The copyright of the above-mentioned described thesis rests with the author or the University to which it was submitted. No portion of the text derived from it may be published without the prior written consent of the author or University (as may be appropriate). *Short quotations may be included in the text of a thesis* or dissertation for purposes of illustration, comment or criticism, provided full acknowledgement is made of the source, author and University.

The copyright of the above-mentioned described thesis rests with the author or the University to which it was submitted. No portion of the text derived from it may be published without the prior written consent of the author or University (as may be appropriate). *Short quotations may be included in the text of a thesis* or dissertation for purposes of illustration, comment or criticism, provided full acknowledgement is made of the source, author and University.

GEOLOGY, GEOCHEMISTRY, AND TECTONO-METALLOGENIC EVOLUTION OF NEOPROTEROZOIC GOLD DEPOSITS IN THE KADUBU AREA, KIVU, DEMOCRATIC REPUBLIC OF CONGO.

****

PART 1 - 2

KABUNGULU MUTOKA AMBROSE WALEMBA.

A thesis submitted to the Faculty of Science, University of the Witwatersrand, Johannesburg, in fulfilment of the requirements for the Degree of

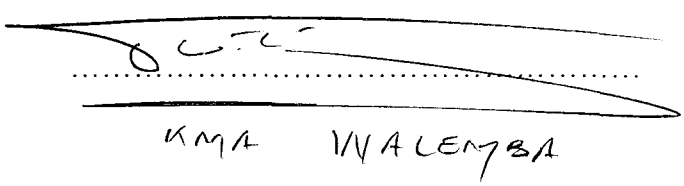
Doctor of Philosophy in Science.

Johannesburg, 2001

DECLARATION.

****

I declare that this thesis is my own, unaided work. It is being submitted for the degree of Doctor of Philosophy in the University of the Witwatersrand, Johannesburg. It has not been submitted before for any degree or examination in any other University.



KMA WALEMBA

.....10th.....day of ....SEPTEMBER.....2001.

ABSTRACT.

****

The aims of this study are to compile the first geological and structural map of the Kadubu area of eastern DR Congo and to elucidate the genesis and evolution of the gold and base- metal mineralizations and their geological setting .

The Kadubu area constitutes the type area of the Itombwe synclinorium Supergroup; situated in the western branch of the East African Rift system and is located between 28 ^{0}33' – 28^0 50' longitude east and the 2^0 45' – 2^0 57' latitude south, covering about 750 s.q.km, (30 km x 25 km). It is made up of a metaturbidite sequence exhibiting characteristic Bouma cycles bordered by major thrust-faults.

The study has entailled the use of modern techniques, from systematic geological mapping to ore genesis studies through structural, tectonic, petrographic, geochronological and geochemical analysis.

The Kadubu metamorphic complex consists of two geochemically and structurally distinct groups: The lower Kadubu group and the upper Kadubu group. The Tshondo fault/ shear zone is a clear tectonic, metamorphic and geochemical discontinuity within the Kadubu area. The Kadubu metaturbidite sequence has been intruded by a late to post-orogenic, alkaline, metaluminous albitite rock. Kasika leucogranite is also intruded into the Kibaran metasediments in the southwesthernmost corner of the study area. This granite is peraluminous, subalkaline, S-type, of syn-to post collisional type. Combined field, geochemical and isotopic data enables constraints to be placed on the origin of the Kasika granite and the Twangiza albitite.

These bounding faults together with major internal, normal shear-faults, strike-slip faults and high-angle reverse faults are interpreted to have a listric geometry and to flatten at depth.They are inferred to pass into major mid-crustal detachment faults forming a west-vergent thrust system. The inferred detachment faulting is interpreted as occurring at the interface of the Itombwe supergroup and the Kibaran basement.

This sequence has been folded into upright, north to northwest -trending, tight to isoclinal folds. Three multiphase deformations [D_1,D_2(compressions)&D_3(extension)], have been metamorphosed to lower-middle greenschist facies. The metamorphic grade increases gradually towards the west with the lower tectonostratigraphic level ranging from subgreenschist to greenschist facies.

^{39}Ar / ^{40}Ar, Rb/Sr and Sm/Nd ratios constrain the history of deformation, metamorphism, magmatism and mineralization. Both field evidence and radiogenic ages indicate Neoproterozoic events.The Kasika granite yielded mean ages of 529 ±5 Ma and 436 ± 8 Ma (^{39}Ar/^{40}Ar) and 703±14 Ma (Rb/Sr).

The Albitite rock yielded an age of 1078 ± 27Ma implying that this albitite is related to a Kibaran granite. The initial Sr isotope ratios (^{87}Sr/ ^{86}Sr) for respectively feldspar (albitite) and apatite & mica (granite) have a mean of 0.734298 ± 0.0001 and [0.885419(apatite) & 18.277000(mica)] respectively. Sm/ Nd isotope ratios for feldspar (albitite) and apatite (granite) are respectively 0.14852 and 0.36422. Sr and Nd isotopic ratios indicate a common crustal source and suggest a genetic relationship between the albitite and granite.

$^{39}Ar/^{40}Ar$ dating of metamorphic muscovite in cleaved phyllite gives an age of 575 ± 83 Ma. This dated muscovite comes from within the D_2 -NNW directed tigh to isoclinal –dominated structural domain and this age is interpreted as coinciding with F_2 folding.

The structure of the Kadubu area is essentially a "detachment (nappe) – thrust stack" that has resulted from compressional thrust tectonics that was later transformed into strike-slip dominated tectonics. The structure and age (530- 540 Ma) of the complex accords with a Pan African collisional history.
The Itombwe basin has evolved as a strike-slip pull-apart basin. The basin was formed in a strike-slip setting with pull-apart structures showing transitions from compressional (transpression) to extensional (transtension) regimes. The pull-apart basin was associated with strike-slip displacements along overstepping *en-echelon* faults. The geochemistry of the clastic metasediments suggest a tectonic model for the Kadubu area (Itombwe synclinorium) as an intracontinental extensional rift receiving clastic detritus from the adjacent uplifted Kibaran basement. Glacial influence on deposition of the Kadubu (meta)sediments has been recognized.

Mineralization within the Kadubu area is represented by two important gold deposits (Twangiza and Tshondo) and one tin deposit (The Kashwa sheeted tin deposit). Small occurrences of gold (Kakere, Mufwa and Mwanza), travertine deposits, thermal hot springs (The Luidja and Bugoyi hot-springs) and alluvial terraces (Nambo ..) are also recognized in the study area.

In the Twangiza deposit, the combined results from studies of mineral paragenesis, geologic relationships, geochemistry and geochronology ($^{40}Ar/^{39}Ar$, Rb-Sr and Sm-Nd) have been synthesized to provide a coherent composite of the relationships between the different tectonothermal events (deformation, metamorphism, magmatism and mineralization).

Two separate phases of mineralization are indicated, the earlier comprising sulphide veining localized within classic saddle reef structures and containing the highest Au, and a later, fault controlled style of quartz reef, synchronous with dextral strike-slip faulting. The cross-cutting fault controlled reef stage of mineralization is associated with ground preparation and kinematic emplacement of albitite rock and is related to hydrothermal fluids migrating out of the Twangiza fault feeder zone. The first phase of mineralization corresponds to stages I & II gold mineralization, while the late phase correspond to Stage III gold mineralization. It is suggested that the $^{40}Ar/^{39}Ar$ ages (mean: 522 ± 15Ma) of hydrothermal muscovites from the Twangiza deposit provides a good estimate of timing of the saddle reef gold mineralization.

In the Twangiza region, small intrusive albitite porphyries, crescent shaped and with dimensions of about 200m x 50m, were also perfectly placed for driving the ore-forming hydrothermal system. The spatial association between albitite intrusion and gold mineralization reflects the paramount importance of structure in the localization of gold mineralization. Based on field relations, textural and geochemical evidence as well as geochronological information, it is argued that the albitite intrusions pre-date emplacement of saddle reefs and fault reefs by at least 53 Ma .

Four types of fluid inclusions have been recognized: H_2O-NaCl-CO_2- Salt; H_2O-NaCl-CO_2 and H_2O- NaCl- Salt; H_2O- NaCl. Thermobarometric evolution occurred in two stages:
*.- Fluid inclusions from the H_2O-NaCl-CO_2 +/- salt system correspond to a drop of pressure and an opening in a lithostatic regime and accompanied by early Au and As ore deposition .
*.- Fluid inclusions from the H_2O -NaCl +/- Salt system correspond to a drop in temperature and an opening in a hydrostatic regime. They are associated with late Au, As and Sb ore deposition. The great variability of temperature and salinity of these inclusions suggests a range of fluids from meteoric to a mixture of meteoric and magmatic. The hypothesis of magmatic derivation under alternating hydrostatic and lithostatic conditions seems to explain the gross features of the data.

Isotopic analyses (C, O, S) of pyrite and carbonate veins from QV_1 and QV_2 (Twangiza) and TV_2 (Tshondo) constrain the characteristics of the ore-forming source fluid and the source rocks. The isotopic data collectively indicate that the vein fluids were exotic with respect to the upper Kadubu group. Based on this study, the hydrothermal fluids which generated the vein minerals examined, are considered to have originated from a magmatic source. This model derives the heat and gold mobilizing fluid from the associated Kasika leucogranite.

The $^{40}Ar/^{39}Ar$ age of 533-559 Ma (mean age of 546 ± 8Ma) for quartz -tourmaline-tin veining broadly agrees with the geological and structural observations that deformation and veining were initiated during a Pan African event, at which time bedding planes and tensional features related to faulting would have been the major anisotropy available for fluid migration.

A close association in time (522 ± 15Ma for gold and 533 -559Ma for tin respectively) and space (8.5 km apart) also support the general concept of a genetic link between the Twangiza gold deposit and the Kashwa tin deposit. Field and geochemical evidence indicate that albitite porphyry intrusions spatially related to gold mineralization in the Twangiza deposit may be genetically related to the Kashwa sheeted tin vein system, both being related to the Kasika granitoid batholith inferred at depth. Gold and tin mineralization form one continous ore spectrum.

Spatial and temporal distribution of gold and tin deposits in the Kadubu area suggest the presence of a metamorphic core complex /detachment fault model to explain the source for the mineralization. In this model, intense hydrothermal circulation, silicification, brecciation and even magmatism (granitization, greisenization and albitization), are features seen on permeable detachment zones, with mineralization occurring along cover/basement contacts as well as along relatively high-angled reverse, and/or listric faults. High-angled, listric (e.g. Tshondo) or reverse(e.g.Twangiza) faults emanating from the detachment fault sole, have channeled mineralized fluids to higher levels.

The genetic model for the Kadubu gold-bearing deposits invokes degassing of magmatic hydrothermal fluids, mixing with basinal fluids and partial meteoric and/or connate fluids . Minor convecting formational and contact metamorphic fluids were probable also involved in an overall brittle deformational environment within a collisional and transpressive geodynamic regime.

DEDICATION.

****

To : - My parents ; Walemba Kabungulu Pius and Mukombelwa Astrid .

- In memory of my brother ; Walemba Nzolo Pius Jr.

1946 - 1999.

ACKNOWLEDGEMENTS.

****

I would sincerely like to thank the Anglo American Plc / AED for the initiation of this project and for providing financial and logistical support. I am extremely grateful for the continued assistance and encouragement of the management and staff of AAC/AED. In particular the enthusiasm of Messrs R.D. Corrans, J.C. Moncur, G.L. Palmer, S. Marsh, H.Voet, C.Clopper, and Mrs L.Wadsworth, D. Holahan, W. Ancill, Carmen, P.A. Hillier are greatly appreciated.

I am most grateful to my supervisor, Prof. Morris. J. Viljoen, for the invaluable guidance during all phases of this study, for his encouragement and support, for his neverending willingness, for discussions and his constructive critisism.

Prof. Spike McCathy, head of the Geology Department is thanked for affording me the opportunity to conduct this research in the stimulating environment of the Geology Department at Wits University.

Very special thanks are extended to Dr. P.A.de Groot of the Geology Department, Wits University for his enthusiastic support throughout this project, particularly for assistance for sulphur isotope analyses and for having read draft portions of this thesis.

The work has further benefited from discussions and constructive critisism on fluid inclusion studies by Dr. Yong Yao, of the Geology Department, Wits University.

I am grateful to the following people and institutions who played an important role in the collection of analytical data:

- Prof. M.J.Witcomb and Mrs C.Lalkhan for help with the Scanning electron microscope at the Electron Microscope Unit, University of the Witwatersrand.
- Prof. B. Verhagen for use of the mass spectrometer for carbon and oxygen isotope analyses at the Schonland Research Centre for Nuclear Sciences, University of the Witwatersrand.
- Dr. P. Murphy, for use of the Raman microspectroscopic facility at the Department of Physic, University of the Witwatersrand.
- Dr. W. Jordaan and Dr. J.Bester at the Council for Geoscience, Pretoria for assistance with sulphur isotope analysis on a Finigan Mat250 mass spectrometer.

- Dr. D. Phillips, Mrs. V.M. Robb, and Mrs. G.B. Kiviets, at the Anglo American Research Laboratories for Argon - Argon dating.
- Mr. R. Holdsworth at the Anglo American Research Laboratories for his assistance with XRD, XRF, and ICP analyses.
- Ms.S. Farrell at the Geology Department,Wits for her assistance with XRF and XRD analyses.
- Mrs. N. Day for the use of Ion microprobe facility at the Geology Department,Rand Afrikaans University.
- Dr.F. J. Kruger for the use of the analytical facilities of the Hugh Allsopp Laboratory at the Bernard Price Institute for Geophysical Research, Wits University.
- Dr. C. Harris for his assistance with the mass spectrometer for oxygen isotope analysis at the Department of Geochemistry, University of Cape Town.
- Prof. R.T. Lubala at the Geology Department,University of Lubumbashi for his geological advices in the field.
- Prof. C. Anhaeusser, Prof. L.Robb, Prof. R.Viljoen, Prof. G. Cawthorn, Dr. S. Master , Dr. G. Cooper, Dr. G. Charlesworth, Dr. R. Gibson, Dr. J. Hancox, Dr. D. Brandt, Dr. R.Boer and Dr. G. Drennam are thanked for their interest in the project and their support.
- The Department of Geology, at Wits is also thanked for the use of in-house facilities.

Thanks also to Ms Judy Wilmot, Mrs E. Sole and Mrs S.Cannel for their administrative help. Messrs M. Miles and A. Mathebula are thanked for their technical support and the preparation of thin and polished sections. Mr T. K. Kinyema for his fraternity.

All the Post-graduates of the Geology Department of the University, (Stewart Foya, Christine Rainaud, Andy Hirner, Robert Kiefer, JP Hunt, Bisrat Yibas, Steve Johnson, Sabine Hautke....) are thanked for the many hours of discussion on geology, life, and the universe.
Thanks a lot for the great time I had.
Very special thanks are due to Serah, my wife for all her love and her relentless support and understanding which accompanied me during some very significant phases of this work.
Last, but not least, I want to thank my father, my mother and my brothers to whom this thesis is dedicated and all my family.

Thanks Lord.

CONTENTS.

PART.I.- INTRODUCTION AND GEOLOGICAL SETTING.

CHAPTER 1.- INTRODUCTION.

1.1.- AIMS, SCOPE AND OBJECTIVES OF THIS STUDY..... 1

1.2.- METHODS OF INVESTIGATION..... 2

1.3.- HISTORICAL REVIEW AND PREVIOUS WORKS..... 8

CHAPTER 2.- GEOLOGICAL FRAMEWORK.

2.1.- INTRODUCTION..... 11

2.2.- THE KIBARAN BELT OF CENTRAL AFRICA..... 11

2.3.- ITOMBWE SYNCLINORIUM SUPERGROUP..... 23

2.4.- TECTONICS, RIFTING AND MAGMATIC PROCESSES IN THE WESTERN BRANCH OF THE EAST AFRICAN RIFT SYSTEM..... 28

PART.II.- GEOLOGY AND TECTONIC EVOLUTION OF THE KADUBU AREA.

CHAPTER 3.- INTRODUCTION.

3.1- INTRODUCTION AND GEOGRAPHIC SETTING..... 33

3.2.- GEOMORPHOLOGY AND PREVIOUS WORK..... 33

CHAPTER 4.-TECTONIC LINEAMENT AND LITHOLOGICAL DISCRIMINATION.

4.1.- INTRODUCTION..... 38

4.2.- GEOMORPHIC CRITERIA..... 39

4.3.- LINEAMENT ANALYSIS (PATTERN , DENSITY AND LENGTH) 40

4.4.- LANDSAT LINEAMENT CORRIDORS AND STRUCTURAL INTERPRETATION..... 41

4.5.- DISCRIMINATION..... 47

4.6.- MAGNETIC FEATURES..... 48

4.7.- SUMMARY AND DISCUSSION..... 51

CHAPTER 5.- LITHOSTRATIGRAPHY, PETROGRAPHY AND GEOCHEMISTRY.

5.1.- GENERAL STATEMENT..... 53

5.2.- LIHOSTRATIGRAPHY AND PETROGRAPHY..... 54

5.2.1.- KIBARAN BASEMENT.....54
5.2.1.1.- INTRODUCTION.....54
5.2.1.2.- KASIKA FORMATION.....54
5.2.1.3.- BANGWE FORMATION.....54
5.2.2.- THE LOWER KADUBU GROUP.....55
5.2.2.1.- KIGOGO CONGLOMERATE FORMATION.....55
5.2.2.2.- KALAMA FORMATION.....55
5.2.2.3.- MUDUBWE FORMATION.....57
5.2.3.- THE UPPER KADUBU GROUP.....59
5.2.3.1.-NYA-KASIBA SEDIMENTARY FORMATION.....59
5.2.3.2.- TSIBANGU FORMATION.....61
5.3.- RECENT FORMATIONS.....69
5.3.1.- THE GWESHE BASALT.....69
5.3.2.- ACTIVE GEOTHERMAL SYSTEM AND TRAVERTINE DEPOSIT.....69
5.3.3.- NAMBO STONE LINE GRAVEL TERRACE.....82
5.4.- PETROGRAPHY AND GEOCHEMISTRY OF IGNEOUS ROCKS.....91
5.4.1.- KASIKA TIN-GRANITE.....91
5.4.2.- TWANGIZA ALBITITE.....119
5.5.- SUMMARY AND DISCUSSION.....146

CHAPTER 6.- STRUCTURE AND DEFORMATION.

6.1.- INTRODUCTION.....149
6.2.- TECTONOSTRATIGRAPHY.....149
6.2.1.- FOLD GEOMETRY.....150
6.2.2.- FAULT SYSTEMS.....151
6.3.- TIME SEQUENCE OF DEFORMATION.....153
6.3.1.- D_1 PHASE OF DEFORMATION : COMPRESSION.....153
6.3.2.- D_2 PHASE OF DEFORMATION : COMPRESSION.....154
6.3.3.- D_3 PHASE OF DEFORMATION : EXTENSION.....155
6.4.- KINEMATIC INTERPRETATION.....155
6.4.1.- INTRODUCTION.....155
6.4.2.- COMPRESSIVE PHASES.....155
6.4.3.- STRIKE-SLIP PHASE.....155
6.4.4.- THE RELATIONSHIP BETWEEN THE TWANGIZA ALBITITE AND D_2 STRUCTURE.....159
6.5.- SUMMARY AND DISCUSSION.....159

CHAPTER 7.- METAMORPHISM.

7.1.- INTRODUCTION.....165
7.2.- PETROGRAPHY AND PHASE RELATIONS.....165
7.2.1.- MINERAL ASSEMBLAGE.....166
7.2.2.- WHOLE-ROCK COMPOSITIONS.....167
7.3.- MICROTECTONISM AND METAMORPHISM.....167
7.3.1.- INTRODUCTION.....167
7.3.2.- TECTONO-METAMORPHIC PHASE: D_1 - M_1.....169
7.3.3.-TECTONO-METAMORPHIC PHASE: D_2 - M_2.....169
7.4.- METAMORPHIC EVOLUTION.....169
7.4.1.- GROWTH AND STABILITY OF MINERALS.....170
7.4.2.- CHRONOLOGY AND TECTONIC FRAMEWORK: $^{40}Ar/^{39}Ar$ DATING.....170
7.5.- SUMMARY AND DISCUSSION.....175

CHAPTER 8.- GEOCHEMISTRY AND TECTONIC SETTING OF CLASTIC METASEDIMENTS

8.1.- INTRODUCTION.....177
8.2.- GENERAL GEOCHEMICAL FEATURES AND CLASSIFICATION.....177
8.3.- SOURCE CHARACTERISTIC AND DEPOSITIONAL ENVIRONMENT.....178
8.3.1.- COMPOSITIONAL CHARACTERISTICS.....187
8.3.2.- GLACIOGENIC DEPOSITS: PALEOCLIMATE SIGNIFICANCES AND GEOCHRONOLOGICAL IMPLICATIONS.....200
8.4.- SUMMARY AND DISCUSSIONS.....203

CHAPTER 9.- INTERPRETATIONS.....204

CHAPTER 10.- SUMMARY OF THE GEOLOGY AND TECTONIC EVOLUTION OF THE KADUBU AREA.....206

PART III.- MINERALIZATION.

CHAPTER 11.- INTRODUCTION .

11.1.- GENERAL STATEMENT.....211
11.2.- LINEAMENT TECTONICS OF KADUBU ORE DEPOSITS.....211
11.2.1.- GENERAL ASPECTS.....211
11.2.2.- REGIONAL LINEAMENT SYSTEMS.....212
11.2.3.- LINEAMENT - ORE RELATION.....212
11.2.4.- SUMMARY.....215

CHAPTER 12.- THE TWANGIZA GOLD DEPOSIT.

12.1.- INTRODUCTION.....216

12.2.- LOCATION OF THE DEPOSIT.....216

12.3.- EXPLORATION HISTORY.....216

12.4.- GOLD MINERALIZATION.....223

12.4.1.- REGIONAL SETTING AND DEPOSIT -SCALE GEOLOGY.....223

12.4.2.- STRUCTURAL STYLE AND DEPOSIT ARCHITECTURE.....223

12.4.3.- VEIN MINERALOGY AND PARAGENESIS.....239

12.4.4.- WALL-ROCK ALTERATION AND RELATIVE CHEMICAL CHANGES.....253

12.4.5.- SUPERGENE ENVIRONMENT.....257

12.4.6.- ORE-ELEMENT ASSOCIATION.....257

12.4.7.- SUMMARY AND DISCUSSIONS.....258

12.5.- ORE MINERALOGY.....263

12.5.1.- INTRODUCTION.....263

12.5.2.- MORPHOLOGY AND TEXTURE.....264

12.5.3.- CHEMISTRY SIGNATURES.....276

12.5.4.- SUMMARY AND DISCUSSION.....292

12.6.- CHEMICAL MASS TRANSFER AND THE PATH OF METASOMATIC REACTIONS.

12.6.1.- INTRODUCTION.....295

12.6.2.- DESCRIPTION OF VEIN MINERALOGY AND PARAGENESIS FOR SELECTED SAMPLES.....295

12.6.3.- MINERAL AND ALTERATION GEOCHEMISTRY.....299

12.6.4.- SUMMARY AND DISCUSSIONS.....317

12.7.- $^{40}Ar/^{39}Ar$, Rb-sr and Sm-Nd AGES CONSTRAINTS ON THE TIMING OF GOLD MINERALIZATION.....322

12.7.1.- INTRODUCTION.....322

12.7.2.- DESCRIPTION OF THE SAMPLES.....322

12.7.3.- RESULTS.....323

12.7.4.- RELATIVE TIMING OF GOLD MINERALIZATION.....327

12.7.5.- SUMMARY AND DISCUSSION.....329

12.8.- FLUID INCLUSIONS.....333

12.8.1.- INTRODUCTION.....333

12.8.2.- PETROGRAPHY.....333

12.8.3.- MICROTHERMOMETRY.....339

12.8.4.- RAMAN SPECTROSCOPY.....351

12.8.5.- DISCUSSIONS.....354

12.8.6.- SUMMARY AND DISCUSSION.....360

12.9.- STABLE ISOTOPE SYSTEMATICS.....361
12.9.1.- INTRODUCTION.....361
12.9.2.- ANALYTICAL RESULTS.....361
12.9.3.- COMBINED OXYGEN AND CARBON ISOTOPES ON CARBONATES.....364
12.9.4.- SULPHUR ISOTOPES.....369
12.9.5.- SUMMARY AND DISCUSSION.....373
12.10.- GENETIC MODEL FOR THE TWANGIZA GOLD DEPOSIT.....374
12.10.1.- REVIEW OF RELEVANT RESEARCH AND THEORIES.....374
12.10.2.- NATURE AND CONDITIONS OF ORE-BEARING FLUIDS.....376
12.10.3.- GOLD TRANSPORT AND PRECIPITATION.....377
12.10.4.- FLUID FOCUSING.....379
12.10.5.- SOURCE(S) OF FLUID(S) AND ORE METAL COMPONENTS.....380
12.10.6.- GENETIC MODEL.....384
12.10.7.- SUMMARY.....387

CHAPTER 13.- THE TSHONDO GOLD DEPOSIT.

13.1.- INTRODUCTION.....389
13.2.- GOLD MINERALIZATION.....389
13.3.- OXYGEN ISOTOPE.....394
13.4.- SUMMARY AND DISCUSSIONS.....409

CHAPTER 14.- KASHWA TIN DEPOSIT.

14.1.- INTRODUCTION.....410
14.2.- THE HYDROTHERMAL TIN-BEARING VEINS AND STRUCTURE.....410
14.3.- GEOCHEMISTRY.....418
14.4.- OXYGEN ISOTOPE.....418
14.5.- $^{40}Ar/^{39}Ar$ DATING.....421
14.6.- STRESS FIELDS AND EMPLACEMENT OF THE HYDROTHERMAL TIN - BEARING VEINS ...425
14.7.- GENETIC LINK BETWEEN GOLD AND TIN MINERALIZATION.....426
14.8.- SUMMARY AND DISCUSSION.....427

PART IV :- SUMMARY AND CONCLUSIONS.....430
REFERENCES.....442
APPENDIX.....492

LIST OF FIGURES.

PART I.

Fig.I.1:- Structural setting of Archean cratons and Proterozoic mobile belts in Central and Eastern Africa , showing the Itombwe synclinorium and the Kadubu area. (Compiled from Cahen et al., 1984, Pohl, 1994, Daly, 1986, Ring et al., 1997, with additions).

Fig.I.2:- Topographical expression of the study area: mountainous with deeply incised valleys and alpine grassland .

Fig.I.3:- Artisanal workers in the Shabunda region. Ulindi alluvial gravel.

Fig.I.4:- Location of the Kadubu study area within a sketch map of Kibaran basins after Klerkx,J., 1988.

Fig.I.5a:- Configuration of the upper Proterozoic Pan-African belt system with extensions into South America, Antartica and Australia on a pre-drift reassembly of the Gondwana continent (modified after Porada .,1985).

Fig.I.5b:- Outline of the IMSLEK terranes that collide with the Congo Craton and Arabian - Nubian Shield to form the Mozambique belt between 800 and 650 Ma. (after Meert et al., 1995).

Fig.I.5c:- Gondwana paleomagnetic poles in the age range 810-585 Ma rotated to the Gondwana configuration of de Wit et al., (1988) , with the African poles fixed. (after Meert et al., 1995).

Fig.I.5d:- Gondwana paleomagnetic poles (south poles) for the interval 550-510 Ma rotated to Africa coordinates. (after Meert et al., 1995).

Fig.I.6a:- Sketch map showing the Late Proterozoic tectonic setting of Central Africa. This comprises a pair of opposed thrust belts separated by the continental scale Mwembeshi shear zone (after Daly, 1989).

Fig.I.6b:- Approximate position of Pan-African rift sequences in southern Africa and South America [modified after Porada (1989)] . Note that an Angola plate is distinguished from the Congo plate with the West Congolian and the Lufilian belts separating them. (after Frimmel , H.E and Frank, W. (1998).

Fig.I.7: - Locality map of the Itombwe plateaux and location of the Kadubu study area.

Fig.I.8:- Structural sketch of the East African Rift System including proposed NW-SE trending wrench zones..

Fig.I.9:- Simplified map of the western branch of the East African rift system subdivised into three segments and showing four volcanic provinces.

Fig.I.10:- Three-dimensional model of spoon-shaped rift basins and accomodation zones between basins (after Ebinger, 1989b) .

Fig.I.11:- Spatial distribution and rock types of 19 alkaline massifs located along the Western branch of the East African rift System. The Bukavu and Kamituga volcanic regions are also shown in relation to the study area.

PART II.

Fig.II.1:- Topography of East Africa derived from 30arc second DEM, showing lineament corridors and location of the Kadubu area.

Fig.II.2:- Locality map of the Kadubu study area.

Fig.II.3:- Extract of DIF image 600 X 750 pixels, of the East Africa showing lineament corridors through the Kadubu study area .

Fig.II.4:- Topographical expression of the study area : grassland and Kadubu river in the central part of the study area, and rainforest environment and Lushwege river in the southwestermost corner of the study area.

Fig.II.5:- Landsat TM 457 image of the study area.

Fig.II.6:- Enhanced magnetic anomaly map of the Kadubu study area.

Fig.II.7:- Tectonic lineaments ; generalised Landsat TM interpretation of the study area.

Fig.II.8:- The map of the subdivision of the Kadubu area into three zones.

Fig.II.9:- The map of the subdivision of the Kadubu area into three domains.

Fig.II.10:- Rose diagram for all of the 356 linear features for the whole area and its structural trends .

Fig.II.11:- Rose diagram of lineaments of the Monana zone (zone 1) and its structural trends.

Fig.II.12:- Rose diagram of lineaments of the Mwana zone (zone 2) and its structural trends

Fig.II.13:- Rose diagram of lineaments of the Kilungutwe zone (zone 3) and its structural trends.

Fig.II.14:- Rose diagram of the upper Kadubu group lineaments and its structural trends.

Fig.II.15:- Rose diagram of the lower Kadubu group lineaments and its structural trends.

Fig.II.16:- Geological and structural map of the Kadubu study area.

Fig.II.17:- Kalama formation . Quartzite interbedded with variegated mica schist. Kilungutwe river in the southwesternmost of the study area.

Fig.II.18:- Mudubwe formation. Alternating sequence of phyllite, schist and quartzitic sandstone. Kilungutwe river in the southernmost of the study area.

Fig.II.19:- Cross -laminations within the phyllitic Mudubwe formation.Kitwabaluzi locality.

Fig.II.20:- Oligomictic conglomerate with laminated facies and turbidites . Note graded laminations identifying origin as turbidites. Mukuka river, Nya -Kasiba locality.

Fig.II.21:- The graphitic black shale overlying the quartzitic oligomictic conglomerate. Mukuka river, Nya -Kasiba locality.

Fig.II.22:- Fold and cleavage morphology within interbedded black shale, silstone and sandstone of the Kadubu area. Luidja locality.

Fig.II.23:- Photomicrograph of black shale.

Fig.II.24:- Phyllite (sericite schist) exhibiting a well -defined fissility and slaty cleavage.

Fig.II.25:- Photomicrograph of phyllite.

Fig.II.26:- Arkosic sandstone.

Fig.II.27:- Intensely deformed and sheared polymictic conglomerate. Kahanda locality.

Fig.II.28:- Hand specimen of polymictic conglomerate, showing quartz vein and granites pebbles.

Fig.II.29:- Ngweshe basalt. Bugoyi locality.

Fig.II.30:- Tuffaceous volcanic rock. Bugoyi locality.

Fig.II.31:- Luidja (Monana) hot-spring .

Fig.II.32:- Bugoyi hot-spring travertine.

Fig.II.33:- Detail of a paludal tufa. A typical waterfall site producing modern tufas in association with macrophyte hummocks (bryophytes) and hanging angiosperm roots.

Fig.II.34:- Ternary diagram (MgO-CaO-LOI) and binary plots (Log MgO/CaO vs Log MgO/CaO ; Log Na_2O/CaO vs Log Na_2O/CaO).

Fig.II.35:- Schemas of the main features of geothermal systems and the environments of hydrothermal ore deposition (after Henley & Hedenquist.,1983).

Fig.II.36 :- Model for the evolution of an incised valley and its subsequent filling (after Shanley and McCabe.,1993).

Fig.II.37a:- Nambo stone line gravel terrace. Paired terraces and incised valley.

Fig.II.37b:- Detail of Nambo pedological profile.

Fig.II.38:- Various ternary ($Fe_2O_3/SiO_2/Al_2O_3$; $MgO/MnO/P_2O_3$), binary (Al_2O_3 versus Fe_2O_3 ; SiO_2 versus Al_2O_3 , Fe_2O_3) and frequency diagram of Fe_2O_{3T} plots for the Nambo terrace.

Fig.II.39:- The stratigraphic column of the Kadubu area within the Itombwe synclinorium.

Fig.II.40:- Kasika granite outcrop showing intrusive stock units. Lumetekelo river, Kasika locality.

Fig.II.41:- Hand specimen of coarse-grained porphyritic Kasika granite showing texture and mineralogy .

Fig.II.42:- Photomicrograph of Kasika granite.

Fig.II.43:- SiO_2 versus total alkalis diagrams for the Kasika granite. Symbols : half-circle = I-type granite; circle= S- type granite. The average of I and S -type granites from the Lachlan fold belt of Chapell and White, 1992.

Fig.II.44:- ACNK versus ANK diagram for the Kasika granite, Ternary diagram of $CaO-Al_2O_3-(Na_2O+K_2O)$ and Binary plot of SiO_2 versus $Al_2O_3/(CaO-3.3*P_2O_5+Na_2O+K_2O)$ showing the peraluminous chemistry of the Kasika granite.

Fig.II.45:- Harker variation diagrams for selected major elements from the Kasika granite. Symbols as in Fig.II.43, unless otherwise indicated.

Fig.II.46:- Binary plots (Al_2O_3 vs CaO ; Fe_2OT vs TiO_2 ; Fe_2OT vs P_2O_5 ; K_2O vs Na_2O ; MgO vs CaO) for the Kasika granite.

Fig.II.47:- The subdivision of subalkalic rocks using the K_2O versus silica diagram. Kasika granite plot in the fields of high -K and medium - K (after Le Maitre et al., 1989) and high -K , calc-alkaline series and calc-alkaline series (after Rickwood , 1989) .

Fig.II.48:- The ($Al_2O_3 - K_2O - CaO + Na_2O$) of Nesbitt and Young (1984, 1989) showing the weathering trends for Kasika granite.

Fig.II.49:- Harker variation diagrams for selected trace elements from Kasika granite.

Fig.II.50:- Chondrite -normalized trace element patterns for Kasika granite. Elements are arranged with increasing incompatibility, from right to left.

Fig.II.51:- Multi -element variation diagrams illustrating the geochemical characteristics of the Kasika granite. Normalizing values after Sun and McDonough, (1989).

Fig.II.52:- Chondrite -normalized REE patterns for the Kasika granite .

Fig.II.53:- Spider diagrams for the Kasika granite.

Fig.II.54:- $^{40}Ar/^{39}Ar$ age spectrum versus cumulative fraction of ^{39}Ar released from a muscovite grain (KW 44-1) from leucogranite sample KW 44.

Fig.II.55:- $^{40}Ar/^{39}Ar$ step-heating analyses for three feldspar grains from tonalite sample KW 44.

Fig.II.56:- Rb-Sr isochron for thin -slab profiles of samples KW 44 apatite and KW 44 mica

Fig.II.57:- Diagram of total alkalis versus SiO_2 for the Kasika granite. The original plot is from Cox et al., (1979) and Le Bas et al., (1986). The line dividing alkalic and sub-alkalic magma series is from Miyashiro (1978).

Fig.II.58:- Triangular QAP diagram of Streckeisen (1976) showing CIPW normative mineral compositions of the Kasika granite.

Fig.II.59:- Binary plot of Na_2O versus K_2O for the Kasika granite.

Fig.II.60:- Ternary plots (An-Or-Ab and Q-Or-Ab) for the Kasika granite.

Fig.II.61:- Triangular QAP diagram (Streckeisen, 1976; Bowden and al., 1984). Fields of S, I and A - type granites are from Whalen and Curie ,(1990).

Fig.II.62:- SiO_2 vs $Al_2O_3/CaO-3.3*P_2O_5+Na_2O+K_2O)$ diagram .

Fig.II.63:- SiO_2 vs Fe_2O_3T/MgO diagram .

Fig.II.64:- Plots of Zr versus SiO_2 , Zn versus SiO_2 , showing the I-type character of the Kasika granite (after Collins et al., 1982).

Fig.II.65:- Plots of Y versus SiO_2 , Nb versus SiO_2 showing the I-type character of the Kasika granite (after Collins et al., 1982).

Fig.II.66:- Plots of the Kasika granite in the tectonomagmatic discriminative diagrams of Pearce et al., 1984. (Y+Nb vs Rb; Y vs Nb ; SiO_2 vs Rb ; SiO_2 vs Nb).

Fig.II.67:- Kasika granite in the diagrams of Maniar and Picolli, (1989) .

Fig.II.68:- Ternary Rb-Sr-Ba diagram showing the characteristics of Kasika granite.

Fig.II.69:- Log-log diagrams of incompatible (Rb) versus compatible elements (Ba, Sr) after Cocherie et al.,(1994).

Fig.II.70:- Bivariat plot of P_2O_5 versus Rb .

Fig.II.71:- MgO versus Ni diagram of Elthon (1998).

Fig.II.72:- SiO_2 versus CaO / ($K_2O = Na_2O$) diagram of Feng and Kerrich , (1992).

Fig.II.73:- Twangiza albitite outcrops: weathered, yellowish-brown, soft with mottled appearance.

Fig.II.74:- Close observation of the Twangiza albitite outcrop. The rock is compact with mottled and granular appearance.

Fig.II.75:- Hand specimem of albitite rock cut by two sets of quartz-veins with halo of silicification and carbonatization extending from the veins. Pyrite and green mica occurring in the zone of bleaching.

Fig.II.76:- Hand specimen of weathered halo of altered albitite rock cut by QV_2 (quartz/iron after sulphide vein) and exhibiting coarse rutile grains in alteration zone.

Fig.II.77:- Albitite injection within the black shale. Fracture control of alteration haloes is evident.

Fig.II.78:- Photomicrograph of albitite rock.

Fig.II.79:- Silky talc -carbonate rock associated with albitite.

Fig.II.80:- Igneous spectrum diagram of Hughes (1972).

Fig.II.81:- SiO_2 versus alkalis diagram .

Fig.II.82:- ACNK versus ANK diagram , SiO_2 versus alkalis diagram, and Zr/P versus TiO_2 .

Fig.II.83:- Harker variation diagrams for selected major oxide elements from the Twangiza albitite.

Fig.II.84:- Frequency diagram of Fe_2O_3/ FeO.

Fig.II.85:- The (Na_2O +CaO)- Al_2O_3- K_2O diagram of Nesbitt and Young (1984, 1989) showing the weathering trends for Twangiza albitite.

Fig.II.86:- Triangular QAP diagram of Streckeisen (1976) showing CIPW normative mineral compositions of the Twangiza albitite.

Fig.II.87:- Na_2O / SiO_2 versus Na_2O/Al_2O_3 and K_2O/ SiO_2 versus K_2O/ Al_2O_3 plots , showing albitite samples described in this study.

Fig.II.88:- Harker and other variation diagrams for selected trace elements from the Twangiza albitite illustrating some important chemical characteristics.

Fig.II.89:- Chondrite - normalized REE patterns for the Twangiza albitite.

Fig.II.90:- Spider diagrams for Twangiza albitite.

Fig.II.91:- Plots of Twangiza albitite in the tectonomagmatic discriminative diagrams of Pearce et al., 1983, 1984.(Y+Nb vs Rb; Y vs Nb ; SiO_2 vs Rb ; SiO_2 vs Nb .

Fig.II.92:- Twangiza albitite in the diagrams of Maniar and Picolli, (1989).

Fig.II.93:- Composition of Twangiza albitite in terms of a $CaO-Na_2O+K_2O - Al_2O_3$ ternary diagram and showing the typical field of A-type granitoids.

Fig.II.94:- Ternary Rb-Sr-Ba diagram showing the characteristics of Twangiza albitite.

Fig.II.95:- Total alkali versus silica diagram of Le Bas et al., (1986), for Twangiza albitite.

Fig.II.96:- Geochemical tectonic classification diagrams for Twangiza albitite.

Fig.II.97:- Discriminant diagrams of Maniar and Picolli, (1984, 1989) for Twangiza albitite.

Fig.II.98:- Tectonic discriminant diagram of A-type granitoids of Elby (1992).

Fig.II.99:- Comparison of REE abundance, demonstrating genetic independence between the metaturbidite of the Kadubu area as a possible source for direct partial melting of the Twangiza albitite intrusion.

Fig.II.100:- Comparison of REE abundances demonstrating genetic dependence between the Kasika leucogranite and the Twangiza albitite.

Fig.II.101:- Enrichment - depletion diagram showing the enrichment factors for selected major and trace elements from the Kadubu area. The diagram compare the relative concentrations of the Twangiza albitite (KW 1A) and the Kasika granite (KW 44).

Fig.II.102:- Kasika granite and Twangiza albitite within the ternary diagram of Kjarsgaard and Hamilton (1989).

Fig.II.103:- The binary plot of SiO_2 versus total alkalis of Twangiza albitite.

Fig.II.104:- Y versus SiO_2 showing albitite field comparatively to granite field described in this study .

Fig.II.105:- Zr versus TiO_2 showing respectively fields of Twangiza albitite and spatially associated Kasika granite. The diagram shows considerable overlap between Twangiza albitite porphyry and Kasika leucogranite.

Fig.II.106:- Models for postmagmatic alteration in rare-element granitoids.

Fig.II.107:- Kinematic indicators within the polymitic conglomerate .

Fig.II.108:- Synthetic set of Riedel shears.

Fig.II.109:- Albitic margins occuring as mm to cm wide bands. Twangiza gold deposit.

Fig.II.110:- Contact of albitite and black shale in oxide zone showing brecciation. Adit G20 , level 2130 ; Twangiza gold deposit.

Fig.II.111:- Contact of albitite and black shale showing no deformation and albitization of black shale suggesting passive emplacement of albitite pluton. Adit G19 , level 2130 Twangiza gold deposit.

Fig.II.112:- Contact of albitite and black shale showing margin banding. Twangiza gold deposit.

Fig.II.113:- Thrust -fault zone within albitite .

Fig.II.114:- Folded albitite rock exhibiting D_2 deformation and thrust -fault zone within albitite rock and suggesting a synkinematic emplacement and cooling of albitite pluton.

Fig.II.115:- Enrichment / depletion diagrams showing the enrichment factors for selected major and trace elements in samples from Kadubu area. The diagrams compare the relative concentration respectively of the upper Kadubu group polymictic conglomerate and phyllite and lower Kadubu group metagreywacke and phyllite.

Fig.II.116:- Photomicrograph of a carbonaceous- sericite- quartz schist (KW 152), from the upper Kadubu group.

Fig.II.117:- Covariation of major elements versus SiO_2 for the Kadubu metasediments.

Fig.II.118:- Chemical classification of the Kadubu metasediments as predominantly metagreywackes and lithic sandstones.

Fig.II.119:- Position of the Kadubu metasediments on Al_2O_3/SiO_2 versus SiO_2 diagram after Lisitsyn, 1978.

Fig.II.120:- Bivariate plots of Ni versus TiO_2 . Symbols of the fields of PAAS, Bendigo shale and Upper continental crust.

Fig.II.121:- Plot of incompatible trace elements (Nb, Y, Zr) against SiO_2 content for the Kadubu metasediments. Notice the high Nb, Y, and Zr contents relative to average upper continental crust.

Fig.II.122:- Binary plots of Cr versus Ni and Co versus V for Kadubu metasediments.

Fig.II.123:- Binary plots of Y versus CaO, P_2O_5, Sr, and Rb versus K_2O , Sr.

Fig.II.124:- Binary plots of Ba versus Sr , V versus Cr and TiO_2 versus Zr/Nb.

Fig.II.125:- Kadubu metasediments on the Ternary diagram (K_2O - Na_2O - CaO) of Le Maitre , (1976) .

Fig.II.126:- Kadubu metasediments on the weathering discrimination diagram of Nesbitt and Young (1984, 1989) . Major molar proportions plot [(CaO+Na_2O)-K_2O-Al_2O_3]

Fig.II.127:- Upper and lower Kadubu group phyllites on the enrichment/depletion diagram.

Fig.II.128:- Enrichment-depletion diagram showing the enrichment factors for selected major and trace elements from Kadubu area. The diagram compares the relative concentration of the polymitic conglomerate (KW 107B) from the upper Kadubu group and the metagreywacke (KW 330) from the lower Kadubu group.

Fig.II.129:- Kadubu metasedimentary rocks on the Fe_2O_{3T} + MgO versus K_2O/Na_2O, TiO_2, and Al_2O_3/SiO_2 discriminant diagrams of Bathia, 1983.

Fig.II.130:- Kadubu metasediments on the discrminant diagrams of Roser and Korsch,1986.

Fig.II.131:- Kadubu metasediments on the ternary diagram [Al_2O_3- Fe_2O_{3T} /MgO -(CaO + Na_2O + K_2O)] .

Fig.II.132:- Various plots (Sr/Y vs Rb, Sr vs Rb ; TiO_2 Lax20 vs Ni/La ; K_2O vs Ba) for Kadubu metasediments.

Fig.II.133:- Binary plots of Fe_2O_{3T} versus mafic elements (Ni, V, Cr, Co, TiO_2 , MgO) for Kadubu metasediments .

Fig.II.134:- Binary plots of MgO versus ferromagnesian elements (MnO, Fe_2O_{3T} , Cr + Ni, Cr + Ni + Co).

Fig.II.135:- Binary plots of Al_2O_3 versus TiO_2 , V, MgO, K_2O, and Na_2O.

Fig.II.136:- Binary plots of Au versus Co, TiO2, Hg, Ag for Kadubu metasediments.

Fig.II.137:- Chondrite -normalized REE diagram for Kadubu metasediments.

Fig.II.138:- PAAS-normalized REE diagrams, shale composite NA-normalized REE diagram and upper crust- normalized REE patterns for the Kadubu metasediments.

Fig.II.139:- Spider diagrams of the Kadubu metasediments.

PART III.

Fig.III.1:- Extract of Gif image 600x750 pixels

Fig.III.2:- Twangiza gold deposit looking SE, NE and N and showing trenches and adits.

Fig.III.3:- Geological and structural map of the Twangiza region.

Fig.III.4:- Twangiza gold deposit showing trenches and adits (continued).

Fig.III.5:- Cross - section along G18/level 2130 .

Fig.III.6:- Black shale sample with " calciting -out ".

Fig.III.7:- Hydrothermally altered black shale.

Fig.III.8:- Siltstone hand specimen .

Fig.III.9:- Metagreywacke outcrop.

Fig.III.10:- Albitite outcrop.

Fig.III.11:- Saddle reef mineralization at an interface between two black shale beds.

Fig.III.12:- Brittle-ductile shear zone within black shale.

Fig.III.13:- Shearing and veining within black shale.

Fig.III.14:- Shear zone in black shale, rotation of (S) fabric towards © in centre zone.

Fig.III.15:- Gold distribution values within the cross section along G18/level 2130.

Fig.III.16:- Distribution of ore shoots relative to the geometry of the deposit at level 2100.

Fig.III.17:- Fault reef and spur vein outcrops of the Twangiza deposit. [Outcrop of vein sets QV_1; QV_2; QV_3].

Fig.III.18:- Outcrop of vein set QV_1; QV_2; QV_3; QV_4.

Fig.III.19:- Outcrop of vein set QV_1; QV_2; QV_3; QV_4.

Fig.III.20:- Outcrop of vein set QV_2 ; QV_3; QV_4.

Fig.III.21:- Outcrop of vein set QV_1; QV_2; QV_3; QV_4.

Fig.III.22:- Out crop of vein set QV_4.

Fig.III.23a:- Sketch of the main types of gold- sulphide/quartz vein systems.

Fig.III.23b:- Sketches showing the different styles of structural control of mineralized veins.

Fig.III.24:- Generalised form of saddle reefs at Bendigo and schematic fluid circulation pattern around saddle reefs and related fault-hosted deposits (Cox et al., 1991).

Fig.III.25:- Wall-rock alteration assemblage and paragenesis for black shale host rock and QV_2 vein.

Fig.III.26:- Wall-rock alteration assemblage and paragenesis for albitite host rock and QV_3 vein.

Fig.III.27:- Stage II mineralization with multiple episodes of vein opening and filling.

Fig.III.28:- Stage III mineralization with massive carbonate.

Fig.III.29:- Box work with iron oxide along fracture planes.

Fig.III.30:- Propyllitic alteration with mid-argillaceous alteration (halloysite and allophane).

Fig.III.31:- Chemical variations accros alteration selvedges bordering a sulphide vein (QV_2), plotted in the unfolded tetrahedron : [(FeO+MgO) -CaO- K_2O- Na_2O]. The arrows reflect the approximate path from unaltered to visibly altered wall- rock.

Fig.III.32:- Relative chemical variations in altered rock bordering a quartz-carbonate vein (QV_3), plotted in the unfolded tetrahedron [CaO- K_2O-Na_2O-(Fe_2O_2 +MgO)] system. The arrows reflect the approximate path from unaltered to visibly altered wall-rock.

Fig.III.33:- Equant grain of pyrite with triple junction and straight boundaries.

Fig.III.34:- Pyritohedron crystals of pyrite. Some of them are striated with triple points. Twangiza gold deposit.

Fig.III.35:- Photomicrograph of pyrite grains from the Twangiza deposit.(TL and PL).

Fig.III.36:- Photomicrograph of pyrite grains from the Twangiza deposit.(TL and PL).

Fig.III.37:- SEM photomicrographs of pyrite grain from the Twangiza deposit. (Mag: x20, x40, x200, x750).

Fig.III.38:- SEM photomicrographs of pyrite grain from the Twangiza deposit. (Mag: x200, x750, x4000, x4000).

Fig.III.39:- SEM photomicrographs of pyrite grain from the Twangiza deposit. (Mag: x40, x200, x750).

Fig.III.40:- Photomicrograph of arsenopyrite and gold grains from the Twangiza gold deposit.

Fig.III.41:- Hand specimens of native gold from Twangiza gold deposit.

Fig.III.42:- Nuggets of gold from Twangiza gold deposit.

Fig.III.43:- Photomicrograph of gold grains.

Fig.III.44:- SEM of native gold from the Twangiza gold deposit. (Mag: x10, x200, x750, x4000 , x9000).

Fig.III.45:- Histograms of Au contents of pyrite and arsenical pyrite .

Fig.III.46:- Histograms of respectively As, S, and Fe contents of pyrite and arsenical pyrite.

Fig.III.47:- Ternary diagram (S- Fe- As*100) of pyrite from the Twangiza deposit.

Fig.III.48:- Scatter diagrams of .S, Fe, As, Ag, Hg, Cd, Pd and Cu with Au in gold grains.

Fig.III.49:- Correlation of Cu, Hg, Pd and Cd versus Au in pyrite.

Fig.III.50:- Binary plot of $\delta^{34}S$ versus S for Twangiza pyrite with the regression lines.

Fig.III.51:- Enrichment /depletion diagram of the Twangiza pyrite compared to standard mesothermal pyrite of Ho et al., (1991).

Fig.III.52:- Spider plots for elements of the ore suite of the Twangiza deposit compared to standard mesothermal pyrite of Ho et al., (1991) and to pyrite from the Witwatersrand gold deposit of Haulbauer , (1983)..

Fig.III.53:- Scatter diagrams of S, Fe, As, Ag, Hg, Cd, Pd and Cu with Au in arsenopyrite.

Fig.III.54:- Arsenopyrite compositions in atomic % in ternary system Fe- As - S.

Fig.III.55:- The spectra of individual gold grains.

Fig.III.56:- Correlation diagrams of Au versus As, Ag, Fe, S, Pd, Cu, and Cd with the regression lines.

Fig.III.57:- Frequency diagrams of gold grains for the Twangiza deposit .

Fig.III.58:- Histograms of respectively Au, Fe, As, S , Ag,Cu, Pd, in gold from the Twangiza deposit.

Fig.III.59:- Histograms of respectively fineness , the ratios Au/Ag , Au/Fe, and Au/S.

Fig.III.60:- Polished slab of QV_2 multi -stage tension vein with three" ribbons" of vein minerals and associated altered black shale wall -rock .(alteration zonation along black shale host rock).

Fig.III.61:- Polished slab of QV_1 vein and associated altered albitite wall -rock. (alteration halo along albitite host rock).

Fig.III.62:- Scatter diagrams of Zr versus SiO_2 , TiO_2 , Al_2O_3, Fe_2O_3, MgO, La, Nb, Y of QV_1 in albitite.

Fig.III.63:- Correlation diagrams of Al_2O_3 versus Na_2O, Fe_2O_3, CaO, SiO_2 , TiO_2 , MgO, of QV_1 in albitite.

Fig.III.64:- Binary plot of LOI versus (Na_2O+CaO) of albitite samples.

Fig.III.65:- Binary plots of SiO_2 versus K_2O /Al_2O_3 and Fe_2O_3 / Al_2O_3

Fig.III.66:- REE patterns from the fresh albitite sample compared to the most altered and/or mineralized samples.

Fig.III.67:- Scatter diagrams of Zr versus Al_2O_3, SiO_2 , TiO_2 , MgO, Fe_2O_3, La, Nb, Y.,within the QV_2 in black shale.

Fig.III.68:- Correlation diagrams of Al_2O_3 versus Na_2O, Fe_2O_3, CaO, SiO_2 , TiO_2 , MgO, within the QV_2 in black shale.

Fig.III.69:- REE patterns from the fresh black shale sample compared to the most altered and/or mineralized samples.

Fig.III.70:- Chondrite normalized REE patterns for altered black shale metasediments associated with vein-type (QV_2) sulphide mineralization.

Fig.III.71:- Chondrite normalized REE patterns for altered albitite associated with vein type QV_1 mineralization.

Fig.III.72:- Comparison of major and trace elements between most altered albitite sample, close to a QV_1 vein, and a similar unaltered sample not associated with mineralization.

Fig.III.73:- Comparison of major and trace elements between most altered black shale sample, close to a QV_2 vein, and a similar unaltered sample not associated with mineralization

Fig.III.74:- Ternary diagram of molecular Al_2O_3-(CaO+Na_2O+K_2O)-(FeO+MgO) showing compositional variations and metasomatism in the analysed hydrothermally altered samples. (*a*: Black shale, *b*: Albitite , and *c*: Black shale +Albitite) .

Fig.III.75:- Trace element plots for the Kadubu black shale metasediments associated with the vein-type QV_2 sulphide mineralization.

Fig.III.76:- Element distribution in black shale from Twangiza deposit showing significant variation within 150mm from a QV_2 vein.

Fig.III.77:- 3D portrayal of elemental distribution in black shale from the Twangiza deposit, plotted against increasing distance from QV_2 vein.

Fig.III.78:- Variation of As, and Au relative to distance from a QV_2 vein.

Fig.III.79:- Ni, V, Cr, and Co variation within 150mm of a QV_2 vein into black shale host rock.

Fig.III.80:- 3D portrayal of elemental distribution of Ni, V,Cr and Co in black shale from the Twangiza deposit, plotted against increasing distance from QV_2 vein.

Fig.III.81:- Mass change profiles for selected major element oxides and trace elements, plotted against increasing distance from a QV_1 vein , across the albitite alteration haloe.

Fig.III.82:- 3D portrayal of mass change profiles for selected major element oxides and trace elements, plotted against increasing distance from a QV_1 vein , accros the albitite alteration haloe.

Fig.III.83:- Variation of As along a profile within an albitite haloe.

Fig.III.84:- Hand specimen of alteration material adjoining a weathered QV_2 vein associated with albitite host rock.

Fig.III.85:- Some geochemical characteristic of the weathered albitite, and enrichment / depletion diagram between the first and second zones of weathered albitite host rock.

Fig.III.86:- Elemental distribution in weathered albitite from the Twangiza deposit, plotted against increasing distance from a QV_2 vein.

Fig.III.87:- 3D portrayal elemental distribution in weathered albitite from the Twangiza deposit, plotted against increasing distance from a QV_2 vein.

Fig.III.88:- Photomicrograph of hydrothermally altered and mineralizaed black shale.

Fig.III.89:- $^{40}Ar/^{39}Ar$ age spectra derived from resistance furnace step-heating for hydrothermal muscovite samples.

Fig.III.90:- Handspecimen of quartz-vein (QV_1) with sulphide mineralization used for fluid inclusion studies.

Fig.III.91:- Photomicrograph of quartz-vein (QV_1) with sulphide mineralization used for fluid inclusion studies.

Fig.III.92:- Optical photomicrographs of selected fluid inclusion types in a quartz sulphide vein from the Twangiza deposit taken in transmitted light.

Fig.III.93:- Optical photomicrographs of selected fluid inclusion types in a quartz sulphide vein from the Twangiza deposit taken in transmitted light.

Fig.III.94:- Size of fluid inclusions. (Type I, II, III & IV).

Fig.III.95:- Degree of fill of fluid inclusions.(Type I, II, III & IV).

Fig.III.96:- Frequency histogram of melting of CO_2, from microthermometric data . (Type I : H_2O-NaCL -CO_2 -DM and Type II: H_2O-NaCL -CO_2).

Fig.III.97:- Frequency histogram of melting of Ice , from microthermometric data. (Type I, &II, and Type III & IV).

Fig.III.98:- Frequency histogram of melting of ice, from microthermometric data. (Type II and Type IV).

Fig.III.99:- Frequency histogram of final melting of ice, from microthermometric data. (Type II and Type IV).

Fig.III.100:- Frequency histogram of melting of salt, , from microthermometric data. (Type I : H_2 O-NaCL -CO_2 -DM and Type III: H_2O- NaCL -DM).

Fig.III.101:- Frequency histogram of temperature of homogenization of CO_2 , from microthermometric data. (Type I and Type II).

Fig.III.102:- Optical photomicrograph and SEM photomicrographs of quartz vein (QV_1) - hosted decrepitates of fluid inclusions. (Mag: x 85, x 950, x 2300).

Fig.III.103:- Frequency histogram of temperature of homogenization total , from microthermometric data. (Type III: H_2O-NaCl -DM and Type IV: H_2O- NaCl).

Fig.III.104:- Frequency histogram of salinity from microthermometric data. (Type I ,Type II, Type III, Type IV) .

Fig.III.105:- Binary plot of temperature of homogenization and temperature of melting of NaCl

Fig.III.106:- Relationship between homogenization temperatures and salinities. Homogenization temperatures versus salinity diagram for fluid inclusions in quartz - sulphide vein from the Twangiza deposit .

Fig.III.107:- The Raman spectrum of quartz and CO_2 from fluid inclusions from quartz vein (QV_1).

Fig.III.108:- The Raman spectrum of quartz and CO_2 from fluid inclusions from quartz vein (QV_1) .

Fig.III.109:- Histogram of carbonate isotope data (PDB) on carbonate from the Twangiza gold deposit.

Fig.III.110:- Histogram of oxygen isotope data (SMOW) on carbonate from the Twangiza gold deposit.

Fig.III.111:- Histogram of oxygen isotope data (PDB) on carbonate from the Twangiza gold deposit.

Fig.III.112:- The oxygen and carbon isotope compositions of vein calcite and ferroan dolomites from gold ore at Twangiza plotted on the oxygen and carbon isotope diagram for carbonates and for carbon isotopic values of carbon- bearing phases from different settings.(Kerrich , 1987).

Fig.III.113:- The oxygen and carbon isotope compositions of vein calcite and ferroan dolomites from gold ore at Twangiza, compared to mean values for the $\delta^{13}C$ and $\delta^{18}O$ of ferroan dolomites associated with gold deposits of the Abitibi greenstone belt. (Kerrich , 1987).

Fig.III.114:- $\delta^{13}C$ data points indicated relative to ranges of values given by Ohmoto,(1986), for carbon derived from external reservoir, mantle or carbonate source.

Fig.III.115:- Histogram of sulphur isotope data (PDB) from pyrite of the Twangiza deposit .

Fig.III.116:- Schematic diagram of fluid reservoirs.Twangiza gold deposit.

Fig.III.117:- Schematic diagram of genetic model for the Twangiza gold deposit.

Fig.III.118:- The Tshondo gold deposit , looking south.

Fig.III.119:- Artisanal workings, Tshondo gold deposit.

Fig.III.120:- Quartz and sulphide veining , Tshondo gold deposit.

Fig.III.121:- Photomicrograph of native gold. Tshondo gold deposit.

Fig.III.122:- SEM images of native gold from the Tshondo deposit. (Mag: x 30,x 75, x 85, x 200).

Fig.III.123:- SEM images of native gold from the Tshondo deposit. (Mag: x 750, x 4000 , x 9000, x6000).

Fig.III.124:- The spectra of individual gold grains . Tshondo gold deposit.

Fig.III.125:- Histograms of Au, Fe, As, and S respectively from theTshondo deposit.

Fig.III.126:- Histograms of Ag, Cu, Pd, and Cd respectively from theTshondo deposit.

Fig.III.127:- Correlation diagrams of Au, versus As, Ag, S, Fe, Pd, Cu, and Cd from a TV_2 from the Tshondo gold deposit. Ion microprobe results.

Fig.III.128:- Histograms of the fineness and of the ratios Au/Ag, Au/Fe and Au/S respectively from the Tshondo deposit.

Fig.III.129:- Histogram of $\delta^{18}O$ values, Tshondo gold deposit.

Fig.III.130:- View of Kashwa tin deposit looking northeast.

Fig.III.131:- Artisanal working within the Kashwa river, with tin output.

Fig.III.132:- Sheeted tin veins, Kashwa tin deposit.

Fig.III.133:- Vein type system , Kashwa tin deposit.

Fig.III.134:- Hand specimen, tin vein ore, Kashwa tin deposit.

Fig.III.135:- Hand specimen of tin vein ore, Kashwa tin deposit.

Fig.III.136:- Wall-rock alteration in the form of silicification and tourmalinization of black shale unit within the Kashwa tin deposit.

Fig.III.137:- Previous working within a quartz-tourmaline veining and showing silicification and tourmalinization of black shale wall-rock .

Fig.III.138:- Histograms of the ratios of Sn/W and Sn/F from a tin vein,Kashwa tin deposit.

Fig.III.139:- Histogram of $\delta^{18}O$ values of the Kashwa sheeted tin deposit.

Fig.III.140:- Photomicrograph of a quartz-tourmaline vein containing tin from the Kashwa .

LIST OF TABLES.

PART. I.

Table.I.1:- Kibaran evolution in Central Africa .

Table.I.2:- List of 19 alkaline massifs located along the Western Rift with available radiometric data.

PART. II.

Table.II.1:- Chemical composition of the Bugoyi Travertine.

Table.II.2:- Taupo volcanic zone fluid characteristics (Data from Henley & Hedenquist 1983).

Table.II.3:- Chemical data from the Nambo stone line terrace profile.

Table.II.4:- Representative major oxides, trace elements and REE abundances for the Kasika granite and CIPW-norms for selected samples .

Table.II.5:- Summary of major and trace element geochemistry of the Kasika leucogranite compared with S - and I-type granites from Chappell and White (1992).

Table.II.6:- Previous isotopic data from the Kasika granite.

Table.II.7:- $^{40}Ar/^{39}Ar$ laser probe analytical results for single muscovite and feldspar grains from the Kasika granite ; Kadubu area.

Table.II.8:- Rb- Sr and Sm-Nd isotope data for the Kasika granite.

Table.II.9:- Chemical composition of the Twangiza albitite.

Table.II.10:- CIPW - norms of the Twangiza albitite.

Table.II.11:- Rb- Sr and Sm-Nd isotope data for the Twangiza albitite.

Table.II.12:- Magmatic and postmagmatic processes and products in rare-element granitoids.

Table.II.13:- Whole-rock compositions of the mineral assemblage from phyllites, diamictites and metagreywackes from respectively the upper and lower Kadubu group.

Table.II.14:- The relative growth and stability of the minerals during the metamorphic and deformational evolution.

Table.II.15:- $^{40}Ar/^{39}Ar$ laser probe analytical results for single muscovite from black shale; Kadubu area.

Table.II.16:- Chemical composition of the Kadubu metasediments.

Table.II.17:- Chemical composition of Average Shale and Major sandstones types.

Table.II.18:- Chemical composition of the fine-grained portion of the diamictite matrix from the polymictic conglomerate of the Tsibangu Formation.

PART. III.

Table.III.1:- Metasomatic zoning within albitite rock.

Table.III.2:- Quantitative ion-microanalyses of pyrite.

Table.III.3:- Quantitative ion-microanalyses of arsenopyrite.

Table.III.4:- Quantitative ion-microanalyses for gold.

Table.III.5:- Average fineness values for gold from different depositional environments.

Table.III.6:- Major and trace elements from alteration haloes of QV_2 vein in black shale.

Table.III.7:- Major and trace elements from alteration haloes of QV_1 vein in albitite rock.

Table.III.8:- Major and trace elements from alteration haloes of QV_2 vein in albitite rock.

Table.III.9:- $^{40}Ar/^{39}Ar$ laser probe analytical results for muscovite grains from hydrothermally altered and mineralized black shale. Twangiza gold deposit.

Table.III.10:- Schematic sketch illustrating the nomenclature and timing relationships of deformation, metamorphism , magmatism and mineralization in the Kadubu area.

Table.III.11:- Microthermometric data for mesured fluid inclusions in theTwangiza gold deposit.

Table.III.12:- Synthesis of microthermometric fluid inclusion data.

Table.III.13:- Isotopic data for selected veins and wall-rock from the Twangiza gold deposit.

Table.III.14:- Chemical composition of quartz/sulphide vein (TV_2) from the Tshondo gold deposit..

Table.III.15:- Chemical composition of wall-rock associated with quartz/sulphide vein (TV_2) from the Tshondo gold deposit.

Table.III.16:- Quantitative ion-microanalyses of gold from the Tshondo gold deposit.

Table.III.17:- Results of oxygen isotope of hydrothermal quartz vein (TV_2) from the Tshondo gold deposit.

Table.III.18:- Chemical composition of the hydrothermal tin -bearing vein from the Kashwa sheeted tin deposit.

Table.III.19:- Result of oxygen isotope of hydrothermal quartz -tourmaline vein from the Kashwa sheeted tin deposit.

Table.III.20:- $^{40}Ar/^{39}Ar$ laser probe analytical results for a sericite mineral from a quartz - tourmaline vein from Kashwa tin deposit.

PART.I.- INTRODUCTION AND GEOLOGICAL SETTING.

****

CHAPTER 1.- INTRODUCTION.

1.1.- AIMS, SCOPE AND OBJECTIVES OF THIS STUDY.

The principal aims and objectives of the present study are:

*- To construct the first semi-regional geological and structural maps of the Kadubu area;

*- To elucidate the genesis and evolution of the gold and base-metal mineralization and its geological setting, in the light of modern and current geological concepts using various modern techniques.

Major questions addressed in this study are :

*.- What is the nature and the spatial and temporal distribution of ore minerals and their parageneses;

*.- From what source, when, in what sequence, by what process, by what mechanism and in what environment were gold and base-metals deposited in the Kadubu area ?

All of these questions include and involve subhypotheses relating to regional occurrences and tectonic setting, mineralization styles and grade, structural and host-rock controls, fluid-rock interaction, gold and metal associations, timing of gold mineralization, gold transport and depositional conditions, the source of the fluids: magmatic, metamorphic, meteoric or mixed origin , locally derived or externally and/or from a deep-seated source ?

The area of study, as well as all gold-bearing deposits within the Kivu gold metallogenic province (ca, 181,500 sq. km with Au, Sn, W, Nb, Ta, Be, Li, B, U,....) have not before been the subject of detailed studies using current and modern concepts.

This study is the first of its kind and will contribute to the knowledge of this metallogenic province and particularly, the Kadubu gold-bearing deposits in the Western Branch of the East African Rift System (WBEARS).

1.2.- METHODS OF INVESTIGATION.

1.2.1.- INTRODUCTION.

The Kivu region is geographicaly located in the Eastern part of the Democratic Republic of the Congo (DRC),(formerly Zaire), between $25^0$00'-$29^0$30' longitude east and $1^0$00'–$6^0$00'latitude south.

The tectono-metallogenic evolution of the vast Kivu gold metallogenic province, which contains over 50 known gold and base-metal mineral occurrences, is poorly documented and understood. For sake of clarity and considering the time constraints, an intensive study of a limited and selected geographical area (Kadubu area: ~ 750 sq.km) was undertaken, rather than a subregional reconnaissance study. This area contains two gold deposits of economic interest (Twangiza and Tshondo), three additional known gold occurrences (Nambo, Mufwa and Kakere) and one tin-tungsten deposit (Kashwa). Fig.I.1. shows the location of the Kadubu study area within the geological framework of the Central and Eastern African continent.

1.2.2.- FIELDWORK.

Two field seasons were spent in the study area (July 10th to December 6th,1995 and June15th to October 15th 1996). During the first field season, a 1: 50,000 scale semi-regional geological and structural map, using aerial photographs, supported by satellite imagery in conjuction with field checking and observations was compiled.

Field traverses were planned and carried out taking into consideration the topographical expression and geomorphology of the study area. The tographical relief shows up to 2261m of variation from the bed of the Kadubu river (about 900m a.m.s.l.) to the top of Mayi ya Kanon mountain (3161m a.m.s.l ; maximum elevation). The field study involved traversing up and down steep slopes across rugged mountainous terrane with deeply incised valleys (Fig.I.2).

1.2.3.- LABORATORY STUDIES.

Laboratory investigation included : mineralogical studies of 275 thin and polished sections, geochemical analyses by XRF, XRD, REE and ICP1 of 501 samples giving rise up to 12.091 elements, radiogenic isotopes (Rb/Sr & Sm/Nd) studies of 7 samples, $^{38}Ar/^{40}Ar$ dating of 5 samples, fluid inclusions studies of 5 double polished sections, Raman spectroscopy analysis of fluid inclusions, stable isotopes (C, O, S) studies, scanning electron microscopy analysis and ion microprobe analysis.

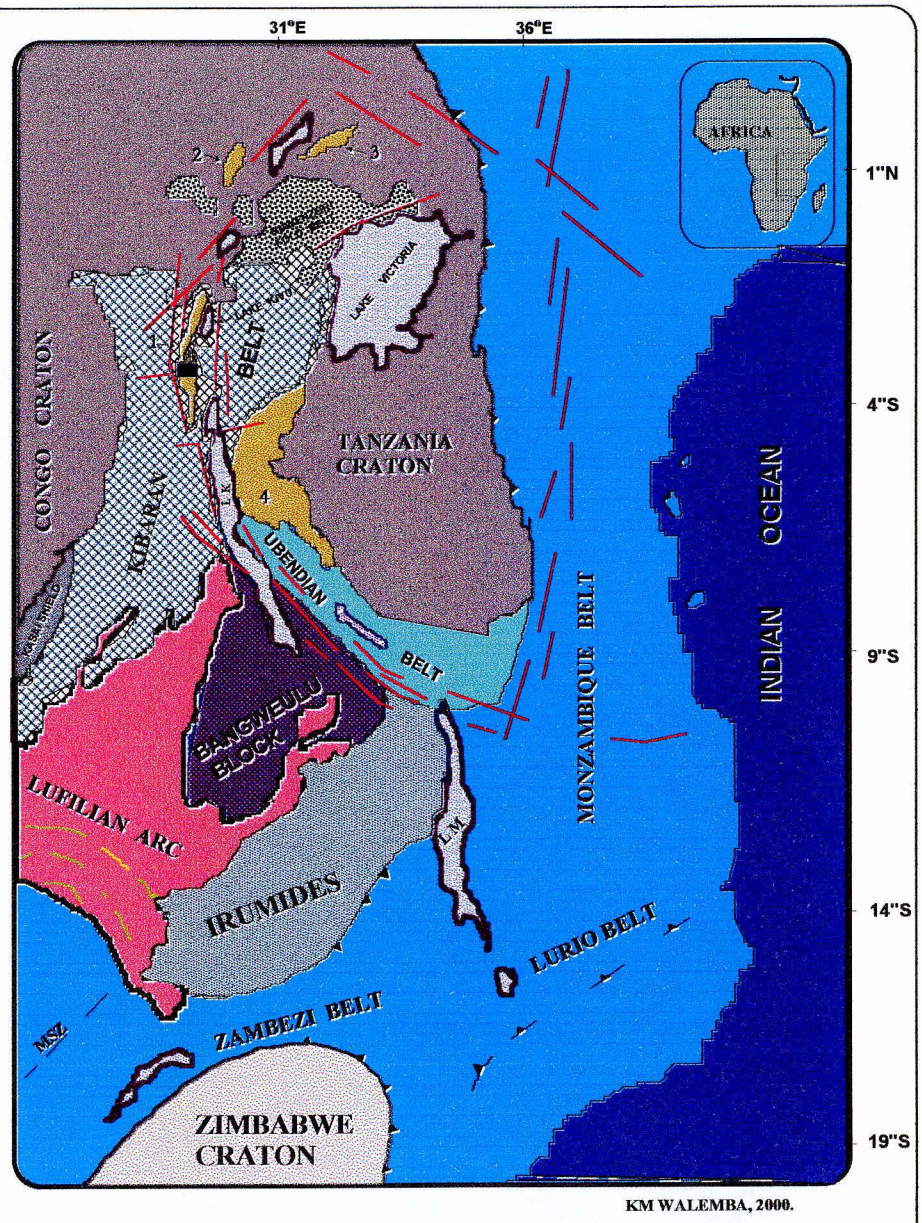
The details relative to these different laboratory studies are listed in appendices.

1.3.- HISTORICAL REVIEW AND PREVIOUS WORK.

The Kivu region has been an established gold producing region for centuries. During the past fifteen years or so, small-scale gold mining has been reactivated, largely as a result of the promulgation of the 1982 act; liberalizing artisanal gold exploitation in the DRC. Presently, over a thousand small-scale miners are actively engaged in gold extraction operations in the overall region of Kivu, principally from four sources (Fig. I.3) :

*- Alluvial gravel workings along the active rivers and their tributaries;
*- Gravel terraces along the rivers;
*- Eluvial material adjacent to gold quartz-veins and veinlets;
*- Gold from pits and trenches on quartz and /or sulphides veins, stockworks and breccia zones.

The alluvial gold is recovered by panning or washing the mined alluvium in locally made sluice boxes. Gold in quartz-veins is recovered by amalgamation using mercury or by crushing and pulverization in wooden or steel mortar. The output of artisanal exploitation is estimated at over a thousand kg per year of gold. (Walemba ,K.M.,1994; Palmer,G.L.and Moncur, J.C.,1994). Fig. I.3. show artisanal workers in the Shabunda region.



Scale : 1 : 12 500 000

Fig. I.1 :-
Structural setting of Archean cratons and Proterozoic mobile belts in Central and Eastern Africa showing the Itombwe Supergroup and the Kadubu study area. (Compiled from Cahen et al., 1984, Daly,1986; Pohl, 1994 ; Ring et al., 1997 ; with addition). L M : Lake Malawi MSZ : Mwembeshi shear zone. 1: Itombwe basin; 2 : Bunyoro basin; 3: Irumu basin; 4 : Bukomba - Malagarasia. L K : Lake Tanganyika.
■ :- The Kadubu study area. —— Major faults of the rift valleys.



Kadubu river

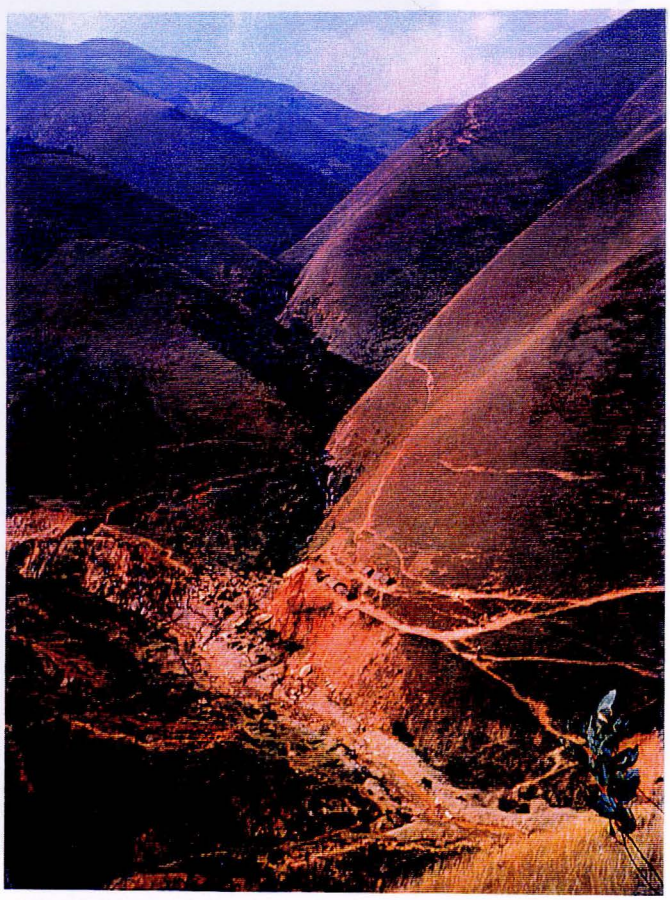


Fig.I.2 : Topographical expression of the study area: mountainous with deeply incised valleys and alpine grassland .

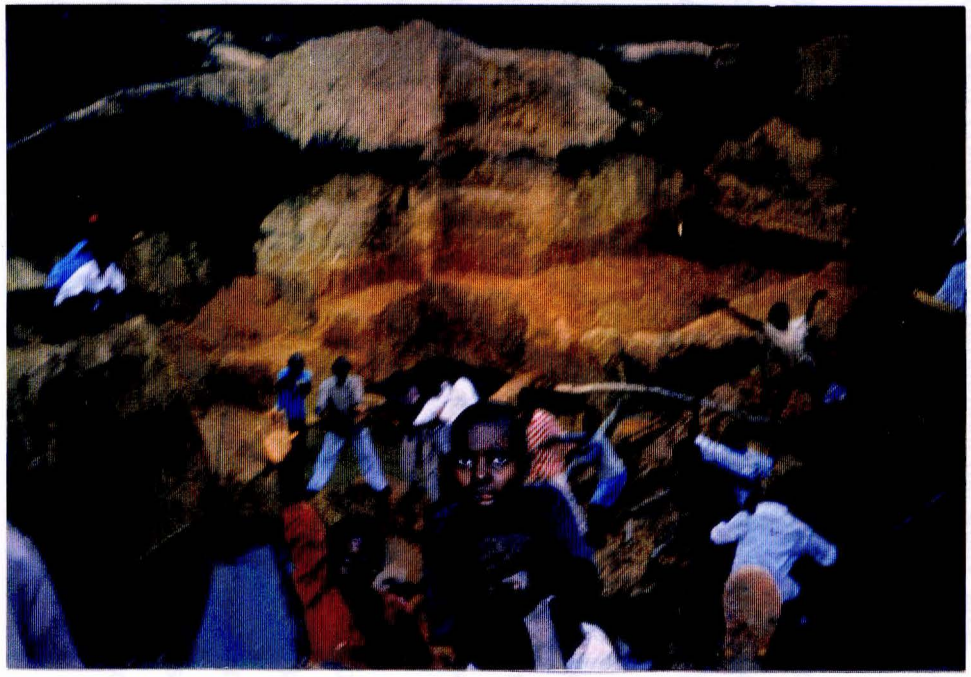


Fig.I.3:- -Artisanal workers in the Shabunda region. Ulindi alluvial gravel.

Detailed geological mapping was undertaken along selected traverses and lithology and sedimentary structures were documented. In addition, traverses were undertaken along well-exposed stream sections of the Kadubu, Monana and Kilungutwe rivers in order to facilitate measurement of stratigraphic successions. Important additional informations of large scale structures and stratigraphic boundaries have been obtained from aerial photographs supported by Landsat imagery (bands 4,5 and 7 colour composite) and aeromagnetic data.
A large number of structural data were collected in the field in order to understand the structural evolution of the area and associated stress regime. Selected samples from different stratigraphic horizons were collected from throughout the study area.

Good outcrops occur in most parts of the study area, specially along the Nya-Kaziba - Kitwabaluzi road. This road being almost perpendicular to the major trend of the Kadubu area, (N-S trending structure), was investigated as a matter of priority. Alluvium and soil covered areas yielded few exposures and are poorly understood.(Fig.I.1, Fig.I.2, Fig.II.2).

The second field season's work was focused largely within the mineralized zones, particularly the Twangiza and Tshondo gold deposits.Detailed observations and measurements of structural features were carried out on surface and in underground working on quartz /sulphide vein, in competent albitite and in black shale.
Representative oriented rock specimens were collected for mineralogical investigations and geochemical studies. Small-scale structural data were also accumulated and interpreted to elucidate the tectonic history of the mineralized zones and the structural controls to gold mineralization. More than 15 geological and structural maps for the Kadubu area and Twangiza and Kashwa deposits were compiled in the course of this study. Among the more important ones are the following :

*- Geological and structural map of the Kadubu area ,
*- Structural and tectonic lineament map of the study area ,
*- Generalised magnetic field interpretation map of the Kadubu area ,
*- Geological and structural map of the Twangiza Region ,
*- Gold isochon maps of the Twangiza deposit.

For many of these deposits, no research has previously been done. For some deposits certain detailed studies as well as regional syntheses are dated before 1954, and need re- evaluation. Some local observations have been made on the gold deposits and the scope of these studies and their conclusions are listed below:

*- De laVallee Poussin.,1933; described the spatial relationship between gold mineralization and the two granitoid intrusions (G3 and G4), recognized in the Kivu region ;

*-Goffard.G., 1933 ; pointed out the fact that, in many cases , gold is closely linked to the basic rocks such as gabbro and diorite ,and controlled by brittle tectonics of the region;

*- Van Aubel.,1934a and 1934b ; investigated the area located between $27^0$40'-28^0 50' E and 2^0 30' - 2^0 40' S . He compiled a detailed section of the stratigraphic succession of this area and the sequence of igneous rock intrusions related to gold mineralization. He noted that the alignement of auriferous veins, the great basic dykes and a fault zone demarcated by thermal springs, are parallel to and follow the general orientation of the Kibaran belt. Gold quartz-vein lodes predominate in the Kivu gold metallogenic province;

*- Van Aubel .,1936; postulated the paragenetic association of gold and tin mineralization;

*.- Blaise.F., 1934 ; investigated the relationship between the tectonics and mineralization (Au, Sn), in the area located at (1^0 40' - 2^0 00' S ; 28^0 30'- 29^0 00' E) ;

*- Passau, .G., 1945 ; studied alluvial gold-silver mineralization in the Lubero region (roughly, $28^0$15'-$28^0$30'E ; $0^0$15'N-$0^0$15'S) and linked the genesis of gold- silver mineralization to the granodiorite intruded in this region ;

*- Bethune.P. and Borgniez.G.,1950 ; studied respectively the gold deposit of the Lubongola area in the Shabunda region and the Mobale gold-deposit in the Kamituga region. These two deposits are quartz-veins type and have been mined previously.

*- Polinard, E., 1954; undertook a synthesis of gold mineralization in Central Africa and concluded that most concentrations of gold are linked to the quartz-veins and were genetically hydrothermal .

CHAPTER 2 .- GEOLOGICAL FRAMEWORK.

2.1.- INTRODUCTION.

In the Kivu region, two fold chains have been recognized : The Kibaran belt and the Itombwe Synclinorium Supergroup (Boutakoff, 1939; Cahen , 1954; 1978a; 1979; Cahen et al., 1979; 1984; Villeneuve, 1976; 1976a; 1977)(Fig.I.1).

The existence of the "Rusizian belt " has been for a long time a matter of debate. The Rusizian belt was considered by previous workers as an extension of the Ubendian belt into the north Kivu area from northern Malawi, through Zambia and southwestern Tanzania in a general NW-SE direction. (Boutakoff,1939; Van Aubel,1934a; Cahen,1954; Cahen et al.,1970a; Lepersonne,1974; Cahen et al.,1984; Lavreau,1985; Daly.,1986; Daly. ,1988 ; Klerkx, J.,1988; Theunissen, 1989; Ring, 1993; Ring et al.,1997). However, the real status of " Rusizian " basement is very badly known and nothing is known on lithology or structural characteristics. Rusizian attributed rocks by previous workers (Cahen, 1967) have been after considered as part of migmatic gneisses occurring in Kibaran belt (Theunissen, 1989).

A common problem in regions of superimposed orogenes is the unravelling of the tectonic characteristics of the earliest orogeny.

In the Kivu region; Central Africa, very little recent work has been carried out and with the present state of knowledge, the overall situation of these two Supergroups can be summarised as follows :

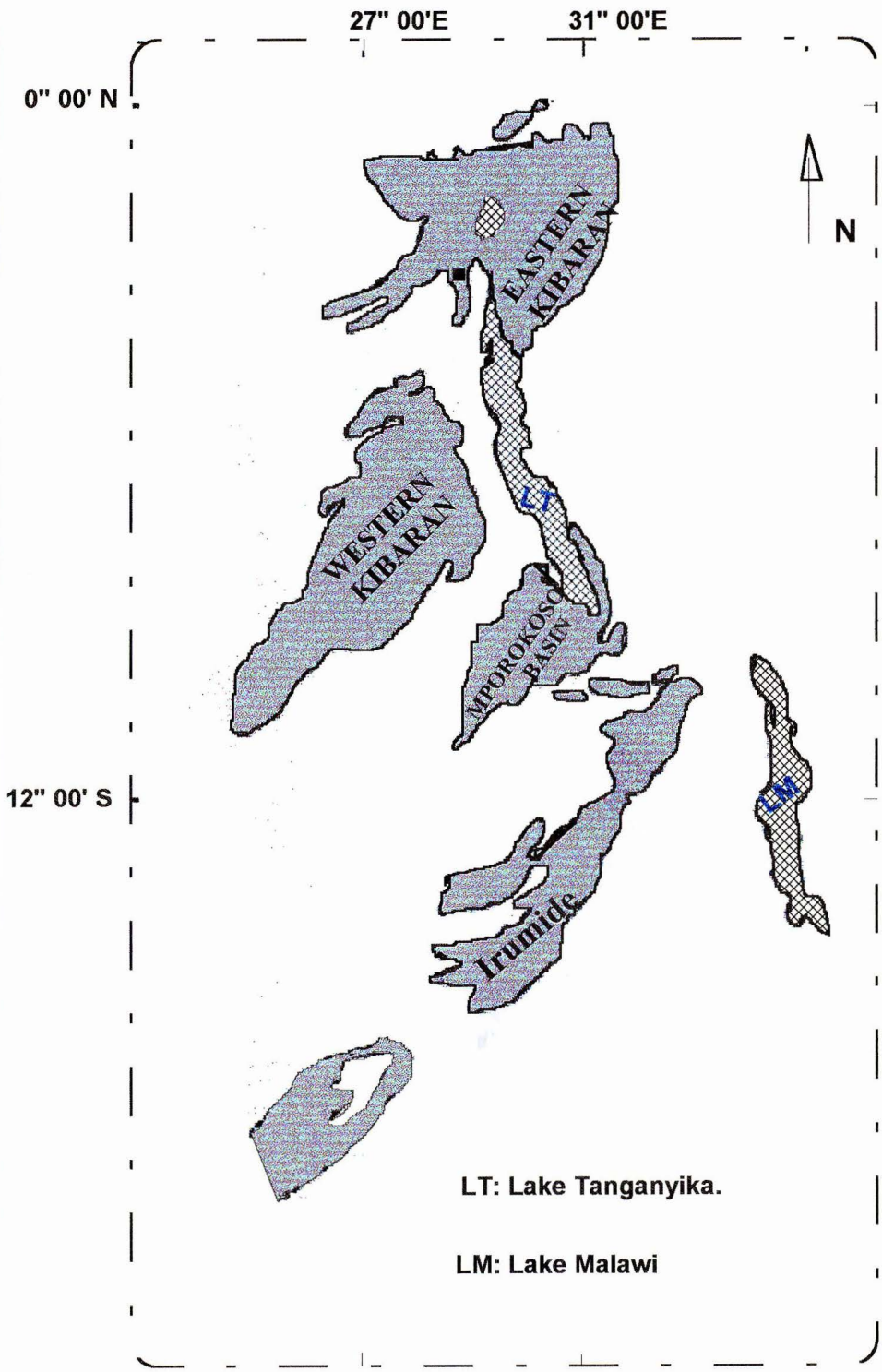
2.2.- THE KIBARAN BELT OF CENTRAL AFRICA. (*ca 1400- 900 Ma*).

2.2.1.- INTRODUCTION.

The Kibaran linear belt is situated along the eastern edge of the Congo craton and stabilized at ca.2Ga.(Fig.,I.1;Fig.,I.4). Formerly, four different names were used for the same chain independently in each region: Kibaran in Katanga /DRC (Robert,1931); Burundian in Kivu / DRC, Burundi and Rwanda (Delhaye and Salle,1928): Muva-Ankole in Tanzania (Kigoma conference of African Geological survey, 1931); and Karagwe- Ankolean in Uganda (Combe, 1926).

Fig.I.4.- Location of the Kadubu study area within a sketch map of the Kibaran basins . (After Klerkx, J., 1988 with additions).

■ The Kadubu study area.



It extends almost continuously from the Katanga province in southern DRC , with the type area being in the Kibaran mountains and Lubudi valley; through southwestern Uganda (Ankole), Eastern DRC (Kivu), Burundi, Rwanda and northwestern Tanzania (Karagwe). Its overall length is nearly 1700 km, and it attains a width of up 500Km .Two thirds of the belt are located in the DRC, including the type locality of the Kibaran mountains.

Folded Lufilian arc rocks occur to the southeast of the Kibaran belt with the Kasai shield being the foreland of the belt. (Fig.I.1).

The belt is the northwesternmost of a series of Mesoproterozoics belts, forming roughly parallel domains in eastern or southern Africa (Irumide belt, Malawi-Mozambique or Lurio belt, Namaqua - Natal belts) to which " Kibaran " (sensu - lato) name and ages have been assigned.(*ca. 2050 - 976 Ma*,Cahen et al.,1984 ; *ca.1400 900 Ma.*,Pohl,1994 ;*1600 -1000 Ma.*,Thomas et al.,1989) (Fig,I.1; Fig,I.4.)

The Kibaran events were also recorded from southernmost Mozambique (Sacchi et al.,1984; Daly.,1986; Key et al.,1989; Pinna et al.,1993), Namibia (Hoal et al.,1989), Angola (Carvalho et al.,1987), Nigeria (Grant et al.,1972; Ekwueme and Caen,1989); and Brazil (Porada,1979). The correlation of the Kibaran segments from western, central and southern Africa and Brazil would represent an important stage for the integration of Africa into the Rodinia Supercontinent

2.2.2.- LITHOSTRATIGRAPHY.

In all areas of the Kibaran, a three-fold lithostratigraphic division, with lateral and vertical changes, is recognized: Lower Group, Middle-Group and Upper Group (Cahen et al.,1984; Caron et al.,1986 ; Pohl.,1994).

The Lower group (1200-5100 m) is composed of a basal conglomerate and dark, laminated pelitic sedimentary rocks with intercalations of siltstones, sandstones, mature quartzites, and tuff. Some of these successions are of turbiditic origin. Dolerite intrusives are also present.

The Middle group (1000-2600m) is reddish to purple in color, and more arenaceous with minor basaltic and dacitic volcanic rocks.

The Upper group (>1500m) consits of immature clastic sediments with a basal polymictic coarse conglomerate, ferruginous quartzite, siltstone and shale. It occurs in major syclinoria structures only.

2.2.3.- STRUCTURE AND METAMORPHISM.

Structurally, four periods of deformation are recognised within the Kibaran belt (Cahen et al,1984, Pohl, 1992;1994) :

*.- D1 : This takes the form of an S1 schistosity parallel to bedding, with associated minor often isoclinal D1 folds, and thrusts related to the synkinematic emplacement of the granite plutons.

*.- D2 : NW-SE trending folds D2 and an S2 axial planar cleavage. This was the climax of Kibaran deformation which induced the main structural features of the Kibaran belt.

*.- D'2 : NW-SE oriented shearing, subparallel to the major folds, closed the D2 folding and thrusting events.

*.- D3 : N-S axes cutting D2-folds at sharp angles, formed during renewed upright folding. Outcrop patterns created by fold interference occur.

*.- D4: Shear folding and cataclastic deformation affecting alkaline and carbonatitic intrusions. Shortening across the belt was probably less than 50%.

Generally, Kibaran metasediments are of very low grade, except around the granitic intrusions where high grade metamorphism (amphibolite facies, high-T/low-P type, with andalusite and staurolite in the metapelites) appears and migmatites may occur.

The tectono-metamorphic events; M1-D1, and M2-D2 have been recognised as the main phases.

2.2.4.- MAGMATISM, GEOCHRONOLOGY AND METALLOGENY.

Four types of granites (G1,G2,G3,G4), are distinguished as a result of the field and petrographical observations, supported by Rb/Sr and U/Pb age data (Boutakoff,1939; Gerards and Ledent., 1970;1976; Cahen et al.,1984; Klerkx et al.,1984, Lavreau,1984; Fernandez-Alonso et al., 1986; Tack et al.,1994) :

The two first, G1 and G2, are syn-orogenic and dated respectively; G1: ca 1370 +/- 25Ma,G2: ca 1310 +/- 25Ma. G1 is a porphyritic gneissose two-mica or biotite adamellite with low initial Sr- ratio whereas G2 is a non- porphyritic peraluminous adamellitic orthogneiss.

The two last , G3 and G4 , are post-orogenic, accompanied by abundant pegmatites and dated respectively ; G3: ca 1094 +/-50Ma, G4: ca 976 +/-10Ma. G3 is an alkaline biotite granite, rift related in origin whereas G4 or "tin granite " is accompanied by abundant pegmatites and veins containing Au, Sn, W, Nb, Ta, Be, Cu, Pb, phosphate, tourmaline and U mineralization.

" Tin granites" are leucocratic, equigranular "aplitic"or pegmatitic, sub-alkaline,strongly peraluminous, often cataclastic , locally sheared , and clearly crosscutting , with an average initial Sr ratio of 0.7721 (Fernandez-Alonso el al.,1986; Tack el al.,1994). Petrographically, tin granite consists of quartz, microcline, albite, and muscovite (biotite), with accessory apatite, zircon and tourmaline.

Kibaran granitoids occur frequently in anticlinorial or tectonically elevated structures. A strong structural control of both intrusion sites of the tin granites and the mineralization related to a compressive phase has been documented.(Fernandez-Alonso el al.,1986).

Three types of base-metal mineralization related to the geological evolution of the Kibaran have been distinguished (Tissot et al.,1982; Pohl,1992, Gosse,1992) :

1*- Mineralization associated with the 1275 Ma mafic layered intrusions.

Mafic / ultramafic bodies (e.g, Kabanga/Tanzania - Musongati/ Burundi) may contains Ni-(Cu, Co)- Fe, V, Ti, Au, PGM and sulphide mineralization.

2*- Mineralization associated with the tin granites.

This is the most important type with four subgroups of the G4 tin granite -associated mineralization (Varlamoff, 1975, Baudin et al., 1984):

2.1.- Pegmatites with Sn, Nb/Ta (Li, Be, U/Th).

2.2.- Quartz-veins with Sn, W (Au, U, Bi, pyrite, siderite).

2.3.- Talc deposits developed by hydrothermal alteration of dolomites and /or mafic magmatic rocks .

2.4.- Auriferous silicification zones, quartz-veins and breccias, with native Au, pyrite, arsenopyrite, (magnetite, specularite and PGM).

3*- Mineralization related to alkaline complexes and carbonatites.

Post-Kibaran deposits associated with the Neoproterozoic; Pan-African (700- 500Ma) intrusive activity related to crustal extension and to magmas of sub-crustal derivation, in a consolidated cratonic setting.

2.2.5.- POST-OROGENIC EVENTS.

The end of the Kibaran belt is marked by the Lufilian – Zambezi orogeny (950 – 800 Ma). Later events include the formation of the Itombwe supergroup (900- 500 Ma?), the intrusion of alkaline complexes (700-500Ma) and carbonatites (ca. 500Ma), the Pan African resetting of mineral ages (600 - 500Ma), and the formation of the East African rift system (Cainozoic-0 Ma).

2.2.6.- " PAN-AFRICAN " EVENT.

The " Pan -African " episode refers to polyphase tectonometamorphic events that occurred between 800 and 400 Ma within Gondwana. There appear to be at least two separate tectonic events within Central and East Africa that were previously ascribed to a rather ill-defined " Pan - African " event .

The *East African Orogen (800-650 Ma)* which represents a separate tectonic event within the Pan -African of Central Gondwana(Stern ,1994) and a later collision ; *Kuunga Orogen* which ocurred at around *550 Ma* between Australo- Antarctica and Congo - ANS (Arabian - Nubian - Shield) - IMSLEK (India, Madagascar, Sri Lanka, a strip of the East Antarctic Craton including Enderby Land and Dronning Maud land , and the Kalahari Craton) and represents the final suturing of the Gondwana continent (Meert et al., 1995). (Fig. I.5a, Fig. I.5b, Fig. I.5c, Fig. I.6a, Fig. I.6b).
Recent paleomagnetic data suggest that the Congo craton may not have been part of the supercontinent Rodinia in the configuration envisioned by Dalziel (1992), (Meert et al., 1995).

The Rodinia configuration, as proposed by Dalziel (1992) and Stern (1994) is considered valid for the time period from *1100 to 750 Ma*. By *750 Ma*, evidence for rifting within Rodinia suggests that the supercontinent is beginning to break apart. The beakup of Rodinia is synchronous with the assembly of Gondwana although the sequence and timing of events leading to the final assembly of Gondwana are debated. { Burke and Dewey, (1972), Sacchi et al., (1984), Daly (1986, 1988), Porada, (1989), Key et al.,(1989), Dalziel (1992), Kroner, (1993), Stern (1994), Meert and Van der Voo (1994) }.

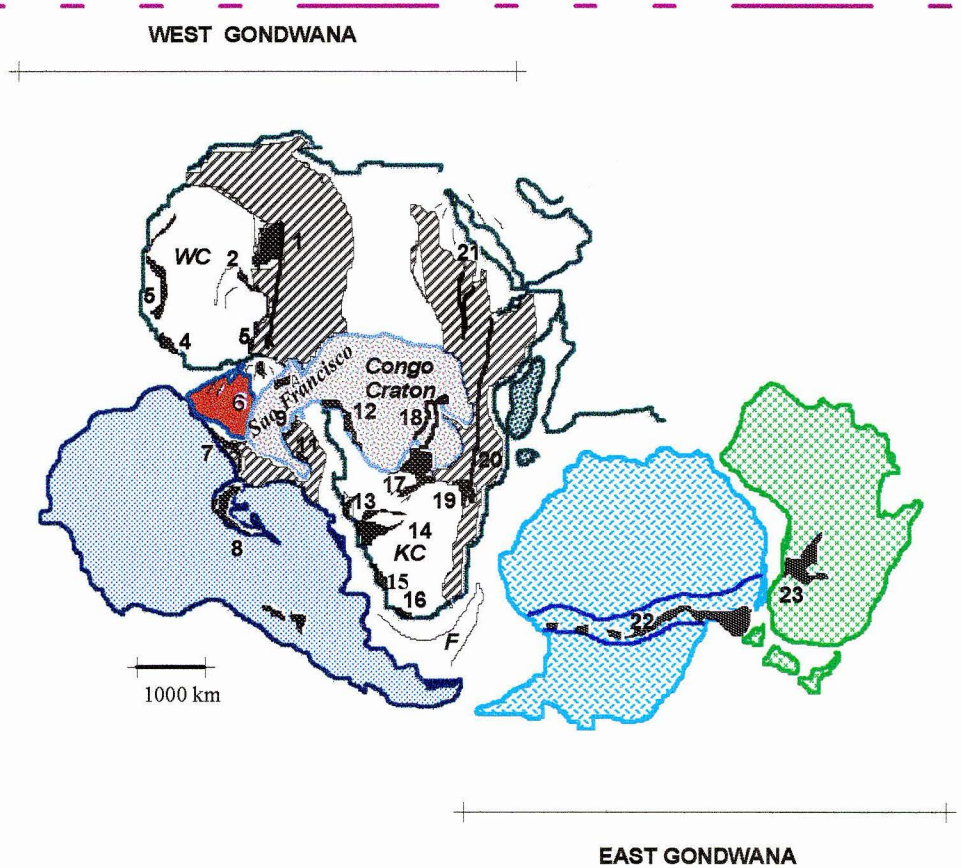


Fig.I.5a :- Configuration of the upper Proterozoic Pan - African belt system with extension into South America, Antarctica and Australia on pre-drift reassembly of the Gondwana continent (modified after Porada ,1989)

Black = Upper Proterozoic " geosyclinal" deposits.
Dotted = Upper Proterozoic Aulacogen deposits.
Hatching = areas of Upper Proterozoic to Lower Palaeozoic tectono- thermal basement rejuvenation.
WC = West African Craton; KC = Kalahari Craton ; F = Falkland plateau ;
1 = Pharusian belt ; 2 = Gourma Aulacogen ; 3 = Dahomeyan belt ; 4 = Rokelide belt ;
5 = Mauritanide belt (party Hercynian); 6 = Northeastern fold belt (Borborema province) ;
7 = Araguaia belt ; 8 = Paraguay belt ; 9 = Sierra Pampeanas ; 10 = Ribeira belt ;
11 = Mantiqueira belt ; 12 = West Congolian belt ; 13 = Kaoka belt ; 14 = Damara belt ;
15 = Gariep belt ; 16 = Saldania belt ; 17 = Lufilian Arc ; 18 = Katanga Aulacogen ;
19 = Zambezi belt ; 20 = Mozambique belt; 21 = Red sea fold belt ; 22 = Transantarctic belt ;
23 = Adelaide belt. (after Porada, 1989, with additions).

KMA Walemba, 2000

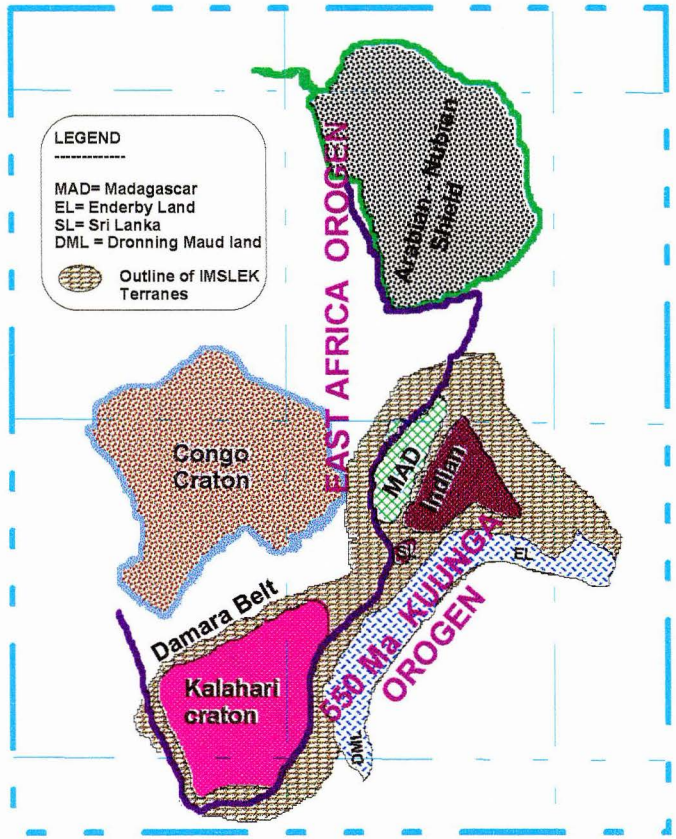


Fig.I.5b

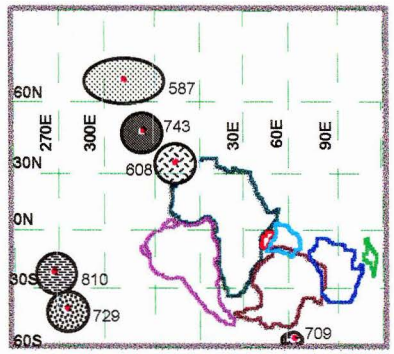


Fig.I.5C

LEGEND
- Congo craton poles.
- West African Craton poles.
- Australian poles.
- Rio Plata Craton poles.
- Indian poles.
- Arabian - Nubian shield pole.

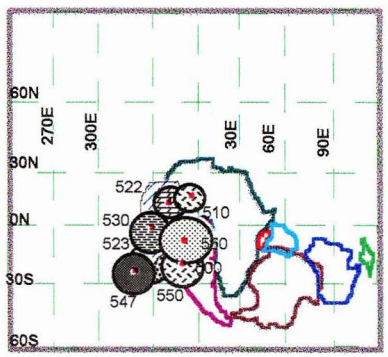


Fig.I.5d

Gondwana Path
550 - 510 Ma

Fig.I.5b:- Outline of the IMSLEK terranes that collide with the Congo Craton and Arabian - Numbian Shield (ANS) to form the Mozambique Belt between 800 - and 650 Ma . This collision is followed 100 - 250 m.y later (550 Ma) by the collision of Australia - Antarctica with IMSLEK - Congo - Arabian / Nubian shield during the Kuunga Orogeny with possible sutures now exposed in Sri Lanka and East Antarctica. (After Meert et al., 1995).

Fig.I.5c and Fig.I.5d:- Gondwana paleomagnetic poles in the ages range 810 - 585 Ma rotated to the Gondwana configuration of De Wit et al ., (1988) with the African poles fixed . Gondwana paleomagnetic poles (south poles) for the interval 550 - 510 Ma rotated to Africa coordinates. (After Meert et al., 1995).

KMA Walemba, 2000

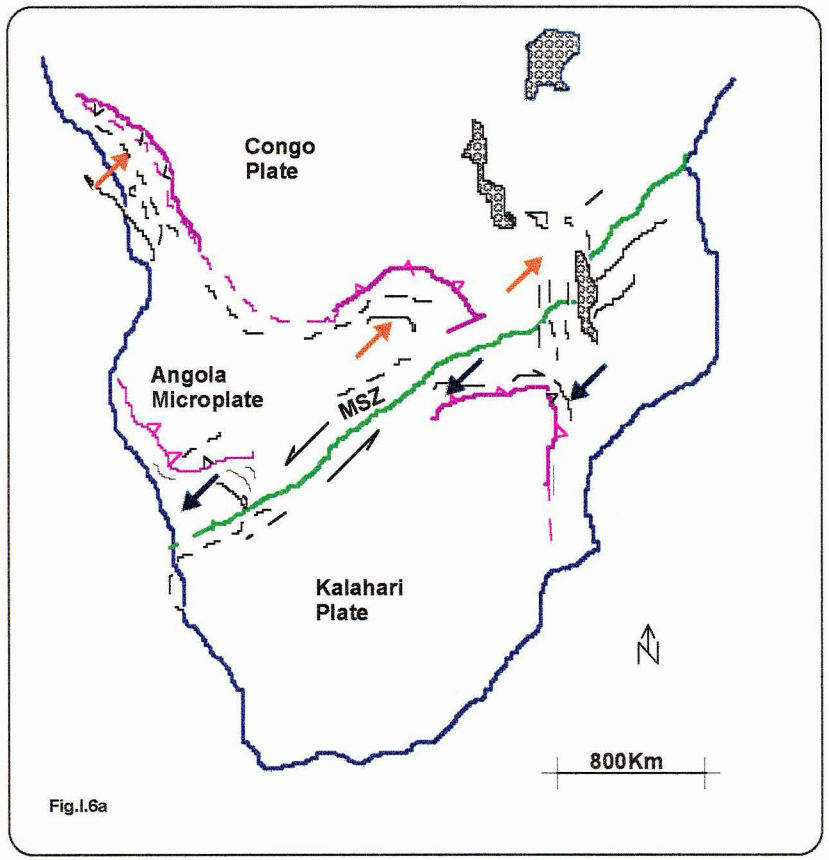


Fig.I.6a

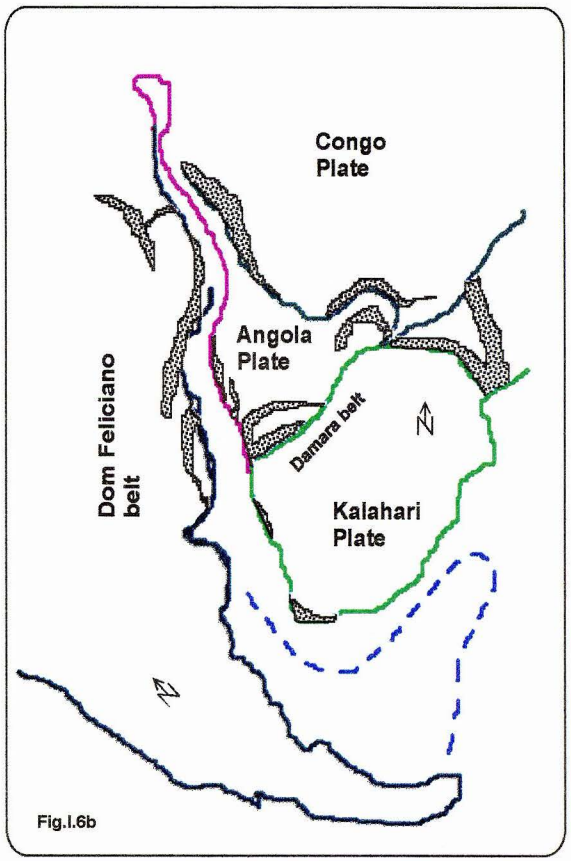


Fig.I.6b

Fig.I.6a :- Sketch map showing the Late Proterozoic tectonic setting of Central Africa .
This comprises a pair of opposed thrust belts separated by the continent scale Mwembeshi shear zone (MSZ).
(After Daly, 1989).

Fig.I.6b :- Approximate position of Pan African rift sequences in southern Africa and South America (Modified after Porada,1989).
Note that an Angola plate is distinguished from the Congo plate with the West Congolian and the Lufilian belts separating them .
(after Frimmel, H.E and Frank, W. 1998).

Conventionaly, the assembly of Gondwana is perceived as a large-scale collision between West (Africa and South America) and East (India, Antarctica and Australia) Gondwana along the Monzambique orogenic belt.
More recent Proterozoic plate models treat West Gondwana as a series of distinct cratonic blocks assembled during a sequence of orogenic events spanning *200Ma (680-480 Ma)* and East Gondwana as a coherent unit from at least *1300 Ma* until its beak -up in the Mesozoic (Torsvik et al., 1996).

However, Meert and Van der Voo (1995) and Wilson et al., (1995) propose that East Gondwana was assembled through polyphase accretion of cratonic blocks between *770* and *550Ma.*

Collision of East Gondwana with the African plate and intraplate closure of the West Congolian belt, Lufilian Arc, and Zambezi belt, ocurred during the Pan African event, followed by continental collision.
With proceeding convergence and collision along the successively closing Proto-South Atlantic Ocean, strike-slip faulting and local cross-folding and thrusting occurred in the older belts. (Porada, 1979,1989), (Fig.I.1 ; Fig.I.5a ; Fig.I.5b, Fig.I.5c; Fig.I.6a; Fig.I.6b).

Sacchi et al.,(1984) and Daly (1986, 1988) identified structures in the south Mozambiquan belt and in the Irumide belt, respectively, which they have interpreted as representing continent-continent collision sutures. The sutures which lie far SE of the present study area, were the result of continent-continent collision in which the relative plate motions were in an approximatelly NW-SE direction. This event which took place during mid-to late Kibaran, seems to have generated considerable compresssional stress which affected the entire region extending up to and possibly beyond the NE of DRC.

In the northen part of the Mozambique orogenic belt, there was a second period of uplift and major erosion. At ~ 620 Ma, intra-cratonic (post-collision), strike-slip vertical structures roughly parallel to the N –S orogenic strike were generated (Key et al., 1989). Tectonism lasted until ~ 530Ma, with open folding, brittle shearing and related minor intrusives.

Oblique collision occurred at some time prior to ~ *620Ma* between a western Tanzanian craton and an eastern Kibaran plate (Key et al.,1989). The relationships among individual Upper Proterozoic Pan African belt systems are far from being well understood.

Subsequent uplift and cooling extended beyond the orogen into the western foreland to give regional mineral ages of ~ *480 Ma* (Cahen et al.,1984).

The Pan – African thermal event resulted in the widespread resseting of K -Ar ages *at ~ 500 – 450 Ma* (Daly, 1986).

2.2.7.- MODELS FOR THE GEODYNAMIC EVOLUTION OF THE KIBARAN BELT.

Various aspects of the evolution of the Kibaran belt including fundamental geology and metallogeny are still under debate. More field and especially laboratory studies are needed in order to constrain the evolution of the entire Kibaran belt.

Previous geodynamic models for the belt include: The " syncollisional " model of Kampunzu et al., 1986; the " decollement " model of Klerkx et al.,1987, Pohl.,1997; the " collapse " model of Tack et al.,1994 and the "extensional detachment " model of Fernandez – Alonso and Theunissen.,1998. (Table.I.1). All these models need re-evaluation as the constraining field and supporting petrographic and geochemical evidences are still poorly documented .

Some outstanding problems include (Tack., 1997) :

1.- The time problem:

Ca.1400 -950 Ma, spanning more than 400 Ma, is a very long time period of evolution, if the belt is to be modelled in terms of conventional plate tectonic processes.

Tack et al., 1995, suggest that the term " Kibaran " should be restricted to the period ca. 1500-1200 Ma and the term " Grenvillian " to the orogenic period ca. 1200 – 1000Ma .

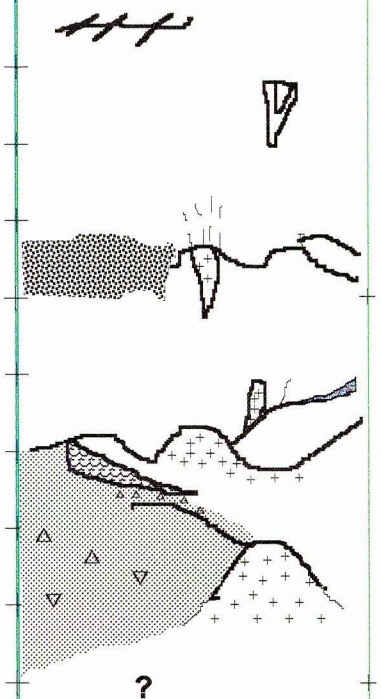
2.- The space problem:

In the vast area underlain by Kibaran rocks, particularly in the DRC segment, much research in the fields of systematic geological mapping, detailed structural analysis , geophysical data and geochemical studies remain to be undertaken.

3.- The terminology problem :

The chronostratigraphic term " Mesoproterozoic " (1.6 – 1.0 Ga) is often misused as a synonym for the orogenic term " Kibaran " A need for an appropriate (re) definition of the Kibaran event in Africa, within the Mesoproterozoic era is stressed.

Table I.1:- Kibaran evolution in Central Africa after Pohl, 1997 (Data from Cahen et al., 1984; Klerkx et al., 1984; Lavreau, 1984 ; Theunissen, 1984).



Ma	LITHOLOGY	DEFORMATION	METAMORPHISM	MAGMATIC ROCKS
500			Resetting of mineral ages. ~ 550 Ma	
		D4- Shear folding. cataclasis ~ 680 Ma		
	" Molasse " Itombwe Clastics (DRC) Bukoban sandstones (Tanzania)			o Syenite etc
			Local contact →	o G4 - Tin granites 977 +/-13Ma Ri = 0.7721
1000		D3- N-S folds, thrusts. ~ 950 Ma		o G3 - Subalkalic, biotite
			Local contact →	o Ultramafic / mafic intrusions
		D2:- Strike - slip shearing		o G2 Biotite granite
		D2:- Upright folds - S2 NE or NW . ~ 1100 Ma	M2:- very low , thermal aureoles	
	Pre-D2 :- 10000m			
	Metapelites, Sandstones, Quartzites, grits, Conglomerates, Rare carbonates and silicified stromatolites	D1:- Schistosity S1 // So Thrusting. 1250-1200 Ma	M1:- Very low to greenschist (amphibolite) facies.	o G1b - Biot/Musc granitoids o G1a - Biotite granitoids o Rhyodacites 1353+/-44 and basic volcanics inter-stratified with sediments.
1500	Basement : Granites, metamorphics Ubendian, Buganda- Toro, Archean			

2.3.- ITOMBWE SYNCLINORIUM SUPERGROUP (*ca 976 – 575 Ma , this study*).

2.3.1.-INTRODUCTION.

The Itombwe Supergroup is one of a series of basins (troughs) located in Central Africa and situated between major tectonic lineanments. Other basins include: Bunyoro, Irumu, Bukoban-Malagarasian (Fig.I.1).

Early workers (Lhoest, 1946; Peeters, 1951; Agassiz, 1954) linked the Itombwe supergroup to the Kibaran system, but recent studies has interpreted the Itombwe as an intra- mountainous molasse basin (trough), of post-Kibaran age (Cahen et al.,1984, Pohl, 1994), or a Rift basin (Villeneuve,1983).

The present study area; (Kadubu), which forms a part of the Itombwe synclinorium, represents the first area to be investigated in detailed using modern techniques, from systematic geological mapping to ore genesis through structural, tectonic, petrographic, geochronological and geochemical analysis.(Fig.I.7).

2.3.2.- PREVIOUS WORK.

With a north-south trending structure, the Itombwe synclinorium , was first described by Lhoest (1946) and has been thought by all early workers to belong to the Kibaran system. (Lhoest., 1946,. 1964 ; Agassiz, 1954 ; Peeters., 1951, 1952 , 1954, 1955,1956 ; Pasteel., 1961 ; Bles., 1972). The recent studies by Lepersonne (1971), Villeneuve (1976a;1976b; 1977;1978a;1979), Lavreau, (1977a) and Chorowitz and Mukonki,(1980),on the basis of one-off studies and Landsat imagery, link the Itombwe Supergroup to the Neoproterozoic, post-Kibaran.

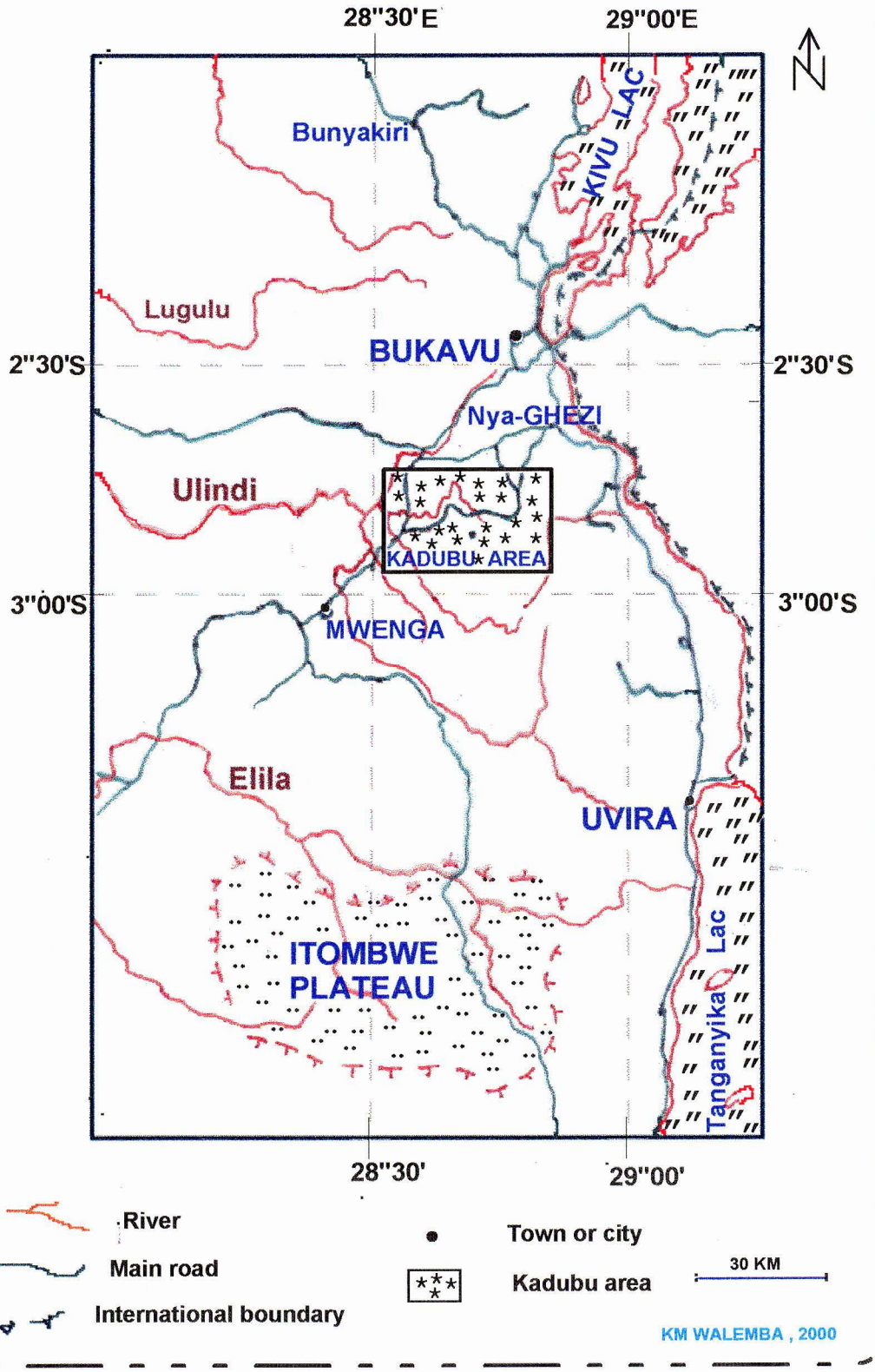
Studies undertaken by the above authors and their conclusions include the following :

*- Lhoest has constructed a cross-section along $4^0$00'S, in the extreme south.

*- Peeters, (op.cit) has constructed some cross-sections between $3^0$00'S – 4^0 00'S.

*- Villeneuve (op.cit), has mapped the northeastern part of the basin along the western bank of lake Kivu to the foot of Mount Kahozi, (2^0 23'S , $28^0$31'E).

Fig.I.7:- Locality map of the Itombwe plateau and location of the Kadubu study area.



*- Lavreau (op.cit) , on the basis of Landsat imagery and the previous studies, developed the notion of overall structural continuity of the Itombwe Synclinorium from south (3^0 40'S – $4^0$00'S) to north ($1^0$20'S – 1^0 25'S).

*- Cahen et al.,1984, extended this Itombwe structure to the south ($5^0$40'S).

*.- Sorotchinsky,1952, made the first petrographic study of albitite rocks within the Kadubu area.

*.- On the basis of the age dating of G 4, granite, Cahen et al., 1979, gave an approximate age to the Itombwe synclinorium Supergroup of between 1310 – 648 Ma, the age of D2 Kibaran deformation and shearfolding.

2.3.3.- REGIONAL GEOLOGICAL SETTING.

The Itombwe supergroup is subdivided into two lithostratigraphic groups: The lower Kadubu group and the Upper Kadubu group. These terrains rest unconformably upon more metamorphosed formations (gneiss, micaschist and quartzite) ascribed to the Kibaran belt in the south. In the northern part, the Itombwe supergroup is underlain by Kibaran metasedimentary formations.

The Itombwe synclinorium has not been the focus of any recent systematic geological mapping and geochemical studies applying modern techniques.

The Itombwe synclinorium has been interpreted as an intra- mountainous molasse basin (trough), of post-Kibaran age (Cahen et al.,1984, Pohl, 1994), or a Rift basin (Villeneuve,1983) .

Klerkx el al., (1998) point out that different Meso-and Neoproterozoic sedimentary basins have been developed along the ductile shear belt as a result of repeated sinistral wrench fault reactivation.

Dating of these Synclinoria is still a matter of debate. A Neoproterozoic (Pan – African) age (1310 – 648 Ma) was attributed to the Itombwe supergroup by Cahen et al.,1979, who used only photogeological mapping and geological cross sections based on correlations with lithologies observed hundreds of kilometres away. No geochronological studies have been undertaken to resolve this uncertainty.

The present study area; (Kadubu), which forms a part of the Itombwe synclinorium, represents the first area to be investigated in detail using modern techniques, from systematic geological mapping to ore genesis through structural, tectonic, petrographic, geochronological and geochemical analysis.

2.4- TECTONICS, RIFTING AND MAGMATIC PROCESSES IN THE WESTERN BRANCH OF THE EAST AFRICAN RIFT SYSTEM.

2.4.1.- INTRODUCTION.

The Phanerozoic evolution of the African plate, stabilised at the end of the Pan -African tectono-thermal event (ca. 600 – 500 Ma ago), and has been characterized by more recent diachronous uplift and /or rifting and magmatism. The spatial setting of the main Phanerozoic rifts in Central Africa and some associated magmatism are shown in Fig. I.8 and Fig. I.9. Phanerozoic rift basin evolution in Africa has been influenced by the pre-existing basement structure inherited from Precambrian tectonics (Daly et al.,1989). No orogenic phenomenon has affected the Western Branch of the East African Rift System (WBEARS) for the past 500Ma or so.

The 2000-km – long WBEARS has an overall sigmoidal shape and is segmented along its length into individual, asymmetric basins, many of which contain lakes, (Malawi, Rukwa, Tanganyika, Kivu, Edward, Albert). Three segments are distinguished: north, centre and south. (Fig.,I.9).

The north includes the lakes Albert, Edward, Kivu and the north Tanganyika with eight separate basins(Fig.I.9). The central segment comprise the central part of Lake Tanganyika, Lake Rukwa and the north part of Lake Malawi with three separate basins. The south segment comprises the Lake Malawi rift and the smaller basins of Mozambique (Daly et al.,1989).

2.4.2.- TECTONICS AND RIFTING.

The WBEARS is bordered by a high-angled normal fault system bounding one side of spoon-shaped basins and with depth- to- detachment estimated at 20–30 km: Extending along the length of the rift are a series of *en echelon* border-fault segments linked by oblique –slip transfer faults, ramps, and monoclines within comparatively high- strain accommodation zones.

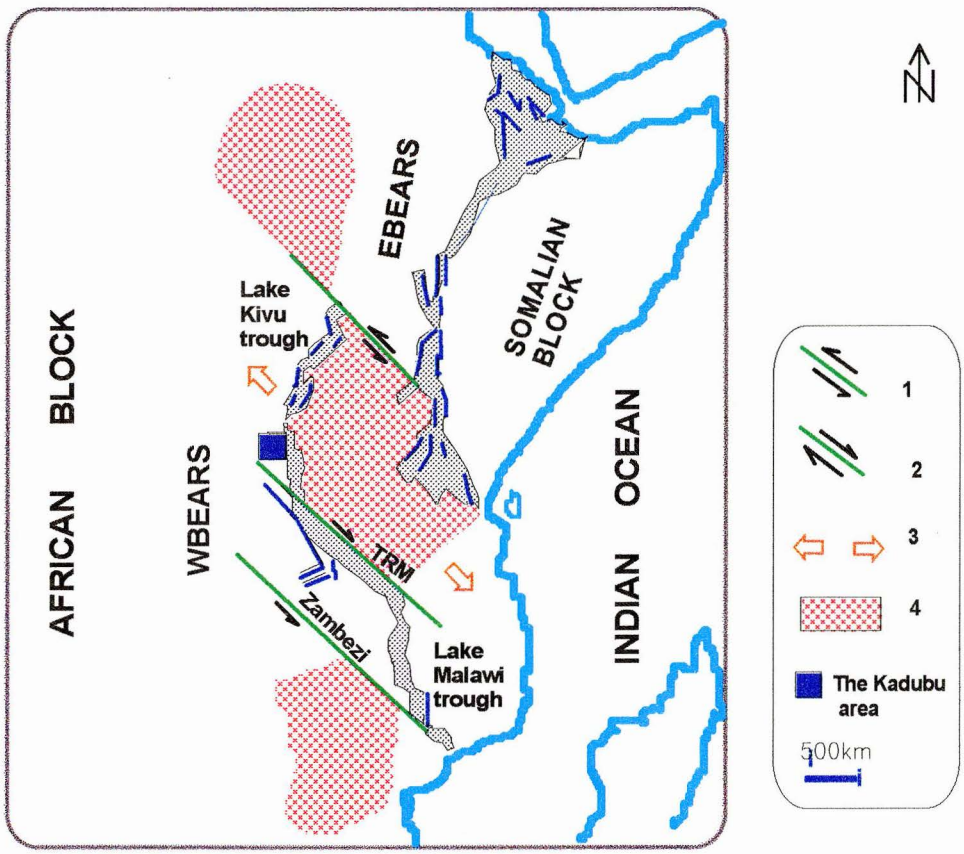


Fig.I.8:- Structural sketch of the East African Rift system including proposed NE trending wrench zones.
1-2- 3 :- Direction of movement.
4 :- Ancient craton (Precambrian).
TRM :- Tanganyika, Rukwa, Malawi transform fault.
WBEARS : - Western branch of the East African rift system.
EBEARS : - Eastern branch of the East African rift system.
(After Tiercelin et al., 1988).

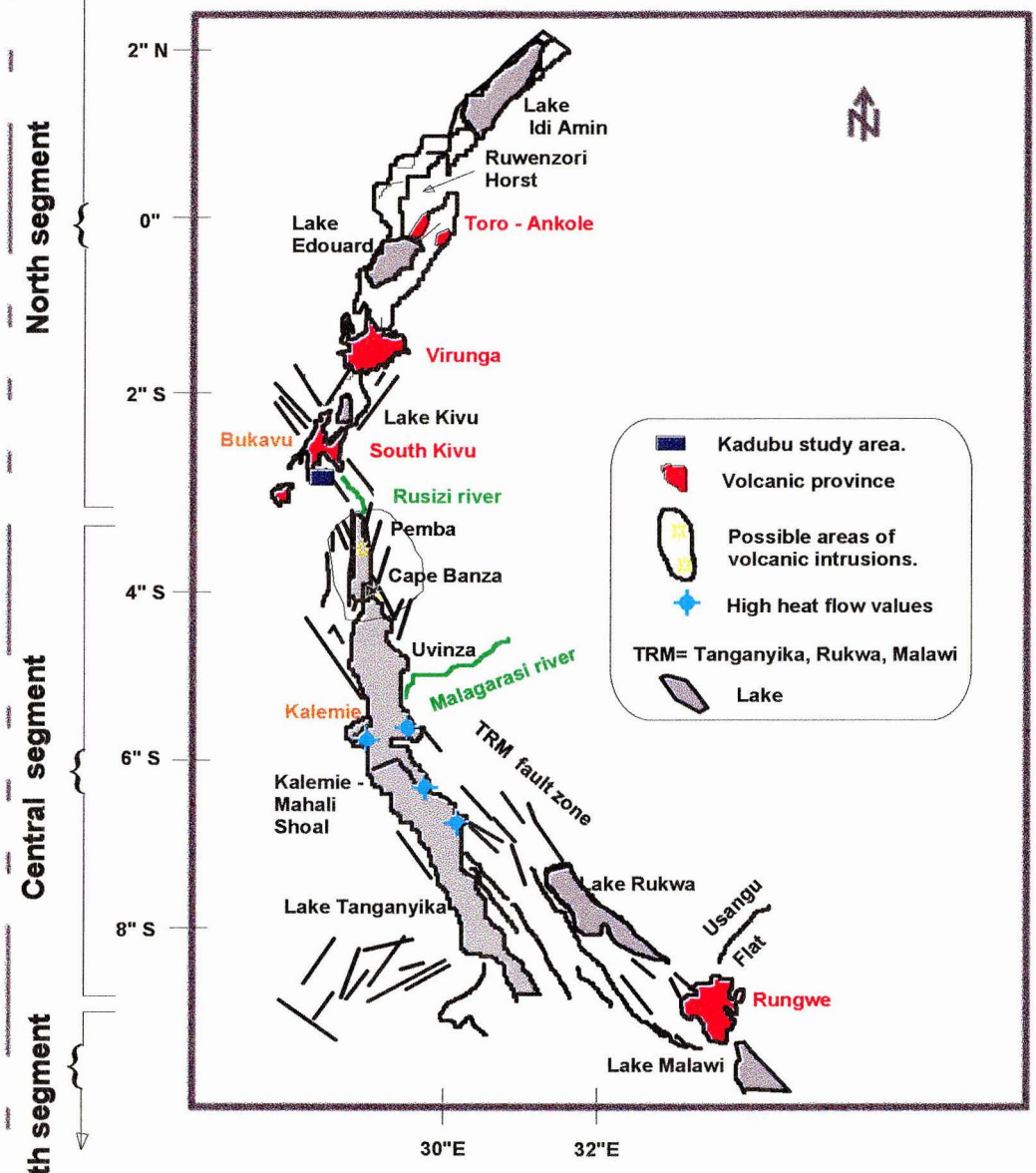


Fig.I.9:- Simplified map of the western branch of the East African rift system subdivided into three segments and showing four volcanic provinces (Toro-Ankole, Virunga, South Kivu, and Rungwe). Compiled from Daly et al., 1989 and Coussement et al., 1991.

KMA Walemba

These high-angle border faults penetrate to lower crustal levels, as indicated by seismicity data. (Ebinger,1989b; Ebinger et al.,1991) (Fig.I.10; Fig.I.11).

In the WBEARS, geophysical studies concentrated on rift Lakes, have shown that the topographical depressions are bordered on one or both sides by uplifted rift flanks comprising steeply dipping normal fault systems with cumulative displacements of up to 10Km.
Some faulted basins are separated by structural highs and cross- rift ramps or faults and suggest sedimentary basin depths of 4 - 6 Km (Morley.,1988, Lezzar et al.,1996, Upcott et al.,1996). (Fig.,I.10).
In the northern segment, the basement ridges have a NW - SE strike and the border fault segments vary from 60 to 120 Km in length and form the major morphological features of the region (Fig.I10). In the central segment, the major border faults are linear in outcrop, have a NW-SE trend, are continuous for 300 – 500Km along strike, have en echelon arrangement, and define a deformation zone, 150Km wide and 900Km long (Karson and Curts, 1989). The present study area, Kadubu is located within this deformation zone (Fig.I.1 ; Fig.I.10).

Daly et al., 1989, point out the fact that steep shear zones are sites of rift nucleation and play a fundamental role in the mechanisms of rift propagation and subsequent continental break up. A regional east – west extension direction is indicated by kinematic constraints from several basins. Estimates of crustal extension are less than 15% (< 10Km).

In the Kivu region, three representative basins (West Kivu, East Kivu and Rusizi are bordered along one side by high-angle normal faults with 2 – to 5 km throws (Fig.I.10). In plan view, ~ 100Km –long systems of linear border faults form curvilinear border fault segments bounding these three basins. The opposite sides of these asymetric basins are bounded by lower relief faulted monoclines or en echelon ramps. Maximun estimates of East - West crustal extension within basins are less than 25% (< 16Km), and planar border faults may penetrate the crust.
(Ebinger, 1989a, 1991) (Fig.I.10).
A complex history of hydrological connections and changes in shoreline configuration in northern Lake Tanganyika has resulted from a combination of volcanic doming, border fault evolution and climatically induced lake-level fluctuations (Lezzar et al.,1996, Cohen et al.,1997).

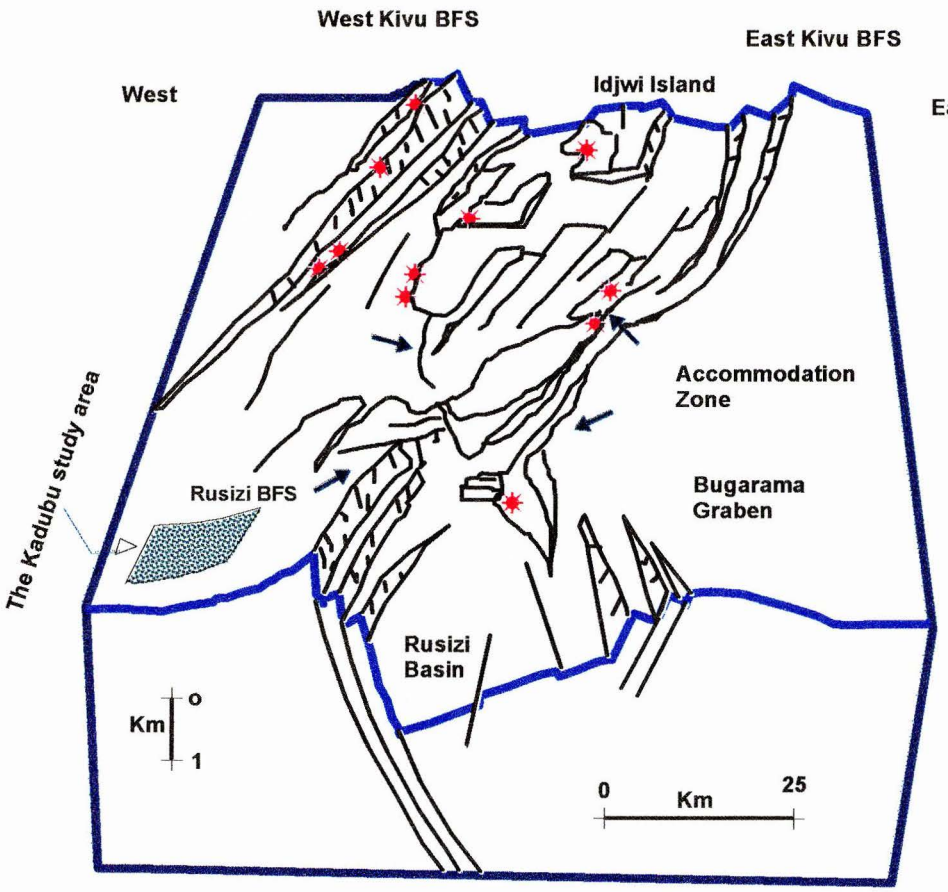


Fig.I.10 :- Three-dimensional model of spoon-shaped rift basins and accommodation zone between basins. (Scale approximate). ✸ **:- Volcanic centers.**

BFS is Border Fault Segment. Arrows point to ~ 30 km - wide , ~20 km -long accommodation zone. Border fault segments are regionally curvilinear in plan view, and ~ 100 km-long basins are spoon-shaped. (after Ebinger, C.J. 1989b, with additions).

KMA Walemba, 2000

The kinematic evolution of the East African Rift system (EARS) is interpreted in a succession of four major stages, characterized by a progressive rotation of compression direction from horizontal (strike-slip regime) to vertical (extension regime), with the extension axis remaining in a fixed horizontal NW-SE to E- W direction (Chorowicsz et a., 1987, Tiercelin et al., 1988, Versfelt and Rosendahl, 1989, Delvaux, 1991).

In westen Tanzania, the WBEARS is commonly cited as having resulted from Phanerozoic reactivation of the Paleoproterozoic Ubendian belt. (Theunissen et al., 1996). Active sublacustrine hydrothermal seeps (thermal spring) and associated massive sulfides and hydrocarbon mineral deposits were discovered in the north Tanganyika trough and are located at the intersection of major north-south normal faults and northwest-southeast faults belonging to the Tanganyika-Rukwa-Malawi (TRM) strike-slip fault zone (Tiercelin et al.,1989,1992; Tanganhydro group,1992). The mineralization associated with the thermal springs consists mainly of pyrite, marcasite, kaolinite, quartz, natroalunite within sulphide –quartz veins and stockworks.

Lake Kivu contains about 50 cubic kilometres of methane [up to 0.37 liter per liter of water] and carbon dioxide [up to 1.4 liter per liter of water](at standard temperaure and pressure) in its deep water. Most of the methane was formed by bacteria from abiogenetic carbon dioxide and hydrogen, rather than being of volcanic origin or having formed from decomposing organic matter (Damas., 1937 ,Deuser et al., 1973).

2.4.3.- MAGMATISM.

2.4.3.1.- ALKALINE PLUTONIC COMPLEXES .

More than 25 alkaline plutonic complexes with comparable ages, rock types, and anorogenic features have been identified in the WBEARS (Tack et al.,1984, 1994,1996). Their spatial distribution along the rift, show two alkaline plutonic alignments of Mesoproterozoic (ca, 1250 Ma) and Neoproterozoic ages (ca ,750 Ma) and their geological setting is controlled by structural weakness in the lithosphere suggesting that the present-day WBEARS was already a zone of weakness in late Precambrian times (Fig. I.10, Fig., I.11 ; Table.I.2) .

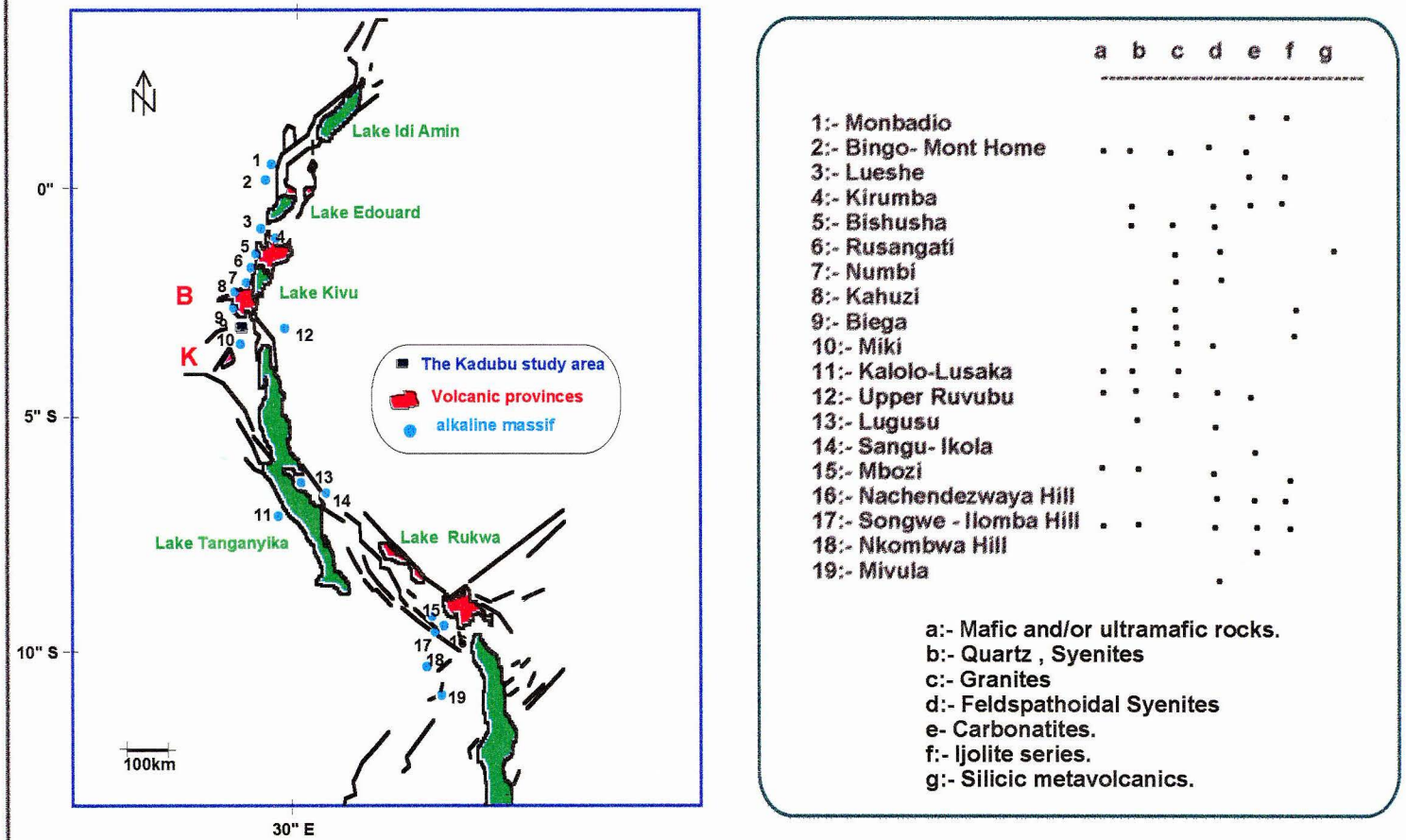


Fig.I.11:- Spatial distribution and rock type of 19 alkaline massifs located along the Western branch of the East African rift system . The Bukavu (B) and Kamituga (K) volcanic regions are also shown in relation to the study area.(After Lubala et al., 1987)

Table. I.2:- List of 19 alkaline massifs located along the westren branch of the East African rift system with available radiometric data.

Complexes	Radiometric ages	Nature and number of dated samples.
1:- Monbadio		
2:- Bingo- Mont Home		
3:- Lueshe	516 +/- 26 (K, Ar)	1 Bi
4:- Kirumba	259 +/- 13 (K, Ar)	1 WR
	501 +/- 72 (Rb - Sr)	1 WR, 1 PL, 1 Mi.
	+/- 580 (Rb - Sr)	1 Bi
	688 +/- 33* (Rb - Sr)	1 Bi
5:- Bishusha		
6:- Rusangati		
7:- Numbi	+/- 520 (Rb - Sr)	1 Bi
8:- Kahuzi	493 +/- 12 to 452 +/- 11 (K - Ar)	2 WR + 2 Bi
	134 +/- 7 (K- Ar)	1 WR
	55 +/- 3 (K - Ar)	1 WR
	728 +/- 25 (Rb - Sr)	6 WR
9:- Biega	555 +/- 13 to 442 +/- 11 (K - Ar)	2 WR + 2 Bi
10:- Miki		
11:- Kalolo-Lusaka	781 +/- 83* (Rb - Sr)	3 WR
	604 +/- 50* (Rb - Sr)	2 WR + 2 F + 1 Hb
	1106 +/- 27 (K - Ar)	1 Hb
	877 +/- 23 (K - Ar)	1 Hb
12:- Upper Ruvubu	774 +/- 88 (Rb - Sr)	3 WR
	699 +/- 13 (Rb - Sr)	9 WR
	707 +/- 17 (Rb - Sr)	7 WR
	739 +/- 7 (U - Pb)	2 Zr
13:- Lugusu		
14:- Sangu- Ikola		
15:- Mbozi	745 +/- 25 (K - Ar)	1 Bi
	743 +/- 30 (K - Ar)	1 Bi
16:- Nachendezwaya Hil		
17:- Songwe - Ilomba Hill	685 +/- 62 (Rb - Sr)	3 WR
	655 (Pb)	1 Zr
	500 (K - Ar)	1 Bi
18:- Nkombwa Hill	680 +/- 25 (K - Ar)	1 Ph
19:- Mivula	550 +/- 20 (K - Ar)	1 Bi

* Recalculated with λ^{47} Rb = $1.42.10^{-11}$ Y^{-1} and errors at 2 σ level.
WR = Whole rock ; Bi = Biotite; Pl = Plagioclase ; Mi = Microcline; F = Feldspar;
Hb = Hornblende, Zr = Zircon, Ph = Phlogopite. (After Lubala et al., 1987).

KMA Walemba, 2000

Major pre-existing zones of weakness orientated parallel to the direction of relative continental separation may determine the position of the transforms that develop in the new ocean (Sykes, 1978, Reyre, 1983). According to Black et al., 1985, alkaline magmatism precedes and succeeds the opening of an ocean. Intrusion areas are located along old lines of weakness near the ends of transform faults and may extend far inland.

2.4.3.2.- VOLCANISM.

Three distinct volcanic regions have been distinguished in the Kivu province. From north to south, there are the Virunga, the Bukavu and the Mwenga- Kamituga regions (Fig.I.10, Fig. I.11). Highly undersaturated K-rich and Na-rich lavas associated with carbonatites are restricted to the WBEARS system where they cut Kibaran and Ubendian basements (Thorpe and Smith.,1974).

In the Bukavu region, the volcanic sequence commence with tholeiites which are also the most abundant (ca 18 – 6 Ma). These are followed and partly covered by Na alkaline lavas (ca 8 – 1.6 Ma) and finally transitional lavas (10000 years - present) were erupted.(Kampunzu et al., 1998).(Table. I.2),
Auchapt (1985) reports a 16% partial melting for tholeiites, 5% for transitional basalts and 2.5% for basanites.

Continental tholeiites and/or transitional basalts could be related to the pre-rift stage, whereas alkaline and transitional lava to the syn-rift stage. The ultra – alkaline and carbonatite igneous zones are mainly located along transverse fracture zones .
In the south Kivu area, normal faults intersect strike-slip faults and this seems to have determined the location of volcanic activity and seismicity (Pasteels et al., 1989).

Rifting mechanisms (normal and strike-slip) appear to be continuous today as proved by recent volcanic activity and present day-seismic activity .

PART II.- GEOLOGY AND TECTONIC EVOLUTION OF THE KADUBU AREA.

****

CHAPTER.3.- INTRODUCTION.

3.1.- INTRODUCTION AND GEOGRAPHIC SETTING.

The Kadubu area forms a part of the Itombwe synclinorium supergroup and constitutes the type area, being the best preserved segment of this orogenic belt. It includes many gold and tin occurrences being exploited by small-scale mining operations.

The area is located in the Kivu province, of eastern DRC; within the deformation zone of Cenozoic rifting of the WBEARS. It lies roughly 40 kms, southwest of Bukavu and 45 kms, west of the axial trough of the fault depression of the WBEARS (Fig.I,1; Fig.II,1;Fig.II,2).

This study area is located approximately between the $28^0 33' - 28^0 50'$ longitude east and the $2^0 45' - 2^0 57'$ latitude south, covering about 750 s.q.km (30 km x 25 km). Access to the area is well provided by an all-weather gravel road from Bukavu to Nya-ngezi (~ 45 km), followed by 15 kms on a rather poor gravel road. (Fig.II,1;Fig.II,2).

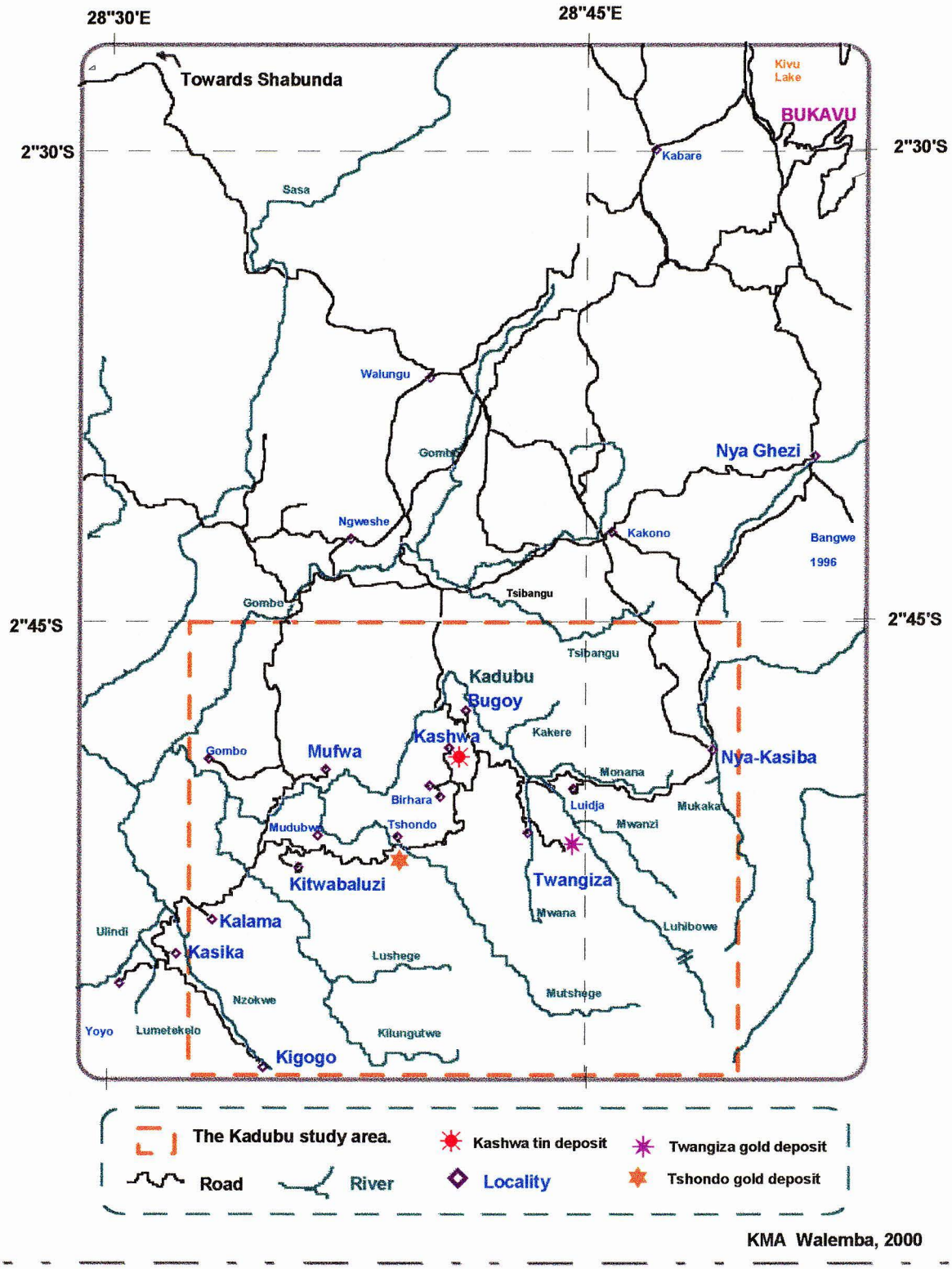
3.2.- - GEOMORPHOLOGY AND PREVIOUS WORK .

The most striking physiographical features of the study area, are the mountain ranges of the WBEARS, which have deeply incised valleys with rain forests within them (Fig.II.3; Fig.II.4). Higher up, the slopes are covered by short savannah type shrubs and at the highest elevation , alpine grassland. In the southernmost, dense rainforest heavy vegetation covers the drainage basins.

Elevations range from 900m to 3161m a.m.s.l., rising from west to east and from north to south. The ridgetops decrease in elevation to the east and south to 900m a.m.s.l. These mountains are dissected into a series of smaller hills and valleys and have steep slopes reaching 45^0 and more.

The area experiences a semihumid, tropical climate influenced by elevation.Temperatures do not vary greatly, seldom exceeding 25^0C (77^0F), with a 4-month "dry season"(May through August) with cooler dry conditions, and a regular " rainy (wet) season ", which more or less guarantees high rainfall during the year.

Fig.II.2 :- Locality map of the Kadubu study area.



KMA Walemba, 2000



Fig.II.3:- Extract of DIF image 600 X 750 pixels, of the East Africa showing lineament corridors through the Kadubu study area .





Fig.II.4:- -Topographical expression of the study area : grassland and Kadubu river in the central part of the study area, and rainforest environment and Lushwege river in the southwestermost corner of the study area.

The mean annual rainfall is about 2,000mm (79 inch, precipitation), falling mainly between September and April.

A deep weathering profile, up to 200m deep is strongly developed, producing some distinctive landforms of which large rills following the line of bedding in phyllite and sandstone are evident. Boxworks in phyllite; and spheroidal weathering around corestones of basalt and conglomerate are a feature.

The Kadubu river drains a large part of the study area and has a catchment area of about 25,000 s.q km. It has five major tributaries: the Luhimbowe, the Monana, the Mutshege, the Mudubwe and the Kilungutwe. All of them rise east and drain west and feed into the Ulindi river system (Fig.II.2) .

Two distinct geomorphic zones occur on the Kadubu river, and its tributaries: a gorge section and a valley section. Some gorges are up to 500m deep and the river occupies the whole of the valley canyon floor.

A wide range of alluvial sediments are present in the river beds, varying in size from boulders through gravel to very fine material in the silt-clay fraction.The coarse material is generally topped by layers of fine and medium sand. Various terrace levels can be identified up to 350m above the present profile of some streams so that quite a complex history of development lies behind the present stream pattern.

Little geological research has been undertaken so far in this are. The earliest and only survey of the Kadubu area was carried out by Peeters.,1952, (opcit) and Sorotchinsky.,1952(opcit).

CHAPTER 4.- TECTONIC LINEAMENTS AND LITHOLOGICAL DISCRIMINATION.

4.1.- INTRODUCTION.

The ERTSI (Landsat) launched in the early 1970s expanded the scope of direct structural observations on a megascopic and gigascopic scale. Conventional field mapping in the study area was supported by remote sensing in the form of aerial photographs (scale: 1:50000) , LANDSAT TM imagery (scale 1:100000) and aeromagnetic survey (Fig.II.5 ;Fig.II.6).



FIGURE II.5:- LANDSAT IMAGE OF THE KADUBU STUDY AREA

LANDSAT TM IMAGERY 457. SCALE: 1: 100 000

FIG.II.6.

DEMOCRATIC REPUBLIC OF CONGO

KADUBU AREA

ENHANCED MAGNETIC ANOMALY MAP

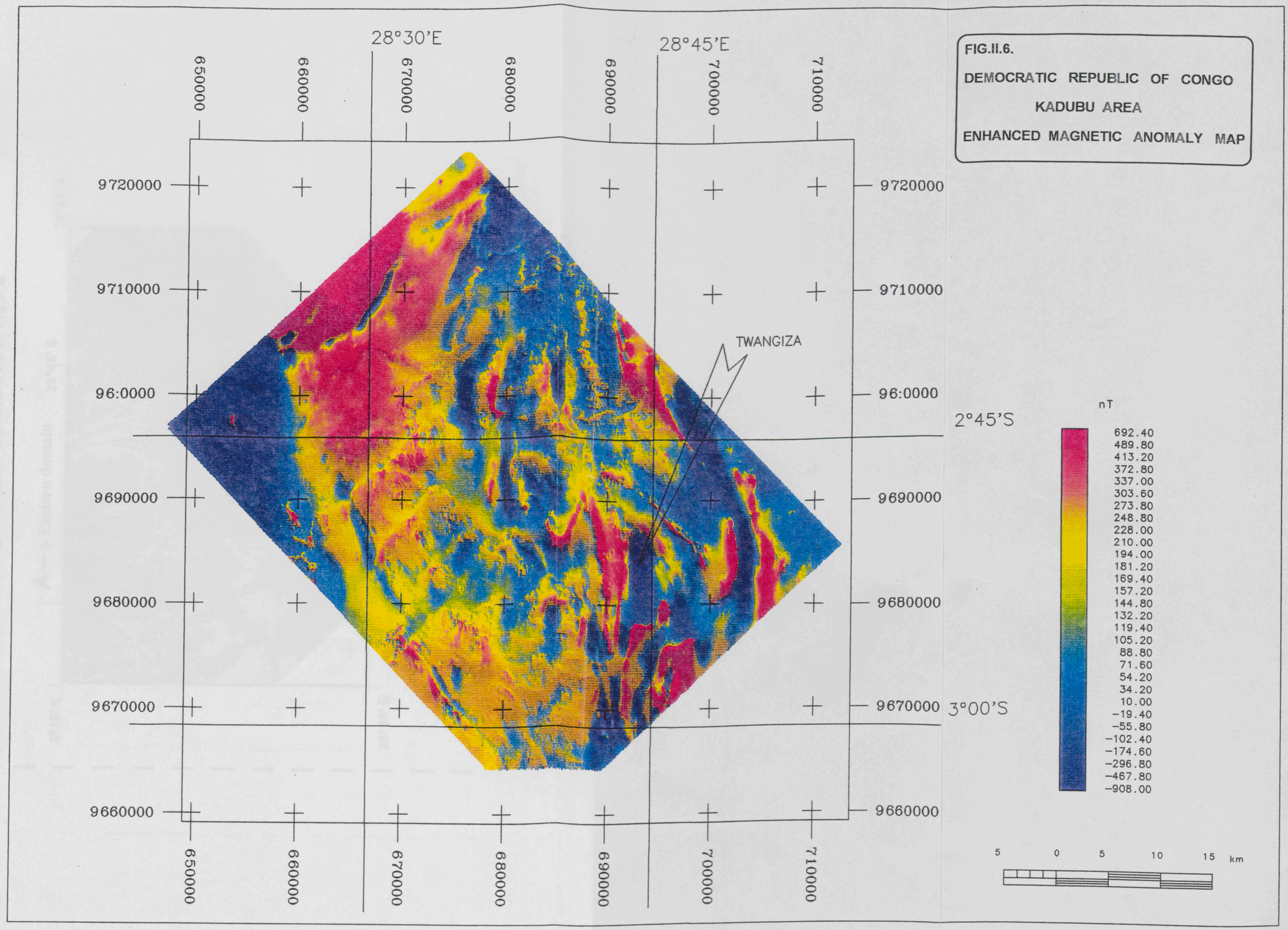


Fig.II.6a:- Total magnetic field map of Kadubu area subdivided into two separate domains of differing magnetic characetere : The western domain and the Eastern domain . Legend of magnetic color signature as in Fig.II.6

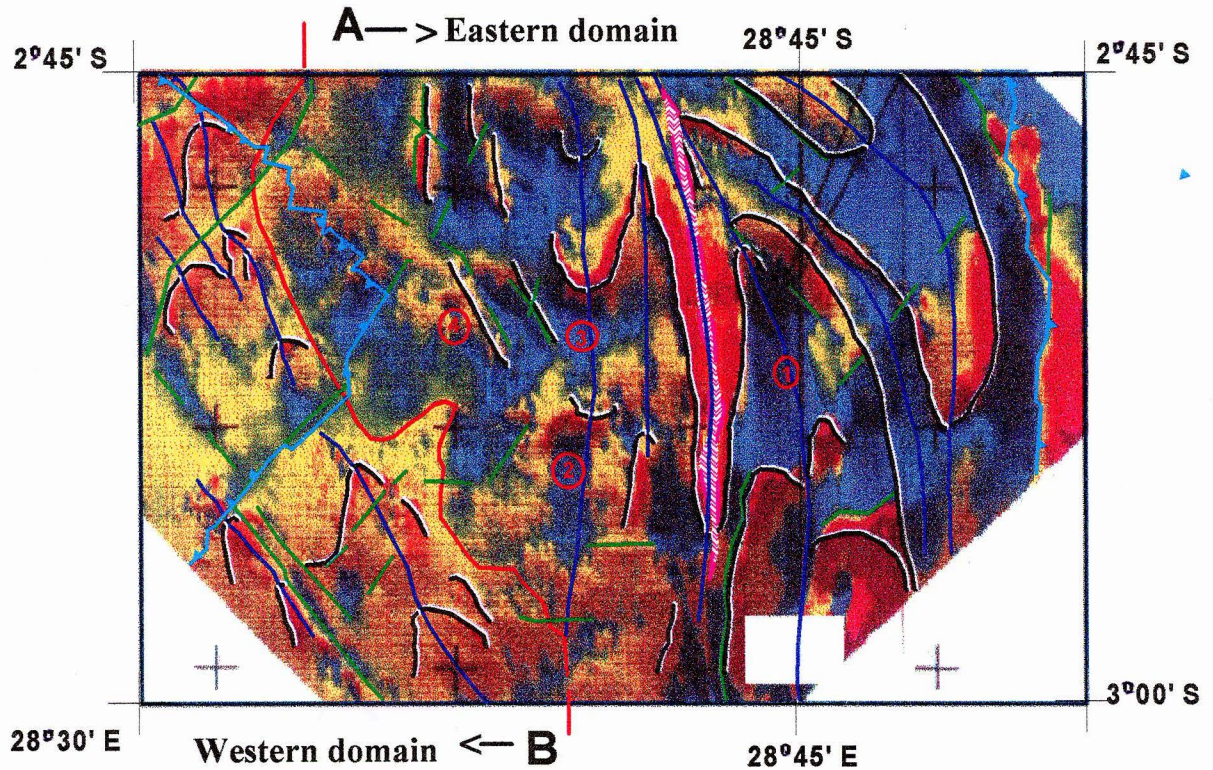
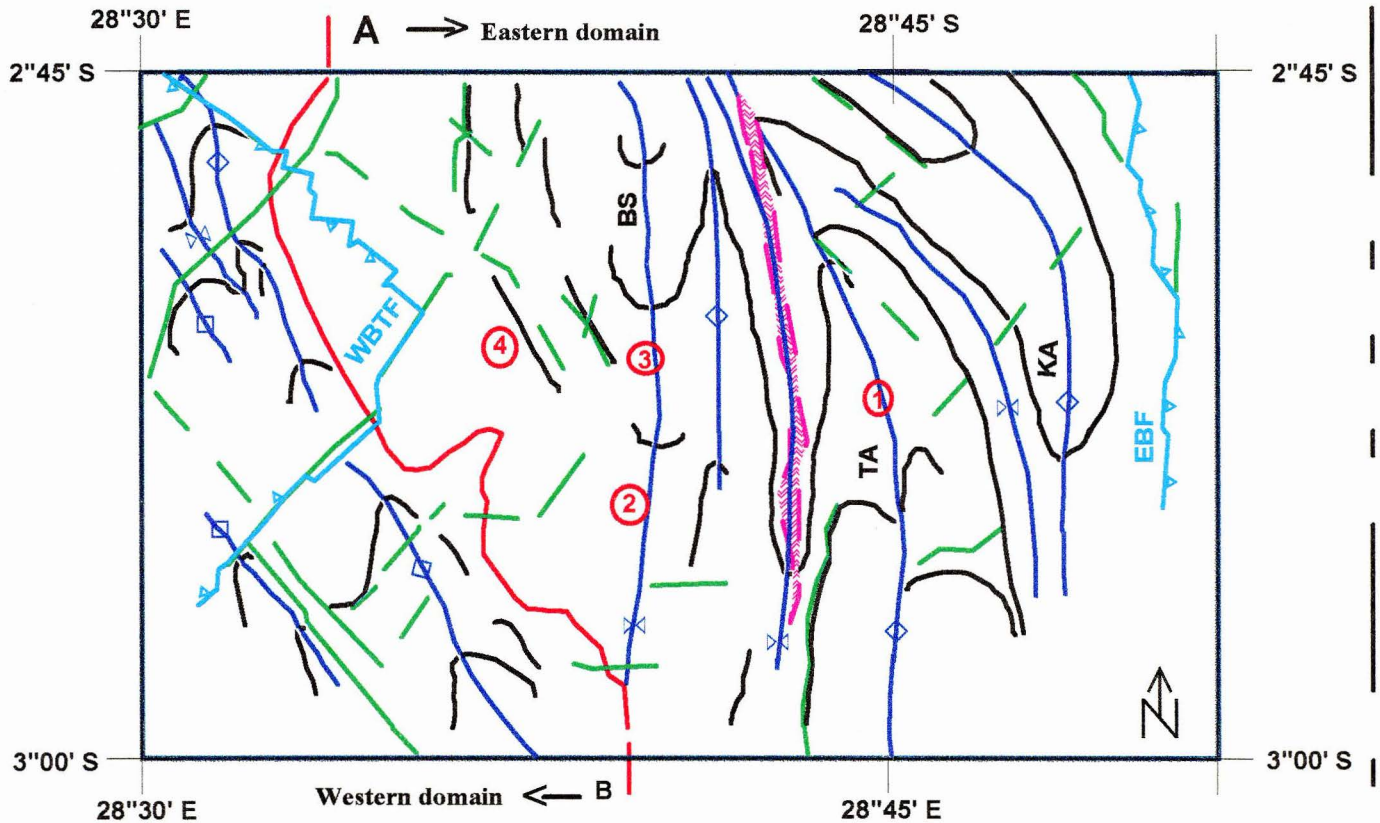


Fig.II.6b : KADUBU AREA .
GENERALISED MAGNETIC INTERPRETATION MAP DERIVED FROM TOTAL MAGNETIC FIELD MAP (FIG.6a).



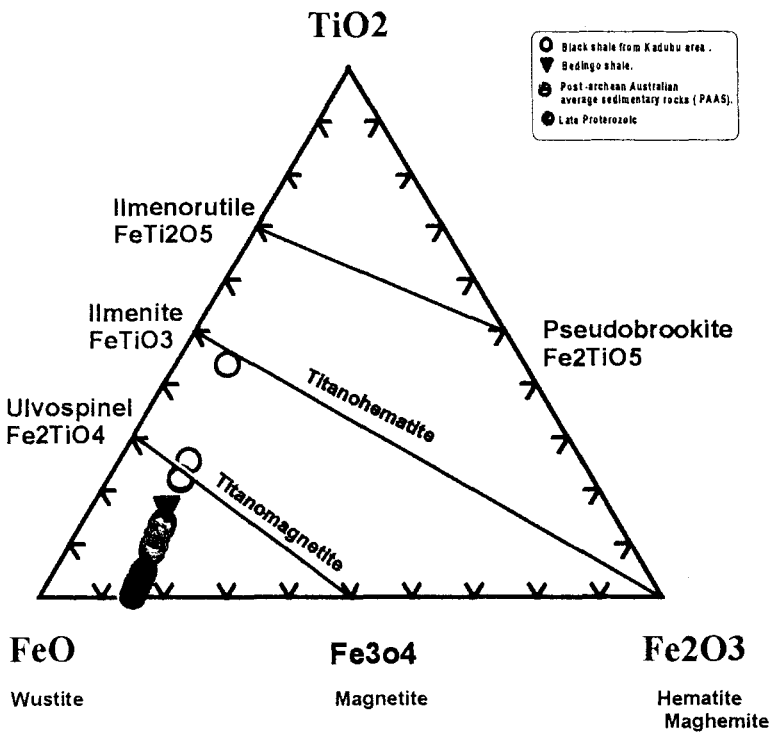


Fig.II.6c:- Iron-titanium oxide mineral from the black shale (Kadubu metasediments) plotted in the ternary compositional diagram of the iron - titanium oxide solid solution diagram for magnetic minerals.

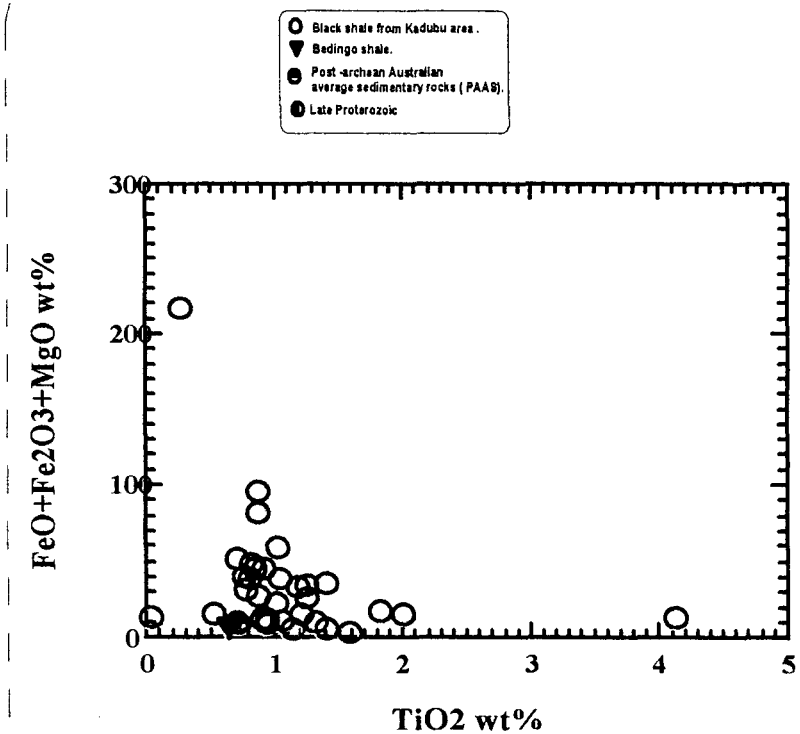


Fig.II.6d : Total Iron + MgO versus TiO2 diagram for black shale samples from Kadubu metasediments.

The LANDSAT TM images were composited using bands 4 ,5 and 7 and the interpretation of the images was accomplished by conventional aerial photographic analysis techniques, taking into account geological and geomorphological pattern recognition through stereoscopic observation. Despite heavy vegetation, particularly in the southernmost part of the study area, major geological structures are manifest through geomorphologic features on the Landsat imagery (Fig.II.5). The available geophysical information has improved knowledge of the disposition of the lithologies and structures(Fig.II.6).

For lithological discrimination, consideration was given to analysis of drainage density and drainage patterns, vegetation differences, landform development, climatic influences on geomorphic processes, and the spectral character of the land surface (tone or/and colour on the images) where available in limited areas .

Subsequent verification in the field of the interpreted geologic relationships was made during field work .

4.2.- GEOMORPHIC CRITERIA.

There is a strong correlation between geomorphology and geology, and major geological features have distinctive shapes and geomorphological expressions. Principal geological features include fractures including lineaments, folds, circular structures, and lithologic domains. The major part of the area studied is drained by streams flowing west towards the Mudubwe locality where they feed into the Ulindi river system.

The Kadubu river and its tributaries run along very narrow to incised valleys bordering the west side of the extension zone of the WBEARS. Three main fabric/lineament directions are: NNW – SSE, NNE – SSW and E-W (Fig.II.2; Fig.II.5).

Anomalous patterns include, pronounced inflections, occurrence of rapids and waterfalls, and barbed junctions. These features suggest capture and diversion of streams, as well as northwest tilting of the overall area in recent times.

4.3.- LINEAMENT ANALYSIS (PATTERN, DENSITY AND LENGTH).

A study was carried out on the lineaments observed on photographs LANDSAT images, and in the field. More than 350 fairly pronounced lineaments were observed, representing mainly faults, fractures and joints. A quantitative analysis and qualitative interpretation was carried out on prominent linear structures obtained from LANDSAT imagery (Fig.II.5; Fig.II.7).

Linear structures have been classified into several groups according to their shape, direction and extent. (Fig.II.8, Fig.II.9). The distribution of lineament is apparently dependent of lithology. Their number is vey high in areas where shales , phyllite and sandstones dominate, and low where there are quartzites and conglomerates. The dominant trends of the Kadubu area is NW to NNW.

The rose diagram for all of the 356 linear features for the whole area in Fig II.7, is shown in Fig. II.10. The Rose diagram, Fig II.10, shows the dominant sets of $N30^0$–80^0W and 50^0 –100^0E lineaments. These lineaments reflect the main structural pattern as observed in the field and reflect significant topographic breaks and drainage realignment. They generally cross cut the belt at high angles and are relatively widespread. Most of them have been reactivated during the recent rifting.

The size of the rosenet core shows that the linear features do not occupy all direction and the two principal orthogonal maxima are precisely ENE and NW- directions that suggest relationship to present – day terrestrial rotation.

A $N\ 0^0 - 20^0$ W trend , less dominant lineaments of a small population has been also recorded and cross cut the belt at lower angle. They are relatively short. Along them, the NW is clearly offset in an apparent sinistral sense. The E-W and NE are weakly dextrally offset. It is notable that Kibaran is structured by N –S trending folds and faults. The $N50^0E$ and $N150^0E$ faults are respectively dextral and sinistral. The E – W trend has been considered as being reactivated Pan African structure.

The (curvi-)linear structural anomalies occurring in the northern part of the study area correlate with basaltic dykes (cinder cones), with the easternmost representing an alluvial gravel deposit.

Two major shear zones running respectively N-S and E- W have been recorded. The first one is a major left lateral shear zone and the second being a right lateral shear zone (Fig.II.5 ; Fig.II.6).

28° 45'

E +510 000

E +520 000

E +530 000

N - 310 000

N - 320 000

N - 330 000

WESTERN BOUNDING THRUST FAULT

EASTERN BOUNDING FAULT

BT

KAKERE

MUFWA

KASHWA

KSZ

LT

MWAZI

TWANGIZA

TSHONDO

BUGOY FAULT

LSZ

BULONGO FAULT

TSHONDO FAULT

TWANGIZA FAULT

28° 45'

N

LEGEND

- Major fault
- Thrust fault, teeth on upper plate
- Major shear-fault with downthrow
- Lineaments: faults, joints, fractures
- Shear zones
- KSZ — Kahanda shear zone
- LSZ — Lungwe shear zone
- Gold deposit
- Tin deposit
- Thermal springs
- LT — Luidja thermal spring
- BT — Bugoy thermal spring
- Cinder cone
- Magnetic Features: Fold, Fault, Shear zone

Figure II.7

DEMOCRATIC REPUBLIC OF CONGO

KADUBU AREA

TECTONIC LINEAMENTS

GENERALISED THEMATIC MAPPER INTERPRETATION

1000m 0 1 2 3 4 5km

Scale 1 : 100 000

GEOLOGY BY: K M WALEMBA (1998)

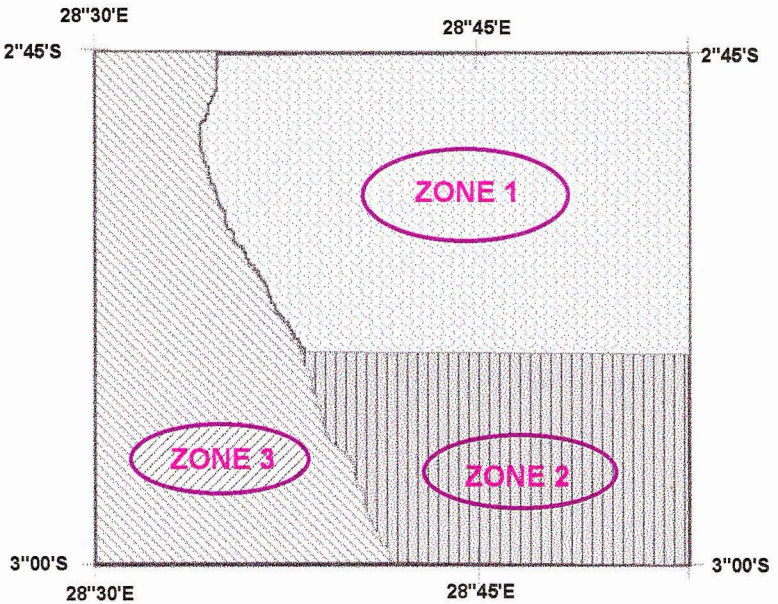


Fig.II.8.- The map of the subdivision of the Kadubu area into three zones in accordance with structural pattern and spatial distribution.:
Zone 1: Monana zone, with a dominant N50" -60" W orientation.
Zone 2 : Mwana zone, with a dominant N60" -100" W orientation.
Zone 3 : Kilungutwe zone, with a dominant N50" -100" E orientation.

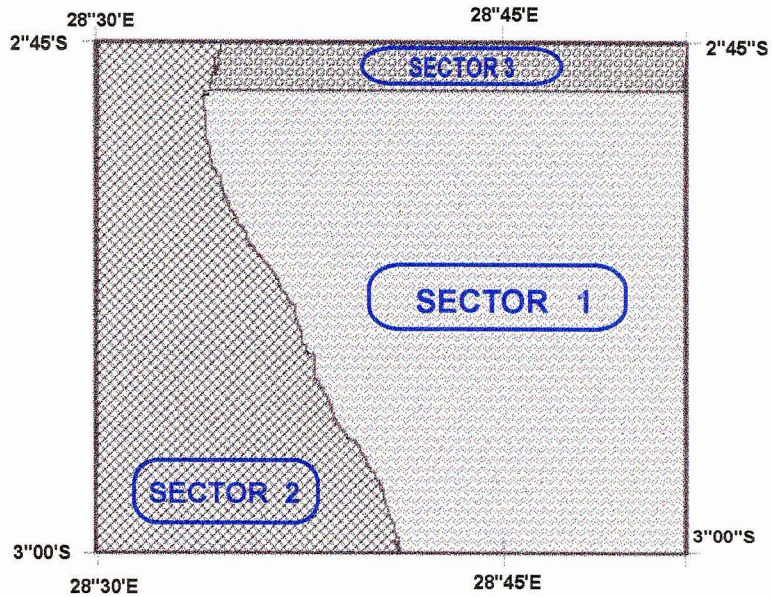
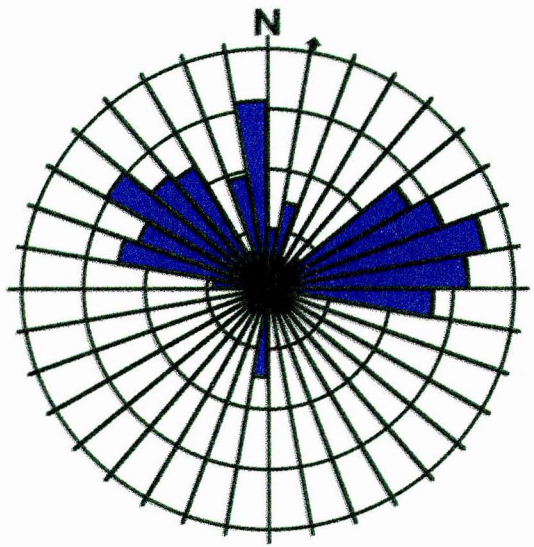
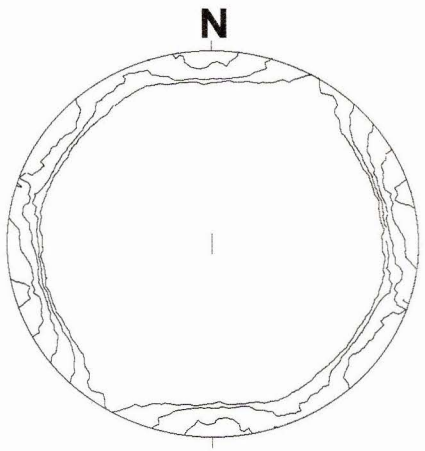


Fig.II.9.- The map of the subdivision of the Kadubu area into three sectors in accordance with lithological discrimination and spatial distribution:
Sector 1 : Shales, phyllites, sandstones, conglomerates.
Sector 2 : Quartzites and schists.
Sector 3 : Lava flow and pyroclastic rocks.

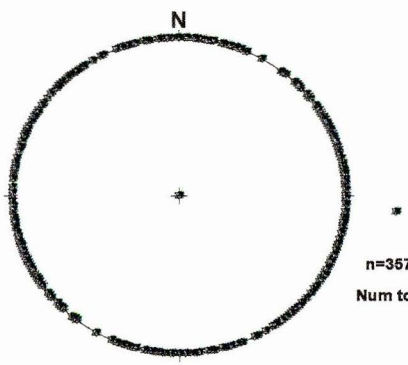


N = 356 ; Mean = 10.37 ; R = 0.483



N = 357
max dens. = 5.61 (at 72/3)
min. dens. = 0.00
Contours at : 0.00, 1.00
2.00, 3.00, 4.00, 5.00,
(Multiples of random distribution)

Equal area projection , lower hemisphere.



n=357 (P)
Num total: 357

Equal area projection, lower hemisphere

Fig.II.10 : - Rose diagram for all the 356 linear features for the whole area and its structural trends.

After the visual analysis of this LANDSAT imagery, three zones have been separated in accordance with the main structural patterns and spatial distribution (Fig.II.8). These zones were analysed separately in order to establish comparision between them:

- *Zone 1* : (Monana zone; delineated by Tshondo fault and from the extremity north to latitude $2^0 52'$) shows a clear dominant $N50^0$ -60^0 W striking lineaments with subsidiary NW and ENE lineaments sets.
- *Zone 2* : (Mwana zone; from latitude $2\ ^0 52'$ to Tshondo fault and south extremity); shows a dominant $N60^0$-80^0 W, $N80^0$-100^0E, and subsidiary $N10^0$-40^0W , $N10^0$-20^0E .
- *Zone 3 :* (Kilungutwe zone; from Tshondo fault to the extremity west) shows a strongly dominant $N50^0$-100^0E orientation and subsidiary $N40^0$-50^0W, $N170^0$-180^0W.

Fig.II.11, Fig.II.12 and Fig.II.13 present respectively the Rosenets of lineaments of these differents zones and their structural trends.

Fig.II.14 , and Fig.II.15, show the Rosenets of these lineaments respectively in Upper Kadubu group (dominant sets: $N150^0$-170^0W; subsidiary sets: $N0^0$-10^0Wand $N120^0$-140^0 W) and Lower Kadubu groups; (dominant sets: $N10^0$-40^0W; subsidiary sets: $N130^0$-160^0W and $N170^0$-180^0W).

4.4.- LANDSAT LINEAMENT CORRIDORS AND STRUCTURAL INTERPRETATION.

Field observations show structural corridors corresponding to subsurface dislocations, and depending on the type of geological environment , either edges or centres of corridors bear a relationship to mineral and oil deposits.Corridors related to ore deposits are commonly 100 – 200 Km in length, with aspect ratios (length / breadth) from 20 to 40. (O'Driscoll, 1981).

In this study area, detailed and integrated study of Landsat lineament plots with other geological data, especially gravity corridors has not yet been carried out. On the drawing of lines through a selected pair of primary gold occurrences, (Twangiza, Tshondo), of which Twangiza belongs, it is interesting to note the correspondance between one of this " alignment" and a major fault zone, (east west trending) bordering the westermost rift valley (Fig.II.3).

Moreover, two lineament corridors are noticeable on GIF image, 30 Arc, DEM image and on Landsat image. Their relationship and association to gold occurrences are remarkable. (Fig.II.2, Fig.II.4, Fig.II.5). Different sets of geo-data are needed to define the structural corridors within the Itombwe synclinorium belt.

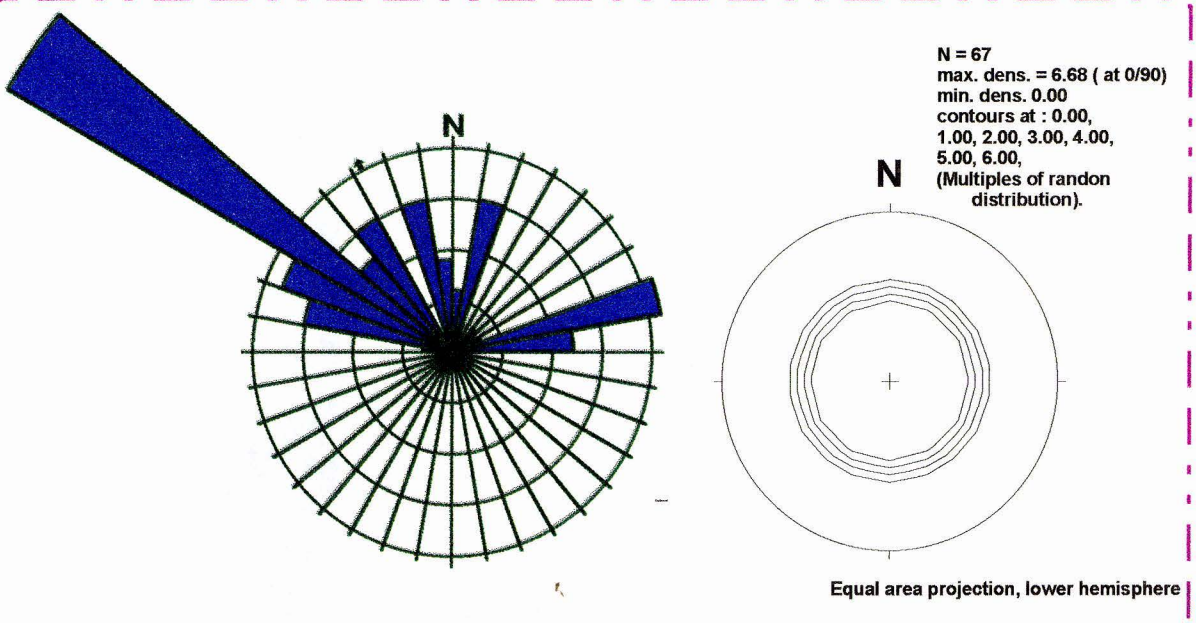


Fig.II.11 :- Rose diagram of lineaments of the Monana zone (zone 1) and its structural trends.

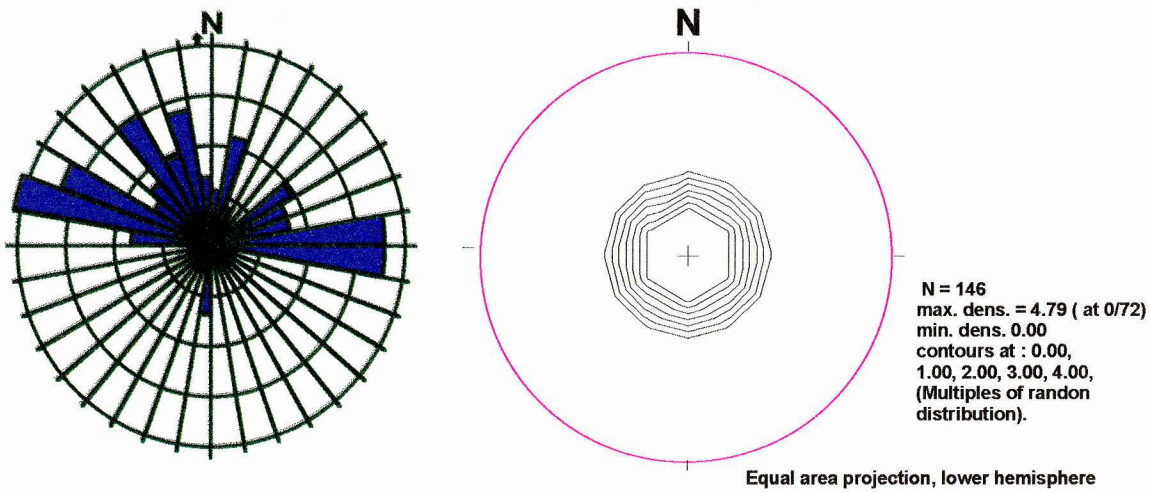


Fig.II.12 :- Rose diagram of lineaments of the Mwana zone (zone 2) and its structural trends.

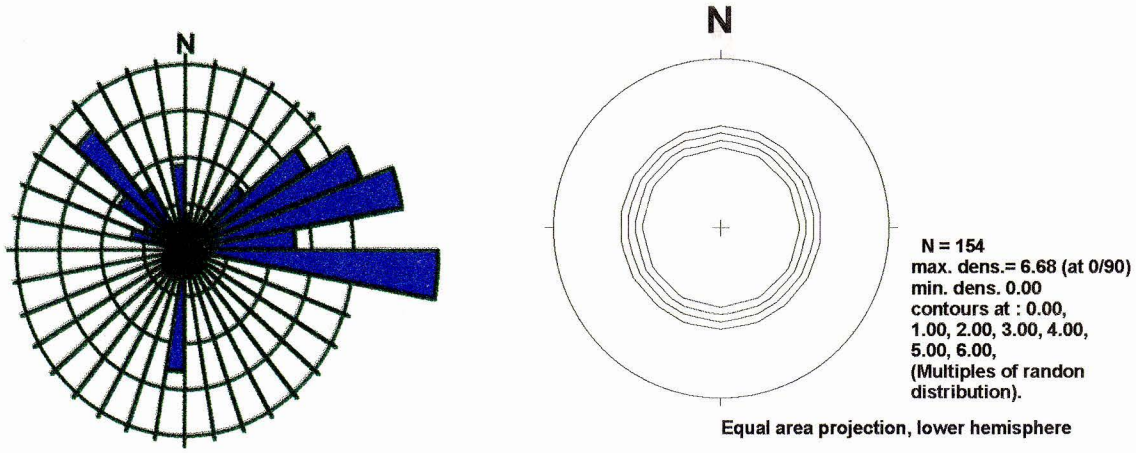
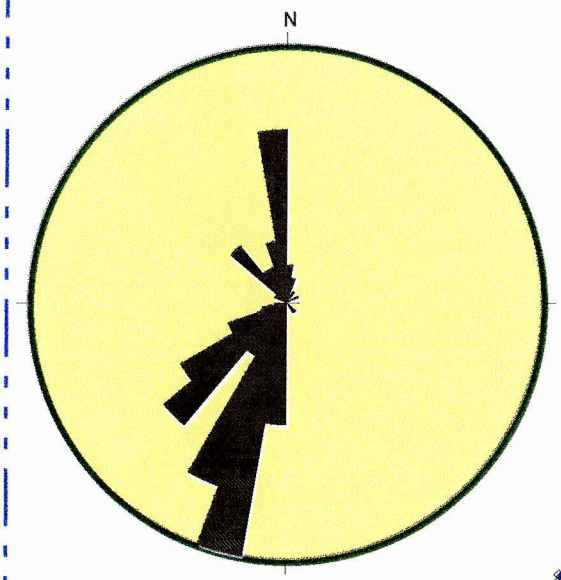
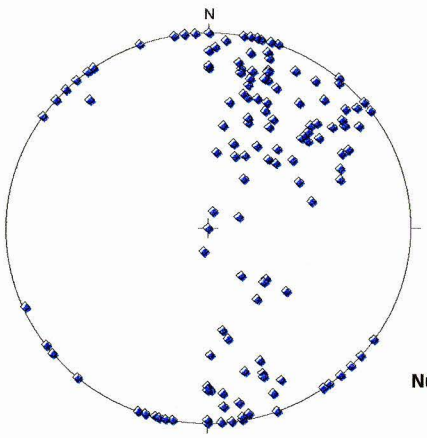


Fig. II.13 :- Rose diagram of lineaments of the Kilungutwe zone (zone 3) and its structural trends.



Num total: 124

Dip Direction: 10 ° classes

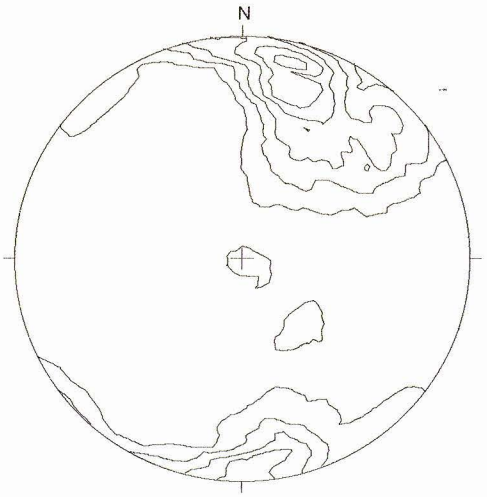


n=123 (P)

n=1 (L)

Num total: 124

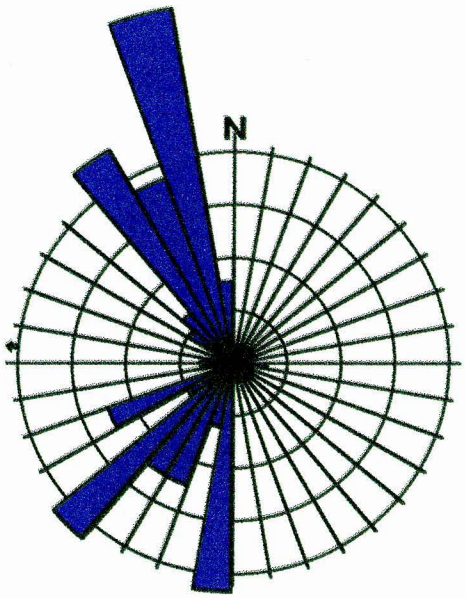
Equal area projection, lower hemisphere



n= 124
max.dens.= 5.26 (at 14/15)
min. dens. = 0.00
contours at : 0.00, 1.00,
2.00, 3.00, 4.00, 5.00,
(Multiples of random distribution)

Equal area projection, lower hemisphere

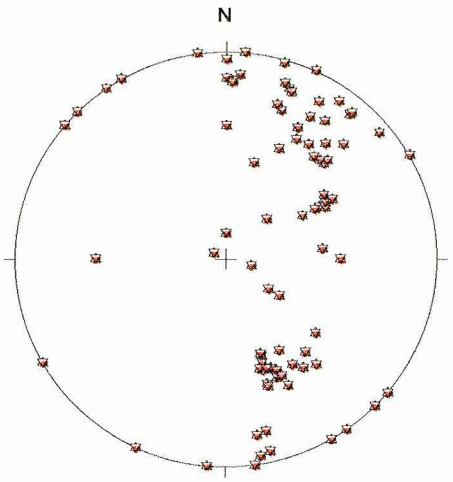
Fig.II.14:- Rose diagram of the upper Kadubu group lineaments and its structurals trends.



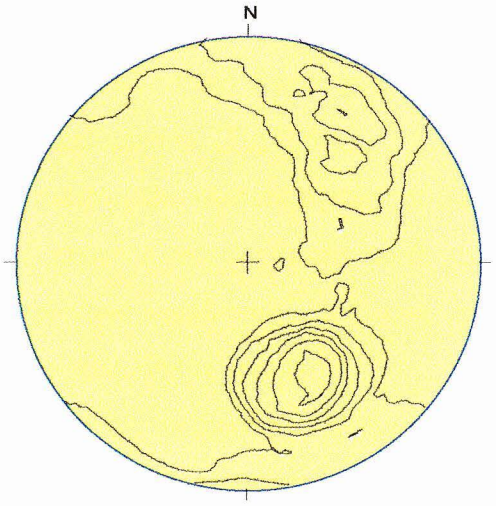
n=129 (P)

n=1 (P)

Num total: 130



Equal area projection, lower hemisphere



n = 127
max. dens . = 6.91 (at 146/46)
min. dens. = 0.00
contours at : 0.00, 1.00, 2.00,
3.00, 4.00, 5.00, 6.00,
(Multiples of randon distribution)

Equal area projection, lower hemisphere

Fig.II.15:- Rose diagram of the lower Kadubu group lineaments and its structural trends.

4.5.- DISCRIMINATION.

Land classification on LANDSAT TM 457, was performed using conventional photointerpretation parameters, including photographic tone, texture, topographic relief, pattern, shape and drainage pattern.

Areas underlain by metasedimentary rocks were readily distinguished on images by their distinct banded appearance. Resistant rocks units (conglomerate, sandstone,quartzite) show greater relief and less resistant beds (phyllite, black shale, schist) are lower due to weathering and erosional processes (etching concept).

Intrusive bodies, particularly albitite rocks, were often not distinct for they are selectively small features and produce landforms similar to bedded metasedimentary rocks.

Three very distinctive major rock sectors were defined in accordance with lithological discrimination and spatial distribution: *Sector 1, Sector2* and *Sector 3* (Fig.II.9) :

Sector 1 covers all the eastern and central portions of the study area, extending from Nya-Kasika to Tshondo villages (Fig.I.7). Among its distinctive characters are deeply dipping layered units, structurally controlled valleys and a high density drainage pattern. The domain exhibits extensive, uniformly textured terrane, criss- crossed by long and curved fractures dissecting metamorphic rocks (Shale, sandstone, phyllite, conglomerate (Fig.II.5).

Sector 2 occupies the western portion of the study area, from Tshondo to Kalama villages. It shows a very persistent north to northwest ridge-and- valley pattern, with selective weathering , indicating interbedded resistant units (quartzites) and non resistant units (schists).

Sector 3 lies in the northern part of the study area and is characterised by lava flow (flood basalt) and associated pyroclastic rocks. These rocks are distinguished by their lobate patterns ,flow structure (channels) and surface characteristics, expressed topographically. They form nearly level plains before dissection, and being resistant to erosion, have produced a plateau : " Ngweshe plateau." (1600 amsl).

Two small dissected volcanic cones are visible in the northern part of this area.

4.6.- MAGNETIC FEATURES .

An aeromagnetic field survey was acquired over the Kadubu area (Fig.II.6). The most important magnetic minerals are iron-titanium oxides which are naturally occuring ferrites. The composition of iron-titanium oxide minerals from black shale of the Kadubu metasediments is graphically illustrated on the ternary oxide diagram (Fig.II.6c) and shows that wustite is the type of ferrimagnetic mineral which influences rock magnetism in this area.

The aeromagnetic map covers a varied geological terranes and shows some various anomaly patterns. Some anomalies are clearly related to surface geology of the Kadubu metasediments and are well defined, whereas others appear to reflect major buried structures of the Kibaran basement and are more diffuse. The pattern of the magnetic anomalies shows also a good concordance/correlation with the geological features recorded and adds a wealth of additional features of structural and stratigraphic importance.

The Kadubu area as outlined on Fig.II.6a is an elongate structure with the major axis striking in a NW - NNW direction. The magnetic anomaly map (Fig.II.6a) suggests that there are abrupt changes in magnetic properties within rock units/ formations. The anomalies includes outcrops of the upper and lower Kadubu groups.

Two main domains of different magnetic character are defined: the Eastern domain of deeper diffuse anomalies and the Western domain of shallow sharper anomalies. (Fig.II.6; Fig.II.6a,b). The Eastern area is dominated by well defined negative anomalies reflecting stratigraphic units in the upper Kadubu metasediments. It contrasts with the more or less " quiet" ; positive area of smooth anomalies to the west. The difference of amplitude of the total magnetic field is significantly higher in eastern domain (> 650 nT and < - 900 nT) than western domain (> + 100 nT to + 400 nT) reflecting primary lithological differences. The linear gradient separating both areas is associated with the Tshondo fault zone . (Fig.II.6a and Fig.II.6b)
Magnetic anomalies induced by volcanism located within the northeastern area are limited in size.

Synform and antiform structures were identified and interpreted as synclines and anticlines with N-S to NW - SE directed axes suggesting a E - W direction of shortening. Extensive linear features are attributed to isoclinally folded formations, comprising black graphitic shales/schists sandstone and conglomerate containing magnetite- bearing units.

The largest part of the eastern domain is characterised by alternate positive and negative anomalies magnetic lineation, ranging from - 900 nT to + 690 nT and trending N to NNW.
Linear N to NW striking positive anomalies best developed in the eastern domain correlate to mapped matrix supported conglomerate of upper Kadubu group. This conglomerate is interpreted to extend as a broad subcircular mass in central part (Bugoyi locality). Furthermore to the east, the linear N striking high anomaly coincide with the lenticular conglomerate of the upper Kadubu group (Nya-Kasiba formation).The elongate very low total magnetic field between them is associated with the black shale and phyllite of the upper Kadubu group (Tsibangu formation).

The Twangiza deposit is interpreted as being situated in the axial zone of a large anticlinal structure flanked by synclinal features, all with NNW trending axial traces.(Fig.II.6a , Fig.II.6b). The pronounced magnetic - low anomaly could be associated with deep -seated granitic intrusions and reflect a possible sub-surface ore bodies. Over the mineralized bodies of the Twangiza deposit, the extent of the lode gold mineralization is picked out clearly by pronounced negative linear magnetic anomalies. These could be caused in part by demagnetization associated with sulphidation of iron oxides which characterises the mineralization.
A series of two other localised negative high anomalies in the central part, are thought to be due to the Tshondo and the Kashwa ore bodies (Fig.II.6a).

The outcropping and suboutcropping quartzite and schist of the lower Kadubu group (Kalama and Mudubwe formations) give rise to prominent anomalies marking the western domain.
The dislocations of contours and the steep and linear form of the gradients in a number of areas suggest major faults while the long, narrow patterns are considered to be due to tectonic shear zones with magnetic impregnation.
A qualitative interpretation of some major anomaly patterns is shows in Fig.II.6a; Fig.II.6b Fig.II.7 and Fig.II.16.

4.7.- SUMMARY AND DISCUSSION.

The Kadubu area constitutes the type area of the Itombwe synclinorium supergroup. The most striking physiographical features of this area are the mountain ranges of the western branch of the east African rift system, which have deeply incised valleys with rain forest within them.
The Kadubu river drains a large part of the study area and has a basin area of 25,000 sq km.
The area experiences a semi humid, tropical climate. Deep weathering profile, is strongly developed producing some distinctive landforms.
Various terrace levels can be developed up to 350m above the present profile of some streams.
The Kadubu river and its tributaries display a high density dentritic to angular pattern, and run along very narrow to incised valleys with two main directions : NNW-SSE and NNE-SSW.

A combination of aerial photographs, Landsat TM imagery and aeromagnetic data readily distinguishes the lithology and structures of the study area.
Linear structures have been classified into several groups according to their shape, direction and extent. The dominant trends of the belt is NW to NNW. Three zones have been separated in accordance with main structural patterns and spatial distribution. The relationship and association of two lineament corridors to gold occurrences are noticeable. Two major shear zones running respectively N-S and E-W have been observed. Three very distinctive major rocks sectors have been separated and defined in accordance with lithological dicrimination and spatial distribution..
Aeromagnetic map shows various anomaly patterns which include linearity, and dislocation of contours. Geomagnetic field displays a good correlation /concordance between the geology and the pattern of magnetic anomalies and define two domains of different magnetic charactere separated by Tshondo fault zone: the eastern domain of deeper diffuse anomalies and the western of shallow sharper anomalies.
Extensive linear features are attributed to isoclinally folded formations comprising black shale /schists containing magnetite- bearing units. The dislocation of contours and the steep and linear form of the gradients in a number of areas suggest major faults while the long, narrow patterns are considered to be tectonic shear zones with magnetic impregnation.
Pronounced negative anomalies pick out clearly the extent of the Twangiza lode gold mineralization.

CHAPTER 5.- LIHOSTRATIGRAPHY, PETROGRAPHY AND GEOCHEMISTRY.

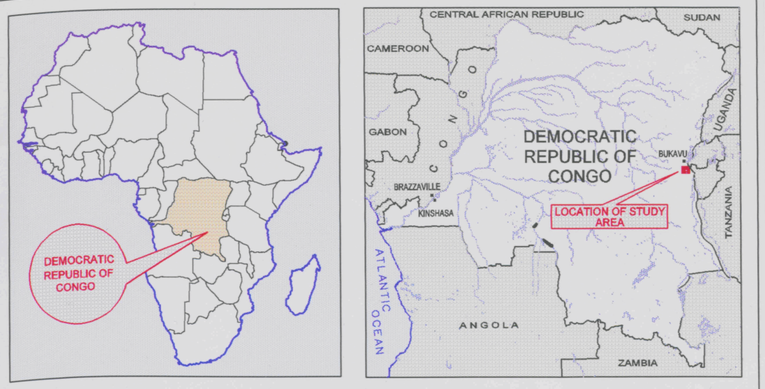
5.1.- GENERAL STATEMENT.

The study area forms a part of the Itombwe synclinorium Supergroup. The synclinorium is arcuate a more or less 35 km wide north-south trending tectonic unit extending for about 125 km; from the Luemba village, south Tanganyila lake, in the south (~ 4^0 00'south), to the north Kivu lake (~ 1^0 30' north), in north. (Fig.I.1; Fig.I.7). Exposures of Kibaran basement rocks occur to the East and West of the area. (Fig.II.6).

The investigated area is composed of three different geological groups subdivided into eight formations, which are intruded by igneous rocks and quartz-veins and /or covered locally by recent formations. From west to east, the main groups include the following: The Kibaran basement composed of the Kasika formation, the lower Kadubu group with three formations , the upper Kadubu group with two formations and again the Kibaran basement with one formation. The lower and upper Kadubu groups are in tectonic contact with the Kibaran basement. An other tectonic contact ; the Tshondo fault, divides both Kadubu groups (Fig.II.16).
The northern part has been mostly covered by rift related basalts.

This classification scheme is based on broad lithologic characteristics. The western group (the lower Kadubu group) consists of a monotonous cyclic sequence of psammitic and phyllitic horizons of the Kalama and Mudubwe formations, whereas, the eastern group (the Upper Kadubu group) is comprised mainly of an alternation of conglomeratic, slaty phyllitic and arenaceous metasediments (The Nya-Kasiba and Tsibangu formations). Fig.II.16.
The basic stratigraphic approach adopted is a lithostratigraphic one based entirely on lithology and is not intended to have a genetic implication. Almost all these metasediments have undergone deep weathering with fresh rocks appearing at depth of up to 250m.

Flyschlike (metasediments) of the upper and lower Kadubu groups were deposited in a linear structural depresssion. The term "flysch" as used herein follows the definition proposed by Hsi (1970) and designates interbedded coarse and fine sediments deposited in a marine geosynclinal environment.



LEGEND

RECENT FORMATIONS

- Alluvial and eluvial erractic
- Stone-line river-terrace gravel
- Basalt and tuffite
- Thermal spring deposit: Calc tuff: Travertine

STRUCTURAL SUCCESSION

	FORMATION	LITHOLOGY
ITOMBWE SYNCLINORIUM SUPERGROUP (NEO PROTEROZOIC)	THE UPPER KADUBU GROUP — TSIBANGU	Matrix supported conglomerate; Phyllite and siltstone schist; Black shale with quartzitic sandstone
	THE UPPER KADUBU GROUP — NYA - KASIBA	Quartzitic conglomerate; Graphitic black shale; Lenticular conglomerate
	TECTONIC CONTACT	
	THE LOWER KADUBU GROUP — MUDUBWE	Cyclic sequence of schists, Greywacke, and pebbly arkosic sandstone
	THE LOWER KADUBU GROUP — KALAMA	Alternation of quartzites and Quartz-sericitic-schists
	THE LOWER KADUBU GROUP — KIGOGO CONGLOMERATE	Conglomerate
	ANGULAR UNCONFORMITY	
KIBARAN BASEMENT (MESOPROTEROZOIC)	BANGWE FORMATION	Quartzitic Bands
	KASIKA FORMATION	Micaschist grading to graphic schist
IGNEOUS ROCKS — TWANGIZA	ALBITITE	Metaluminous
IGNEOUS ROCKS — KASIKA	GRANITE	Leucocratic, peraluminous

- Thermal spring
- Gold deposit
- Tin deposit
- Trigonometrical beacon with ground level in feet
- Geological contacts (Observed and/or inferred)
- Strike and dip of strata
- Strike and dip of foliation plane
- Horizontal strata
- Vertical strata
- Vertical foliation plane
- Thrust fault
- Fault
- Fold
- Fault
- Shear zone

Magnetic Features

- Major shear - fault with down throw
- Strike-slip fault, arrows indicate relative lateral displacement
- Fluid outflow
- Shear zone (KSZ, LSZ)
- Anticline structure
- Axis of anticline
- Axis of syncline
- Syncline structure
- Main roads
- River stream
- Swamp

EAST - WEST CROSS SECTION ALONG LATITUDE 2°53'S

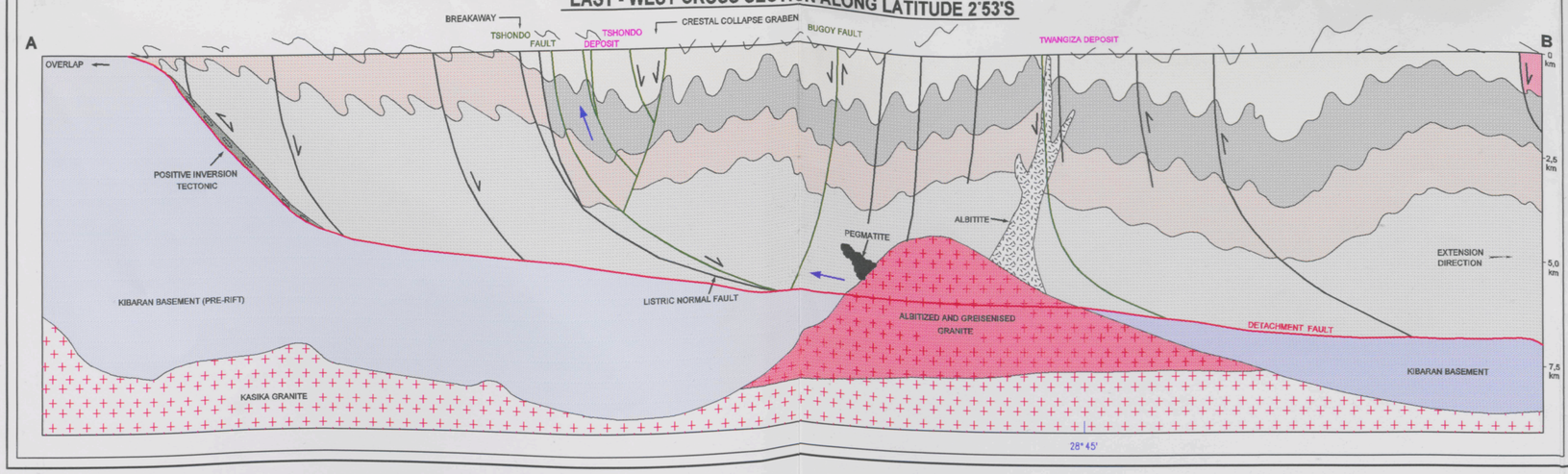


Figure II.16

DEMOCRATIC REPUBLIC OF CONGO

KADUBU AREA

GEOLOGICAL AND STRUCTURAL MAP

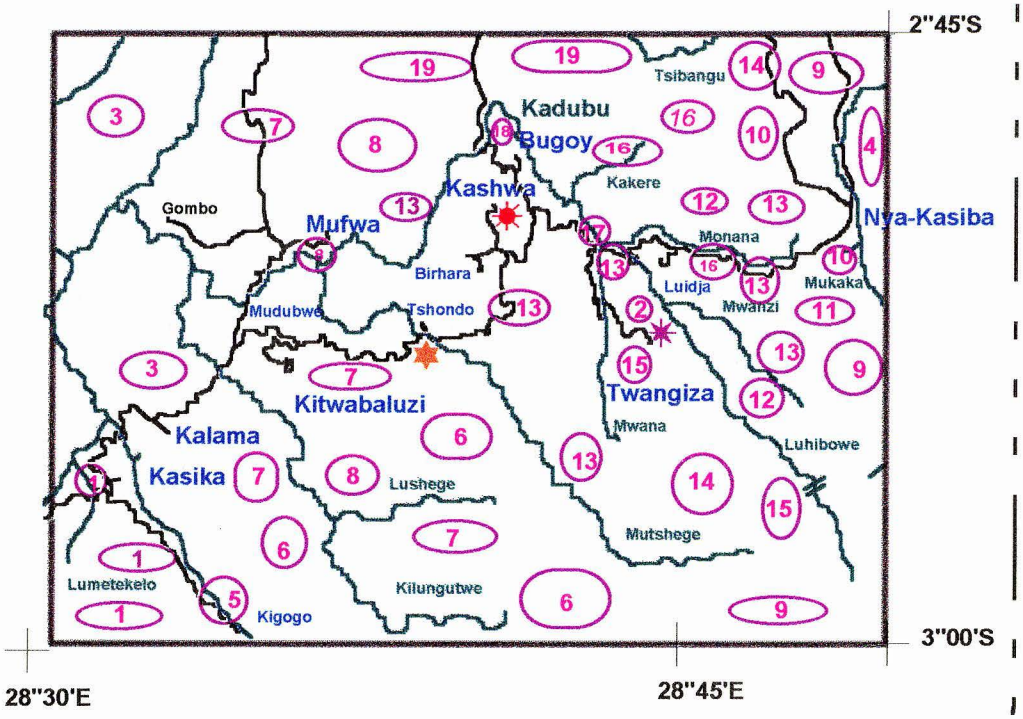
1000m 0 1 2 3 4 5Km

Scale 1 : 100 000

GEOLOGY BY : K M WALEMBA (1998)

GEOCAD CADN3298.DGN

Fig.II.16a :- Spatial distribution of some outcrops of units described within the formations of the lower and upper Kadubu groups.



Recent formations.

19 - The Ngweshe basalt.
18 - Travertine deposit.
17 - Nambo stone line gravel terrace.

The Upper Kadubu group.

16 - Polymictic conglomerate.
15 - Arkosic sandstone
14 - Phyllite :sericite schist and muscovite schist.
13 - Black shale.
12 - Yellow - Phyllite.
11- Graphitic black shale.
10 - Mukuka lenticular conglomerate.
9 - Nya-Kasiba basal conglomerate.

The Lower Kadubu group.

8 - (Meta) greywacke.
7 - Phyllite.
6 - Quartzitic bands with quartz - sericitic - schists.
5 - Kigogo conglomerate

Kibaran basement.

4 - Quartzitic bands.
3 - Micaschist.

Igneous rocks.

2 - Twangiza albitite.
1 - Kasika granite.

Kadubu area

Twangiza gold deposit
Tshondo gold deposit
Kashwa tin deposit

Road
River

KMA Walemba, 2000

Outcrop studies show a complete Bouma sequence (Tsibangu formation) (Bouma, A.H.,1962) that leads to a turbidite model interpretation. No detailed sedimentological work has been done on the sediments, and little is know of the plate tectonic setting of these turbidites.

5.2.- LITHOSTRATIGRAPHY AND PETROGRAPHY .

5.2.1.- KIBARAN BASEMENT.

5.2.1.1.- INTRODUCTION.

The Kibaran formation out crops in the eastern and western extremities of the study area. A bounding fault (to the east) and a bounding thrust fault (to the west) delineate the contacts between the Itombwe synclinorium formations and its basement Kibaran formations (FigII.16).

5.2.1.2.- KASIKA FORMATION (> 500 m >).

This formation, located in the western extremity of the Kadubu study area , is composed of a dark micaschist grading to a black graphitic schist and interbedded with quartzitic bands showing ripple marks (Fig.II.16).

The Kasika granite is intruded into this sequence. A metamorphic change (texture and mineralogy) of the Kasika metasediments occur within the metamorphic aureole around the Kasika granite giving rise to gneiss, mica schist and biotite schist with garnet, disthene and staurotide, quartzite with garnet and tourmaline.

5.2.1.3.- BANGWE FORMATION (> 600m).

Two coarse-grained, saccharoidal, whitish, quartzitic bands, occur in a 100 to 150 m wide quartz schist and sericite schist bed which is brownish to violet in colour, and displays planar cross – bedding (Fig.II.16).

This formation is located in the Luzinzi river , close to Nya-kasiba locality in the eastern part of the study area ; with a north-south striking direction .

5.2.2.-THE LOWER KADUBU GROUP (> 3700 m) .

The Lower Kadubu group is divided into three formations: the Kigogo conglomerate formation, the Kalama formation and the Mudubwe formation. This group consist mostly of fine-grained flysch-type shale /phyllite and turbiditic quartzwackes. Bottom to top, they are as follows:

5.2.2.1.- KIGOGO CONGLOMERATE FORMATION (> 200 m).

This conglomerate, with a clast- supported fabric, is entirely developed in the Kigogo locality and visible along the road between Kasika-Kigogo in the southwesternmost corner of the study area . (Fig.II.16).

The conglomerate is of limited thickness, lenticular and consist mainly of pebbles set in a fine-grained, poorly bedded light-grey to brown- yellowish quartzitic matrix or in a sparse sandy-argillaceous matrix when weathered. The pebbles (0.5cm to 5 cm in size) consist predominantly of angular to subangular quartzites. Veinlets of quartz cross- cut this conglomerate. The conglomerate bed has a strike of N15^{0}W to N80^{0}W, and dips to the east, materializing the base of the Itombwe synclinorium.

Interbedded with the conglomerate and overlying it are steeply dipping finer grained quartzitic sediments composed of quartz and chert fragments in a chloritic matrix . A layer of calcareous dolomites, some 2 to 7m thick overlies the conglomerate . These dolomites are cream-colored and are either well-bedded or have irregular bedding. These rocks are dominated by calcium- and magnesium-carbonate minerals.

5..2.2.2.- KALAMA FORMATION (> 2500 m).

This formation occurs in the southwestern part of the study area (Kalama village) and consists of three quartzitic bands ranging in thickness from 30m to 200m, with sharp lower and upper contacts(Fig.II.16). These quartzitic bands are interbedded with variegated, black and/or bluish sericite schists and micaschist (~ 1m thick) (Fig.II.17).



Fig.II.17:- - Kalama formation . Quartzite interbedded with variegated mica schist. Kilungutwe river in the southwesternmost of the study area.

The quartzite is hard, massive, white or bluish with biotite, muscovite, tourmaline, and locally with garnet and pyrite. It contains crosscutting veinlets of quartz up to ~ 20cm thick.
The quartzite shows clear grading in the more thickly developed units where the grain size is usually coarser. The underside of such larger beds frequently show diagnostic bottom structures such as load casting, groove casting, and flute casts which are generally aligned E-W.

5.2.2.3.- MUDUBWE FORMATION (> 1000 m).

This fornmation consists of an alternating sequence of phyllite, schist, quartzitic sandstone and metagreywacke forming a complex accumulation of metasedimentary rocks. The alternations are generally between 1 and 5 m, although thicker bands are not uncommon. There is a tendency for the finer grained clastics to increase over the coarser grained clastics higher in the sequence The two main rock types of this formation are closely related and form rhythmic units.

5.2.2.3.1.- (Meta)greywacke (> 400 m .

The weathered surface of the metagreywacke is friable, and white to yellowish in colour, with ferrugineous spots, whereas the fresh rock (a quartzwacke), is greyish – black, medium grained and well-sorted. It is sub-mature, massive and may have cross-cutting veinlets. Secondary silicification and recrystallization have affected a large proportion of these greywackes.

The metagreywacke beds have preserved grading and other primary features such as scours, and rare flame structures which are good dissection indicator.

The greywacke units (0.5 to 1 m thick) are massive and dominantly composed of sand-size, subangular to subrounded and moderately to poorly sorted grains of quartz, feldspar and rock fragments scattered in a much finer silty and clayey matrix. Quartz occurs predominantly as angular monocrystalline grains with undulose extinction and polycrystalline fragments. Subangular grains of plagioclase feldspar (oligoclase), are the most abundant, whereas, microcline is rare. The feldspars are mostly altered and clouded with sericite and clay materials. (Fig. II.18).





Fig.II.18:-: - Mudubwe formation. Alternating sequence of phyllite, schist and quartzitic sandstone. Kilungutwe river in the southernmost of the study area.

*5.2.2.3.2.- **Phyllite (> 600 m).***

The phyllite grades into the schist in the southwest part of the area and conformably overlies the greywackes. It is banded and variegated , the banding being defined by centimetre-thick alternations of light silty layers and phyllitic layers. It is multicoloured with a grey- bluish colour predominating when fresh and usually weathering to a fissile reddish-brown material (Fig,II.19).

5.2.3.- THE UPPER KADUBU GROUP (> 3500 m).

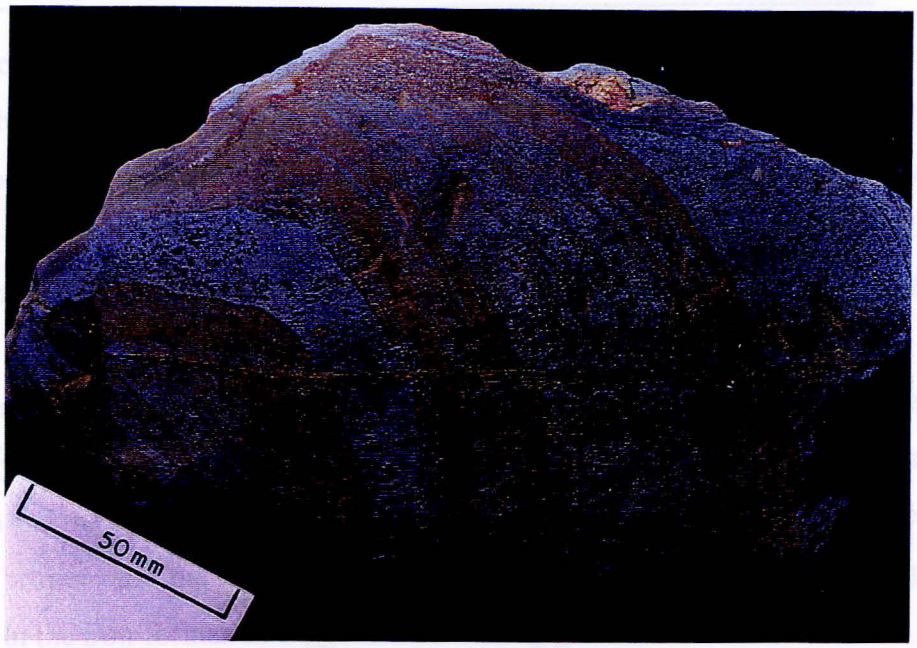
From structural data, two formations with a total of eight lithological units have been defined. These units conformably overlie one another. The upper Kadubu group (Tsibangu formation) unconformably overlies the lower Kadubu group unit (Nya-Kasiba basal conglomerate formation) in the easternmost part of the study area. From bottom to top, they are as follows:

5.2.3.1.- NYA-KASIBA SEDIMENTARY FORMATION (> 1000m).

The Nya – Kasiba formation comprises four units: Nya -Kasiba basal conglomerate, quartzitic lenticular conglomerate, graphitic black shale, and yellow phyllite, with the type locality located within the Nya – Kasiba village .

5.2.3.1.1.- Unit 1 : Nya -Kasiba basal conglomerate (> 500 m).

This is a matrix supported yellowish -grey , conglomerate, up to 500m thick with type locality in the Luzinzi river. The pebbles are mainly quartzitic or quartzitic sandstone in composition, range in size from 2cm to 35cm and are ovoid, polygonal, angular to sub-rounded in shape. The matrix is a fine- grained micaceous quartzite, with ripple-marks. This well-sorted matrix-supported conglomerate passes upward into conglomeratic quartzites that grade into quartz arenites. In both the conglomeratic and the quartzitic units, parallel beds, massive beds and trough cross beds are present. At several localities, soft sediment deformation, such as load casts and oversteepened cross-beds were noted.



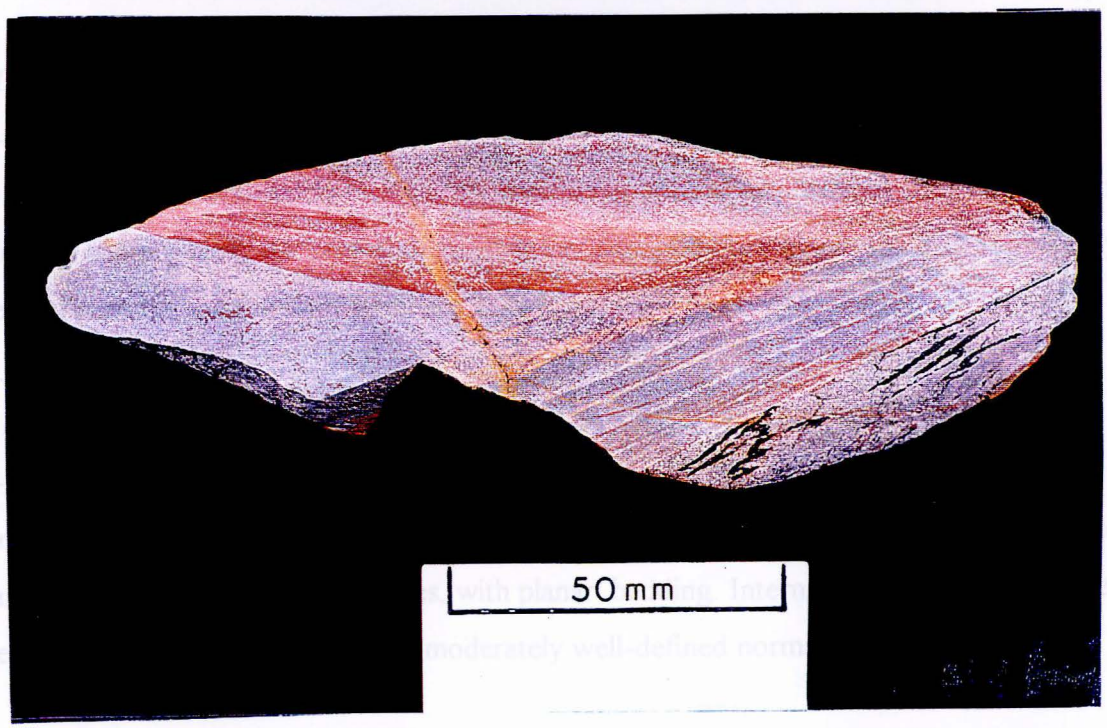


Fig.II.19:- - Cross -laminations within the phyllitic Mudubwe formation. Kitwabaluzi locality.

5.2.3.1.2.-Unit 2 : Mukuka Quartzitic lenticular conglomerate (100-200 m).

Yellowish to light greyish in outcrop, lenticular, laminated , this oligomictic conglomerate consists largely of heterogranular (2cm to 10cm of size), dropstones , and sub-rounded to angular quartzitic pebbles. The matrix consists of a fine-grained micaceous sandstone with ripple-marks and scour –marks. The laminated facies exhibits multiple-graded layers which could have been produced in glacially-influenced environment . Limonitic staining is common. (Fig.II.20).

Iron-rich strata including iron-Formation in the form of laminated -bedded hematite and jasper conformably overlies the Mukuka oligomictic conglomerate and forms a prominent horizon in the Lulindja and the Nganda localities. These appear to be a gradational contact between the iron-formation proper and the underlying Mukuka oligomictic conglomerate. The presence of dropstones in the iron-formation suggests a continuing glacial influence.

5.2.3.1.3.-Unit 3 : Graphitic black shale (50-100 m).

This is a fine-grained and finely laminated, crumbly, graphitic argillaceous rock occurring in the Mukuka river , close to Nya-Kasiba village. The graphitic black shale is rythmically interbedded with the oligomictic lenticular conglomerate. (Fig.II.21).

5.2.3.1.4.-Unit 4 : Yellow-Phyllite (500 - 750 m).

This unit comprises thin-bedded yellow phyllite (sericite schist), with intercalations of fine to medium grained feldspathique quartzites, with planar bedding. Internal sedimentary structures include parallel lamination and poor to moderately well-defined normal distribution grading .

5.2.3.2.- TSIBANGU FORMATION (> 2000 m).

The Tsibangu formation contains the four following units from bottom to top :





Fig.II.20:- Oligomictic conglomerate with laminated facies and turbidites . Note graded laminations identifying origin as turbidites. Mukuka river, Nya -Kasiba locality.

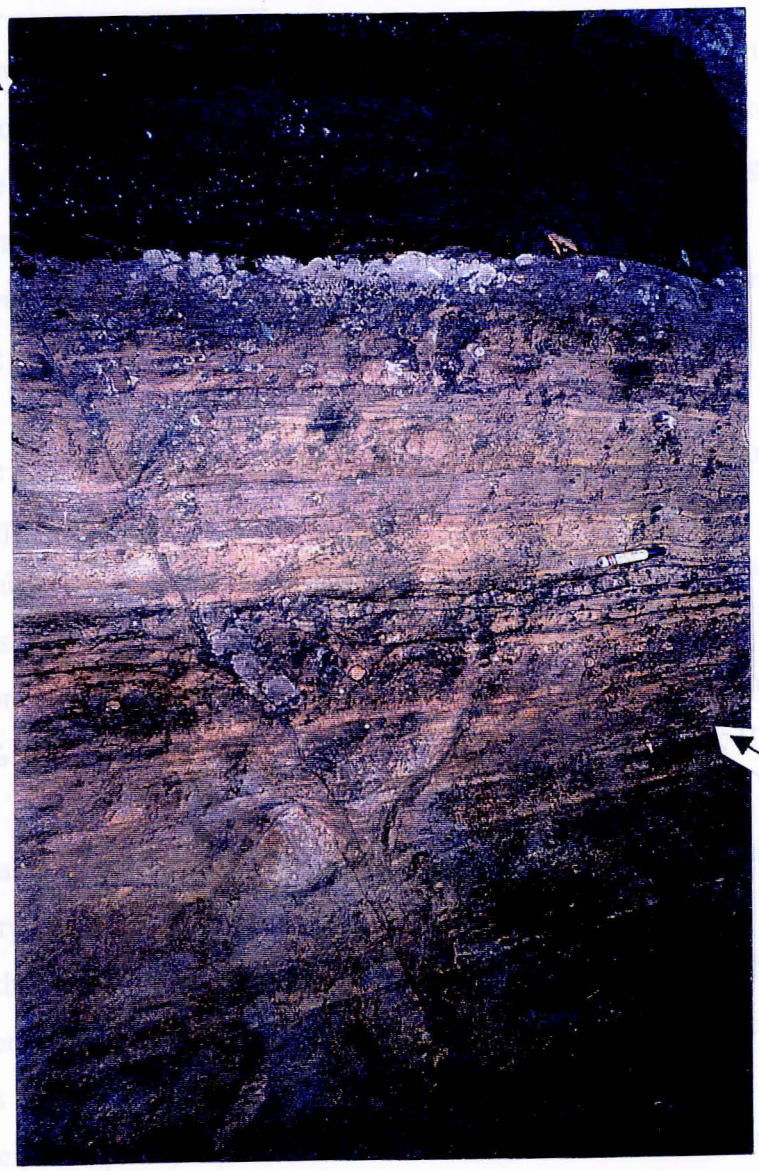


Fig.II.21:- - The graphitic black shale overlying the quartzitic oligomictic conglomerate. Mukuka river, Nya -Kasiba locality. The quartzitic oligomictic conglomerate shows a laminated facies , with dropstones and subrounded clasts and is interpreted as glaciomarine rhytmite. Large and medium exotic igneous clasts were probably dropped from floating ice during deposition of the conglomerate . A late fracture is visible in the rock.

5.2.3.2.1.- ***Unit 1: Black shale (> 600 m).***

The black shale is moderately to strongly graphitic , well- bedded to thinly laminated with some indurated and/or silicified horizons. The fresh black shale is often very hard, sometimes , siliceous, with pyrite and arsenopyrite in the form of cubes, nodules and irregular specks or infillings in the cleavage fracture.

When exposed to weathering, it becomes soft, greyish or whitish in colour with ferruginous veining,and staining on fractures planes which may contain brown clay (Fig.II.22).

Microscopically, the rock is an extremely fine grained, carbon-rich, sercite-quartz schist.
The micaceous component defines a crenulation cleavage with carbon being concentrated along the axes of this cleavage at a high angle to the schistocity. The rock is traversed by quartz-chlorite veins which, to some extent, are parallel to the carbon areas.
The rock is a carbonaceous sericite-quartz schist, with an average composition by volume of : 72% sericite, 15% quartz, 10% carbon, 2-3% chlorite, <1% rutile (Fig., II.23).

*-Sericite , occurs as oriented flakes , up to 0.04mm long, somewhat iron-stained, that define a strong schistosity.

*-Quartz occurs either in deformed veins, up to 3mm wide, transecting the rock at a high angle to foliation, or occurs as a very fine grains , < 0.03mm across, concentrated in lenticular streaks parallel to foliation.

*-Carbon is extremely fine, poorly crystalline material between the mica flakes and concentrated linearly along axes of crenulation cleavage.

*-Chlorite occurs in the outer zone of quartz veins

*-Rutile is rare and occurs as very small grains distributed throughtout sericite.

5.2.3.2.2.- ***Unit 2 : Phyllite : sericite schist and muscovite schist (> 600 m).***

Phyllite forms the bulk of the argillaceous sediments of this unit , is homogenous, with a grey – brownish color on fresh exposures and is located throughtout the central and eastern parts of the study area , with the Luidja area being the type locality (Fig.II.16).



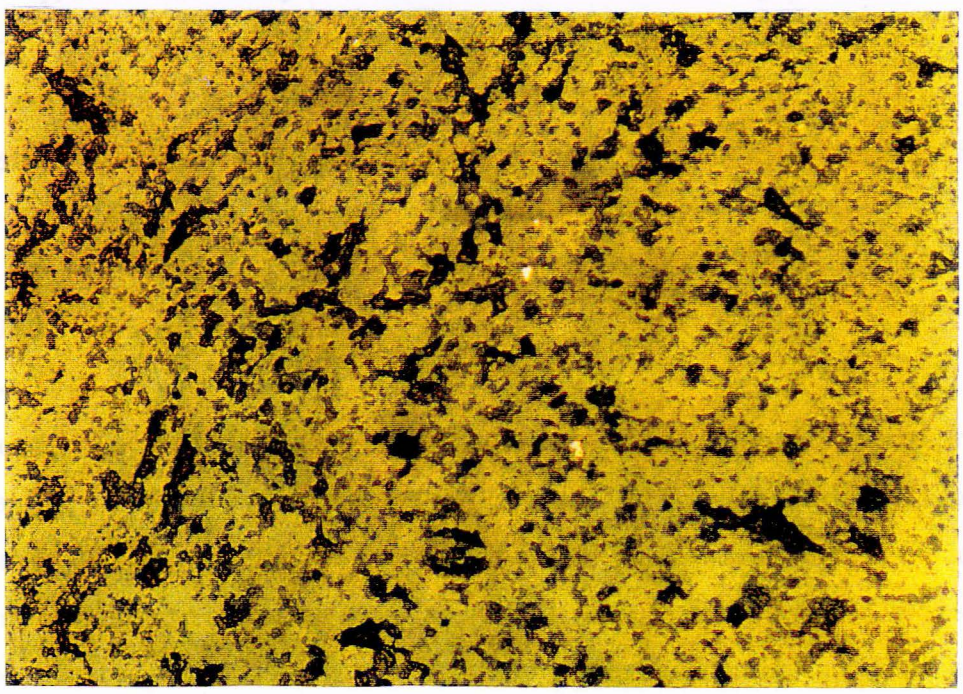


Fig.II.22:- Fold and cleavage morphology within interbedded black shale, silstone and sandstone of the Kadubu area. Luidja locality.

Fig.II.23:- Photomicrograph of black shale.

In outcrop, the rock tends to weather to a redish –purple color and is sometimes grey to dark-grey, and yellowish -grey. The redish –purple could be indicative of iron in the oxidized ferric state, whereas, dark grey is interpreted as indicating a rather high content of organic carbon.

The fresh rock is compact and exhibits a well- defined fissility and slaty cleavage. Thin bands of siltstone are developed in places , the controlling factor being the relative proportion of silt to clay. The siltstone is typically yellowish – grey in colour but with occasional red or purple patches due to local concentrations of iron . The phyllite tends to be slightly fissile in places due to flakes of white mica . The contact between sericite schist and muscovite schist is gradual and alternations of the two rocks occur. The phyllites are rythmically interbedded and interlaminated with the quartzitic sandstone (1 cm to 2 m thick beds) (Fig.II.24).

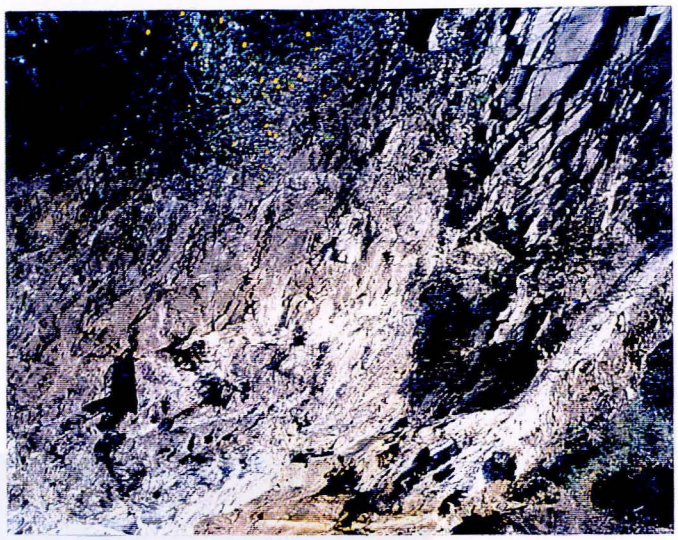
Miroscopically, It consists mainly of a matted mixture of silt- and clay sized grains of quartz, feldspar, clay minerals (mainly illite) associated with chlorite, epidote, opaque minerals, muscovite and apatite. Authigenic coarsely-crystalline calcite patches, chlorite flakes, and epidote grains, in addition to muscovite, were probably formed almost entirely from the diagenetic break-down of the clay fraction of the matrix (Fig.II.25).

5.2.3.2.3.- *Unit 3 : Arkosic Sandstone (> 3 m).*

This unit consists essentially of medium-to coarse-grained arkosic sandstone, poorly sorted , and occurring as thin and massively recrystallised regular bands of 1 to 3m thickness. These are not continous over long distances and are interbedded within black shales. Most of the sandstone is light grey to whitish in colour but locally weathered surfaces may be stained reddish-brown by iron oxide. In the easternmost area, the sandstone grades into a pebbly quartzitic sandstone. (Fig.II.26).

5.2.3.2.4.- *Unit 4 : Polymictic conglomerate (diamictite, tillite) (> 800 m).*

This conglomerate forms the most clearly distinguishable major mappable unit in the central and eastern part of the study area and provides an excellent lithostratigraphic marker horizon.



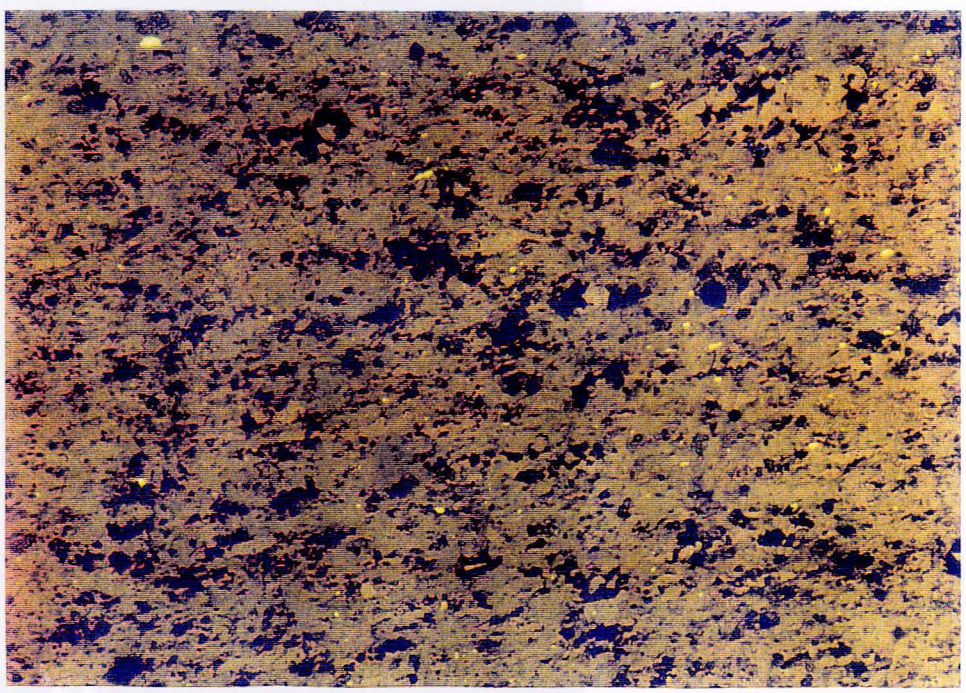


Fig.II.24:- - Phyllite (sericite schist) exhibiting a well -defined fissility and slaty cleavage.

Fig.II.25:- - Photomicrograph of phyllite.



Fig.II.26:- - Arkosic sandstone.

It is a dark, matrix -supported conglomerate, up to 800m thick, strongly silicified, quite hard, and resitant to weathering with scattered large pebbles, cobbles,and boulders in a schistose matrix. The colour varies from blackish (unweathered) to mauvish or greenish (weathered) .

The pebbles are mainly quartzite and include schist, gneiss, granite. The pebbles are sub- rounded to rounded in shape, and range in size from 1cm to 40 cm of size. The orientation of pebbles is elongated parallel to the foliation, mostly N-S to NNW-SSE. The conglomerates are fairly well bedded and show no jointing.

The groundmass is noticeable foliated with a schistose texture probably due to the presence of chlorite. Ripple-marks are evident on upper surfaces of bedded units. (Fig.II.27; Fig.II.28).

5.3.- RECENT FORMATIONS.

5.3.1.- THE NGWESHE BASALT.

The Ngweshe basalt forms a part of the Bukavu volcanic district and covers the northern part of the study area .The volcanic rocks include lavas, tuffs, and two small cinder and ash cones.

Most of the lavas are porphyritic with 1-20 vol % phenocrysts . The fine-grained matrix of the basalt consists of clinopyroxene, plagioclase, leucite, +/- olivine, sanidine and minor mica. Phenocrysts comprise various combinations of the same minerals. The lava is (undersaturated ?) and named according to the modal classification of Streckeisen (1967). (Fig.II.29; (Fig.II.30).

5.3.2.- ACTIVE GEOTHERMAL SYSTEM AND TRAVERTIN DEPOSIT.

5.3.2.1.- INTRODUCTION.

Two active thermal spring systems that are considered to be related to the Kadubu gold –bearing deposits have been recognized in the study area: These are the Bugoyi and the Luidja hot – springs situated 5kms and 7kms respectively from Twangiza gold deposit (Fig.II.7). The hot spring areas in a geothermal field are only small parts of a geothermal system. Travertine deposits are associated with the Bugoyi hot –spring .

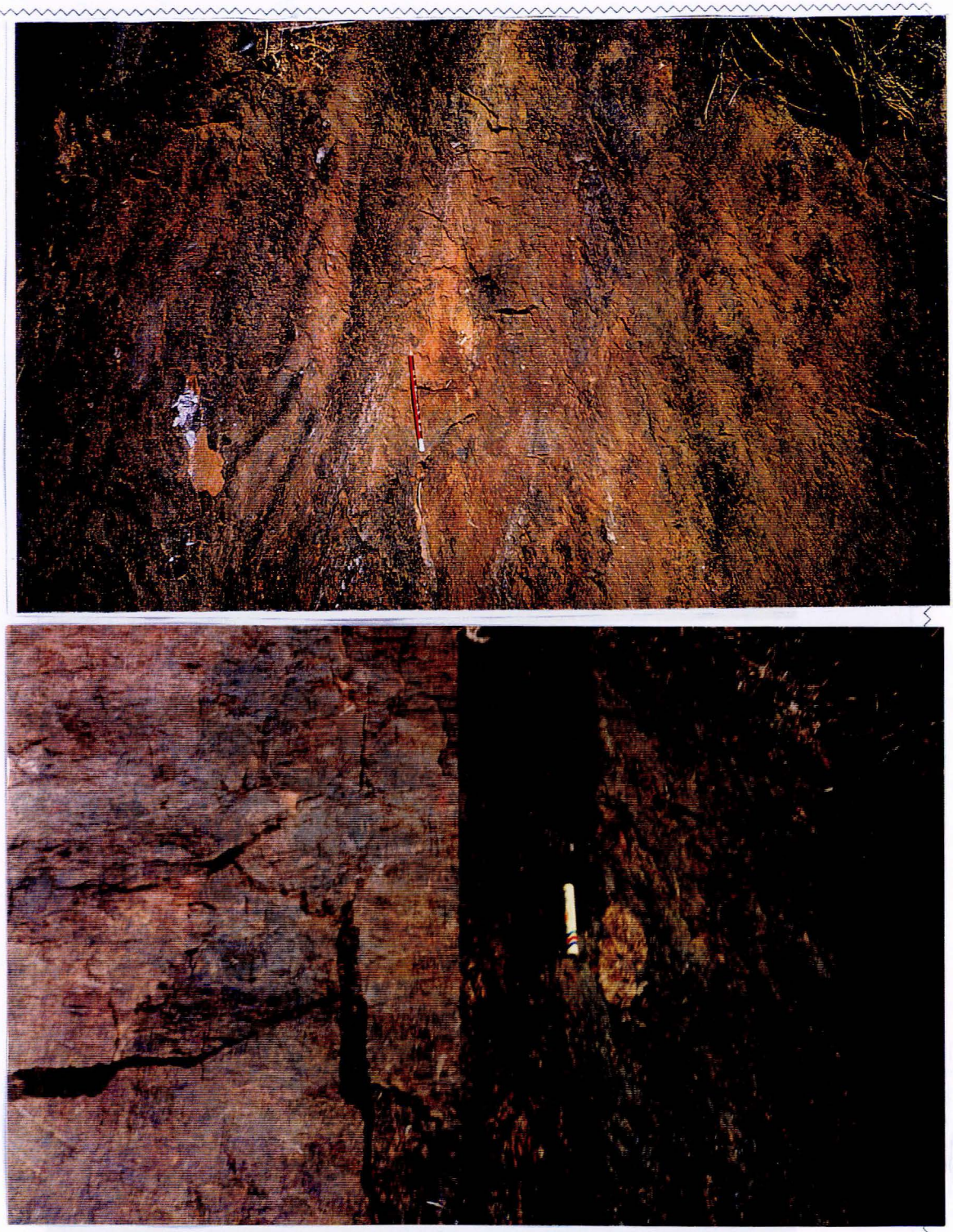


Fig.II.27. -- Intensely deformed and sheared polymictic conglomerate. Clasts of (meta)sedimentary material and quartz veins are highly elongate. Slightly elongate granite clasts are broken and offset. Kahanda locality.



Fig.II.28:- -Hand specimen of polymictic conglomerate , showing quartz vein and granites pebbles.

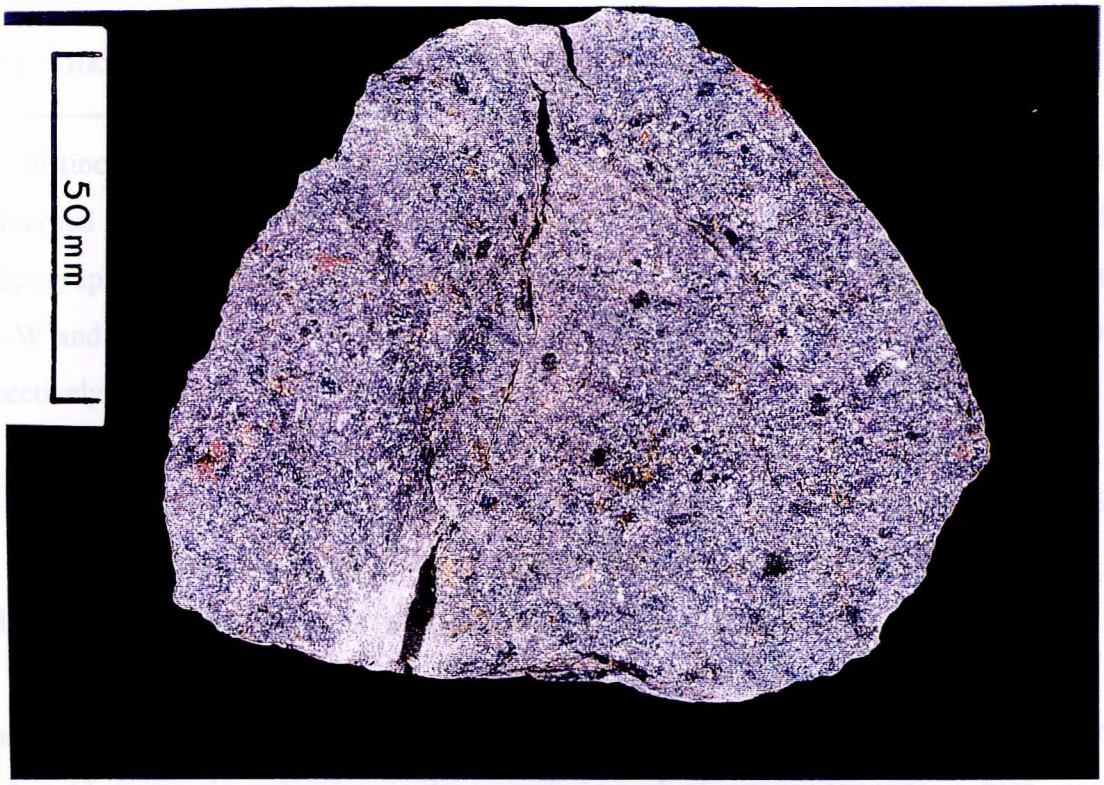




Fig.II.29:- Ngweshe basalt . Bugoyi locality.

Fig.II.30:- - Tuffaceous volcanic rock . Bugoyi locality.

5.3.2.2.- THE LUIDJA-BUGOY HOT SPRINGS.

Two distinctly separate hot spring sites which are approximately 8.5 km apart form the geothermal field recognized in the study area (Fig.II.7).They are fault-controlled and confined to topographic low-points. Spring waters emerge along intersection of major open fractures (E-W and NW trends). The spring waters flow into the rivers (Monana and Tiruembwe respectively) via shallow and narrow channels.

The springs are hot, boiling, and smelling of sulfur with temperatures range of 80^0C to 150^0C and continuous discharges along a 300 to 500 m long zone. Henley and Hedenquist,(1983) and Holl, R.,(1985) give a comprehensive explanation of geothermal system.

Geothermal systems are interpreted in terms of large-scale hydrothermal convection patterns in which cold meteoric water moves downwards in rock structures towards a heat source, absorbing heat and becoming progressively hotter .

The hot water either rises to the surface, if access is possible, and discharge as hot springs, fumaroles or geysers. Hot water reacts, as it rise convectively, with its host rocks and minerals, dissolving some constituents (e.g. silica) and developing a new alteration mineral suite.

The presence of high CO_2 concentrations leads to the extension of boiling conditions to much greater depth than in equivalent gas-free systems. (Holl, R., 1985). Oxidation of H_2S in this near surface environment produces acid-sulphate waters with low chloride contents and pH in the range of 1-4.

Sodium bicarbonate –sulphate waters are common on the margins of systems where steam plus gases condense. They usually have a slightly alkaline pH (7-9) with temperature of < 100-150 ^{o}C (Henley and Hedenquist, 1983).

5.3.2.3.- TRAVERTIN DEPOSITS.

5.3.2.3.1.- FIELD DESCRIPTION.

Travertine is limestone that forms where hot ground waters, rich in calcium and bicarbonate, emerge at springs. Travertine precipitation is rapid and variable, and marked lateral and vertical facies variations are characteristic of these hot spring carbonates. Water chemistry changes quickly as spring waters cool and mix with rain water.

The Luidja hot-spring , within the Luidja locality, exhibits a line of springs ($N30^0W$ & $N70^0E$) discharging freely. It develops extensive marsh deposit accumulated in flats and depressions and consists of yellow-brown mixed lithoclastic and travertine precipitate giving off a sulfur gas smell. Deposition could be observed at the spring vents and continued for many metres downstream. (Fig.II.31).

The Bugoyi hot-spring travertine deposit, the most important, occurs in the Tiruembwe river, located within Bugoyi locality. Proximally, close to the hot spring, white crystalline precipitates form and build cones (Fig.II.32).

Downstream, white crystalline travertine has precipitated to form a terrace system with pool and waterfall (Fig.II.33). Fig.II.33 , is a detail of the Bugoyi travertine showing an oncoidal bed, thin paleosol and phytoclast tufa. This figure shows also the Bugoyi typical waterfall site producing modern tufas in association with macrophyte hummocks (bryophytes) and hanging angiosperm roots. The waterfall is more than 50m high over a black shale bed.

The travertine accumulation crops out as a linear deposit, with thin laminations forming a ridge, 25- 50m high, about a hundred meters wide and extends laterally for approximately five hundred metres. The precise age of the travertine is uncertain but its deposition continues to the present day.

Travertine morphological types include shrub and pisoid. Shrub travertine consists of a porous, friable travertine dominated by small shrub-like growths and pisoid travertine, ranges in shape from spherical, through irregular rounded to irregular subrounded.



Fig.II.31:- - Luidja hot-spring . Monana river , Luidja locality.

Fig.II.32:- - Bugoyi hot-spring travertine. Tiruembwe river. Person for scale.

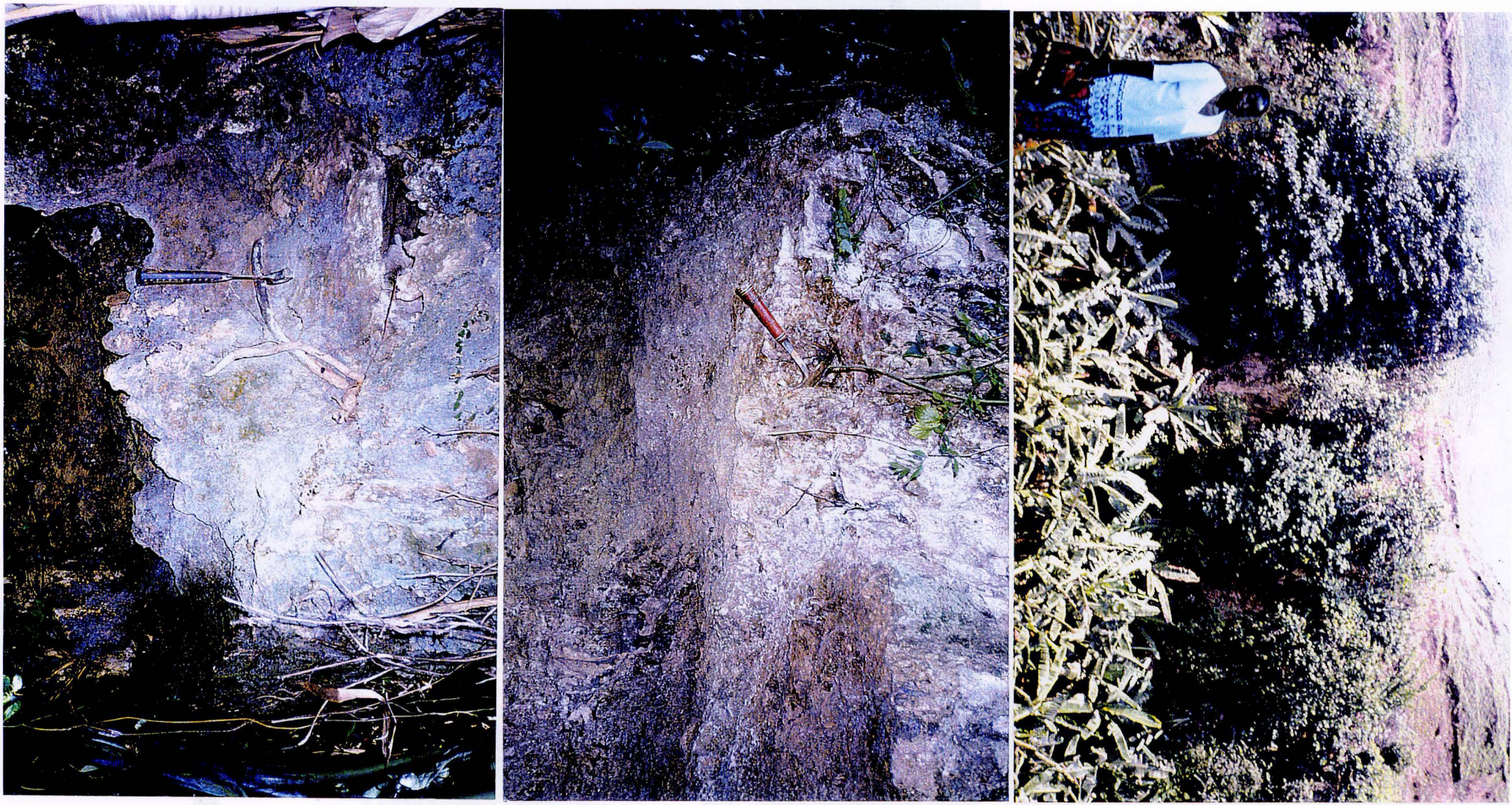






Fig. II.33:- - Detail of a paludal tufa . A typical waterfall site producing modern tufas in association with macrophyte hummocks (bryophytes) and hanging angiosperm roots.

At the waterfall the travertine forms fluted drapes with a fibrous structure and aquatic flora colonize the surface with shrub-like bacterial growths (Fig.II.33).

The beds are horizontal to subhorizontal or gently undulating. The colour is whitish with a pale yellow to pale greenish hue. This discolouration suggest the presence of bacteria. The rock consists of soft, highly porous aragonite associated with minor calcite and various accessory minerals. The aragonite is typically orange, to pale brown. Calcite is white, cream to pink.

5.3.2.3.2.- CHEMISTRY OF BUGOYI TRAVERTINE.

Travertine specimens were taken from the wall of the Bugoyi deposit. The values of the chemical composition of two samples of travertine are shown in Table.II.1.

The low amounts of SiO_2, TiO_2, Al_2O_3 and K_2O represent the contribution of silicate materials to most of the insoluble fraction of this travertine and suggest the presence of opal mineral (Table.II.1). High CaO and LOI values indicate that travertine is essentially built up of calcium carbonate. (Fig. II.34). Iron is mainly present in the travertine as finely scattered oxide.

Mg/Ca ratio may influence precipitation of the $CaCO_3$ polymorphs. (Fig.II.35) .

The chemical characteristics of thermal waters from these different springs have not been analysed.

5.3.2.4.- INTERPRETATION AND SUMMARY.

The requirements for geothermal activity are water, heat, and rapid passage to the surface.

In the Kadubu active geothermal field, water originate as heated meteoric ground water that has seeped down faults and then mixed with condensed steam containing CO_2 and H_2S. A major proportion of meteoric water is required to enable flow. Fluid channels are required and may be produced by natural hydraulic fracturing initiated by normal faults .

It is proposed that the energy that drives the convection system is magmatic and is related to the Kasika leucogranite at depth as well as to the present day rifting process .

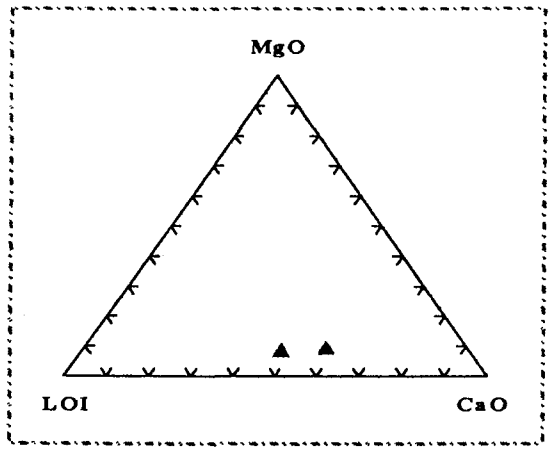
A boiling spring, and the presence of a sulfurous smell, suggests the existence of H_2S, HSO_4, SO_4 etc.. , and implies a deep circulating chloride fluid (Henley & Hedenquist,1983)(Table.II.2).

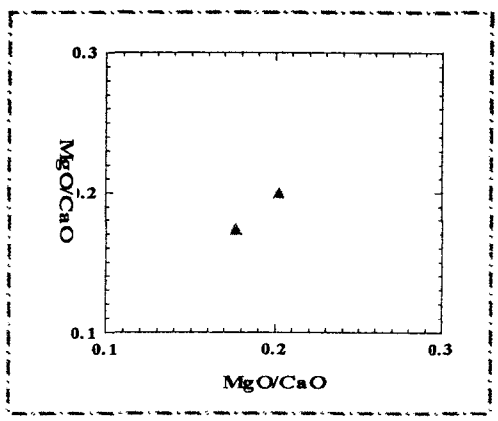
TABLE. II.1 :- CHEMICAL COMPOSITION OF THE BUGOYI TRAVERTINE.

Sample	SiO2	TiO2	Al2O3	Fe2O3	MnO	MgO	CaO	Na2O	K2O	P2O5	F	LOI	Total
KW 716A	13.74	0.21	0.73	1.21	0.04	7.69	38.28	0	0.06	0.04	-	36.6	98.62
KW 716B	17.25	0.39	2.48	-	0.04	7.53	42.92	0.34	0.2	0.26	0.04	25.19	72.29

Sample	FeOT	FeO	Fe2O3T	Cr2O3	V2O5	SO3
KW 716A	8.07	6.96	8.05	-	-	-
KW 716B	-	-	-	0	0	0.06

Sample	Ba	Rb	Sr	Y	Zr	Nb	Th	Pb	Ni	V	Cr	Co
KW 716A	-	-	-	-	-	-	-	-	-	-	-	-
KW 716B	4752.6	-	-	-	-	-	52.98	9.99	-	21.6	-	16.9





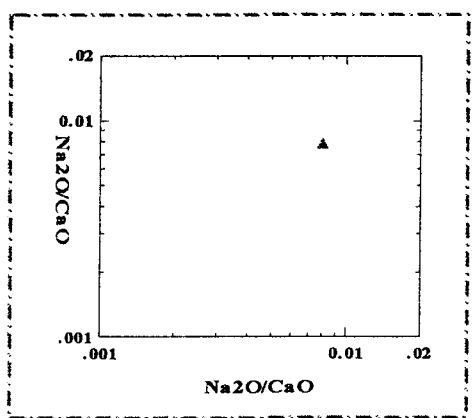


Fig.II.34:- Ternary diagram (MgO - CaO - LOI)
and binary plots (Log MgO/ CaO versus Log MgO / CaO ; Log Na2O / CaO versus Log Na2O / CaO).

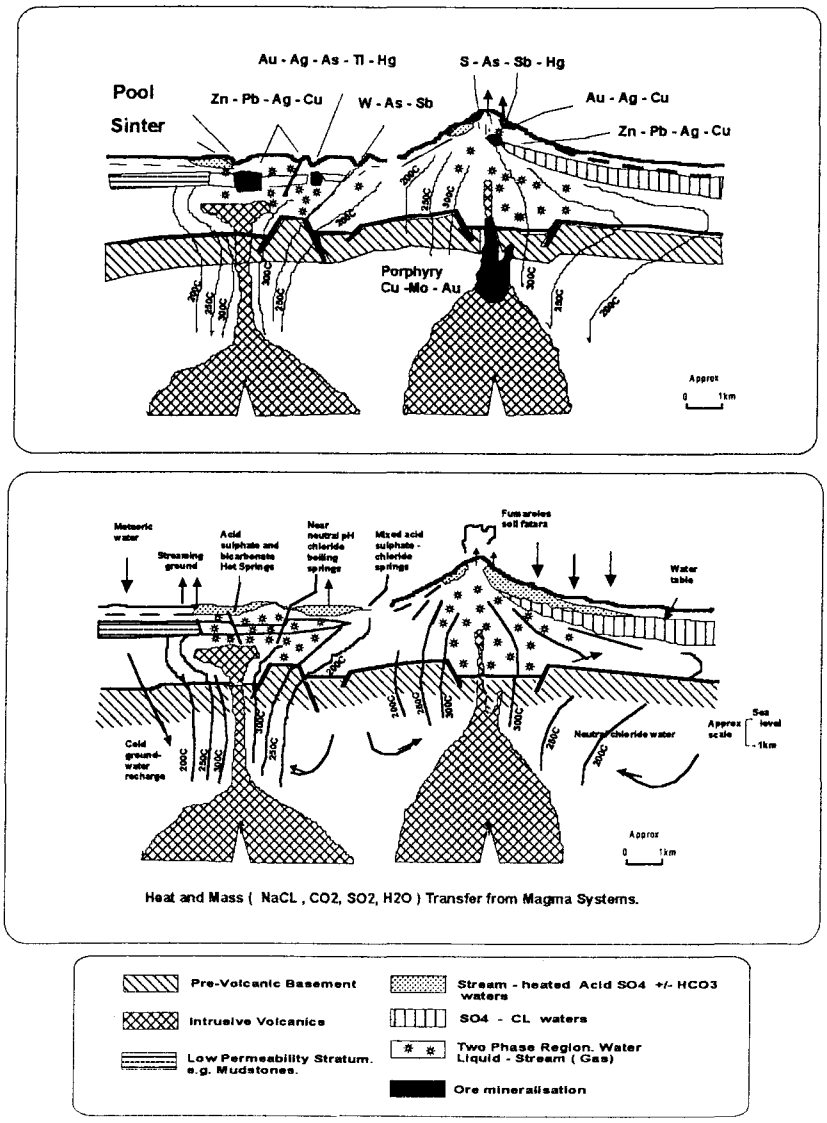


Fig.II.35:- Schemas of the main features of geothermal systems and the environments of Hydrothermal ore deposition. (left: silicic volcanic terrane, right : stratavolcano) (After Henley and Hedenquist, 1983).

Description	Source	Discharge	T C	pH	Cl (ppm)
Chloride	Deep circulation	Boiling spring geyser	200 - 300+	5.5 - 6.5	400 - 1800 + CO2 ; 0.5 - 0.005 m + H2S : 0.02 - 0.0002m + CH4 - H2 - N2 - Ar
Acid sulphate	Surficial condensate	Boiling mud-pool	100 - 130+	< 2 - 3	0
Mixed acid sulphate - chloride	Near surface mixture	Warm - hot spring. Mud -pool	< 100- 130	2 - 4	100 - 500+
Sodium bicarbonate - sulphate	Condensed steam and gas into marginal groundwaters	Warm - hot spring	< 100 - 150	7 - 9	Low

Table. II.2 :- Taupo volcanic Zone fluid characteristics (Data from Henley and Hedenquist, 1983).

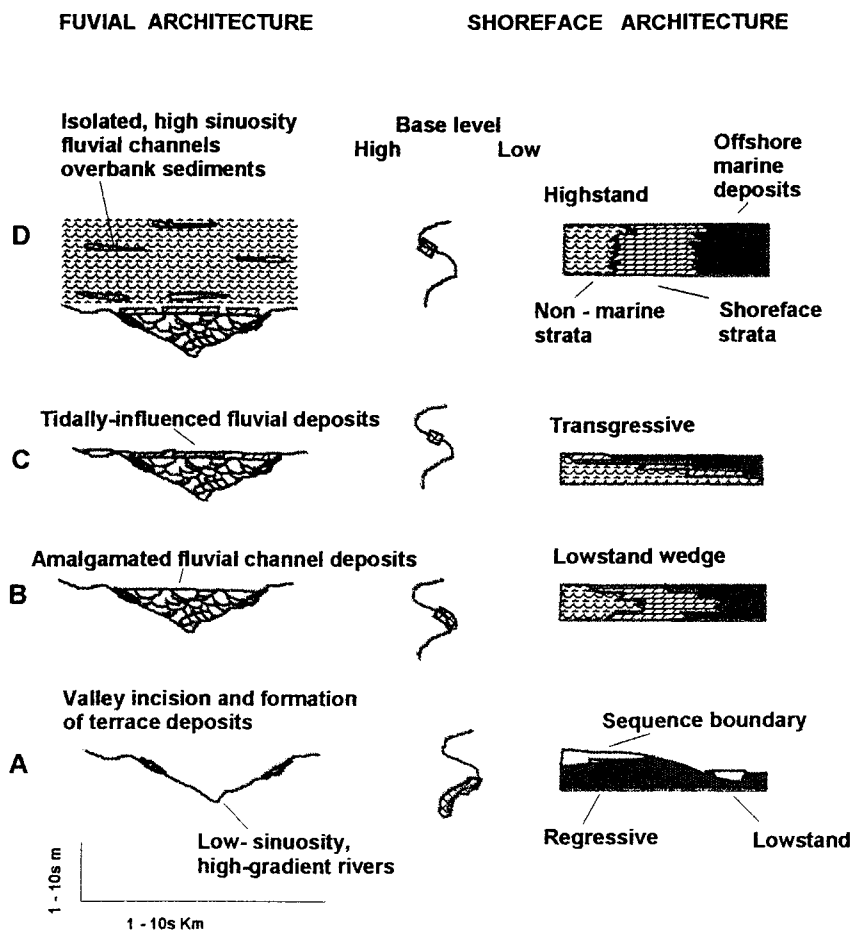


Fig.II.36:- Model for the evolution of an incised valley and its subsequent filling. Coeval changes in nearshore stacking patterns are also shown. Note the incidence of tidal influence and the low channel/ overbank ratio once the rim of palaeovalley has been overtopped. (After Shanley and Mc Cabe, 1993).

Hot springs in the study area could represent a mixing of two hydrotypes ($Ca\text{-}SO_4$ and Na-Cl) with the $Ca\text{-}SO_4$ component prevailing, and with rising gases rich in CO_2 and H_2S.
Travertine deposits are principally associated with $Ca\text{-}SO_4$ and Na-Cl thermal water discharges, but are also precipitated from shallow meteoric waters circulating in metasedimentary formations.

Henley and Hedenquist, (1983) give a model of the main features of geothermal systems and the environments of hydrothermal ore deposition in a volcanic zone (Fig.II.36). The relationship between the active geothermal system in the study area and hydrothermal ore deposits of the region are explored in this study.
According to Healy, (1976); only Quaternary intrusions in the upper crust (< 10km depth), are still active thermally today. Thermal influence due to conductive and convective cooling of the Kasika Kibaran granite, of which tectono-thermal activity is dated at more than 500 Ma old, could not have prevailed to the present day.

However, the presence of two active thermal springs in the area testify to the existence, of a heat source at depth and of an active geothermal system with high heat flow forming large –scale convection patterns operating today .
It is suggested that conductive heat flow originated, from magmatic activity, at depth, reactivated and/or related to the present -day rifting process. Meteoric water is considered to be the main source for the springs.

5.3.3.- NAMBO STONE LINE TERRACE.

5.3.3.1.- INTRODUCTION.

Stream terrace evolution of the Kadubu river was controlled by both climatic change and subsidence. Aggradation followed by rejuvenation of the stream produced the numerous terraces observed in the area. They were probably deposited in consecutive periods with every stage representing an equilibrium in repeated tectonic or erosional processes (Fig.I.7). The most important of these terraces, is the Nambo stone line terrace (Fig.II.37).



Fig.III.37a:- Nambo stone line gravel terrace. Paired terraces and incised valley.



Fig.II.37b:- - Detail of Nambo pedological profile. The upper horizons (H_1 to H_2) are structureless " or "massive " deposited almost entirely directly from suspension. Gravels of (H_3) show faint parallel bedding and overall grading .

Morphologically, the terrace is a flat surface with steep scarp-like slopes bordering the river and found on both sides of the Kadubu river.

Terrace development has given rise to local erosion and in places following of incised valleys by Quaternary deposits with a mature paleosol. Active faults caused the Kadubu river course and terraces to become deformed. Shanley and McCabe, 1993 give a model for the evolution of an incised valley and its subsequent filling (Fig.II.36).

5.3.3.2.- DESCRIPTION OF THE NAMBO TERRACE PEDOLOGICAL PROFILE.

The Nambo terrace pedological profile is composed of four well-differentiated horizons (H_1, H_2, H_3, H_4); from top to bottom (Fig.II.37a, Fig.II.37b):

*- ***H_1*** *Horizon : loose clay horizon; topsoil.*

This horizon consists of fine clayey material with a thickness up to 15m. Very rare isolated blocks of quartz can be observed. The color is brownish to brownish yellow downward.

*- H_2 *Horizon : sandy argillaceous material* , yellow in colour and containing conspicuous quartz grains.

*- ***H_3*** *Horizon : stone line horizon.*

The transition to the H_2 is more or less sharp and well marked. This horizon is marked by a great abundance of coarse fragments accumulated and embedded in a reddish clayey matrix.

The stone line is a continuous horizon of 0.5 to 1.5m thick occuring above the saprolite (H_4). It comprises well rounded, corroded and angular quartz fragments, up to 30cm, and scattered rare iron crust fragments, all set in a iron oxides clay (smectite...) matrix .

These clasts of quartz are of transported alluvial origin, and unconformably sedimented on the black shale bed rock.

*- ***H_4*** *Horizon : Saprolite.*

The contact between H_3 and H_4 is also sharp. H_4 is a weathered black shale exhibiting the schistosity structure of the black shale bed rock .

5.3.3.3.-GEOCHEMISTRY AND ANOMALIES RELATED TO GOLD MINERALIZATION .

Geochemical results above the saprolite were obtained from the channel samples: KW 410 to KW 412 corresponding to H_1, KW 413, corresponding to H_2 and KW 414 and KW 415 to H_3.





Fig.II.37b:- - Detail of Nambo pedological profile. The upper horizons (H_1 to H_2) are structureless " or "massive " deposited almost entirely directly from suspension. Gravels of (H_3) show faint parallel bedding and overall grading. (Continues)

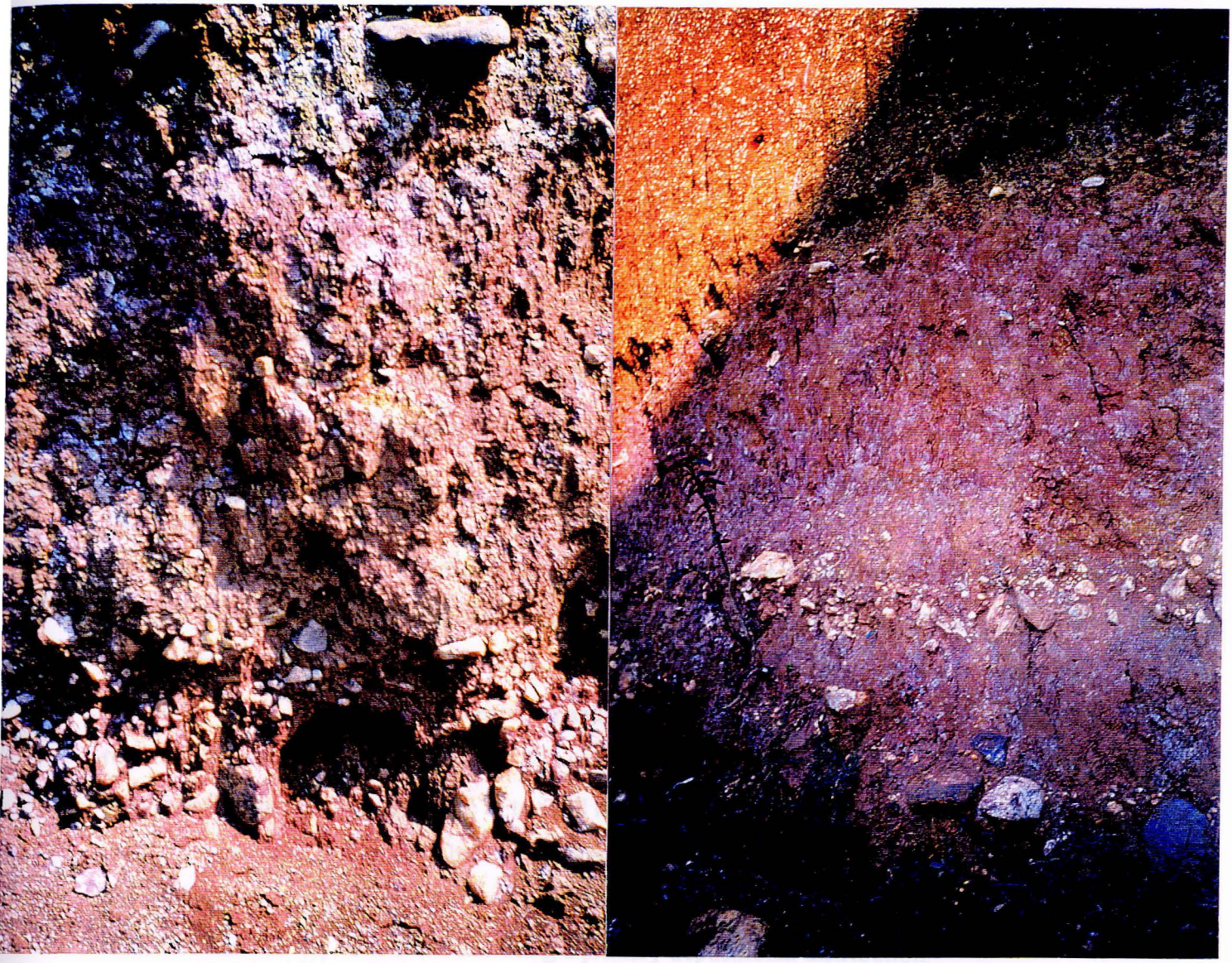




Fig. II.37b: - Detail of Nambo pedological profile. The upper horizons (H_1 to H_2) are structureless " or "massive " deposited almost entirely directly from suspension. Gravels of (H_3) show faint parallel bedding and overall grading. (continues)

Chemical data of the Nambo stone line terrace profile is given in Table.II.3 .

SiO_2 is by far the most abundant constituent with values averaging about 64.28 wt%. This is followed in decreasing abundance by Al_2O_3, Fe_2O_3 and K_2O. The minor oxides (0.1-2.0 wt%), Na_2O, CaO, MgO , P_2O_5 and MnO have been leached and are low in value. Al_2O_3 versus Fe_2O_3 is distinctive for each horizon (Fig.II.38). Major element chemitry is strictly controlled by the mineralogical composition of any horizon. Chemical continuity is observed in the fine matrix sampled from the saprolite H_4 , up to the H_1 horizon.

The profile developed is strongly siliceous, but Fe_2O_3 contents are rather high in the four horizons. Si high : either felsic source or mature sediment. Fe high : ferricrete = dependent on climate conditions with arid periods.

On a Fe_2O_3 - SiO_2 - Al_2O_3 triangular diagram, (Fig.II.38), the data appear to cluster along a silica trend. It is suggested that smectite formation has inferred a migration to the siliceous field.

Various ternary and bivariate plots (Fig.II.38) denote the main chemical and mineralogical evolution related to the main sedimentation and weathering processes, whose combined action resulted in forming the present profile.

Au grade distribution from saprolite to top soil has been evaluated. Gold occurs disseminated in the terrace package, but tends to be concentrated along the stone line horizon H_3 . The high Au contents in the range of 1 ppm to some 10ppm (artisanal workers data) may be observed in the stone line horizon H_3 . The stone line being a primary depositional distribution.

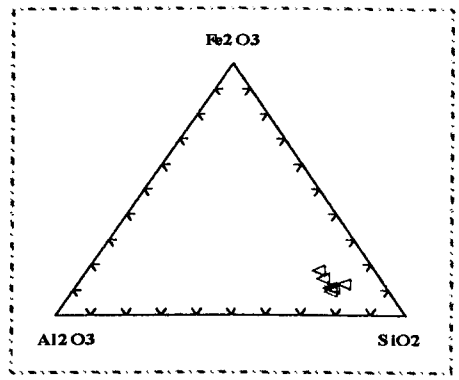
5.3.3.4.- SUMMARY.

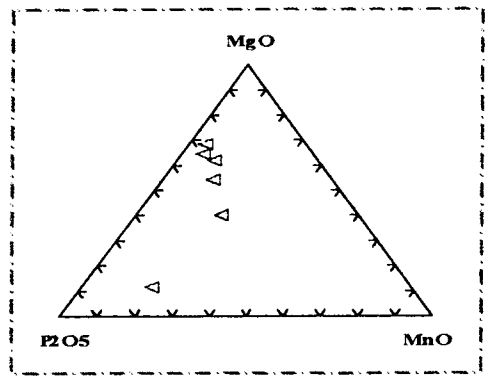
The Nambo terrace pedological profile is characterzed by four main horizons: loose clay , sandy argillaceous material, stone line and saprolite horizon. Major element chemistry is strictly controlled by the mineralogical composition of any horizon.The profile developed is strongly siliceous, but Fe_2O_3 and Al_2O_3 contents are rather high in the four horizons.

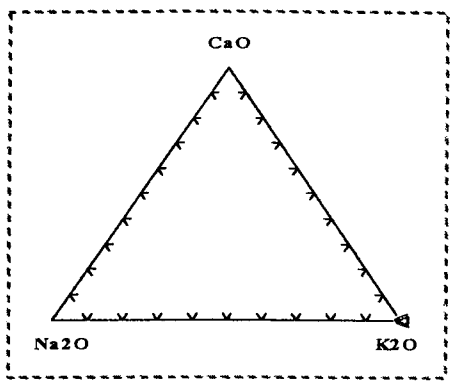
Stream terrace evolution of the Kadubu river was controlled by both climatic change, subsidence and tectonism. Then, climate change and tectonism are interrelated through a complex series of feedback loops. Subsidence, fluctuation of rain volume and the slope of the surface in the area were of sufficient magnitude to deeper incised valleys on erosion. Incision is most likely during times of rapid and large fall of base level. Gold occurs disseminated in the terrace package, but tends to be concentrated along the stone line horizon H_3.

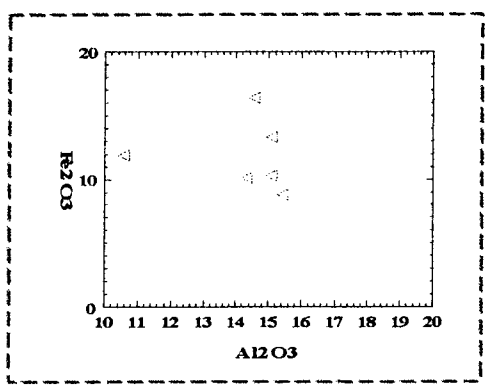
TABLE.II.3 :- CHEMICAL DATA OF THE NAMBO STONE LINE TERRACE PROFILE.

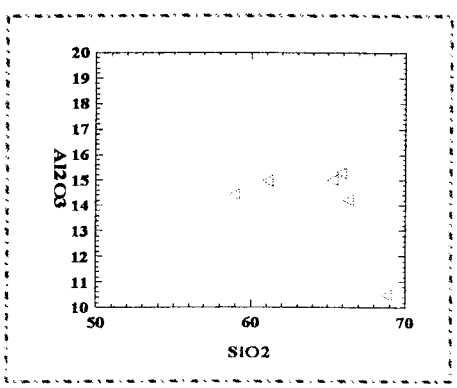
	KW 410	KW 411	KW 412	KW 413	KW 414	KW 415
SiO2 (wt%)	60.97	65.18	68.74	65.78	58.84	66.18
TiO2	1.04	1.61	1.45	1.04	100	1.06
Al2O3	15.02	15.04	10.53	15.35	14.49	14.26
Fe2O3	13.44	10.37	11.95	8.86	16.48	10.2
MnO	0.02	0.06	0.04	0.03	0.06	0.03
MgO	0.38	0.11	0.17	0.2	0.4	0.39
CaO	0	0	0	0	0.01	0
Na2O	0	0	0	0	0	0
K2O	2.19	0.67	0.69	1.22	1.19	2.54
P2O5	0.15	0.1	0.1	0.09	0.23	0.18
LOI	6.51	7.32	5.61	6.55	6.44	5.36
Total	99.72	100.47	99.3	99.14	99.16	100.22
Ag (ppm)	< 0.10	< 0.10	< 0.10	< 0.10	< 0.10	< 0.10
Au	< 0.05	< 0.5	< 0.05	< 0.05	< 0.05	< 0.05

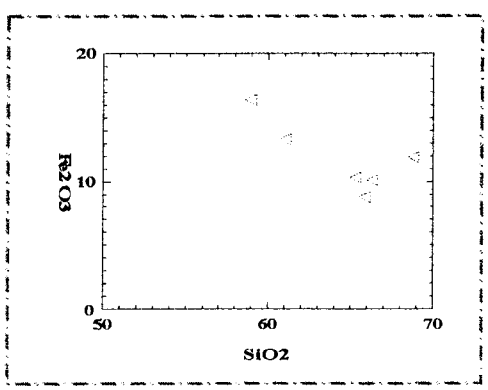












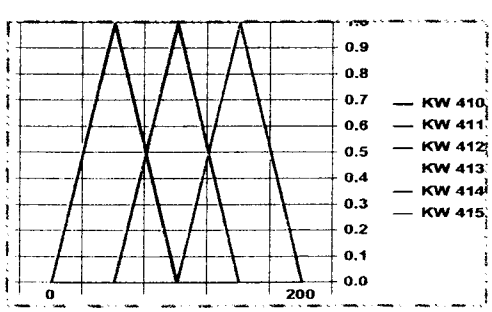
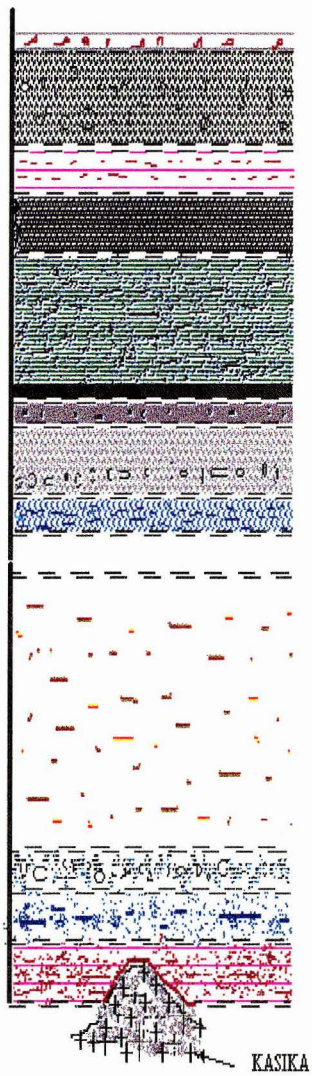


Fig.II.38:- Various ternary (Fe2O3 / SiO2/ Al2O3 ; MgO/MnO/P2O5) and binary (Al2O3 versus Fe2O3, SiO2 versus Al2O3 , SiO2 versus Fe2O3) plots for Nambo.
Frequency diagram of Fe2OT.



UNIT	FORMATION		
Ngweshe basalt.			
Polymictic Conglomerate (Diamictic, Tillite).	TSIBANGU	THE UPPER KADUBU GROUP	THE ITOMBWE SUPERGROUP
Phyllite and siltstone schist.			
Black shale with arkosic sandstone.			
Quartz schist interbedded with sericite schist and mica schist.	NYA-KASIBA		
Graphitic black shale.			
Quartzitic oligomitic conglomerate			
Quartz arenite, matrix-supported Conglomerate with sericite schist			
Phyllite (sericite schist and mica schist).	MUDUBWE	THE LOWER KADUBU GROUP	
(Meta) greywacke.			
Quartzitic bands interbedded with variegated black and /or bluish sericite schists and mica schists.	KALAMA		
Clast - supported conglomerate.	KIGOGO		
Quartzite interbedded with quartz schist and sericite schist.	BANGWE	KIBARAN	
Graphitic schist, quartzitic bands and mica schist.	KASIKA		

500 km

Fig.II.39:- The stratigraphic column of the Kadubu area within the Itombwe Supergroup.

KMA Walemba, 2000.

5.5.- PETROGRAPHY AND GEOCHEMISTRY OF IGNEOUS ROCKS.

5.5.1.- KASIKA TIN-GRANITE.

5.5.1.1.- INTRODUCTION.

This granite occurs in the southwesternmost corner of the study area, between Kasika and Nakitundu , and takes the form of a plutonic complex over 24 s.q. km (4 km x 6 km). It is the closest regional granite to the gold and tin mineralization within the study area, and comprises elongate to irregular shaped, individual intrusive stock units of composite character. (Fig.II.40). These different stocks which comprise the same pluton are intruded into the Kibaran metasediments (Kasika formation) with a N-S striking direction and were formed probably after the peak of metamorphism. The compositional variations range from leucogranite to granodiorite with small enclaves of metasediments dispersed in the pluton.

The granite is flanked and/or surrounded by a swarm of pegmatite dykes and numerous pegmatites with abundant tourmaline cross cut this granite and the surrounding metasediments. The pegmatites occur as dyke-like bodies, a few centimetres to a few metres in width, and up to several tens of metres long. They are coarse- grained rocks (1 cm to 3 cm crystals) with a graphic texture, composed mainly of similar mineralogy and geochemistry to the granite.

This granite (which is not deformed or shattered), together with its associated pegmatites, could be regarded as Syn to Post –kinematic Kibaran age intrusive, with contact aureoles in the surrounding wall- rocks, indicating an allochthonous character and high emplacement level (5 – 9 km depth) .

The genetic relationships between this granite and the pegmatites appears to be established, although the internal evolution of the granite and its origin are much less evident and should be examined in the light of the following data presented (Fig.II.40) .



Fig.II.40:- Kasika granite outcrop showing intrusive stock units. Lumetekelo river, Kasika locality.

5.5.1.2.- PETROGRAPHY.

Samples from the Kasika granite were collected at the Lumetekelo river and analysed petrographically.

Macroscopically, the rock is whitish, to pinkish -white, medium to coarse - grained , equigranular to hypidiomorphic granular, with a weakly porphyritic texture, and with mineral assemblages mainly consisting of medium – grained to pegmatitic quartz, feldspars (orthoclase, microcline , plagioclase and mica (muscovite, +/- biotite), with abundant coarse needles and prismatic crystals of black tourmaline (Fig.II.41). Mineralization phases include columbo-tantalite, cassiterite, and beryl.

Microscopically, the rock is a plagioclase-rich granitoid which displays evidence of granulation. Fine grained quartz and plagioclase occur in trains traversing coarse grained constituents (Tourmaline, muscovite). Perthitic microcline is a minor constituent and ragged aggregates of muscovite occur intergranularly to the other constituents.

The ratio of potash feldspar to plagioclase is approximately 1:6

*- Quartz ; (35 vol.%) ,occurs as anhedral grains, up to 2mm accross, as well as in trains of finely granulated material traversing other phases. It forms allotriomorphic grains with undulatory extinction.

*- Plagioclase ; (50 vol.%) , occurs as subhedral, twinned aggregates displaying some granulation along fractures.

*- K-feldspar ; (8 vol. %) ,occurs as anhedral microcline, up to 4mm in length, occasionally displaying (euthetic) intergrowths.

*- Muscovite; (5 vol. %), occurs as ragged flakes , ~ 1.5mm in length, developed intergranularly to other constituents.

*- Tourmaline ; (2 vol. %)occurs as irregular bodies up to 0.7mm accross, linearly developed..

*- Accessory minerals include garnet occurring as a single chloritised relics and apatite.

(Fig.II.42)



Fig.II.41:- Hand specimen of coarse-grained porphyritic Kasika granite showing texture and mineralogy .

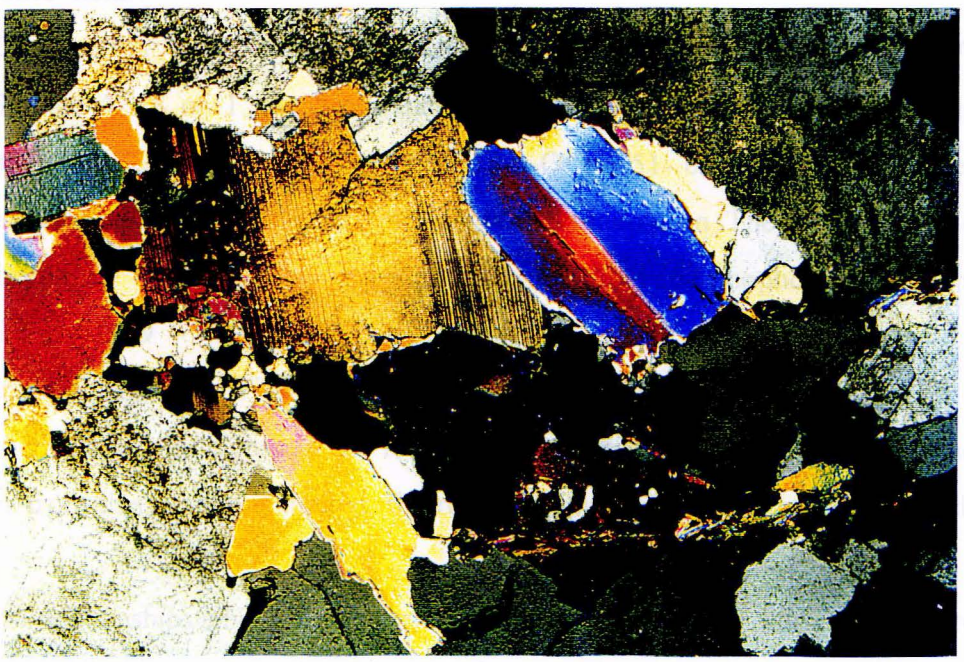


Fig.II.42:- - Photomicrograph of Kasika granite.

5.5.1.3.- GEOCHEMISTRY.

Representative major oxides, trace elements and REE abundances for the Kasika granite are presented in Table. II.4.

5.5.1.3.1.- MAJOR OXIDES.

The Kasika granite exhibit a wide range of chemical composition: SiO_2 contents are high and vary between 70.12 to 73wt %. Total alkalis (K_2O+Na_2O) vary considerably from 4.89 to 11.31 wt%. Al_2O_3 vary between 11.7 to 15.03 wt% , MgO from 0 to 0.57 wt % ,and Fe_2O_3 from 0.26 to 1.98. The abundances of the other oxides ($TiO_2+MnO+CaO+P_2O_5+CuO+NiO+ZnO+ SO_3$) are low: 2.2 to 4.6 wt %.

On an SiO_2 versus total alkalis diagrams (Fig.II.43) they plot respectively in the field of sub-alkaline and calcic with total alkalies (Na_2O+K_2O) increasing with SiO_2. In general they plot in the rhyolite field.

On an ACNK versus ANK diagram (Fig.II.44) they plot in the peraluminous field. A/CNK of 1.32 – 2.33 and A/NK of 1.32 - 2.66 ; indicate a strongly peraluminous chemical signature. The slightly lower CaO (0.2 – 0.73 wt%) and Na_2O (3.51- 6.36wt%) contents reflects the peraluminous character of this leucogranite- granodiorite pluton .The peraluminous chemistry is also indicated by Fig.II.44. The rock is not rich in fluorine and phophorus containing 0.05 – 0.06 wt% F and 0.09 - 0.59 wt% P_2O_5 . (Table II.4).

Harker variation diagrams (Fig II.45), show evolutionary trends with increasing silica contents. Most of them show a little change and form a relatively discrete cluster. Although the number of analyses from this granite is limited, the relationships between and within these cluster are significant..

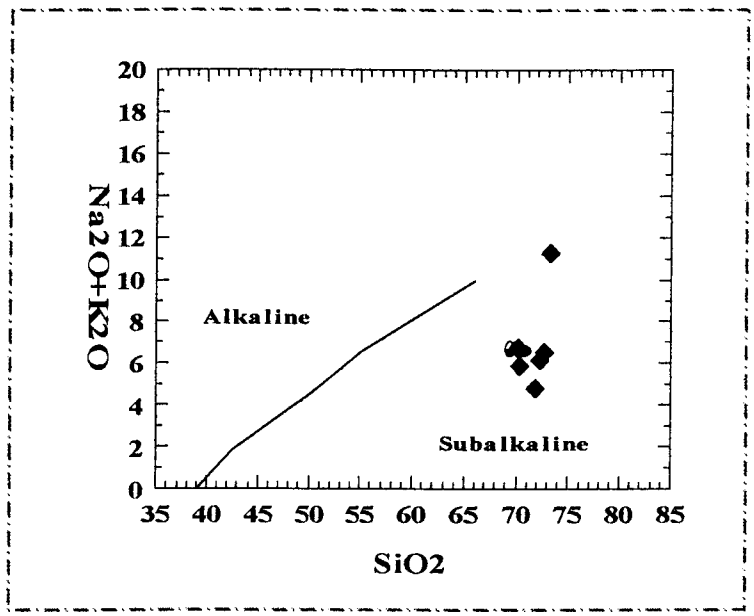
Interelement relationships amongst major constituents can be classified into essentially two types: those which exhibit continuous abundance variations, illustrated by SiO_2 vs.Al_2O_3, MgO vs. CaO, and Na_2O vs. K_2O, Al_2O_3 vs. CaO diagrams (Fig.II.46) and those which tend to produce relatively discrete compositional clusters.

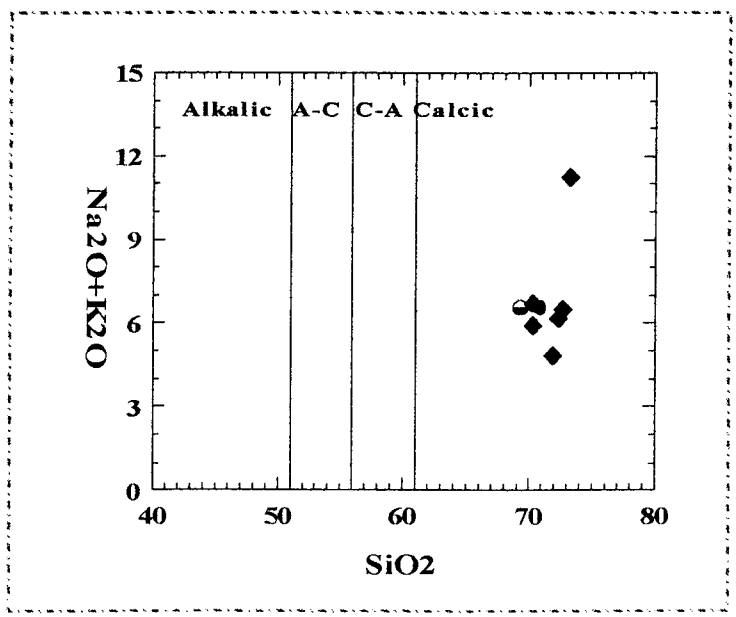
Table II.4: Representative major oxides , trace elements and REE abundances for the Kasika granite and CIPW-norms for selected samples.

Sample	SiO2	TiO2	Al2O3	Fe2O3	FeO	FeOT	MnO	MgO	CaO	Na2O	K2O	P2O5	F	LOI	Total	NiO	CuO	SO3
KW 20A	70.18	0.03	11.7	1.19	6.84	7.93	0.01	0.33	0.55	3.51	2.46	0.13	0.05		90.18	0	0.01	0.03
KW 20B	72.19	0.03	12.53	1.04	5.97	6.93	0.01	0.38	0.73	3.6	2.63	0.47	0.05		93.73	0.01	0.01	0.05
KW 20C	70.12	0.03	12.51	1.04	5.97	6.93	0.01	0.32	0.54	3.39	3.41	0.12	0.05		91.59	0.01	0.01	0.03
KW 20D	72.54	0.02	12.54	1.09	6.27	7.27	0.01	0.57	0.73	3.9	2.68	0.59	0.05		94.79	0.01	0.01	0.05
KW 23	73.11	0.17	15.03	0.26	1.49	1.73	0	0	0.2	6.36	4.95	0.09		0.28	100.46			
KW 44	71.7	0.05	13.03	1.98	11.39	13.2	0.02	0.49	0.69	3.48	1.41	0.35	0.06		93.31	0.01		0.02
KW 44 Apatite																		
KW 44 Mica																		

Sample	Ba	Rb	Sr	Y	Zr	Nb	Th	Pb	Zn	Ni	V	Cr	Ta	Co	U	W	Sn	Mo	Au
KW 20A	37	209	23	1		8	12	17	35		16	7		4					0.05
KW 20B	40	208	27	0		8	11	16	35		11	7		4			3		0.05
KW 20C							12.05	17.05			15.6	7							0.05
KW 20D							11.25	15.5			11	7.2					2.6		0.05
KW 23																			
KW 44		145	18	1	8	16		8	42	3	12	9	1			1	12	1	0.05
KW 44 Apatite		3.73	42.28																
KW 44 Mica		1172	5.32																

Sample	Ag	Rb/Sr	Cu	La	Ce	Pr	Nd	Sm	Eu	Gd	Tb	Dy	Sr87/Sr86	Rb87/Sr86	Nd143/Nd144	Sm147/Nd144	eNd
KW 20A	0.1	9.09															
KW 20B	0.1	7.7		20	16	2	4			1							
KW 20C	0.1																
KW 20D	0.1																
KW 23																	
KW 44	0.1	8.06		3	8		2	1		1		1					
KW 44 Apatite		0.09					212.3	127.9					0.8854	0.259685	0.512669	0.364219	174
KW 44 Mica		220.3											18.277	1732.901			





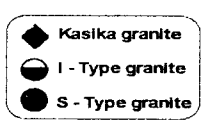
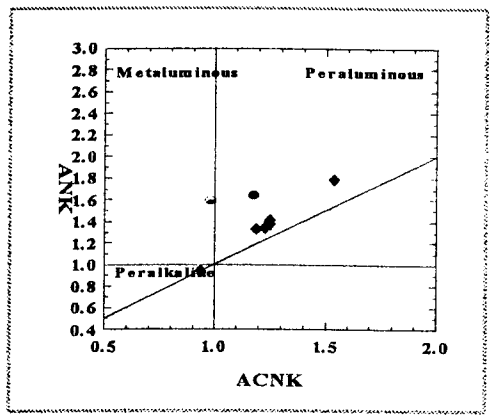
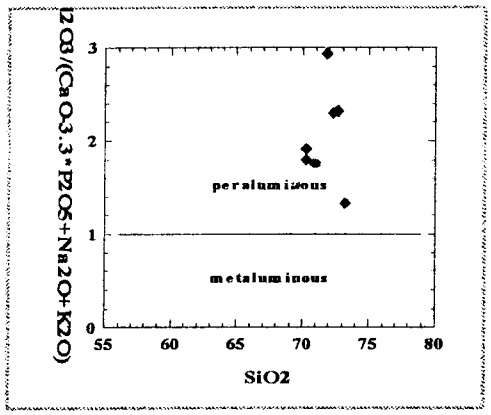
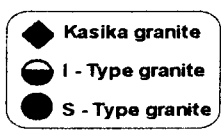
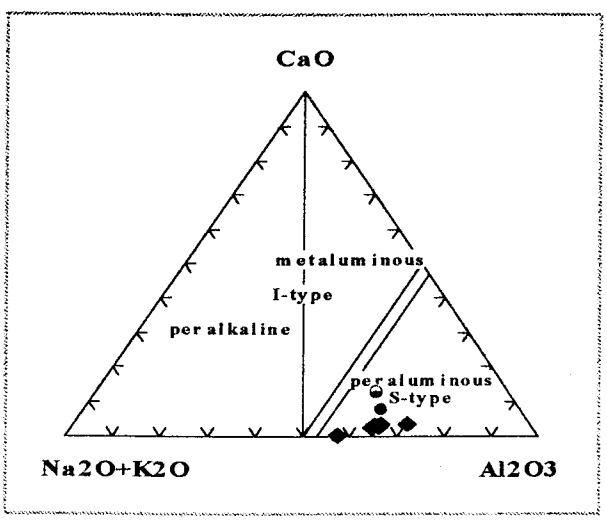


Fig.II.43:- SiO2 versus total alkalis diagrams for the Kasika granite. The average of I and S - type granites from the Lachlan fold belt of Chapell and White, 1992.









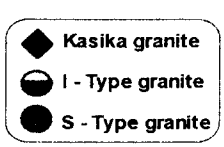


Fig.44:- ACNK - versus ANK diagram for the Kasika granite.
(after Maniar and Piccoli, 1989).
A = Molar value of Al2O3; N = Molar value of Na2O3.
C = Molar value of CaO; K = Molar value of K2O.

*.- Ternary diagram of CaO - Al2O3 - (Na2O+K2O) and
*.- Binary plot of SiO2 versus Al2O3/ (CaO-3.3*P2O5 + Na2O + K2O) showing the peraluminous chemistry of the Kasika granite.

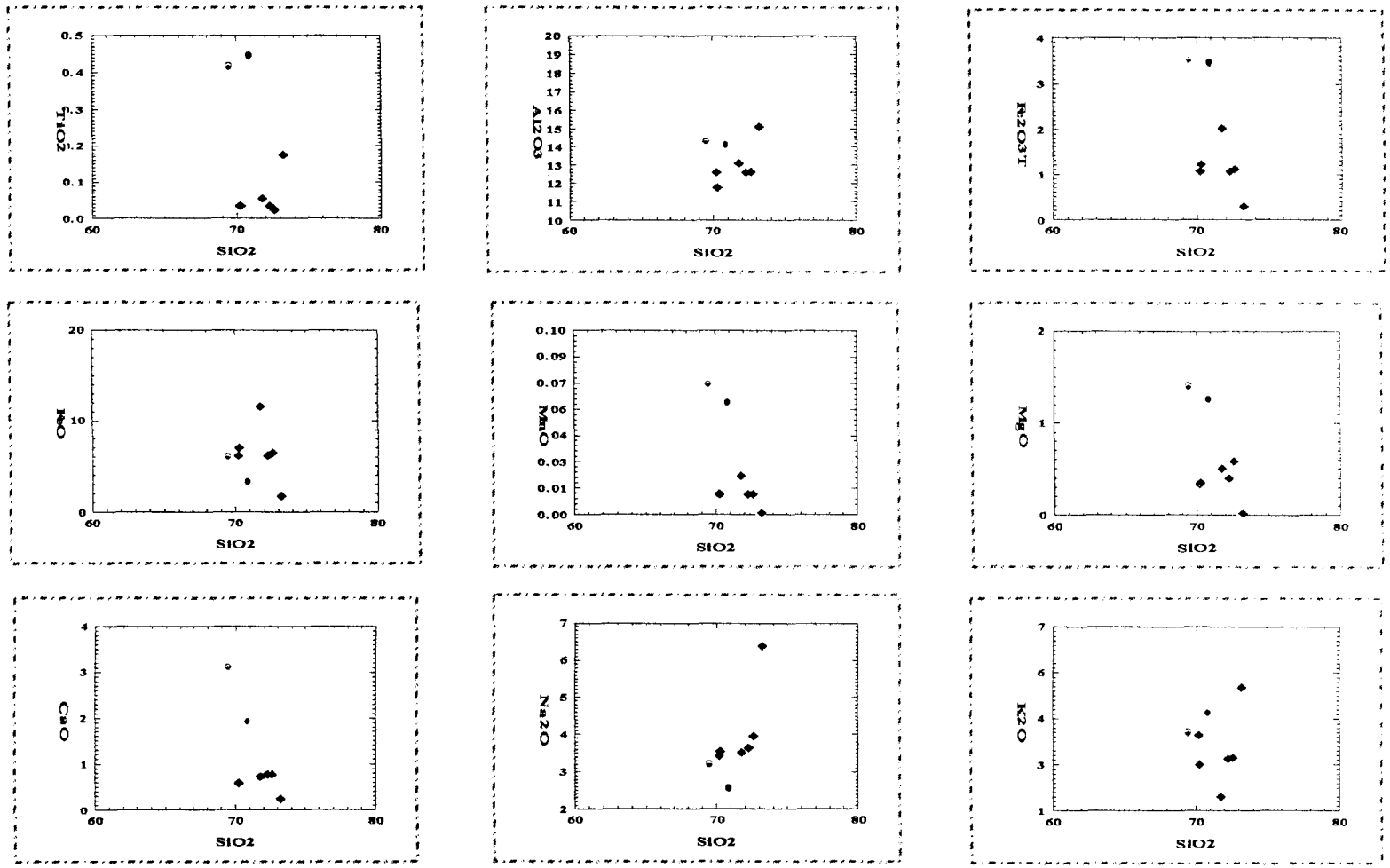


Fig.II.45:- Harker variation diagrams for selected major elements from the Kasika granite.

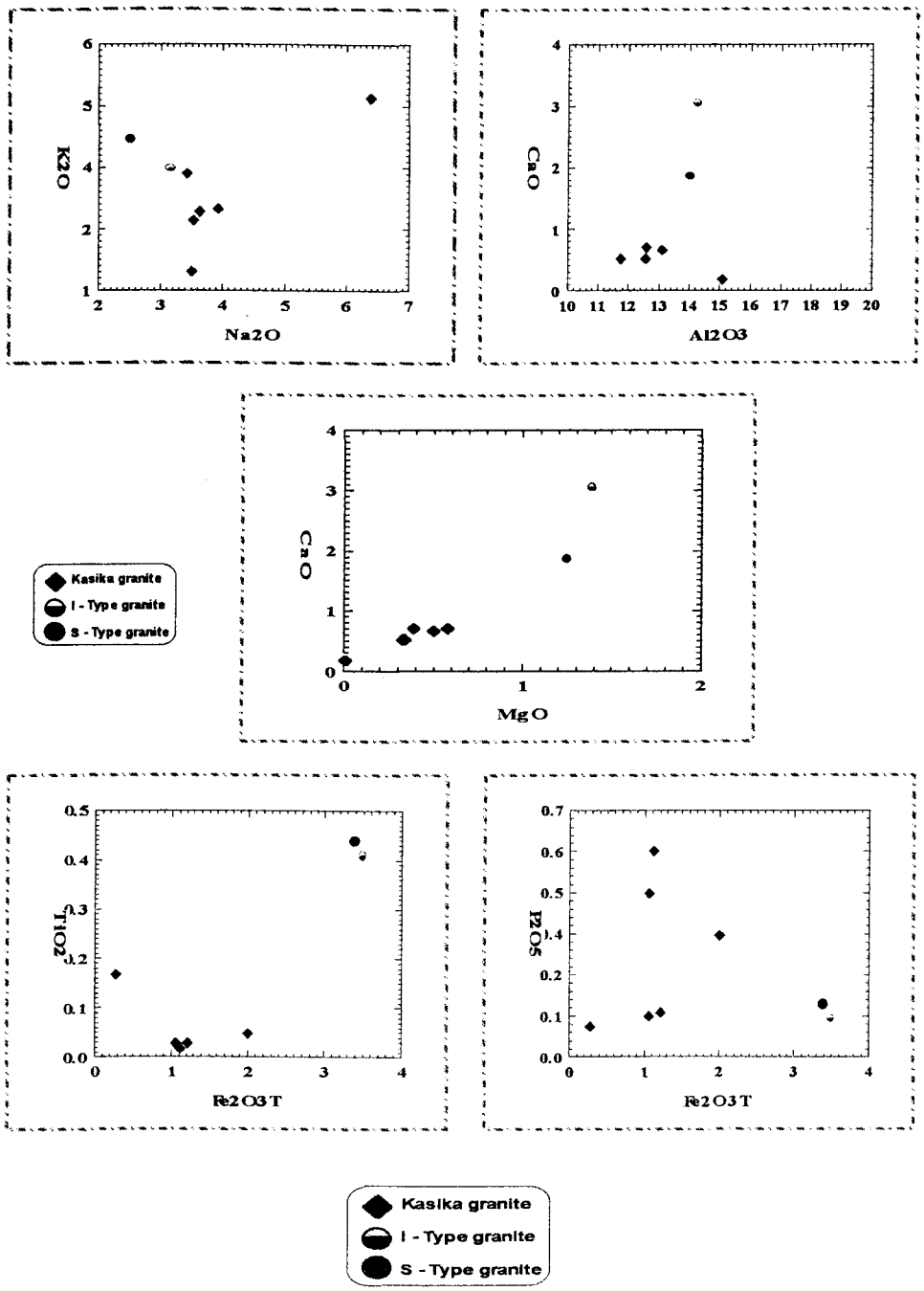


Fig.II.46:- Binary plots (Na2O vs K2O; Al2O vs CaO ; MgO vs CaO ; Fe2OT vs TiO2 ; Fe2OT vs CaO) for the Kasika granite.

On the SiO_2 versus K_2O diagram, the Kasika granite samples plot in the high-K and M-K field (Fig.II.47). More data is needed in order to depict the segmented or scattered trend and its inflections. The Kasika leucogranite pluton is markedly off by the general trend in some plot. The (Na_2O + CaO)- Al_2O_3 – K_2O diagram of Nesbitt and Young (1984,1989), shows the weathering trends for average granite and particularly for Kasika granite. (Fig.II.48) .

5.5.1.3.2.- TRACE ELEMENTS AND REE.

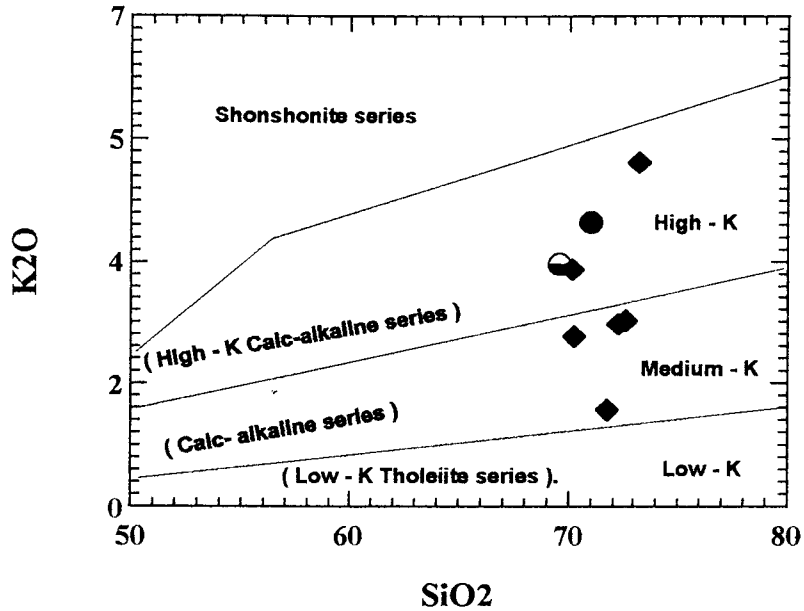
Compared to the average value of a granodiorite model composition of Debon and Le Fort, (1983), the trace element contents show high Rb, and very low, Ba, Co, Sr, and Cr contents. In the Harker diagrams (Fig II.49), all the groups follow the same downward or upward trends. In trace element chondrite-normalised diagrams (Fig II.50), samples show an negative anomalies in La, Nd and Y, moderate to low contents of HFSE (Nb, Zr, Y), and relatively fractionated patterns $(Rb/Lu)_n > 20$. The high degree of magmatic fractionation is demonstrated also by very low K/Rb and high U/Th ratios. The Rb/Sr ratio (> 9) is very high suggesting strong fractionation.

On a multi-element variation diagram (Fig.II.51), the Kasika granite is characterized by marked negative Y, Nd and La anomalies and relatively high levels of Rb, Nb and Zr. The negative anomalies could indicate that fractionation by mineral phases containing these elements took place at some stage in the history of the source area or of the magma.

Chondrite- normalized REE abundances are shown in (Figure II.52) and display a very low total REE content and more steeply sloping distribution and gently fractionated patterns.

Normalized multi-elements diagrams (spider diagrams) based upon a grouping of elements incompatible with respect to a typical mantle mineralogy have been used to depict deviations from a primitive and/or average compositions. These diagrams are an extension of the chondrite-normalized REE diagrams in which other trace elements are added to the traditional REE diagram. The normalizing values are respectively, those of Taylor and McLennan (1985) for chondrite, Sun and McDonough (1989) for primitive mantle, Taylor and McLennan (1985) for upper, lower and average continental crust. Fig.II.53 shows spider diagrams for the Kasika granite.

Fig.II.47:- The subdivision of subalkalic rocks using the K2O versus silica diagram. Kasika granite plot in the fields of high - K and medium - K (after Le Maitre et al., 1989).



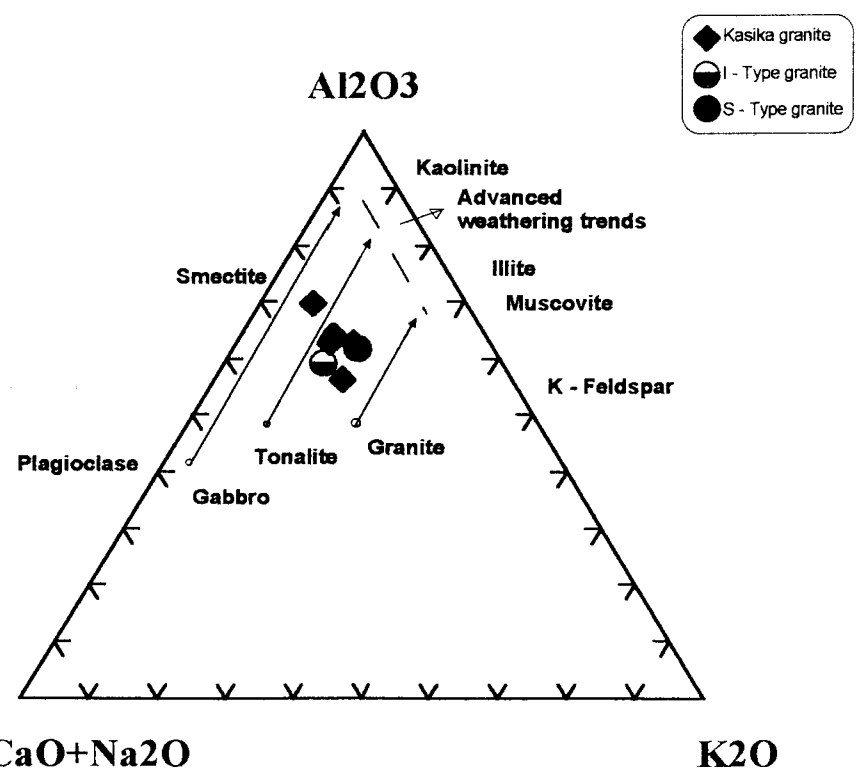


Fig.II.48:- The (Al2O3 - K2O - CaO + Na2O) of Nesbitt and Young (1984, 1989) showing the weathering trends for Kasika granite.

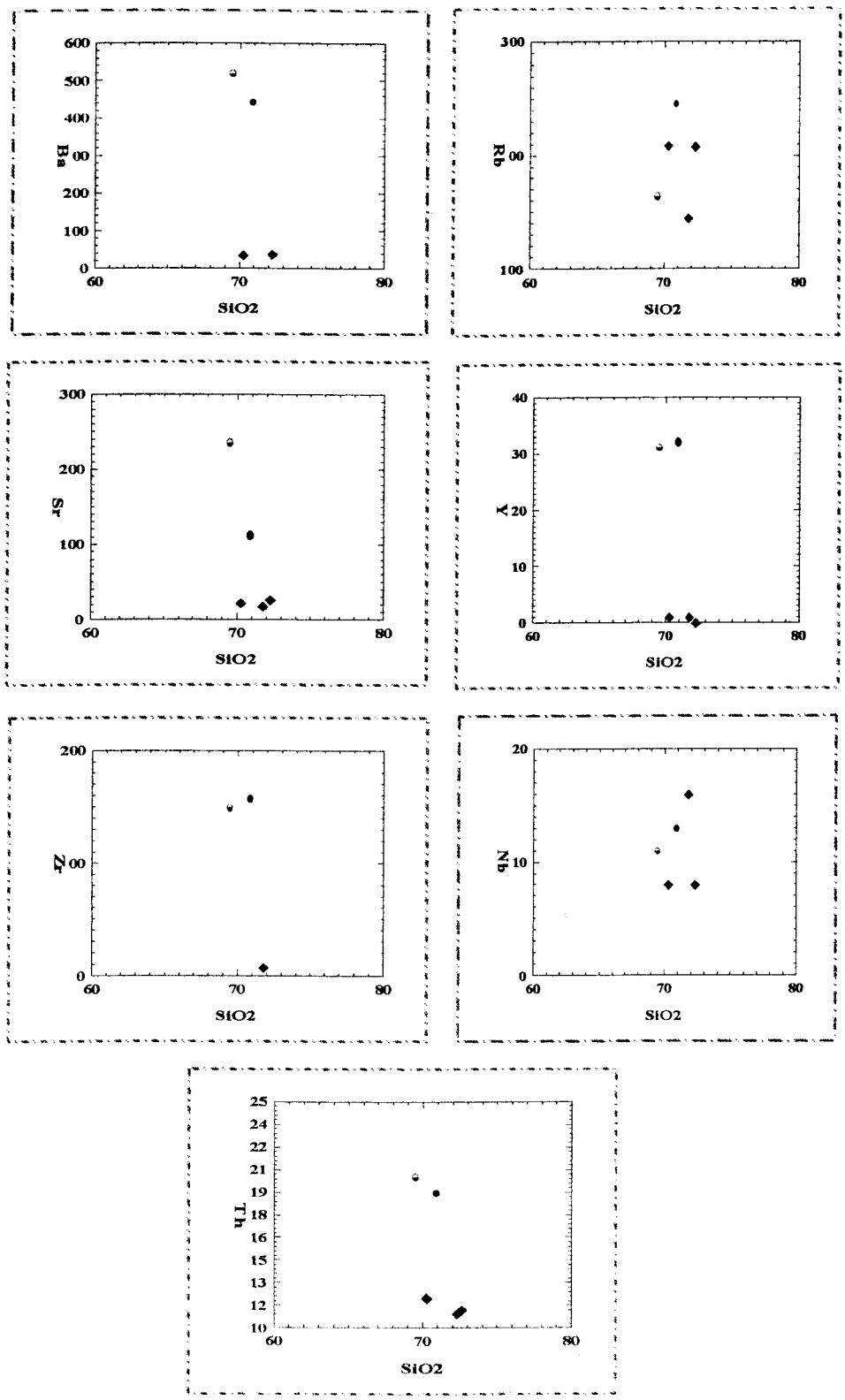
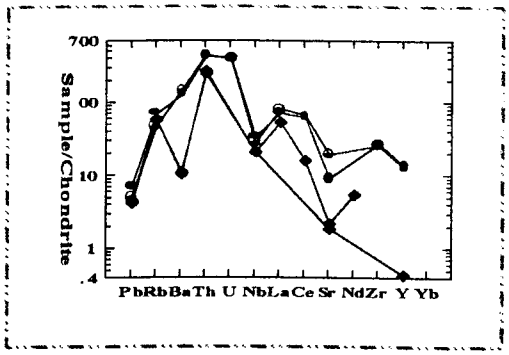


Fig.II.49:- Harker variation diagrams for selected trace elements from the Kasika granite.



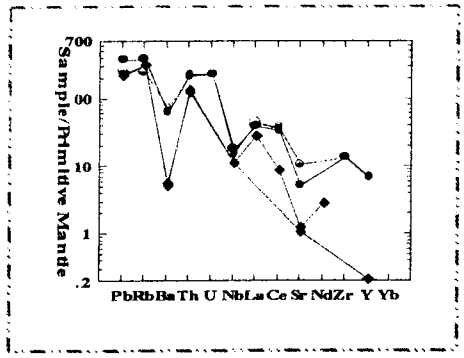
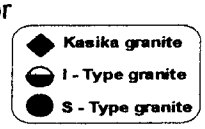
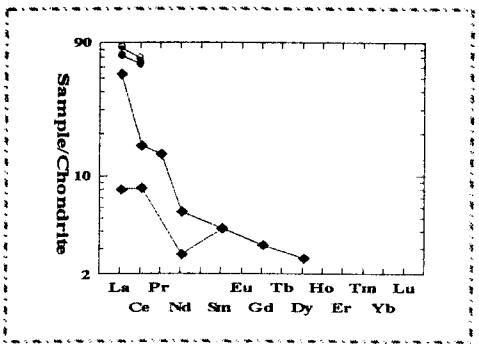


Fig.II.50:- Chondrite - normalized trace element patterns for Kasika granite. Elements are arranged with increasing incompatibility, from right to left.

Fig.II.51:- Multi-element variation diagrams illustrating the geochemical characteristics of the Kasika granite. Normalizing values after Sun and McDonough, (1989).





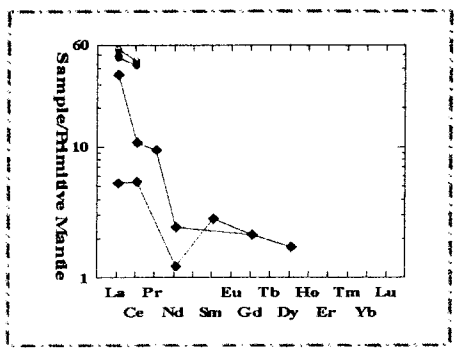
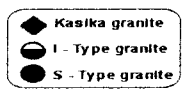
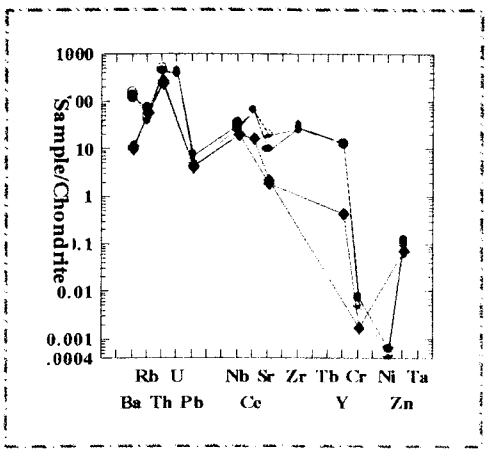


Fig.II.52:- Chondrite - normalized REE patterns for the Kasika granite.





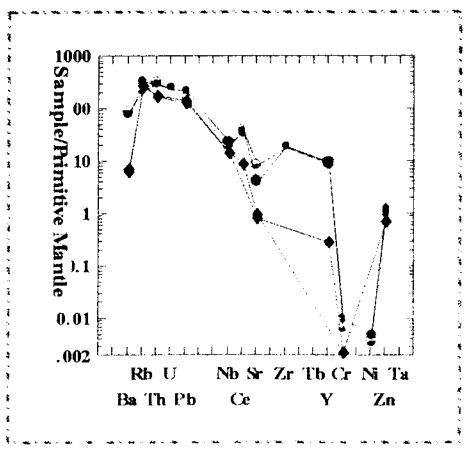
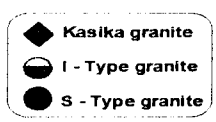


Fig.II.53:- Spider diagrams for the Kasika granite.



The less mobile HFS elemens (Zr,Ti,Nb,Ta) could have been controlled by individual minerals (zircon for Zr and rutile, ilmenite, sphene for Ti, Nb, Ta) and /or the chemistry of the source. The peaks of more mobile LIL elements (Rb, Ba, Sr, Eu) suggest a crustal contamination of magma.

Table.II.5, gives a summary of major and trace elements geochemistry of the Kasika leucogranite compared with S- and I-type granites from Chapell and White (1992).

5.5.1.4.- GEOCHRONOLOGY AND RADIOGENIC ISOTOPES.

5.5.1.4.1.- PREVIOUS DATA.

The Rb/Sr ages dating for the Kasika granite have been reported previously (Ledent and Cahen, 1965, Monteyne-Poulaert et al., 1962) and gave the ages respectively of 1020 ± 50 Ma (Rb/Sr ,whole rock), and 535 ± 16 Ma (Rb/Sr, based on microcline from a pegmatite vein of the Kasika granite). These are the only data from this granite.

Isotopic results from these earlier studies are shown in Table.II.6 for comparison with data presented in this study.

Table. II.6 :- Rb-Sr and Sm-Nd isotopic data of the Kasika granite.

Sample	Rb ppm	Sr ppm	$^{87}Rb/^{86}Sr$	$^{87}Sr/^{86}Sr$	Sm ppm	Nd ppm	$^{147}Sm/^{144}Nd$	$^{143}Nd/^{144}Nd$	Date Ma
RG4757	527	11.9		59					535
									1020

5.5.1.4.2.- $^{40}Ar / ^{39}Ar$ DATING.

Three muscovite and three feldspar grains from sample KW 44 ; a tourmaline-bearing tonalite . were analysed by Dr. D. Philipps at Anglo American Reseach Laboratories. Step-heating analyses undertaken on one muscovite grain yielded a mean age of 528 ± 3 Ma.

Table. II.5.- Summary of major and trace element geochemistry of the Kasika leucogranite compared with S - and I - type granites from Chappell and White (1992).

No	Item	S-Type	I-type	Kasika granite
A. Chemical composition and some distinct ratios.				
A.1	SiO_2 (wt%)	70.91 +/- 2.82	69.50 +/- 4.62	70.12-73
A.2	CaO + Na_2O (wt%)	lower (4.4)	Higher (6.2).	3.71-7.09
A.3	ASI	1.01 - 1.99 .Peralumi-nous (mafic or felsic)	0.69 - 1.10. Metaluminous. (mafic),or slightly Peraluminous.	1.00 - 1.44. Peraluminous
A.4	Fe^{3+} /(Fe^{3+} + Fe^{2+})	0.153	0.29	
A.5	Sr (ppm)	114 (a) ; 43 (b)	147 (a) ; 31 (b)	18-27
A.6	Rb (ppm)	221 (a) ; 475 (b)	219 (a) ; 424 (b)	145-209
A.7	Rb - P_2O_5 diagram	P increases with Rb, with fractionation.	P decreases to very low levels with fractionation	P increases with Rb, with fractionation.
B. Mineral Assemblage.				
B.	Minerals	Al- rich biotite , Al-rich minerals,ilmenite	Felsic: Muscovite, Biotite. Mafic: Hornb,Magnetite,Sphene	Muscovite, Biotite Feldspar, Tourmaline
C. Enclaves.				
C.	Enclaves	Metasedimentary	Metaluminous and/or Hornblende-bearing	Metasedimentary
D. Isotopic Compositions.				
D.1	$dO_{(SMOW)}$ (0/00)	> 10	< 10	
D.2	$^{87}Sr / ^{86}Sr$ ratio	0.708 - 0.720	0.704 - 0.712	0.882812
D.3	E_{Nd}	- 5.8 to -9.2	+ 3.5 to - 8.9	2542.624
E .	Homogeneity	Heterogenous	Homogenous	Heterogenous
F.	Source Rocks	Metasedimentary or Supracrustal	Igneous or Infracrustal.	Metasedimentary or supracrustal
Reference		White and Chapelle (1977) ; Chapelle and White (1992).		This study.

Note: ASI = molar Al2O3 / (Na2O+K2O+CaO), (a)=Unfractionated granite; (b) = Fractionated granite.

The apparent age spectrum for this grain is portrayed in Fig. II.54, Fig. II.55 and Table II.7. Rim and core analyses were carried out on the remaining two muscovite grains. The rim analyses yielded apparent ages ranging from 520 ± 9 Ma to 531 ± 7 Ma , while the core analyses produced apparent ages ranging 521 ± 8 Ma to 549 ± 7 Ma.

Step-heating analyses were undertaken on three individual feldspar grains from sample KW 44. The results are depicted graphically in Fig.II.54. The feldspar grains produced discordant age spectra, where apparent ages generally decreased with increasing temperature. Excluding anomalous results , a mean of 436 ± 8 Ma was calculated for the feldspar grains.

5.5.1.4.3.- INTERPRETATION OF $^{40}Ar/^{39}Ar$ RESULTS.

These ages are not consistent with the field relationship (Kibaran granite) and don't agree with the previous Rb/Sr age of 1020 ± 50 Ma. The Kasika granite being a " G_4 " Kibaran granite, its mean age has been dated at 977 +/- 13 Ma throughout the belt (Cahen et al., 1984).
The shape of the release spectra and the similarity between plateau and total gas ages are compatible with loss of Ar by partial resetting. (Fig.II.54 ; Fig.II.55). $^{40}Ar/^{39}Ar$ ages would suggest that muscovite and feldspar minerals were reset during the Pan-African tectono-thermal event and the age range of 436 to 549 Ma is interpreted as mineral resetting ages .

5.5.1.4.4.- RUBIDIUM / STRONTIUM AND SAMARIUM /NEODYMIUM SYSTEMS.

The relative importance of mantle and crustal contributions to the Kasika leucogranite melt may be considered from isotopic and trace element data. Results of the isotopic analyses and calculated ages are given in Table.II.8. The analysed samples were selected from samples used in previous petrographical and geochemical investigations. Two Rb-Sr analyses were made on apatite and mica.
The samples exhibit a large range of $^{87}Rb/^{86}Sr$ ratios (0.259685 – 1732.901153) , but do not define a statistically acceptable isochron age because of the large variation in $^{87}Sr/^{86}Sr$ initial ratios (Table.II.8).

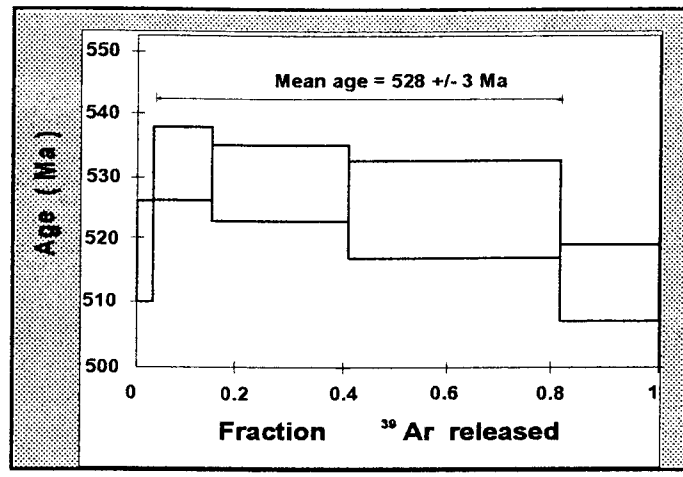


Fig.II.54:- $^{40}Ar / ^{39}Ar$ age spectrum versus cumulative fraction of ^{39}Ar released from muscovite grain KW44-1 from Kasika granite sample KW44. Each rectangle represents a single analysis or temperature step. Temperature increases from left to right and the length of each bar indicates the proportion of $^{39}Ar_K$ released in that step, while the width represents one sigma uncertainties in the age result.

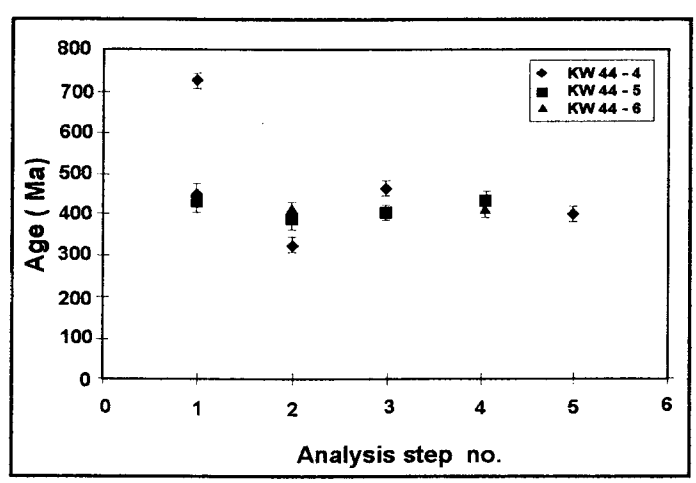


Fig.II.55:- $^{40}Ar / ^{39}Ar$ step - heating analyses for three feldspar grains from the Kasika granite. Sample KW 44.

Table.II.7;- $^{40}Ar/^{39}Ar$ LASER PROBE ANALYTICAL RESULTS FOR SINGLE MUSCOVITE AND FELDSPAR GRAINS FROM THE KASIKA GRANITE. KADUBU AREA.

MINERAL	GRAIN	STEP	INTERFERENCE - CORRECTED PEAK HEIGHTS					$^{37}Ar_{ca}/^{36}Ar_{k}$	ATMOS	AGE (Ma)
	No.	No.	^{40}Ar	^{39}Ar	^{38}Ar	^{37}Ar	^{36}Ar		%	
MUSCOVITE	KW 44-1	1	0.7671+/-0.0014	0.01719+/-0.00022	0.00041+/-0.00004	0.0001+/-0.0001	0.00035+/-0.00002	0.002+/-0.002	1342	518+/-8
		2	2.2134+/-0.0031	0.05332+/-0.00024	0.00018+/-0.00002	0.0005+/-0.0003	0.00029+/-0.00002	0.010+/-0.005	337	532+/-6
		3	5.1272+/-0.0080	0.12651+/-0.00058	0.00019+/-0.00006	0.0017+/-0.0001	0.00038+/-0.00002	0.013+/-0.001	217	529+/-6
		4	7.7725+/-0.0050	0.18527+/-0.00098	0.00023+/-0.00007	0.0012+/-0.0003	0.00037+/-0.00002	0.006+/-0.001	140	525+/-8
		5	3.3388+/-0.0051	0.08583+/-0.00042	0.00017+/-0.00003	0.0008+/-0.0002	0.00019+/-0.00001	0.009+/-0.002	171	513+/-6
	KW 44-2	rim	1.4838+/-0.0023	0.03540+/-0.00027	0.00015+/-0.00004	0.0018+/-0.0002	0.00025+/-0.00002	0.052+/-0.006	530	531+/-7
		core	4.0221+/-0.0010	0.08494+/-0.00061	0.00036+/-0.00007	0.0011+/-0.0001	0.00031+/-0.00001	0.012+/-0.001	227	549+/-7
	KW 44-3	rim	6.0725+/-0.0030	0.15335+/-0.00029	0.00065+/-0.00010	0.0013+/-0.0003	0.00037+/-0.00002	0.008+/-0.002	179	520+/-9
		rim	5.2603+/-0.0065	0.12814+/-0.00092	0.00041+/-0.00006	0.0013+/-0.0003	0.00060+/-0.00001	0.010+/-0.002	337	529+/-1
		core	2.1401+/-0.0130	0.05370+/-0.00055	0.00022+/-0.00003	0.0008+/-0.0002	0.00016+/-0.00002	0.015+/-0.004	227	521+/-8
FELDSPAR	KW 44 - 4	1	0.8495+/-0.0013	0.00797+/-0.00016	0.00917+/-0.00013	0.0128+/-0.0004	0.00065+/-0.00002	1.606+/-0.058	5135	729+/-16
		2	0.1812+/-0.0005	0.00529+/-0.00006	0.00070+/-0.00003	0.0147+/-0.0005	0.00020+/-0.00001	2.788+/-0.106	3237	328+/-22
		3	0.1245+/-0.0005	0.00300+/-0.00007	0.00078+/-0.00005	0.0082+/-0.0003	0.00007+/-0.00002	2.731+/-0.107	1774	484+/-28
		4	0.1799+/-0.0004	0.00416+/-0.00006	0.00123+/-0.00006	0.0118+/-0.0004	0.00016+/-0.00002	2.848+/-0.109	2639	437+/-22
		5	0.3352+/-0.0007	0.00704+/-0.00008	0.00193+/-0.00006	0.0236+/-0.0002	0.00045+/-0.00002	3.347+/-0.051	3942	400+/-12
	KW 44 - 5	1	2.4059+/-0.0100	0.07074+/-0.00009	0.00220+/-0.00006	0.0031+/-0.0003	0.00060+/-0.00002	0.044+/-0.005	745	433+/-5
		2	1.4157+/-0.0008	0.04397+/-0.00023	0.00034+/-0.00002	0.0038+/-0.0003	0.00014+/-0.00002	0.087+/-0.008	310	429+/-5
		3	0.7172+/-0.0004	0.02237+/-0.00020	0.00043+/-0.00006	0.0018+/-0.0003	0.00013+/-0.00002	0.080+/-0.013	526	419+/-6
		4	1.2048+/-0.0004	0.03474+/-0.00009	0.00136+/-0.00003	0.0077+/-0.0002	0.00032+/-0.00002	0.221+/-0.007	747	436+/-6
	KW 44- 6	1	0.9085+/-0.0009	0.01772+/-0.00011	0.00364+/-0.00008	0.0061+/-0.0002	0.00107+/-0.00002	0.343+/-0.018	3437	455+/-7
		2	0.1880+/-0.0004	0.00402+/-0.00004	0.00052+/-0.00004	0.0048+/-0.0001	0.00020+/-0.00001	1.204+/-0.038	3204	432+/-14
		3	0.3289+/-0.0004	0.00704+/-0.00001	0.00138+/-0.00006	0.0110+/-0.0005	0.00038+/-0.00002	1.568+/-0.073	3232	432+/-14

J-Value for KW 44, KW 622A = 0.0086+/-0.0001
J-Value for KW 705 = 0.009+/- 0.0001
J-Value for KW152 = 0.0087+/-0.0001

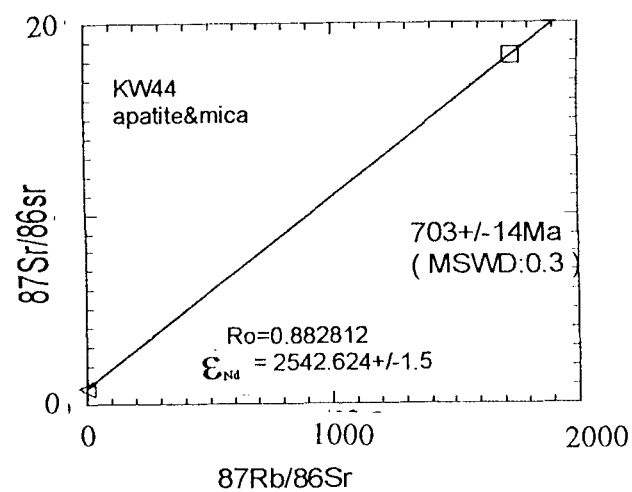
Isotope peak heights are corrected for system blanks, mass discrimination, radioactive decay of ^{37}Ar and ^{39}Ar,and reactor induced interferences on masses 40, 39,38 and 36. Values are recorded as volts (V).

Typical blank levels are: 0.00461 V (^{40}Ar), 0.0001 V (^{39}Ar), 0.00010 V (^{38}Ar), 0.00346 V (^{37}Ar), 0.00030 V (^{36}Ar)

Table II.8. Rb-Sr and Sm- Nd isotopic data used for mineral dating of the Kasika leucogranite.

Samples	Rbppm	Srppm	$^{87}Rb/^{86}Sr$ +/-1se	$^{87}Sr/^{86}Sr$ +/- 1se	Smppm	Ndppm	$^{147}Sm/^{144}Nd$	$^{143}Nd/^{144}Nd$+/-1se
KW44 apatite	3.73	42.28	0.259685	0.885419+/-46	127.9	212.3	0.36422	0.512669+/- 29
KW44 Mica	11.72	5.32	1732.901	18.277+/-26				

Fig.II.56:- Rb - Sr Isochron for thin - slab profiles of samples KW44 apatite and KW 44 mica.



A $^{147}Sm/^{144}Nd$ ratio (0.364219) is high compared to average continental crust (0.125) . An initial $^{87}Sr/^{86}Sr$ ratio is calculated as 0.882812 ± 0.000138 and an epsilon value is 2542.624 ± 1.562 , which give an age of 703 ± 10 Ma. This age correspond to the Katanga – Damara orogeny.

The leucogranite samples have a somewhat higher $^{87}Sr/^{86}Sr$ value (0.885419 to 18.277000) and a lower $^{143}Nd/^{144}Nd$ value (0.512669) .

These ratios of $^{87}Sr/^{86}Sr$ and $^{143}Nd/^{144}Nd$ are too high ,suggesting an enriched mantle or depleted lower - crust origin . Another explanation for the observed high initial strotium ratio could be that the magmas generated in deep source –regions were contaminated by assimilation of Kibaran metasediments. Based on the data presented, a crustal origin could also be retained with the possibility of progressive isotopic re-equilibration of crustal material .

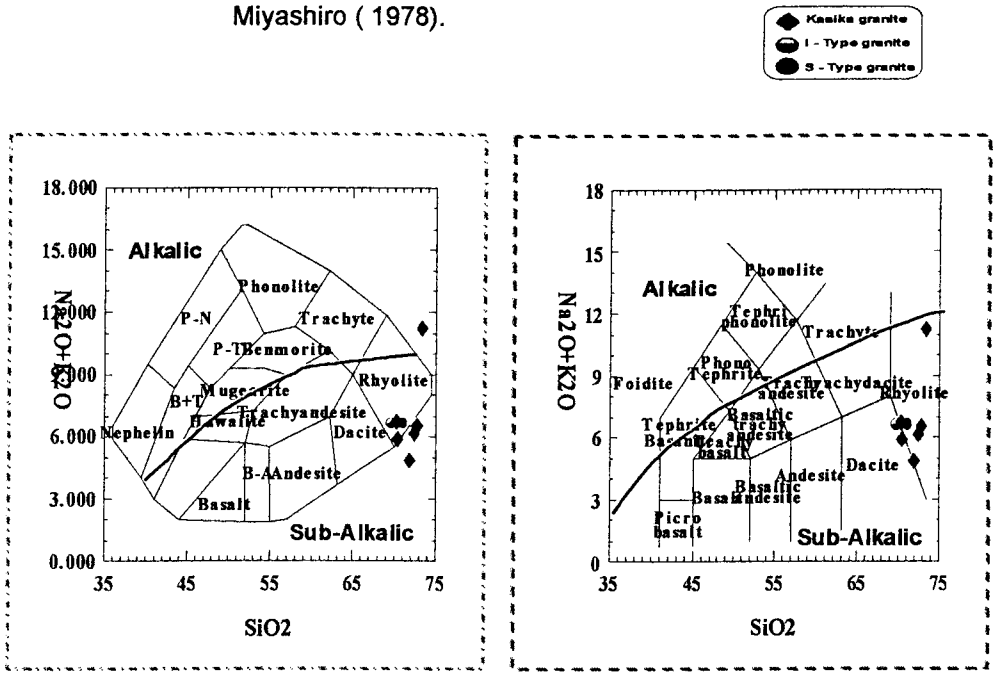
The apatite sample has a $^{87}Rb/^{86}Sr$ value too low to produce precise information about age.
It is instructive to examine these data on an isochron diagram. (Fig.II.56).

5.5.1.5.- PETROGENESIS AND GEOTECTONIC MODEL.

5.5.1.5.1.- PETROGENESIS.

Classification of the Kasika granite is based on petrographic descriptions and whole-rock chemical analyses. Using the total alkali-silica diagram (Cox et al., 1979; Le Bas et al.,1986), the rock is classified as a felsic rock , such as rhyolite, and plots in the subalkaline field.(Fig.II.57).
In the triangular QAP diagram of Streckeisen (1976), (Fig.II.44) the CIPW normative mineral compositions plot in the fields of tonalite, granodiorite and monzogranite. For all of these plots, the compositional variation ranges from tonalite to granite through granodiorite (Fig.II.57; Fig.II.58; Fig.II.59; Fig.II.60).
Petrographically, the rock has a modal proportions of quartz, potash feldspar and plagioclase. These modes are shown in (Fig.II.61) and plot simultaneously in the field of S and I-type granites (after Bowden et al., 1984 and whalen and Curie, 1990).

Fig.II.57:- Diagram of total alkalis versus SiO2 for the Kasika granite
The original plot is from Cox et al., (1979) and Le Bas et al., (1986).
The line dividing alkalic and sub-alkalic magma series is from Miyashiro (1978).



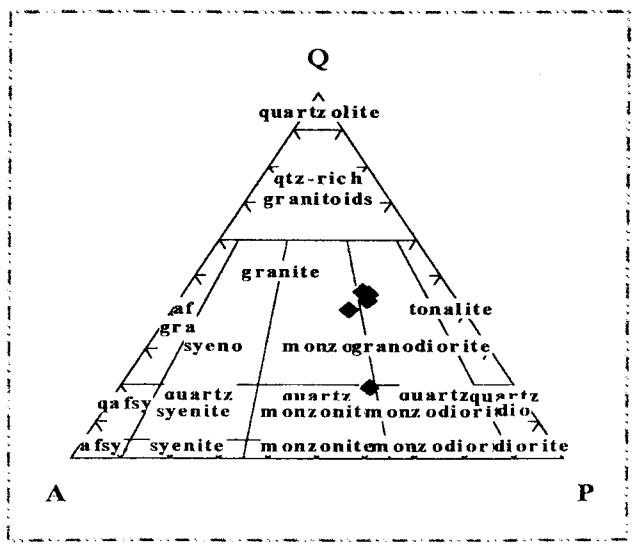
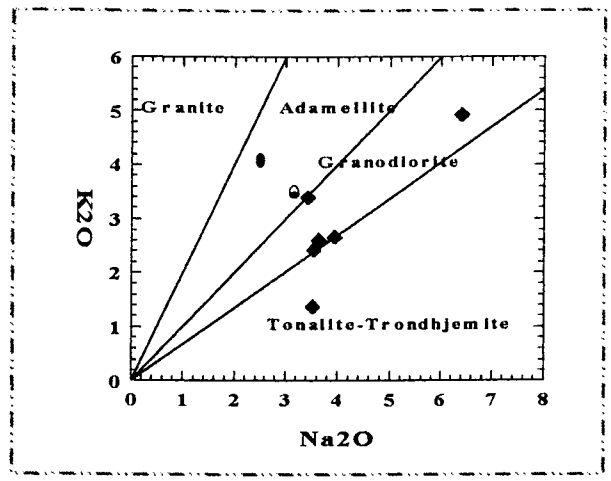


Fig.II.58:- Triangular QAP diagram of Streckeisen (1976) showing CIPW normative mineral compositions of the Kasika granite .



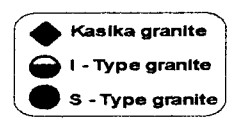
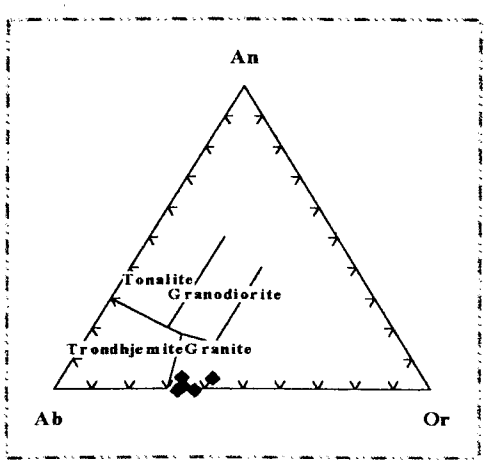
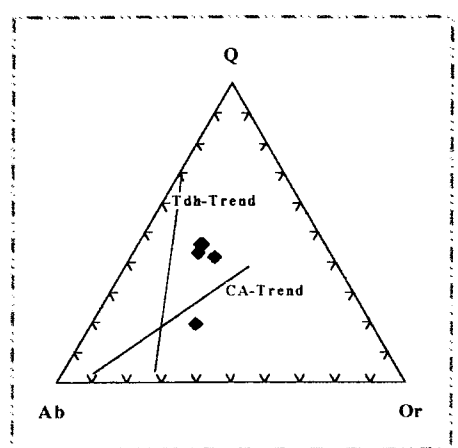


Fig.II.59:- Binary plot of Na2O versus K2O for the Kasika granite.





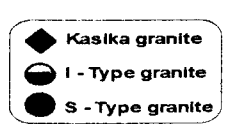


Fig.II.60:- Ternary plots (An - or - Ab and Q - Or - Ab) for the Kasika granite (after Baker, 1979).

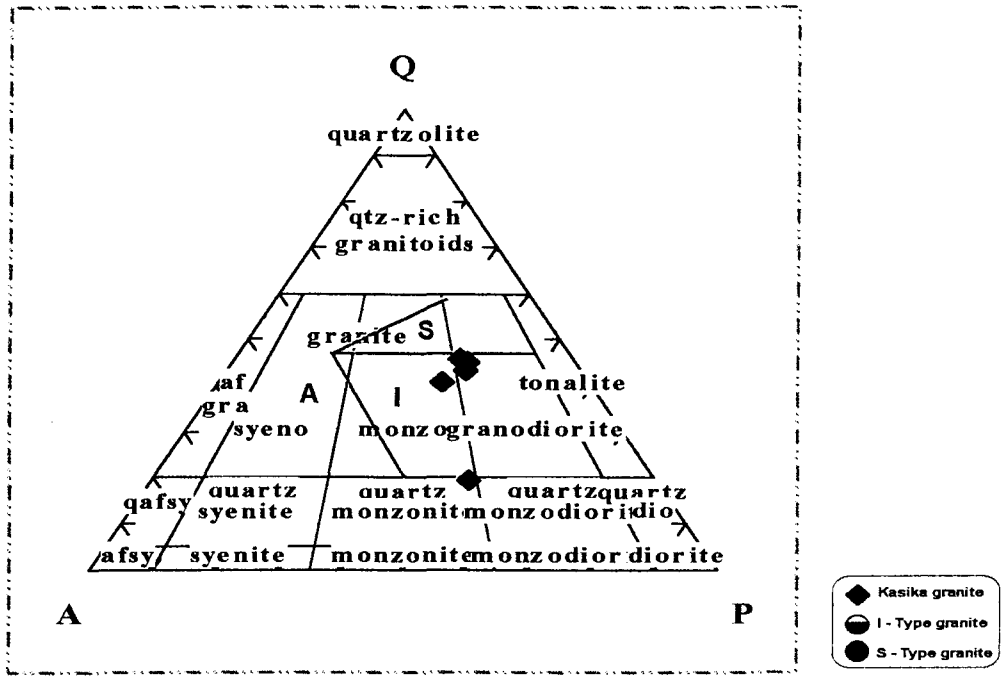


Fig.II.61:- Triangular QAP diagram (Streckeisen , 1976 ; Bowden and al., 1984). Fields of S, I, and A - type granites are from Whalen and Curie (1990)

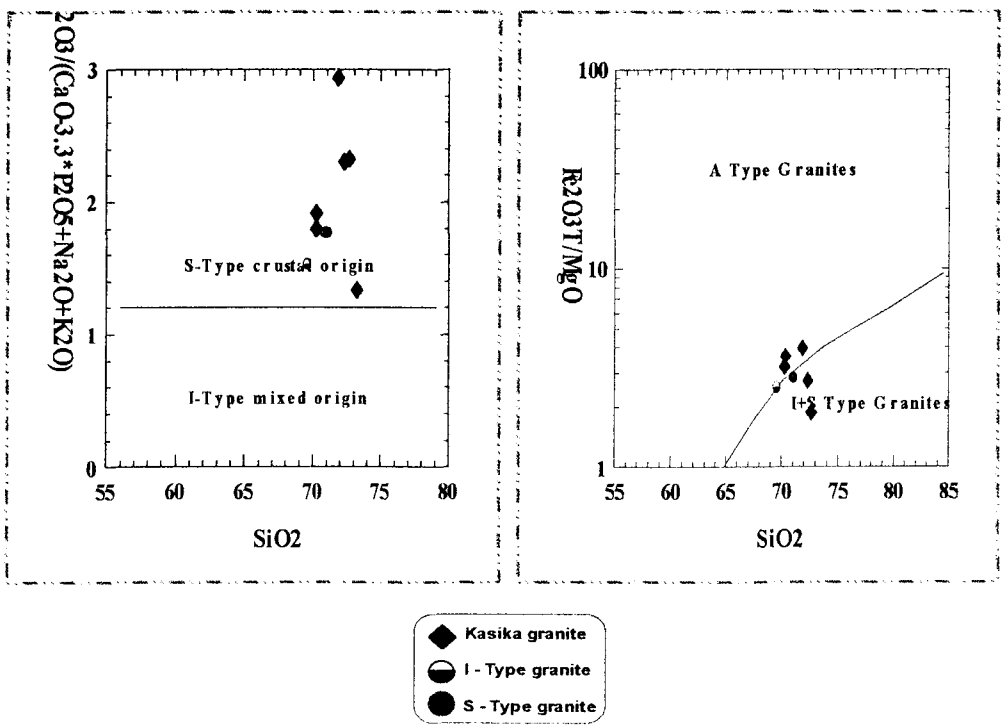


Fig.II.62:- SiO2 versus (Al2O3 / CaO - 3.3*P2O5+Na2O+K2O) diagram.

Fig.II.63:- SiO2 versus (Fe2O3T / MgO) diagram.

In the diagram of SiO_2 vs $Al_2O_3/(CaO - 3.3 * P_2O_5 + Na_2O + K_2O)$, they plot in S-type field. (Fig.II.63). In the SiO_2 versus Fe_2O_{3T}/MgO diagram, they plot in I+S type granite, and close to the border of A type. (Fig.II.63). Abundances of Zr and Zn versus. silica (Collins et al.,1982) show that this granite is not A -type , but an I - type (Fig.II.64). Confirmation of the I-type character is presented also on the SiO_2 versus Y, Nb plots of Fig.II.65.

According to Chapell and White, 1992; the main criteria for distinguishing I- and S- type granites can be summarized as follows:

*.- S-types are always peraluminous [alumina saturation index (ASI > 1.1)] and contain Al-rich minerals (e.g. Al-rich biotite, muscovite, cordierite, garnet , sillimanite, andalusite) . Chemically , they are lower in Na, Ca, Sr, and Fe^{3+} / Fe^{2+} , and higher in Cr and Ni. They have higher $\delta^{18}O$ values (> 10 $^0/_{00}$) and more evolved Sr and Nd isotopic compositions.

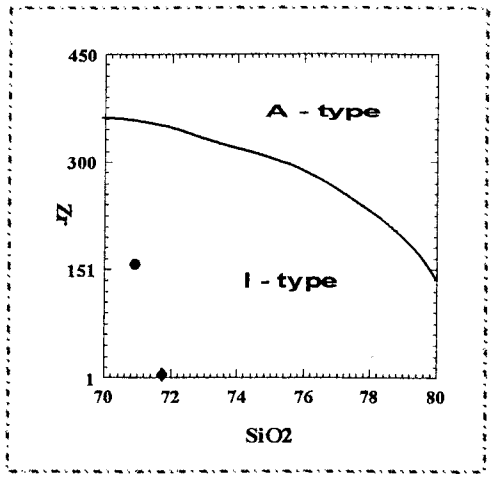
They range in $^{87}Sr/^{86}Sr$ from 0.708 to 0.720 and in ε_{nd} from –5.8 to – 9.2. They contain a diverse assemblage of metasedimentary enclaves .

*.- I-types are metaluminous to weakly peraluminous (ASI<1.1) , and commonly contain biotite, hornblende , and titanite. They range in $^{87}Sr/^{86}Sr$ from 0.704 to 0.712 and in ε_{nd} from +3.5 to – 8.9.Enclaves are commonly metaluminous and hornblende-bearing. Table.II.5

Various discrimination diagrams (Fig II.66; Fig.II.96) for the Kasika granite, plot this granite respectively in the fields of (Syn-COLG) syn-collision granite and VAG (volcanic arc granites) after Pearce et al., (1984), Syn-Collision and Post-Orogenic after Bachelor and Bowden, (1985); Post- Orogenic and Peraluminous (Continental collision granitoids), after Maniar and Piccoli, (1989).

The Kasika granite exhibits chemical characteristics of orogenic (syn-COLG, VAG) tectonic settings (Nb vs. Y and Rb vs. Y+Nb diagrams; Pearce et al, 1984). (Fig.II.66). A simular behaviour is seen in SiO_2 – Rb, SiO_2 – Nb, and SiO_2 – $FeO_T/(FeO+MgO)$ diagrams (Maniar and Piccoli , 1989).(Fig.II.66; Fig.II.67).

The Kasika granite data plot in the fields of Orogenic and Post orogenic granites respectively. (Fig.II.67).



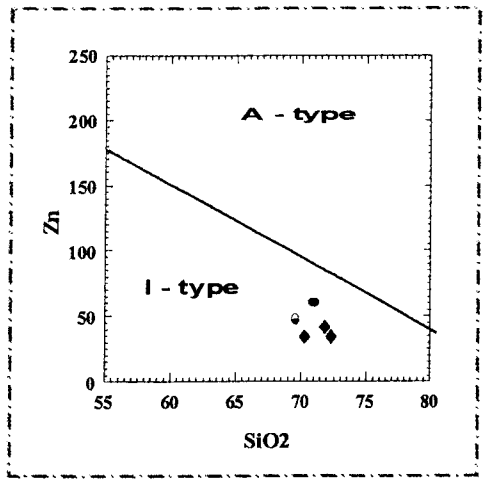
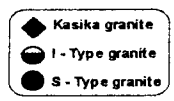
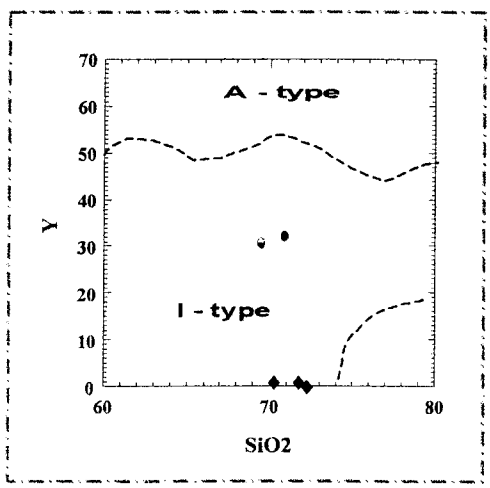


Fig.II.64 : - Plots of Zr versus SiO2 , Zn versus SiO2 , showing the I - type character of the Kasika granite. (after Collins et al., 1982).





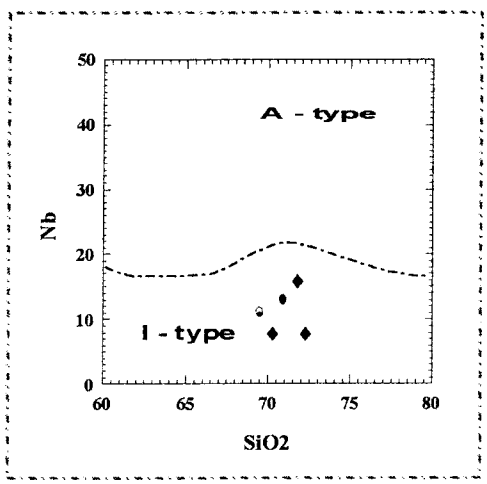
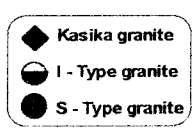


Fig.II.65 : - Plots of Y versus SiO2 , and Nb versus SiO2 showing the I - type character of the Kasika granite. (after Collins et al., 1982).



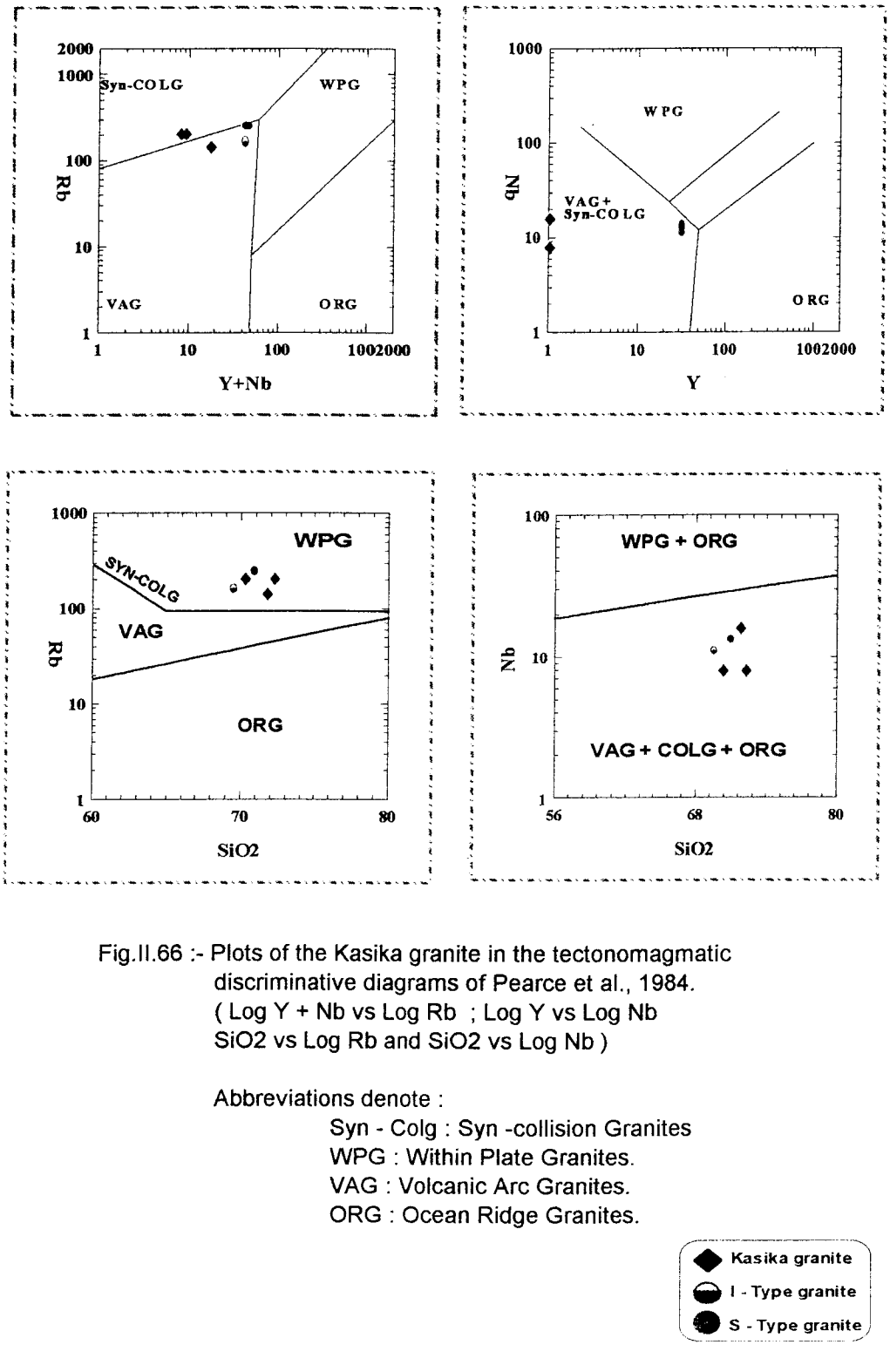


Fig.II.66 :- Plots of the Kasika granite in the tectonomagmatic discriminative diagrams of Pearce et al., 1984.
(Log Y + Nb vs Log Rb ; Log Y vs Log Nb
SiO2 vs Log Rb and SiO2 vs Log Nb)

Abbreviations denote :

Syn - Colg : Syn -collision Granites
WPG : Within Plate Granites.
VAG : Volcanic Arc Granites.
ORG : Ocean Ridge Granites.

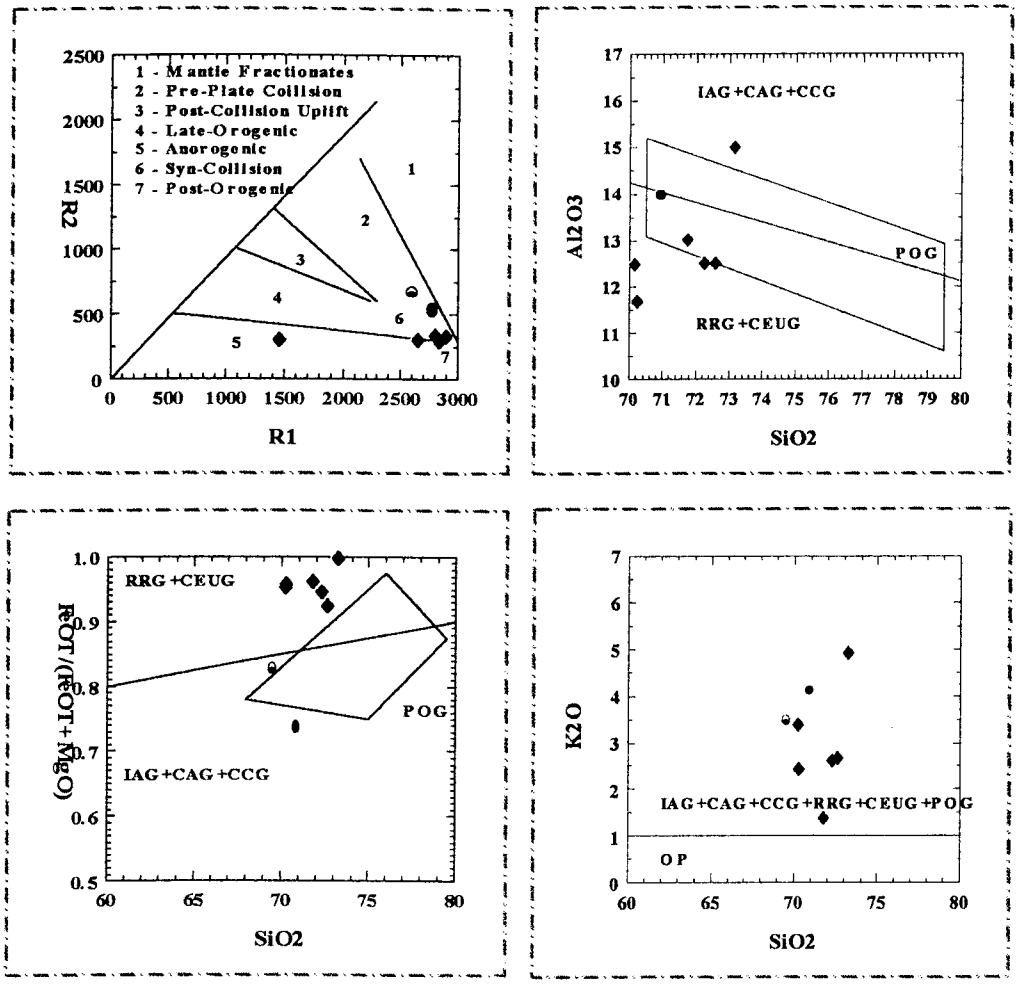


Fig.II.67:- Kasika granite in the discriminant diagrams of Maniar and Picolli (1989) of these the IAG, CAG, CCG and POG are considered orogenic granitoids, and the RRG, CEUG , and OP are considered anorogenic granitoids.

Kasika granite
I - Type granite
S - Type granite

Maniar and Picolli, 1989.

IAG: Island Arc Granitoids
CAG : Continental Collision Granitoids.
RRG: Rift - Related Granitoids.
POG: Post - Orogenic Granitoids.
CEUG: Continental Epeirogenic Uplift Granitoids.
OP : Oceanic Plagiogranites.

R1 - R2 (Bachelor and Bowden, 1985).

R1 = 4 Si - 11(Na + K) - 2 (Fe+Ti)
R2 = 6 Ca + 2 Mg + Al

Several facts support crystal fractionation at the pluton scale:

1.- The Rb -Ba -Sr ternary diagram of El Bouseily, and El Sokkary, (1975) confirm that the Kasika granite is highly differentiated , shows extreme depletions in Sr and Ba and accordingly plots towards the Rb apex of the diagram, a feature typical of albitized and greisenized granites (Fig.II.68).

2.- Negative trends on incompatible (e.g. Rb) versus compatible (e.g. Ba , Sr.) element log-log diagrams characterize the chemical variation produced by crystal fractionation . (Cocherie et al., 1994). (Fig. II.69). The granite is characterized by high Rb/Sr, and Rb/Ba ratios.

3.- On a graph of P_2O_5 against Rb, the leucogranite generally shows no positive correlations. The high P_2O_5 contents of up to 0.59 wt%, appears to be behaving with equal incompatibility to Rb.(Fig. II.70). After, Bea et al.(1994), P is thought to be an incompatible element in leucogranite melt when the activity of Ca is nearly zero and Ca, rather P, is an essential structural constituent of apatite.

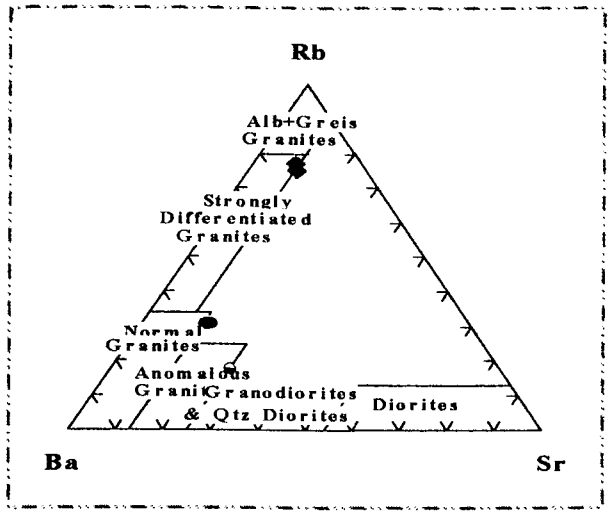
4- Crustal contamination processes provide a further complication in the interpretation of this rock . High Rb, Th and U values are interpreted as reflecting some crustal contamination.

5.- The parental magma is not known. MgO vs. Ni diagram (Fig.II.71) of Elthon (1998) demonstrates its non-primary nature. Very low Ni concentrations of 3 ppm at 0.49 wt% MgO, is below the concentration estimated by Elthon (1989) for primary melts. In this context, it is difficult to infer what the primary source composition may have been.

5.5.1.5.2.- GEOTECTONIC MODEL :

Determining the exact origin and source region of the Kasika leucogranite may not be possible now. Detailed calculations of partial melting, crystal fractionation and assimilation-fractional crystallization processes for the Kasika granite is behond this study. Nonetheless, some general comments and conclusions concerning the origin and evolution of this granodiorite can be made and a generalized model for its petrogenesis proposed.

The Kasika leucogranite -pegmatite system belongs to the silica-oversatured granitic compositions sensu lato. Chemical variation of the granitic complex has been successfully modelled by fractional crystallization .



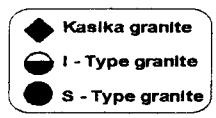
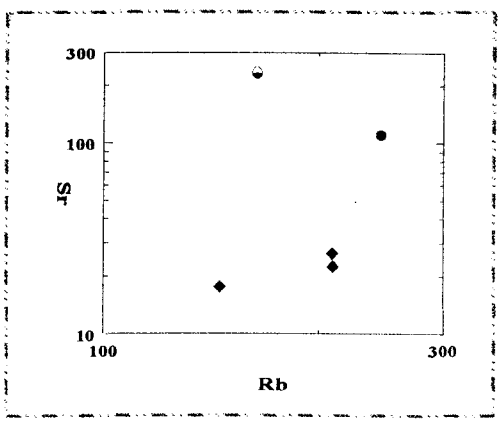
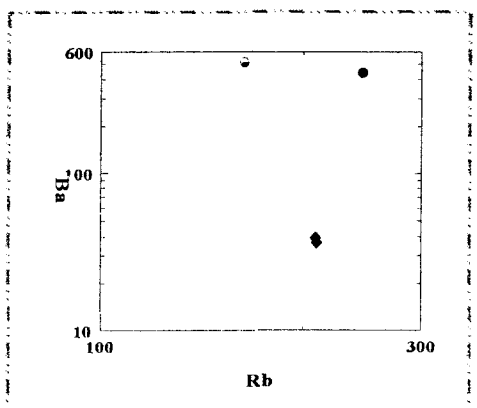


Fig.II.68:- Ternary Rb - Sr - Ba diagram showing the characteristics of the Kasika granite.





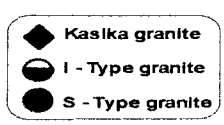


Fig.II.69:- Log - log diagrams of incompatible (Rb) versus compatible elements (Ba, Sr) after Cocherie et al., (1994).

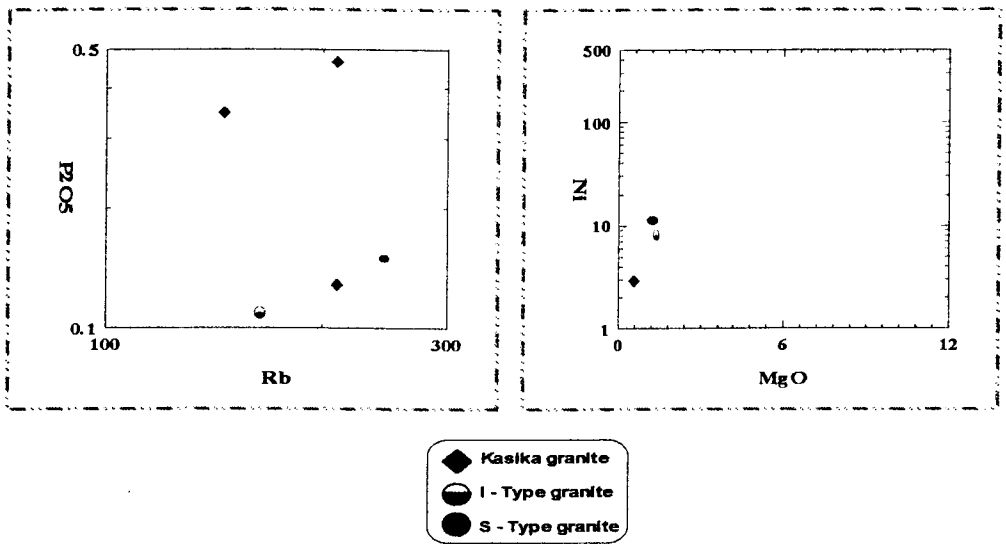


Fig.II.70:- Bivariat plot of P2O5 versus Rb
Fig.II.71:- MgO versus Ni diagram of Ethon (1998).

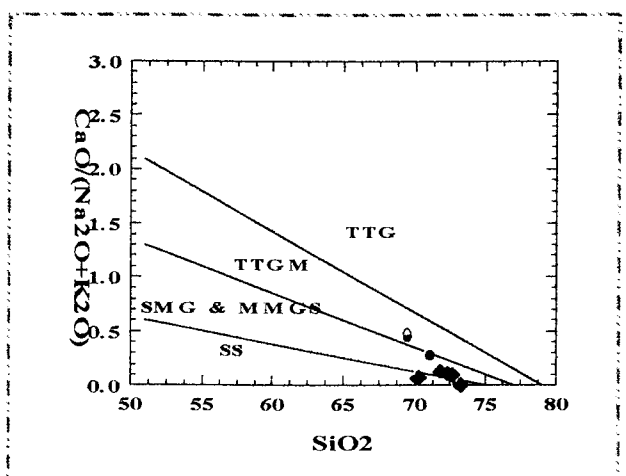
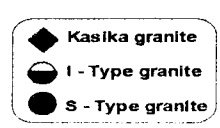


Fig.II.72:- SiO2 versus CaO / (K2O + Na2O) diagram of Feng and Kerrich , (1992).



The mineralogy, chemistry, and isotopic composition of the Kasika granite indicates that it is distinctly more I-type in character than S-type and fits the criteria intermediate for I and S-type granite. In the plot of SiO_2 vs. $CaO/(K_2O+Na_2O)$ (Feng and Kerrich , 1992), the Kasika granite falls into the field of GMG (syncollisional garnet –muscovite granite) series of syn- to late-tectonic type (Fig.II.72) and is consistent with intracrustal melting of various proportions of juvenile mantle-derived rocks and older, crustally derived materials. This is also consistent with the geochemical characteristic of the granite observed in this study.

Two possible sources have been advocated for Phanerozoic syncollisional granitoids, being derived either from the sedimentary wedge attached to the front of a continental margin, or from the hydrated base of thrust sheets (Debon et al., 1986; Harris et al., 1986; Le Fort, 1988). According to Harris et al., 1986; syn-collisional peraluminous intrusions (leucogranites) may be derived from the hydrated bases of continental thrust sheets and are characterized by high Rb/Zr ; Ta/Nd and low K/Rb ratios.

Debon and Le Fort (1983) define three major magmatic associations, namely " cafemic " suites derived from mantle sources, " aluminous " suites derived predominantly by anatexis of continental crust, and " alumino-cafemic " suites intermediate between the two.

The Kasika granite may satisfies the criteria of the " alumino-cafemic " association.

Despite some geochemical similarities to post-orogenic granites, the Kasika leucogranite is better interpreted as a syn-to late- orogenic granite which probably was formed by partial melting of lower –upper crustal /upper mantle source rocks. A mixed crustal / upper mantle source is also indicated by mixed , S and I-type characteristics (e.g. initial $^{87}Sr/^{86}Sr$ of 0.885419 ; Reid and Barton, 1983) and LIL/HFS element ratios.

The Kasika granite is a leucocratic, peraluminous ,SiO_2- and K_2O- rich granite/alkaligranite. Intense crystal fractionation produced highly differentiated pegmatites from granitic melt which may have originated by partial melting of crustal/upper mantle source rocks. Formation probably occurred in a deep Kibaran gneissic and/or granitic environment and at high temperatures (> 800 ^{0}C). The most plausible source for the Kasika granite is the Kibaran gneissic metasediments, which are relatively mature, and contain older crustal materials. The peraluminous Kasika granite plus its pegmatite asssociations also represent modification of pre-existing upper –crust. The Kasika granite – pegmatite system is of syn-to post –orogenic Kibaran affiliation and undepleted basement Kibaran lithologies seem to be the sole source of LCT –type elements (LCT - association for lithium, cesium and tantalum of fertile granite . Cerny, 1991).

5.5.2.- TWANGIZA ALBITITE.

5.5.2.1.- INTRODUCTION.

Albitite rock is found scattered throughout the Twangiza region (Fig.II.5) and in particular within the main deposit. The occurrences have been observed north, northeast and east of the main deposit, and most of them appear to be barren of gold mineralization. In the Twangiza region, gold mineralization is often, but not always associated with the albitite rock . Petrographic and geochemical (major-trace element) data shows the Twangiza albitite intrusion to be of igneous origin and related to a a deep-seated alkalic magmatism. Protoliths are inferred to be the Kasika peraluminous leucocratic granite.

5.5.2.2.- - PETROGRAPHY.

Macroscopically ,the weathered rock has a mottled appearence, is soft, crumbly, and is yellowish-brown to whitish, stained throughout with limonite,and riddled with ferruginous veinlets. From the alteration of albitite, clay minerals (kaolin and montmorillonite) are formed.

The fresh rock is characterized by the appearance of zoned metasomatic columns, with a varying number of minerals and displaying sharp mutual boundaries.
Lithology of the zoned albitite grades from dolomitised albitite to magnesitised albitite , through chloritised albitite (Fig.II.73 ; Fig.II.74). All transitions between these three types can be observed and provides an excellent example of " in situ " differentiation.
The rock is compact, hard, mottled and granular in appearance, coarse-grained to fine- grained, and grading in colour from whitish to dark green, (more magnesium) through light- grey and blue- greenish.

Albite is the main component, followed by iron oxide, iron-magnesium carbonate , chlorite and sericite. Occasionally, the rock is covered by scattered disseminated sulphide (pyrite) grains and a cross-cutting network of spider veinlets. Quartz is generally absent or occurs as a minor. (Fig.II.75; Fig.II.76).

Fig.II.73:- - Twangiza albitite outcrops: weathered, yellowish-brown ,soft with mottled appearance.

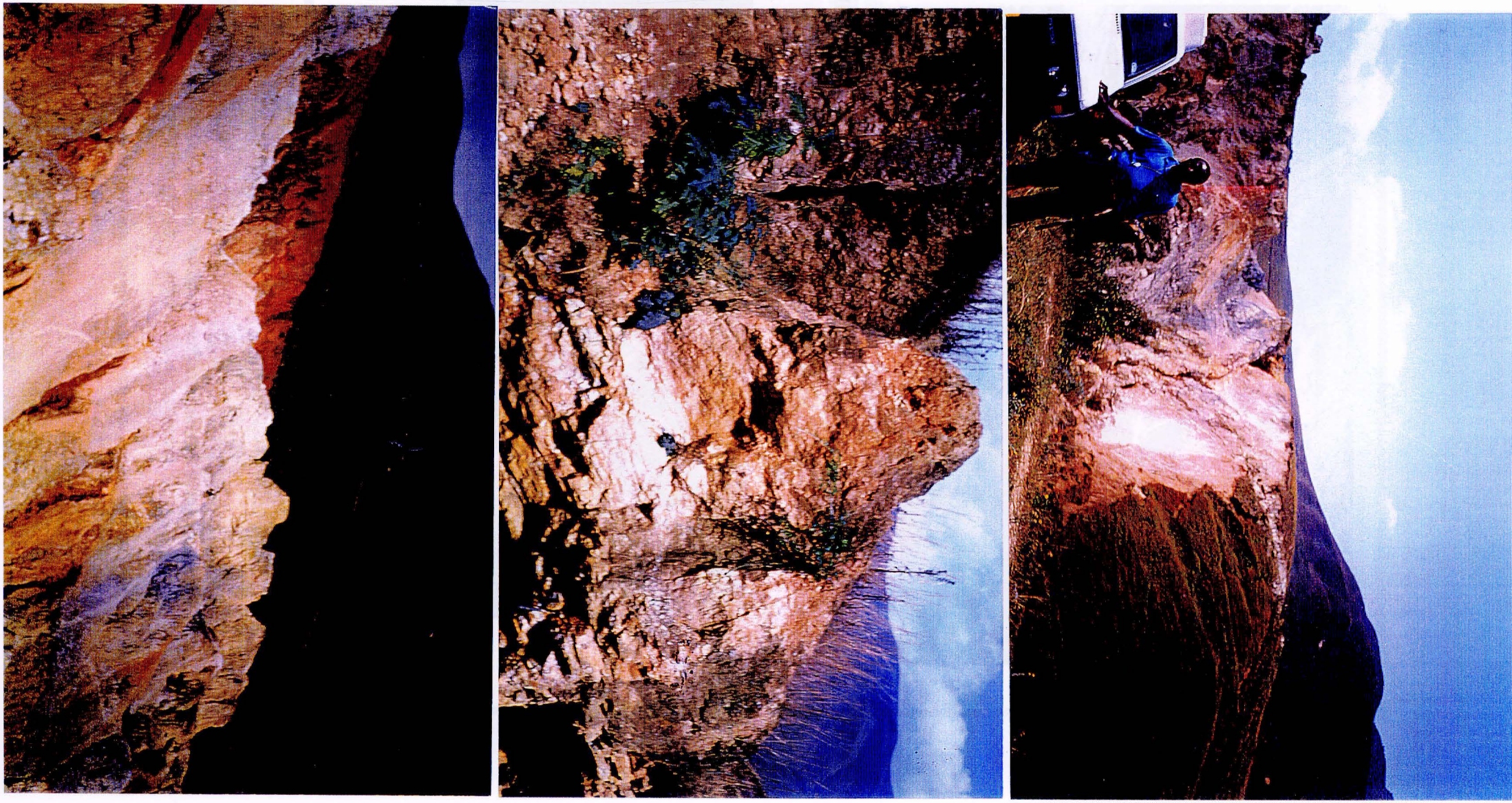




Fig.II.74:- Close observation of the Twangiza albitite rock. The rock is compact with mottled and granular appearance.



Fig.II.75:- : - Hand specimen of albitite rock cut by two sets of quartz-vein with halo of silicification and carbonatization extending from vein. Pyrite and green mica occur in the zone of bleaching.

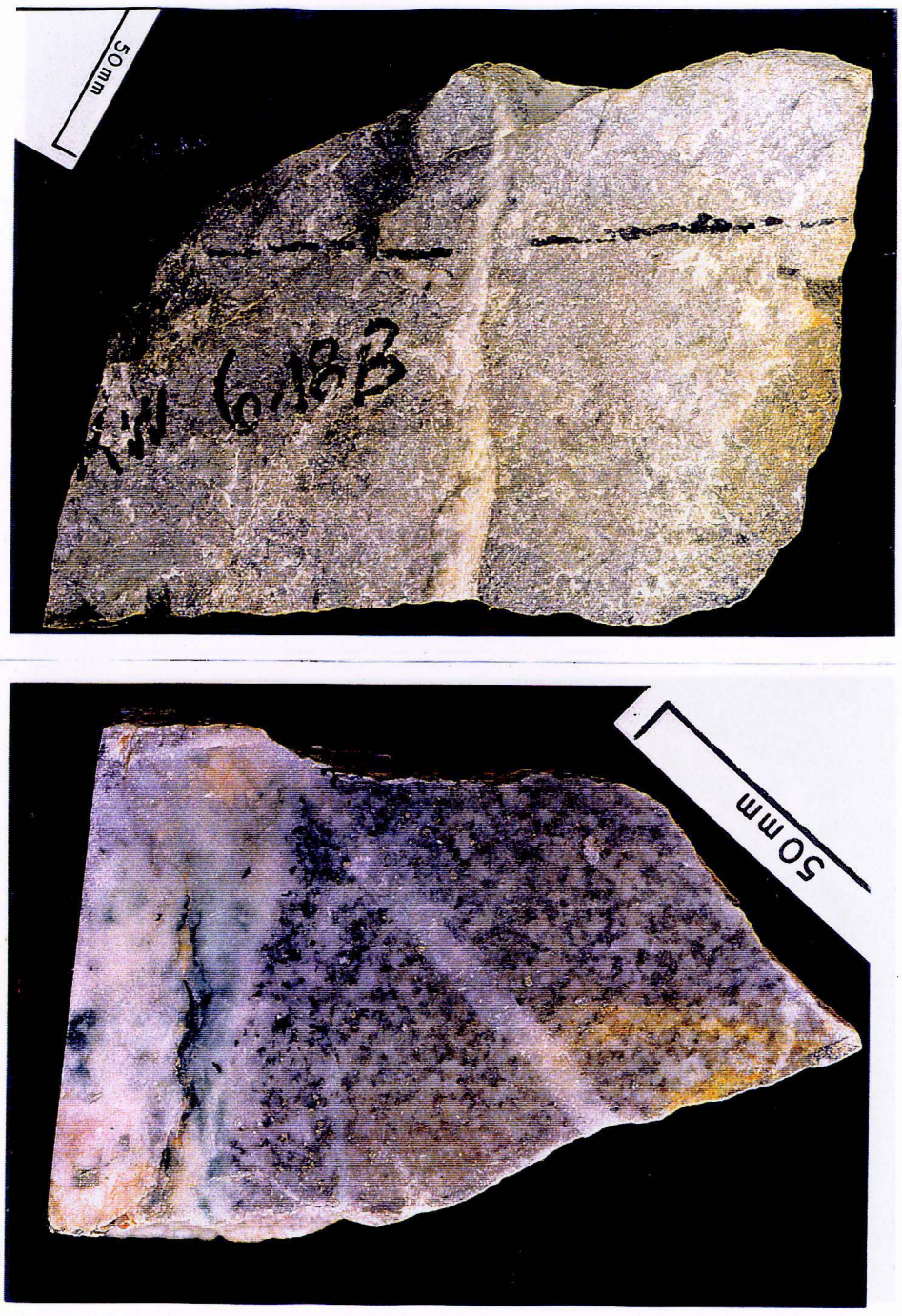


Fig. II.75b:- Hand specimem of albitite rock cut by sets of quartz- carbonate QV_1 veins with halo of silicification and carbonatization extending from the veins. Pyrite and green mica occurring in the zone of bleaching.

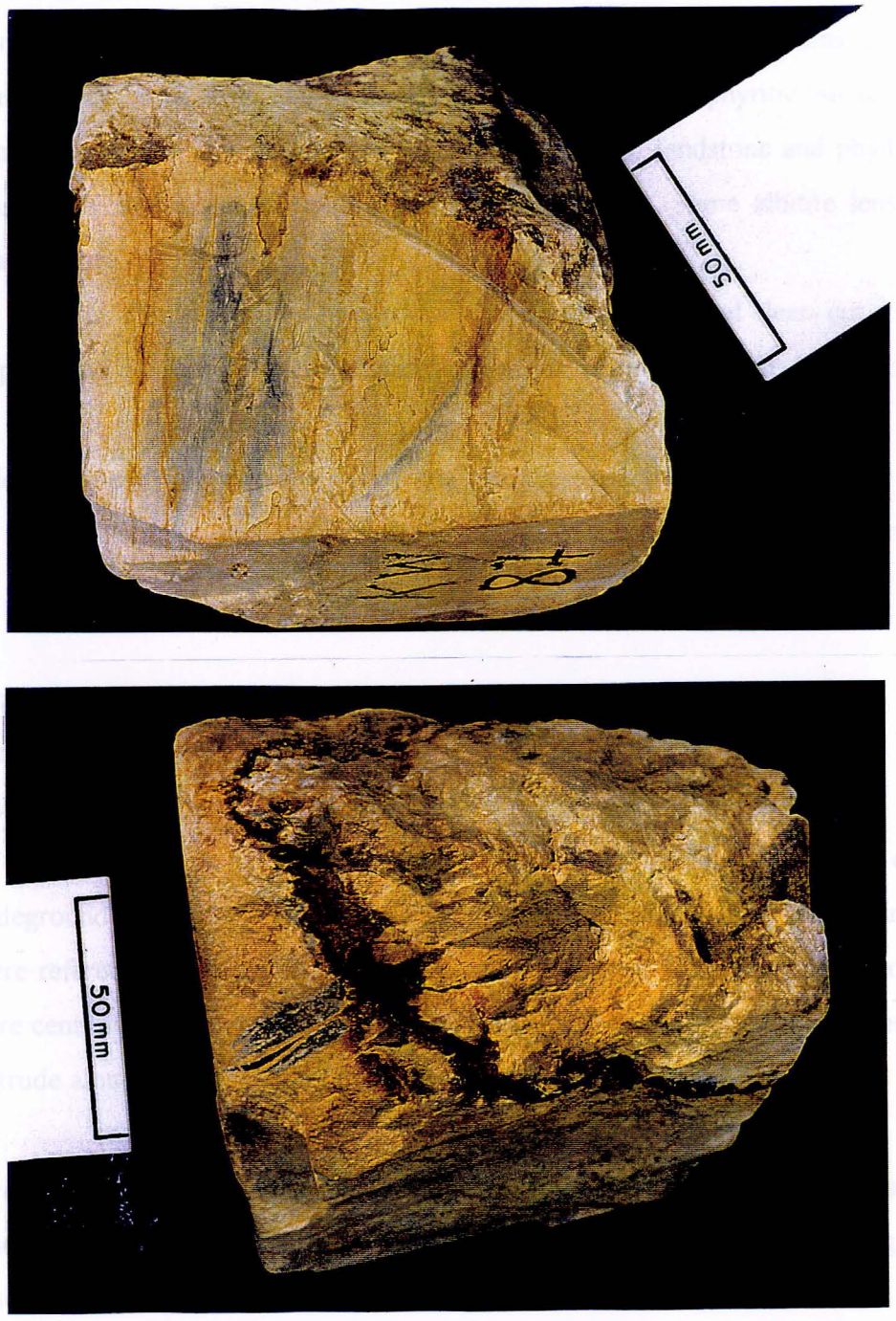


Fig.II.76:- - Hand specimens of weathered halo of altered albitite rock cut by QV_2 (quartz / iron after sulphide vein and exhibiting coarse rutile grains in alteration zone.

The albitite rock is massive with no well developped fabric and contains inclusions of relatively fresh and unstrained black shale.The texture is homogranular to porphyritic but towards the contact with the host rock metasediments (black shale, arkosic sandstone and phyllite), the albitite lenses exhibit a lineation texture and become bedded. Some albitite lenses show dislocation and/or are shifted.

The contact between albitite and their host-rocks is often concordant and clear- cut. However, transition type rocks, the result of metasomatism reactions, from albitite to host rock, exist .

Macroscopically, these intermediate rocks are characterised by high contents of sodic plagioclase, set in a matrix of phyllosilicates. The degree of schistosity varies according to the specimen.

They are :

*- Albite – chlorite schist.

*- Albite – chlorite – quartz schist.

*- Albite – sericite - quartz – chlorite schist.

Evidence of forceful intrusion has been noted in the exocontact zone of intrusions observed in some undeground workings. This albitite rock is surrounded by numerous discrete injections, which is here refered to as marginal since most occur less than 1km from the pluton. Most injections are centimetre-to metre –wide, one to several metres long sheet-like bodies . Other injections intrude along planes of lithological weakness (Fig.II.77).

Microscopically, the albitite rock is an albitite which has been extensively dolomitised, sericitised and chloritised. Relatively coarse pyrite, with associated rutile, is disseminated throughout.

The composition (estimation abundances in vol. %) and texture are as follow:

*- Plagioclase ; (63 vol. %), shows a mass of coarse , up to 1.8mm long, subhedral laths with finer, more anhedral grains occuring intergranularly.

*- Dolomite ; (20 vol.%), occurs as granular aggregates, enclosing fine rutile, pervasively replacing fine grained feldspar.

*- Chlorite ; (7 vol.%), occurs as fine-grained material associated with carbonate.

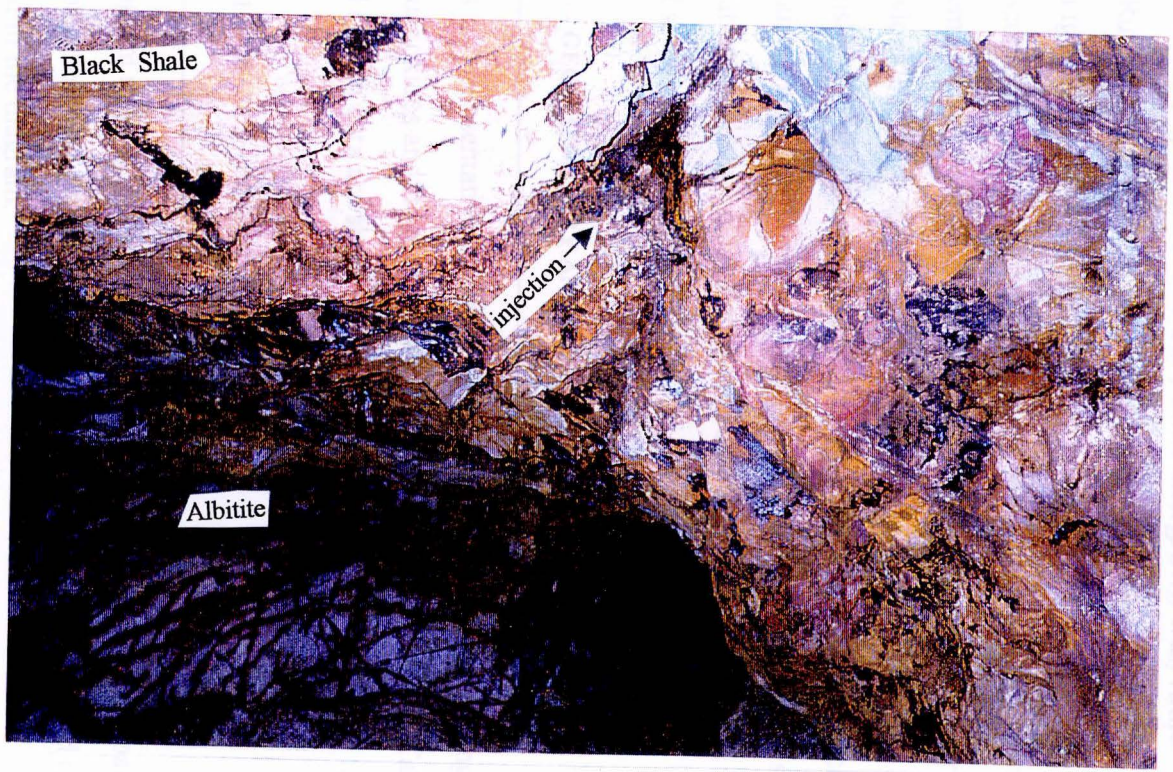


Fig.II.77:- - Albitite injection within the black shale. Fracture control of alteration haloes.

*- Sericite ; (5 vol. %), occurs as extremely fine, with an occasional flake up to 0.08mm long, patchily developed alteration product, particularly of the coarser grained plagioclase.

*- Quartz, (< 1 vol.%), occurs as irregular bodies, < 1.0mm across, interstitial to fedspar.

*- Pyrite , (2 – 3 vol. %), is disseminated and occurs mostly as subhedral to anhedral bodies , up to 0.4mm across , often intergrown with rutile.

*- Rutile ; (1- 2), are found as a clusters of fine material often associated with pyrite. (Fig.II.78).

Microscopic evidence of deformation in the albitite consists of the breaking up of relict replacement to an even distribution of blebby grains in an albite matrix , reducing the grains size to a mylonitic texture and opening of cleavage in albite.

A whitish , silky talc – carbonate rock is associated with albitite rock. This rock consists of a fine-grained, white phyllosilicate matrix surrounding centimetre - sized clots of carbonate. The matrix consits of undulating intergrowths of chlorite and talc and millimetre- sized fan – shaped sprays of talc (Fig.II.79).

5.5.2.3.- - GEOCHEMISTRY AND ISOTOPE GEOCHEMISTRY.

Results of representative analyses of the albitite rock and covering most of the variation of individual oxides and trace elements, are given in Table. II.9 and Table. II.10. The Rb-Sr and Sm-Nd system data are shown in Table. II.11.

5.5.2.3.1.- - MAJOR OXIDES.

The diagram in Fig.II.80, was developed by Hughes in 1972 to separate altered from unaltered rocks based on their Na and K content .Unaltered rocks are believed to plot inside the broad zone depicted in the diagram.

The diagram of Hughes (1972), shows the field of alkalies exchange, particularly albitization (sodic alteration)falling outside of the igneous spectrum field. Some samples fall outside the spectrum in the albitized field and have excess Na for a given total alkali content indicating anomalously high Na contents caused by alteration (Na- metasomatic) processes. Such samples are interpreted as having been albitized.

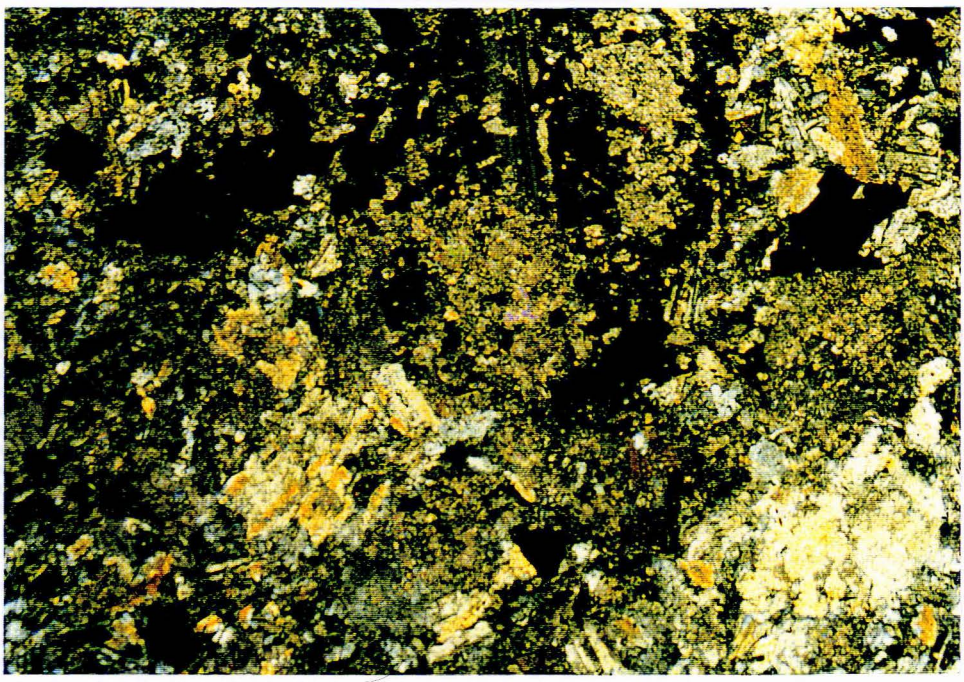


Fig.II.78:- Photomicrograph of albitite rock.

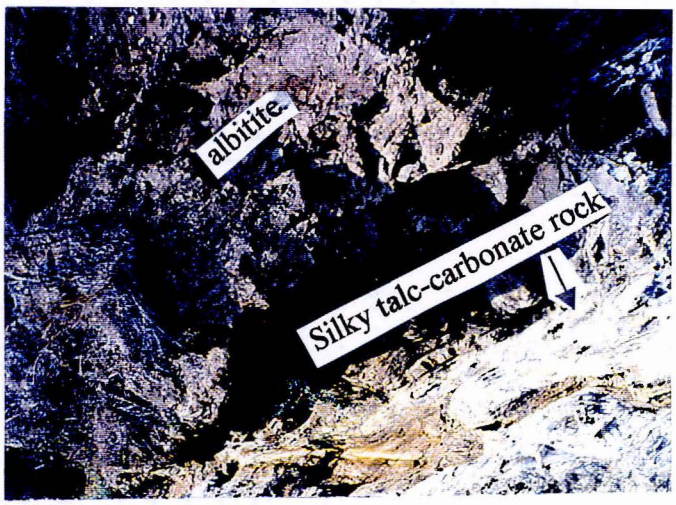


Fig.II.79:- Silky talc-carbonate rock associated with albitite.

Table.II.9 : - CHEMICAL COMPOSITION OF THE TWANGIZA ALBITITE.

Sample	SiO2	TiO2	Al2O3	Fe2O3	FeOT	Fe2O3T	MnO	MgO	CaO	Na2O	K2O	P2O5	F	LOI	Total	Cr2O3	V2O5	Nb2O5	NiO	CuO	ZnO	SO3	FeO
KW 1A	45	1.4	13.5	12.4	82.7	91.72	0.1	7.8	12	2.3	0.1	0.5	0.1	-	95	0.03	0	-	0.03	0.02	0	0.04	71
KW 1B	45	1.4	13.3	12.3	81.9	90.84	0.1	7.8	12	2.4	0.1	0.4	0.1	-	95	0.04	0	-	0.04	0.03	0	0.04	71
KW 1C	46	1.7	16.4	10.8	71.9	79.68	0.1	6.5	10	3.5	0	0.2	-	3	99	-	-	-	-	-	-		62
KW 434C	42	1.9	34.1	0.44	2.93	3.24	0	0.2	0	0	0.1	0.1	-	21	100	-	-	-	-	-	-		2.5
KW 618 Fsj	-	-	-	-	-	-	-	-	-	-	-	-	-	-	-	-	-	-	-	-	-		-
KW 618B1	42	1.9	13.6	12.4	82.7	91.66	0.1	7	7.8	3.2	0.3	0.3	0.1	-	88	0.02	0	-	0.02	0.01	0	-	71
KW 618B2	43	1.8	14.7	3.37	22.5	24.91	0.1	6.2	8.6	5.2	1.2	0.2	-	15	99	-	-	-	-	-	-		19
KW 618B3	39	1.8	13.3	8.91	59.4	65.86	0.1	6	11	3.5	0.9	0.2	-	-	85	-	-	-	0.02	0.01	0	0.1	51
KW 618B4	38	1.7	12.9	8.81	58.7	65.12	0.1	5.9	11	3.3	0.8	0.3	-	-	83	0.01	0	-	0.01	0.03	0	0.12	51
KW 618E2	41	1.9	13.9	3.71	24.7	27.42	0.1	6.4	11	5.5	1.1	0.2	-	-	99	-	-	-	-	-		14.4	21
KW 618E4	43	1.5	14	3.99	26.6	29.49	0.1	5.1	8.9	4.7	2.2	0.3	-	15	99	-	-	-	-	-	-		23
KW 618E5	41	1.8	13.4	3.47	23.1	25.63	0.1	5.3	9.3	5.6	2.1	0.2	-	16	100	-	-	-	-	-	-		20
KW 618E6	43	1.9	14.5	3.47	23.1	25.63	0.1	5.3	9.3	5.6	2.1	0.2	-	15	100	-	-	-	-	-	-		20
KW 618E7	42	2.1	15.5	7.06	47.1	52.18	0.2	6.2	7	5.3	1.5	0.7	-	12	99	-	-	-	-	-	-		41
KW 619	49	1.6	14.3	16.2	108	119.7	0	0.5	0.4	4.5	0.6	0.1	-	12	99	-	-	-	-	-	-		93
KW 620A	47	2.5	17.3	15.7	104	115.8	0.1	6.8	2.4	4	0.1	0.3	-	3.2	99	-	-	-	-	-	-		90
KW 620B	46	2.3	16	14.2	94.4	104.7	0.1	7	3.1	3.3	0.1	0.5	0.1	8	93	0.01	0	-	0.02	0.02	0	0.1	81
KW 623A	41	1.3	15.2	3.31	22.1	24.48	0.1	6.5	9.7	5.3	1.6	0.2	-	15	99	-	-	-	-	-	-		19
KW 87A2	46	1.5	34.5	8.98	59.9	66.37	0	0.8	0	0.3	0.5	0.1	0.5	-	93	0.02	0	-	0.01	0.01	0	0.02	52
KW 87B2	42	1.7	33.3	5.39	35.9	39.83	0	0.4	0	0	0.6	0.1	-	15	99	-	-	-	-	-	-		31
KW2 618E	21	0.2	3.83	23.9	160	176.9	0	12	0.1	3	0.1	0	0	-	78	0.01	0	8.52	0.03	0.03	0	14.31	138

Sample	Ba	Rb	Sr	Y	Zr	Nb	Th	Pb	Zn	Cu	Ni	V	Cr	Ta	Co	U	W	Sn	Mo	Au	Ag	As	Se
KW 1A	68	7	335	24	122	42	-	5	-	-	175	238	396	4	42	12	-	-	0	-	-	8	2
KW 1B	56	7	334	24	121	42	-	5	-	-	174	239	397	2	44	-	-	-	0	-	-	11	1
KW 1C	-	-	-	-	-	-	-	-	-	-	-	-	-	-	-	-	-	-	-	-	-	-	-
KW 434C	-	-	-	-	-	-	-	-	-	-	-	-	-	-	-	-	-	-	-	-	-	-	-
KW 618 Fsj	-	-	-	-	-	-	-	-	-	-	-	-	-	-	-	-	-	-	-	-	-	-	-
KW 618B1	-	15	67	16	107	29	8	-	27	-	76	256	162	-	31	-	-	-	-	-		13	0
KW 618B2	92	48	53	24	122	26	-	-	-	-	31	300	139	-	12	-	-	-		0.5	-	246	-
KW 618B3	49	29	56	16	98	28	13	1	28	49	58	267	148	-	36	3	-	-		0.85	-	49	-
KW 618B4	99	28	65	15	94	27	11	1	27	49	56	268	136	-	29	-	-	-		0.7	-	41	-
KW 618E2	69	47	38	22	22	26	-	-	-	-	38	280	123	-	35	14	19	-	3	-		76	-
KW 618E4	158	72	55	24	171	30	-	-	-	-	37	360	69	-	54	21	21	13	4	-		80	-
KW 618E5	119	45	59	20	135	29	-	-	-	-	16	269	59	-	34	16	23	-	4	-		80	-
KW 618E6	165	58	62	22	163	33	-	-	-	-	17	278	47	-	29	20	24	-	3	-		34	-
KW 618E7	150	45	72	24	171	34	-	-	-	-	50	282	26	-	37	19	-	-		-		28	-
KW 619	61	43	18	31	147	36	-	-	-	13	61	231	206	-	21	14	32	-	4	-		727	-
KW 620A	47	22	79	27	159	33	-	-	12	62	62	335	118	-	37	16	-	-	4	0.35	-	106	-
KW 620B	86	10	90	21	143	38	10	2	30	44	79	291	107	4	44	3	0	-	-	-		251	2
KW 623A	79	61	30	9	83	20	-	-	-	-	15	345	132	-	11	12	-	-	2	-		427	-
KW 87A2	83	23	12	46	404	31	11	-	29	-	33	163	183	-	16	-	8	-	5	0.25	-	2348	-
KW 87B2	-	-	-	-	-	-	-	-	-	-	-	-	-	-	-	-	-	-	-	-	-	-	-
KW2 618E	-	23	27.3	38.3	104	-	160	46	86	-	176	54	64	-	48	27.3	99	-	0.22	-	-	20109	274

Sample	Sb	Bi	Rb/Sr	La	Ce	Pr	Nd	Sm	Eu	Gd	Tb	Dy	Ho	Er	Tm	Yb	Te	Sr87/Sr86	Rb87/Sr86	143Nd/144Nd	m147/Nd144
KW 1A	-	-	0.02	52	69	6	21	5	2	4	-	3	1	2	-	1	1	-	-	-	-
KW 1B	-	-	0.02	-	-	-	-	-	-	-	-	-	-	-	-	-	-	-	-	-	-
KW 1C	-	-	-	-	-	-	-	-	-	-	-	-	-	-	-	-	-	-	-	-	-
KW 434C	-	-	-	-	-	-	-	-	-	-	-	-	-	-	-	-	-	-	-	-	-
KW 618 Fsj	-	-	-	-	-	-	-	-	-	-	-	-	-	-	-	-	-	0.7343	3.347058	0.51259	0.148521
KW 618B1	-	-	0.22	10	18	3	11	2	1	2	-	1	-	-	-	-	-	-	-	-	-
KW 618B2	-	-	0.91	-	-	-	-	-	-	-	-	-	-	-	-	-	-	-	-	-	-
KW 618B3	-	-	0.52	-	-	-	-	-	-	-	-	-	-	-	-	-	-	-	-	-	-
KW 618B4	-	-	0.51	-	-	-	-	-	-	-	-	-	-	-	-	-	-	-	-	-	-
KW 618E2	-	-	1.24	-	-	-	-	-	-	-	-	-	-	-	-	-	-	-	-	-	-
KW 618E4	-	-	1.31	-	-	-	-	-	-	-	-	-	-	-	-	-	-	-	-	-	-
KW 618E5	-	-	0.76	-	-	-	-	-	-	-	-	-	-	-	-	-	-	-	-	-	-
KW 618E6	-	-	0.94	-	-	-	-	-	-	-	-	-	-	-	-	-	-	-	-	-	-
KW 618E7	-	-	0.63	-	-	-	-	-	-	-	-	-	-	-	-	-	-	-	-	-	-
KW 619	-	-	2.39	-	-	-	-	-	-	-	-	-	-	-	-	-	-	-	-	-	-
KW 620A	-	-	0.28	-	-	-	-	-	-	-	-	-	-	-	-	-	-	-	-	-	-
KW 620B	-	1	0.11	12	26	3	12	2	1	3	-	1	-	-	-	-	-	-	-	-	-
KW 623A	-	-	2.03	-	-	-	-	-	-	-	-	-	-	-	-	-	-	-	-	-	-
KW 87A2	-	8	1.92	67.8	166	14	52	9.7	2	9.5	1.4	8.7	1.6	4.9	0.7	4.8	-	-	-	-	-
KW 87B2	-	-	-	-	-	-	-	-	-	-	-	-	-	-	-	-	-	-	-	-	-
KW2 618E	-	518	0.83	-	-	-	-	-	-	-	-	-	-	-	-	-	-	-	-	-	-

Table.II.10 :- CIPW - NORMS OF THE TWANGIZA ALBITITE.

Sample	SiO2	TiO2	Al2O3	Fe2O3	FeO	FeOT	Fe2O3T	MnO	MgO	CaO	Na2O	K2O	P2O5	F	LOI	Total
KW 1A	45	1.35	13.48	12.41	71.39	82.56	91.72	0.13	7.8	11.61	2.3	0.07	0.46	0.07 -		94.83
KW 1B	45.31	1.41	13.34	12.29	70.7	81.76	90.84	0.12	7.8	11.69	2.41	0.05	0.39	0.07 -		95.02
KW 1C	45.99	1.67	16.37	10.78	62.02	71.72	79.68	0.11	6.52	10.45	3.49	0	0.23 -		3.04	98.65
KW 434C	41.52	1.86	34.14	0.44	2.52	2.92	3.24	0	0.22	0	0	0.07	0.05 -		21.41	99.74
KW 618B1	41.53	1.88	13.61	12.4	71.34	82.5	91.66	0.11	6.97	7.8	3.15	0.29	0.32	0.07 -		88.28
KW 618B2	42.73	1.82	14.67	3.37	19.39	22.42	24.91	0.11	6.16	8.61	5.17	1.21	0.21 -		14.52	98.58
KW 618B3	39.4	1.8	13.33	8.91	51.26	59.28	65.86	0.11	5.99	10.53	3.45	0.88	0.21 -	-		84.93
KW 618B4	38.06	1.7	12.9	8.81	50.68	58.61	65.12	0.12	5.91	10.52	3.3	0.8	0.33 -	-		82.76
KW 618E2	40.74	1.93	13.92	3.71	21.34	24.68	27.42	0.14	6.39	10.6	5.48	1.09	0.22 -	-		98.62
KW 618E4	43.22	1.52	14.04	3.99	22.95	26.54	29.49	0.13	5.13	8.9	4.72	2.22	0.3 -		14.96	99.14
KW 618E5	41.37	1.75	13.44	3.47	19.95	23.07	25.63	0.14	5.31	9.29	5.62	2.05	0.24 -		16.3	100.36
KW 618E6	42.77	1.85	14.53	3.47	19.95	23.07	25.63	0.14	5.31	9.29	5.62	2.05	0.24 -		14.74	100.01
KW 618E7	42.31	2.06	15.49	7.06	40.61	46.96	52.18	0.17	6.24	6.98	5.27	1.51	0.67 -		11.66	99.4
KW 619	48.58	1.63	14.31	16.19	93.14	107.71	119.67	0.01	0.54	0.43	4.54	0.6	0.09 -		11.89	98.82
KW 620A	46.57	2.5	17.29	15.66	90.09	104.18	115.75	0.09	6.79	2.36	4.02	0.07	0.32 -		3.22	98.88
KW 620B	46.31	2.26	15.96	14.16	81.46	94.2	104.66	0.06	7	3.09	3.26	0.1	0.46	0.06	8	92.91
KW 623A	40.58	1.34	15.16	3.31	19.04	22.02	24.46	0.12	6.51	9.68	5.3	1.63	0.2 -		15.42	99.25
KW 87A2	46.44	1.49	34.52	8.98	51.66	59.74	66.37	0.01	0.8	0.04	0.3	0.51	0.08	0.5 -		93.31
KW 87B2	42.45	1.74	33.25	5.39	31	35.85	39.83	0	0.42	0	0	0.59	0.1 -		14.63	98.6
KW2 618E	20.65	0.2	3.83	23.93	137.67	159.2	176.88	0	11.82	0.13	2.99	0.11	0.04	0 -		78.11
Av. Alk.syeni	61.86	0.58	16.91	2.32	13.34	15.43	17.14	0.11	0.96	2.54	5.46	5.91	0.19 -	-		96.84

Sample	ACNK	Q	C	Or	Ab	An	Ne	Lc	Ac	Ns	Di	DiWo	DiEn	DiFs	Hy	HyEn
KW 1A	0.96	0	0	-77.56	0	15.81	6.35	61.02	0	0	14.88	7.12	1.09	6.67	0	0
KW 1B	0.94	0	0	-76.43	0	15.36	6.68	60.07	0	0	15.8	7.57	1.17	7.07	0	0
KW 1C	1.17	0	0	-62.33	0	18.39	10.15	48.87	0	0	11.81	5.65	0.84	5.32	0	0
KW 434C	487.71	49.98	42.14	0.51	0	0	0	0	0	0	0	0	0	0	2.13	0.68
KW 618B1	1.21	0	0	-77.55	0	13.88	9.06	61.65	0	0	7.93	3.79	0.53	3.61	0	0
KW 618B2	0.98	0	0	-3.47	0	12.79	22.91	8.14	0	0	22.97	11.33	3.94	7.7	0	0
KW 618B3	0.9	0	0	-73.32	0	13.45	11.64	60.5	0	0	20.86	10	1.64	9.22	0	0
KW 618B4	0.88	0	0	-75.58	0	13.53	11.36	62.05	0	0	20.92	10.03	1.64	9.26	0	0
KW 618E2	0.81	0	0	-28.71	0	9.62	23.8	27.3	0	0	32.9	16.2	5.41	11.28	0	0
KW 618E4	0.89	0	0	-12.39	0	9.85	20.2	19.32	0	0	25.26	12.32	3.35	9.59	0	0
KW 618E5	0.79	0	0	-18.8	0	5.24	25.1	24	0	0	32.43	15.91	4.93	11.59	0	0
KW 618E6	0.86	0	0	-14.04	0	7.94	24.49	20.04	0	0	29.22	14.34	4.46	10.43	0	0
KW 618E7	1.13	0	0	-41.58	0	11.01	18.82	38.05	0	0	10.85	5.24	1.07	4.54	0	0
KW 619	2.57	0	3.12	-40.63	0	0.86	11.56	33.4	0	0	0	0	0	0	0	0
KW 620A	2.68	0	3.81	-59.12	0	5.18	9.92	46.53	0	0	0	0	0	0	0	0
KW 620B	2.47	0	3.43	-50.87	0	7.08	8.58	40.15	0	0	0	0	0	0	0	0
KW 623A	0.91	0	0	-27.41	0	12.39	23.62	28.83	0	0	27.87	13.77	4.92	9.17	0	0
KW 87A2	40.61	2.05	23.11	2.08	1.75	0	0	0	0	0	0	0	0	0	59.9	1.37
KW 87B2	56.36	14.84	28.37	3.03	0	0	0	0	0	0	0	0	0	0	43.94	0.91
KW2 618E	1.19	0	0	-183.89	0	0	5.13	144.45	2.72	0	0.17	0.08	0.01	0.08	0	0
Av. Alk.syeni	1.22	0	0	31.7	32.53	3.78	5.1	0	0	0	5.73	2.73	0.3	2.71	0	0

Sample	HyFs	Ol	OlFo	OlFa	Mt	Hm	Il	Ap	C_I	D_I	A	P
KW 1A	0	57.4	7.4	50	10.97	0	1.54	0.61	84.8	-10.2	-77.56	15.81
KW 1B	0	56.62	7.37	49.26	10.9	0	1.62	0.51	84.94	-9.68	-76.43	15.36
KW 1C	0	52.54	6.59	45.94	10.04	0	2.01	0.32	76.4	-3.3	-62.33	18.39
KW 434C	1.46	0	0	0	0.78	0	4.37	0	7.29	50.49	0.51	0
KW 618B1	0	61.39	7.22	54.17	11.42	0	2.24	0.44	82.97	-6.84	-77.55	13.88
KW 618B2	0	23.96	7.58	16.37	4.79	0	3.34	0.44	55.06	27.58	-3.47	12.79
KW 618B3	0	47	6.51	40.49	9.63	0	2.52	0.34	80	-1.19	-73.32	13.45
KW 618B4	0	47.54	6.56	40.98	9.71	0	2.43	0.54	80.61	-2.17	-75.58	13.53
KW 618E2	0	22.19	6.72	15.47	5.17	0	3.47	0.46	63.73	22.39	-28.71	9.62
KW 618E4	0	24.83	5.97	18.86	5.48	0	2.7	0.61	58.27	27.13	-12.39	9.85
KW 618E5	0	19.91	5.53	14.38	4.97	0	3.24	0.51	60.55	30.3	-18.8	5.24
KW 618E6	0	20.22	5.64	14.58	4.85	0	3.34	0.5	57.64	30.48	-14.04	7.94
KW 618E7	0	43.55	7.69	35.86	8.08	0	3.05	1.14	65.53	15.3	-41.58	11.01
KW 619	0	66.85	0.52	66.33	13.18	0	1.72	0.11	81.75	4.33	-40.63	0.86
KW 620A	0	67.95	6.35	61.61	12.37	0	2.56	0.38	82.87	-2.67	-59.12	5.18
KW 620B	0	66.4	6.98	59.41	11.93	0	2.47	0.58	80.79	-2.13	-50.87	7.08
KW 623A	0	23.07	7.54	15.52	4.73	0	2.47	0.42	58.14	25.05	-27.41	12.39
KW 87A2	58.53	0	0	0	9.09	0	1.95	0.51	70.94	5.88	2.08	1.75
KW 87B2	43.03	0	0	0	6.87	0	2.88	0	53.68	17.87	3.03	0
KW2 618E	0	99.79	10.18	89.61	16.06	0	0.19	0.04	116.2	-34.31	-183.89	0
Av. Alk.syeni	0	14.44	1.3	13.14	3.1	0	1	0.38	24.28	69.32	31.7	36.31

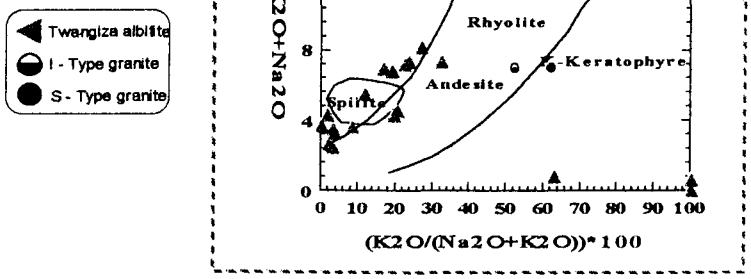


Fig.II.80:- Igneous spectrum diagram of Hughes (1972).

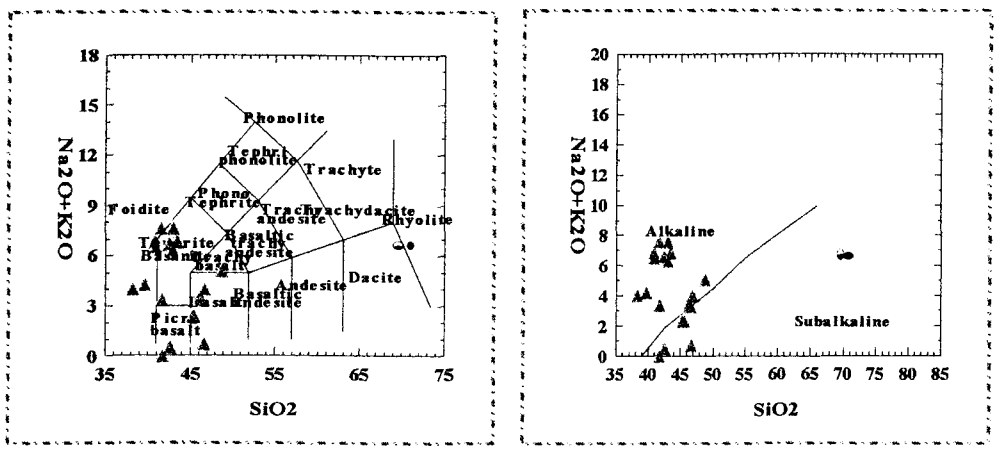
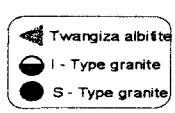


Fig.II.81:- SiO2 versus alkalis diagram.



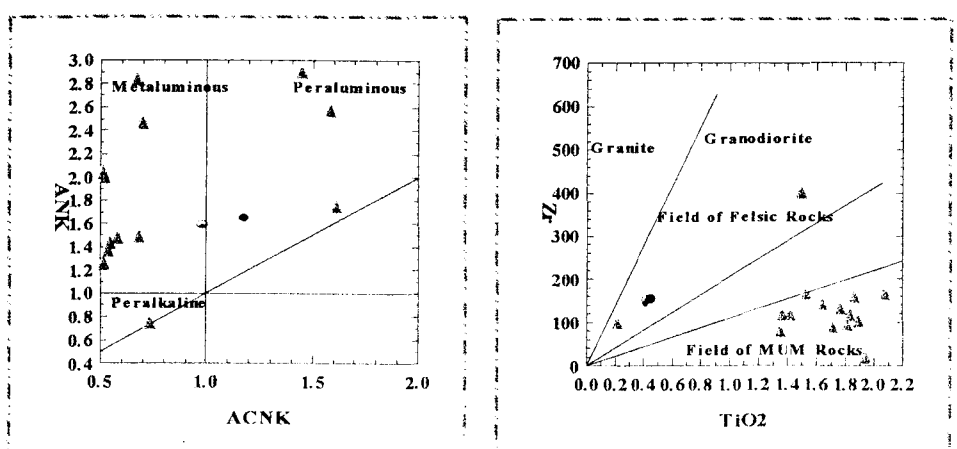
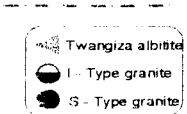


Fig.II.82:- ACNK versus ANK , and Zr versus TiO2 plots.



The majority of the samples fall between the " K " lines, have a so-called normal Na/K ratio, and should represent the " least altered " samples. One sample falls in the potassic alteration field , involving the secondary formation of potash feldspar with possible sericitization and/or biotite which may imply an increase in iron.

On the SiO_2 versus alkalies diagram (Fig.II.81), the samples plot mostly in the alkaline field, with some samples close to the border between alkaline and subalkaline. Three samples fall in the subalkalic field.

On ACNK vs. ANK diagram (Fig.II.82), they fall in the field of metaluminous, with a few slightly peraluminous through peralkaline.

A/CNK = (0.06 - 2.6) and A/NK = (0.2 - 4.2) indicate metaluminous chemistry signature.

This albitite is characterized by very low silica, CaO and MgO contents and a corresponding limited range in other major elements (Table II.9). Harker variation diagrams (Fig.II.83) illustrate some important chemical characteristics of the various rock type and show a slight positive correlation between SiO_2 and many oxide elements (K_2O, FeO, FeO_T, Fe_2O_3, TiO_2, P_2O_5). Some of them (Na_2O, CaO, MnO, Al_2O_3) do not correlate and form a relatively discrete cluster.

The stong positive correlation between Na_2O and K_2O is characteristic for this albitite (Fig.II.83). Enrichment of Na_2O is complemented by depletion of K_2O. The low fractionated character of the albitite, is shown by low SiO_2 (20.65 - 48.58 wt%) and alkalis CaO (0.20-0.73wt%), FeO (1.49- 11.39wt%) and MgO (0.0-0.57wt%) contents, and is also expressed in their trace element contents.(Table.II.9). The iron oxide ratio, Fe_2O_3 /(Fe_2O_3+FeO) = 0.14-0.6 is low. (Fig.II.84). The averall range in major element concentrations is low. SiO_2 is low (20.65- 48.58 wt%), with intermediate Na_2O , CaO, and Al_2O_3 values. Average MgO and K_2O contents are slightly lower. (Table II.9 ;Table II.10). The (Na_2O + CaO) - Al_2O_3 - K_2O diagram of Nesbitt and Young (1984,1989). (Fig.II.85), shows the weathering trends for Twangiza albitite.

In the triangular QAP diagram of Streckeisen (1976) ,(Fig.II.86) the CIPW normative mineral compositions plot in the fields of quartzolite and quarzt-rich granitoids and in the field of I-type granite after Whalen and Curie (1990).

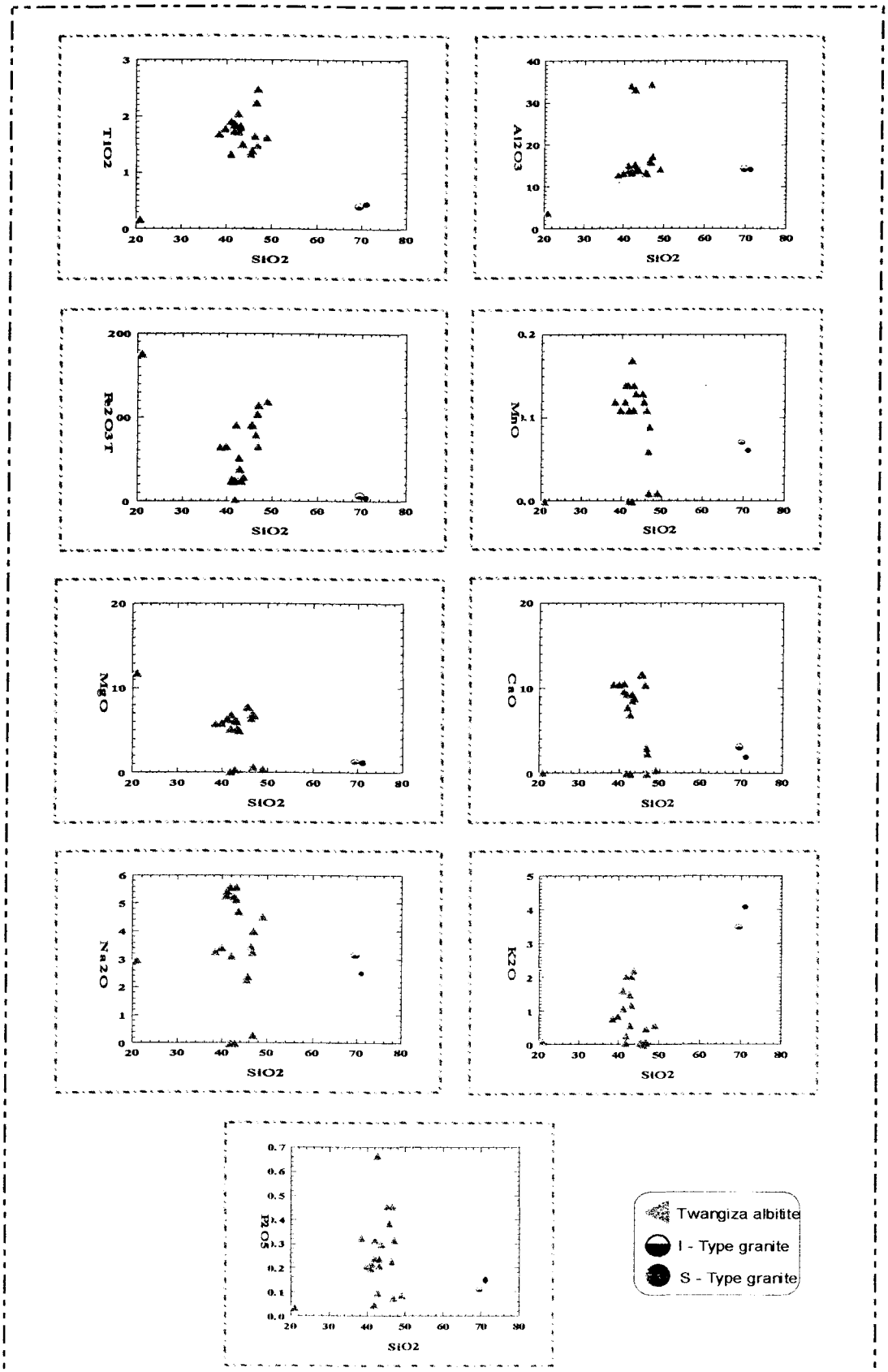
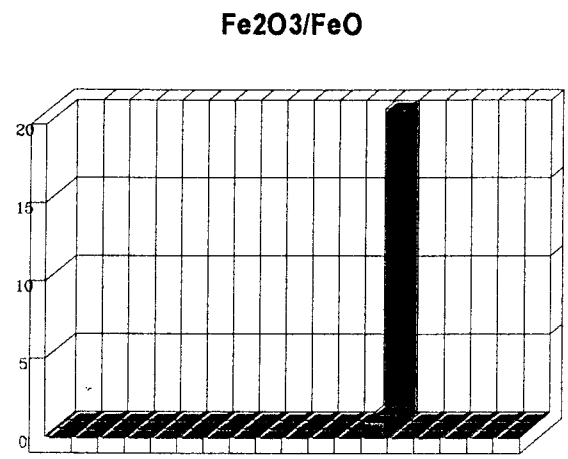


Fig.II.83:- Harker variation diagram for selected major oxide elements from the Twangiza albitite.

Fig.II.84:- Frequency diagram of Fe2O3/FeO



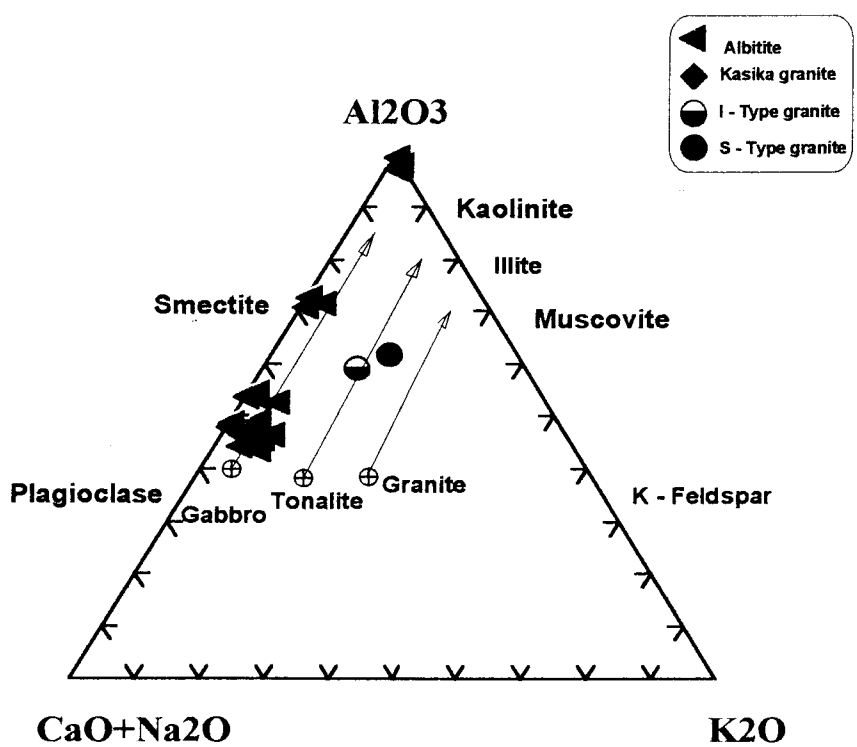


Fig.II.85:- The (Na2O+CaO) - Al2O3 - K2O diagram of Nesbitt and Young (1984, 989) showing the weathering trends for Twangiza albitite.

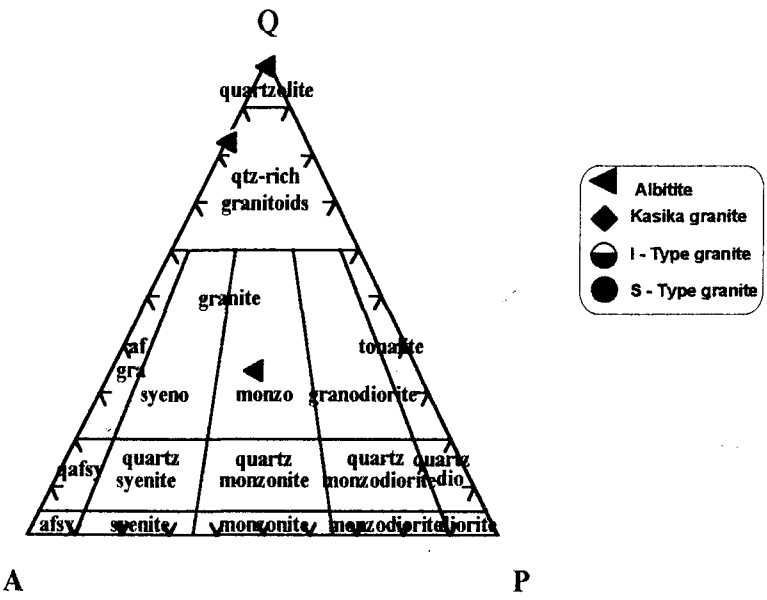


Fig.II.86:- Triangular QAP diagram of Streckeisen (1976) showing CIPW normative mineral compositions of the Twangiza albitite.

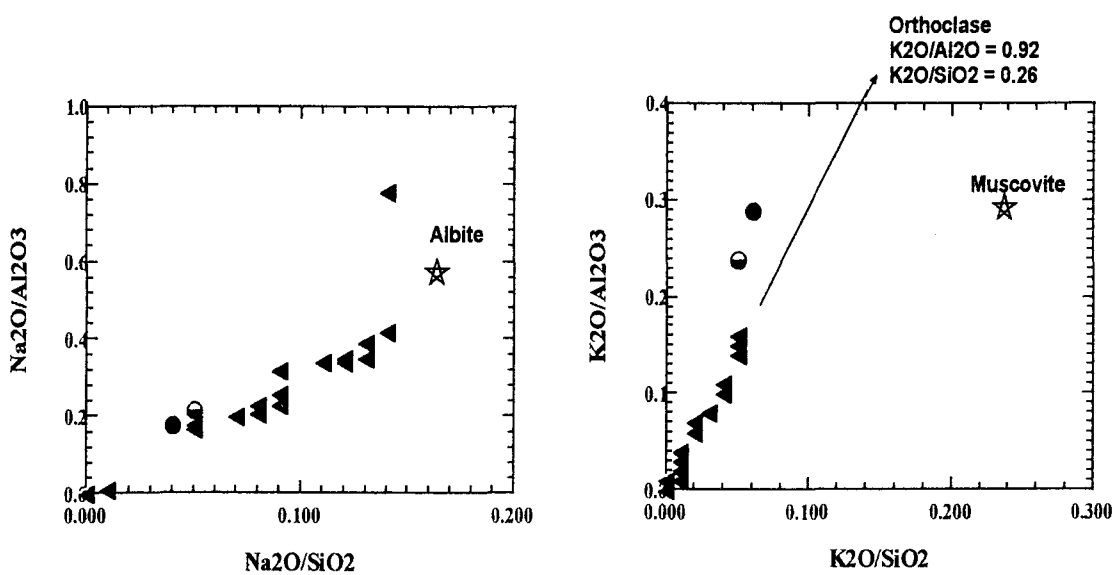


Fig.II.87:- Na2O/SiO2 versus Na2O/ Al2O3 and K2O/SiO2 versus K2O/Al2O3 plots showing albitite samples described in this study.

Petrographic observations, combined with chemical data (particularly K_2O and Na_2O), suggest that sample KW 1 A (albitite from Luidja locality; Fig. II.2) represents the least - altered albitite in the Twangiza region. Albitite samples define a trends away from this albitite sample towards albite. There is a quantitative correlation between the degree of alteration and recrystallization observed in thin section and proximity to albite composition (Fig.II.87).
Mass balance calculations (Gresens, 1967) indicate that albitite at the Twangiza deposit (sample KW 618 E) records increased Na_2O , Al_2O_3 , and MgO relative to less - altered albitite at Luidja locality (Sample KW 1A) . The large amount of chlorite in albitite at the Luidja-Bwami locality, also suggests addition of MgO and /or FeO.

5.5.2.3.2.- TRACE ELEMENTS AND REE.

The albitite samples have low to moderate Ni (31- 174ppm) , and moderate to high LILE concentrations compared to the average syenitic rocks , as shown in Table II.10. (Example include , Rb= 7-48 ppm, Th= 8-13ppm , Ba = 49-92ppm, (Table.II.10). Harker variation diagrams (Fig.II.88), all show a strong correlation between SiO_2 and Y, Zr, Nb, Sr, U, but SiO_2 does not correlate or cluster with other elements (Ba, Th, V, Cr, Co, W, Ni, Mo, La, Ce). A negative correlation is perceptible between SiO_2 and Au, As, Se, and Bi.
There is a strong positive correlation between Rb and Ba and Au and Co. (Fig.II.88) .
The samples have pronounced Nb anomalies (26-42 ppm) and fractionated REE patterns (La / Sm = 5 ppm) including depleted heavy REE and strong light REE enrichment (La= 10-12 ppm). (Fig.II.89). Different spider diagram plots for the Twangiza albitite are shown in Fig.II.90.
The diversity of REE minerals, such as hydrothermal monazite, suggests that the source of sodium –rich fluids may have been deep -seated alkalic (or carbonatitic) intrusions.

5.5.2.3.3.-. RUBIDIUM / STRONTIUM DATING AND SAMARIUM / NEODYMIUM SYSTEMS.

The Sr and Nd isotope ratios are shown in Table.II.11. The Rb – Sr and Sm-Nd systems do not define isochrons. The initial ^{87}Sr /^{86}Sr ratio is 0.734298 ± 11.
The initial $^{143}Nd/^{144}Nd$ ratio (0.512590 ± 23) is consistent with this representing a Kasika granite (0.512669 ± 29) and again suggests a genetic link between these two rock types.

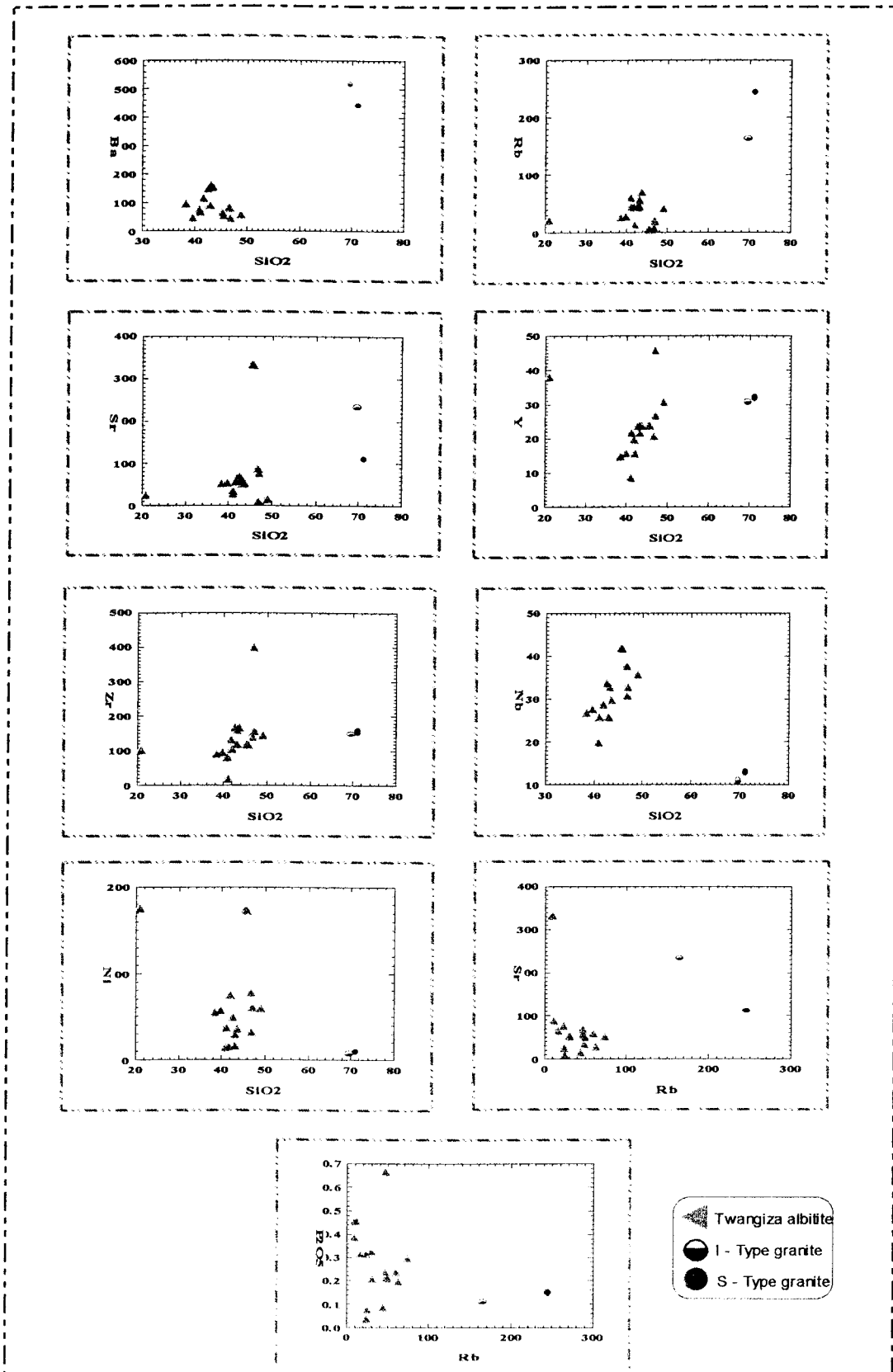
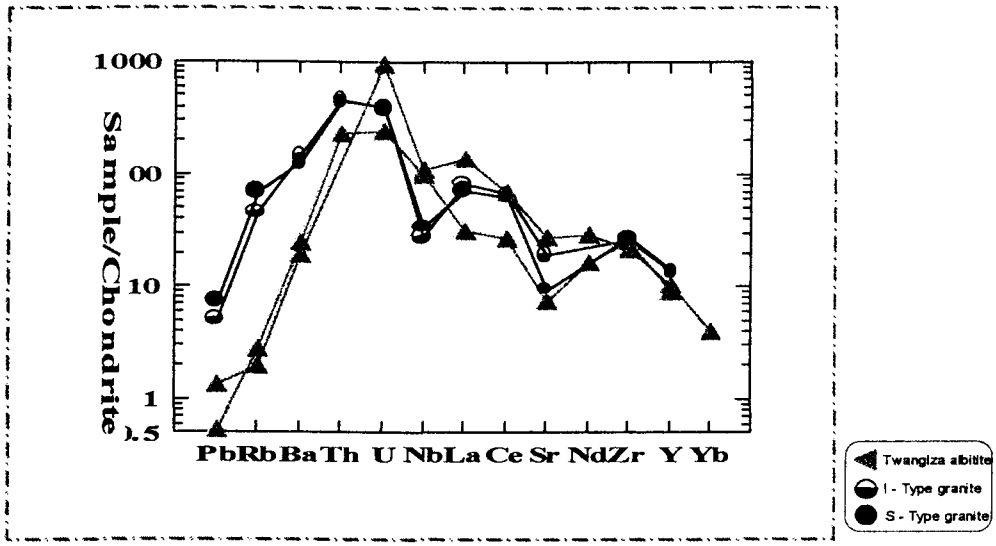


Fig.II.88:- Harker and other variation diagrams for selected trace elements from the Twangiza albitite illustrating some important chemical characteristics.

Fig.II.89:- Chondrite - normalized REE patterns for the Twangiza.



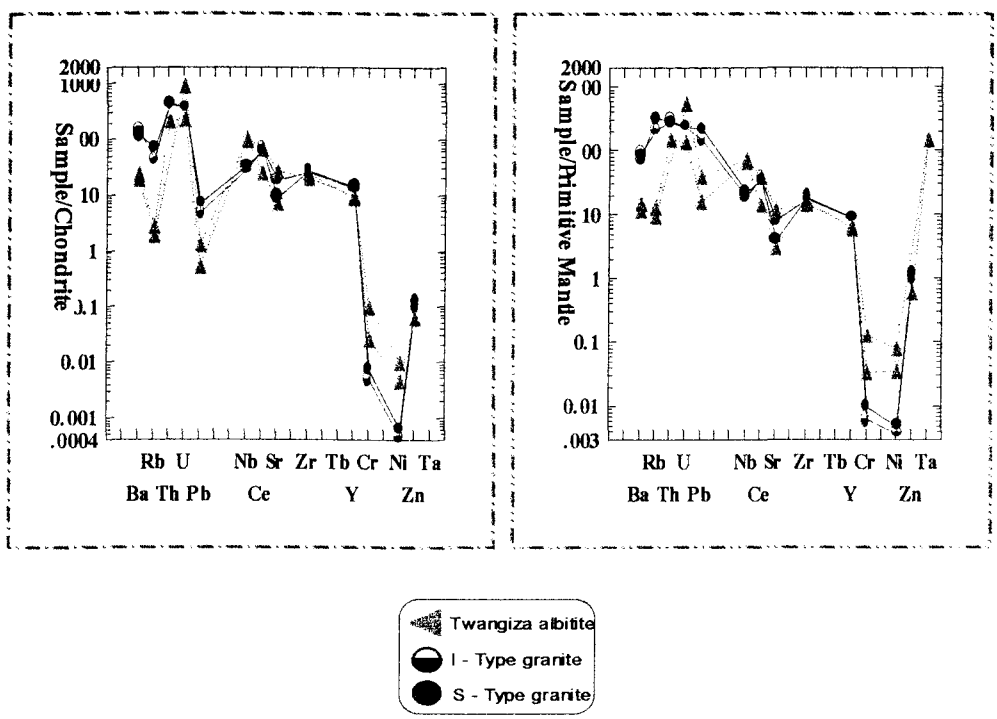


Fig.II.90:- Spider diagrams for Twangiza albitite.

Table II.11:- Rb - Sr and Sm - Nd isotope data for the Twangiza albitite .

Lab #	Sample	Type	Rb ppm	Sr ppm	87Rb / 86 Sr	87Sr / 86Sr +- 1 se	Sm ppm	Nd ppm
E17	KW 618	Feldspar	60.45	52.39	3.347058	0.734298 +/- 11	3.604	14.67

Lab #	Sample	Type	147 Sm / 144 Nd	143Nd / 144Nd +- 1se	Age (Ma)
E17	KW 618	Feldspar	0.148521	0.512590 +/- 23	1078.94 +/- 27

The samples that have a correspondingly similar Nd ratio can be assumed to have evolved from a similar source.

The albitite yielded an age of **1078 ± 27 Ma**, implying that it is related to the Kibaran granites. This age is coeval with a period of Kibaran granitic plutonism in Central Africa (Cahen et al.,1984). Radiogenic isotopes constrain a common source for these two rocks with some contamination.

5.5.2.4.- PETROGENETIC MODEL.

Petrographic, geochemical and isotopic evidence from the Twangiza albitite will be discussed in a endeavour to constrain the origin of this rock. General geotectonic classification schemes (Pearce, 1983, Pearce et al., 1984), illustrate the overall geochemical composition of the Twangiza albitite which plots in the WPG and VAG fields and in the metaluminous I-type to slightly peraluminous. (Fig.II.91; Fig.92; Fig.II.93).

In the diagram of total alkalis versus SiO_2, the albitite falls in the " nepheline ", field with some samples falling within the alkali-rich B+T and basalt fields. (Fig.II.94).
The Classification of the Twangiza albitite is also based on petrographic descriptions and whole-rock chemical analyses. Using the total alkali-silica diagram (Le Bas et al., 1986), the samples are classified as beloging to a suite of rocks ranging in composition from ultramafic to felsic rocks and including picrobasalt, tephrite basanite, trachybasalt, and basalt. (Fig.II.95).

Various geochemical tectonic classification diagrams have been applied to the Twangiza albitite and provide an indication of the tectonic setting of the Twangiza albitite. The Twangiza albitite plots in the field of OFB (Ocean floor basalt), MORB, and Continental arc. (Fig. II.96).
In the discriminant diagrams of Maniar and Picolli, (1984) and (1989), the Twangiza albitite plots mostly in the field of POG (post-orogenic granite). (Fig.II.97). In the Tectonic discriminant diagram of A-type granitoids of Elby, (1992) the Twangiza albitite plots in the subtype A1. (Fig.II.98) . Subtype A1 represents differentiates of magmas derived from sources such as oceanic - island basalts but emplaced in continental rifts or during intraplate magmatism.
According to Eby, (1992), the granitoids of this group were emplaced during intraplate rifting , usually with abundant coeval mafic rocks, or as the result of inferred plume or hotspot activity.

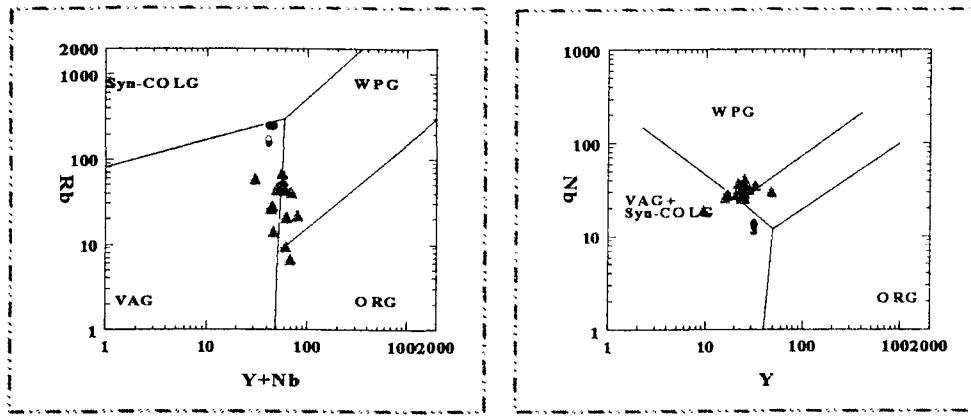
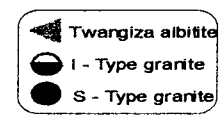
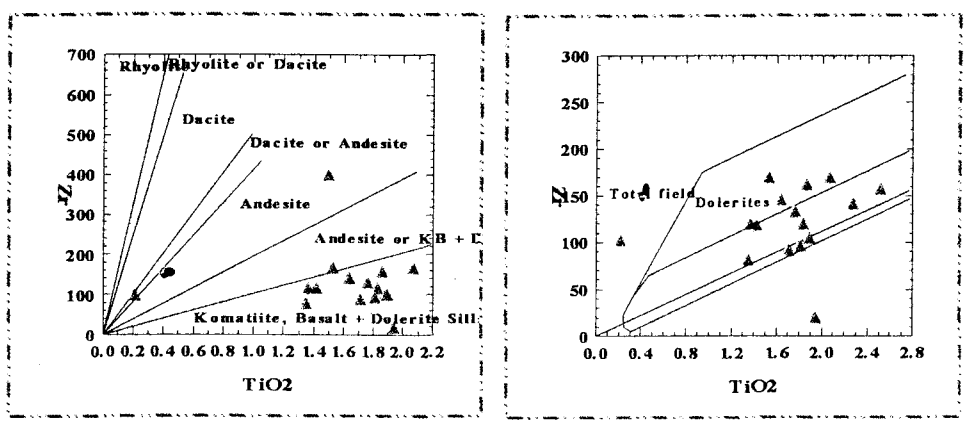
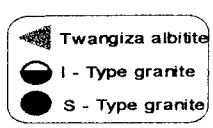


Fig.II.91:- Plots of Twangiza albitite in the tectonomagmatic discriminative diagrams of Pearce et al., (1983, 1984).
(Y + Nb versus Rb ; Y versus Nb; SiO2 versus Rb;
SiO2 versus Nb).







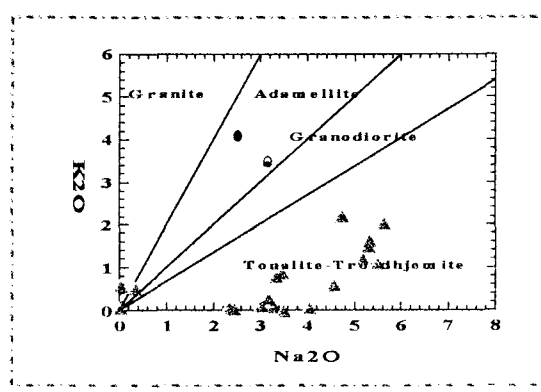
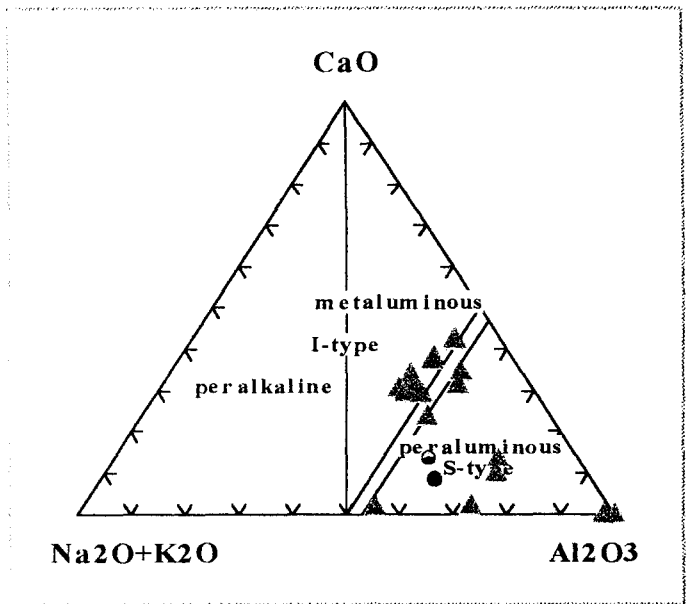


Fig.II.92:- Twangiza albitite in the different diagrams of Maniar and Picolli, (1989).



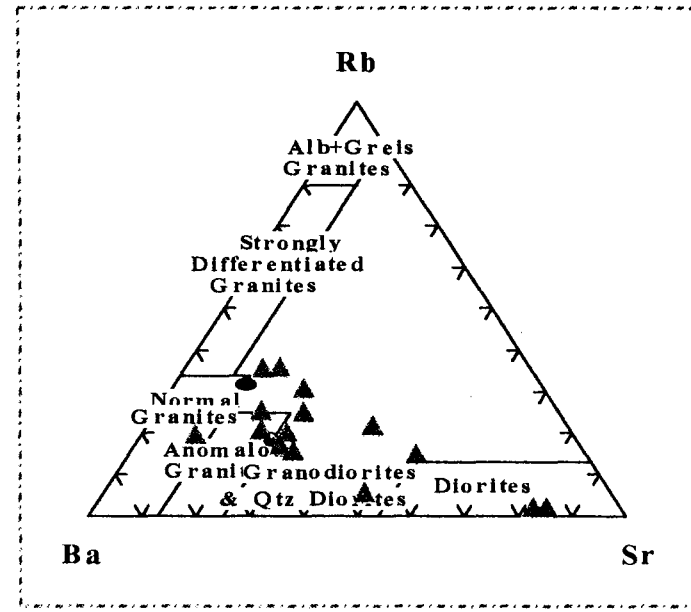


Fig.II.93:- Composition of Twangiza albitite in terms of a CaO - Na2O+K2O - Al2O3 ternary diagram and showing the typical field of A - type granitoids.

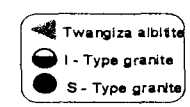
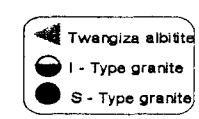


Fig.II.94:- Ternary Rb - Sr - Ba diagram showing the characteristics of Twangiza albitite.



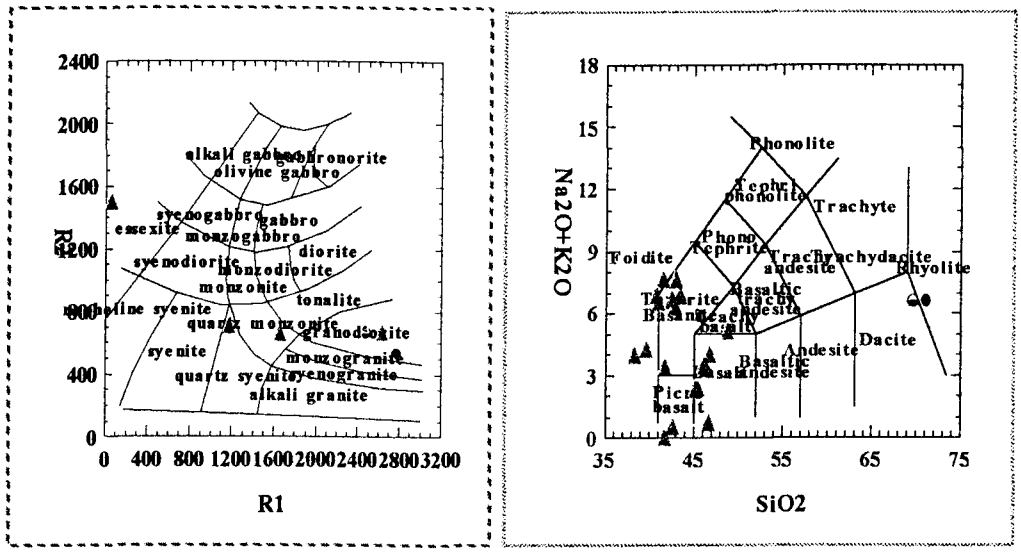
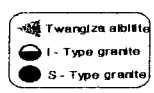
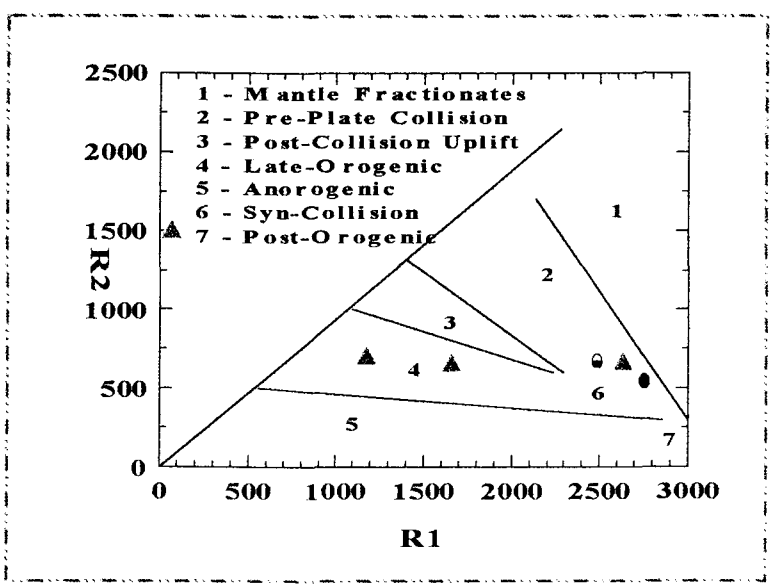


Fig.II.95:- Total alkali versus silica diagram of Le Bas et al., (1986), for Twangiza albitite.





R1 - R2 : (Bachelor and Bowden, 1985).
R1 = 4Si - 11(Na + K) - 2(Fe + Ti)
R2 = 6Ca + 2Mg + Al

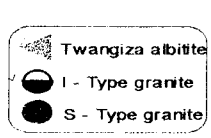


Fig.II.96:- Geochemical tectonic classification diagrams for Twangiza albitite.

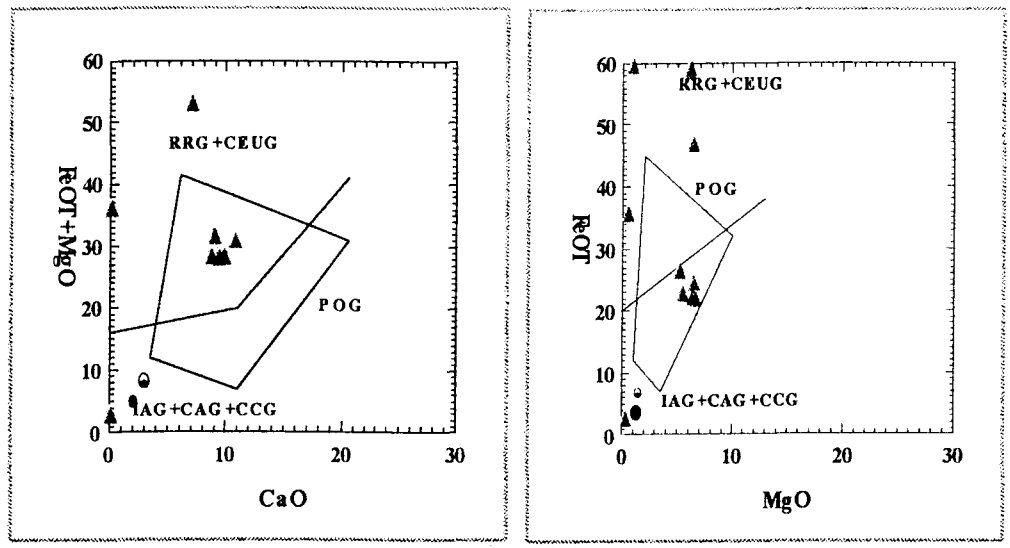
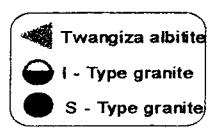


Fig.II.97: Discriminant diagrams of Maniar and Picolli, (1984, 1989) for Twangiza albitite.

Mania and picolli, 1989:

IAG = Island Arc Granitoids.
CAG = Continental Arc Granitoids.
CCG = Continental Collision Granitoids.
RRG = Rift - Related Granitoids.
POG = Post - Orogenic Granitoids.
CEUG = Continental Epeirogenic Uplift Granitoids.
OP = Orogenic Plagiogranites.



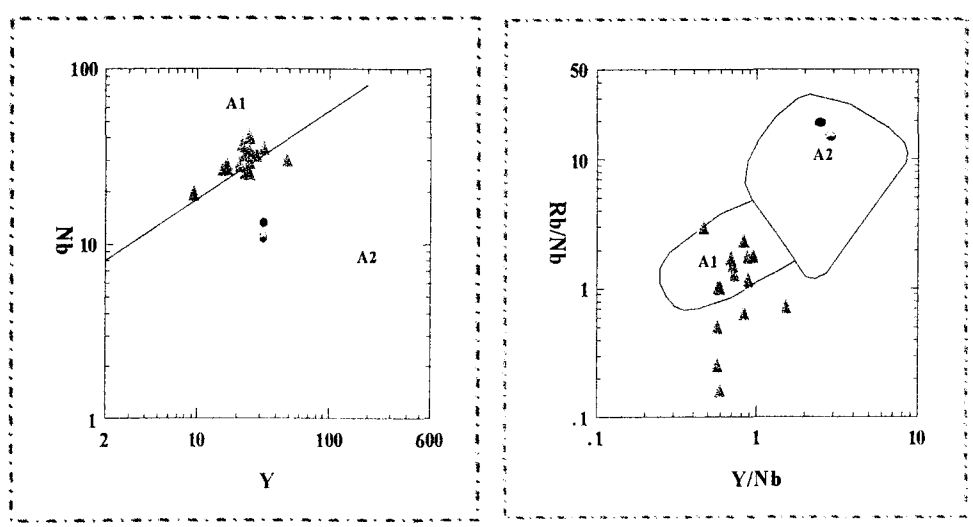
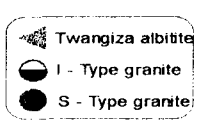


Fig.II.98:- Tectonic discriminant diagram of A-type granitoids of Elby (1992).



The magma could have been generated from crust that has been through a cycle of subduction or continent –continent collision magmatism. Fractionation of batholitic tonalite-granodiorite is a highly probable process because of the compatible fractionation trends and REE abundances .

The representation of the Twangiza albitite on the Rb-Ba-Sr ternary diagram (Fig.II.94) does not reflect a clear differentiation trend. The analyses are clustered in the " anomalous-granites" field which includes magmatic granites subjected to metasomatism and granites that suffered from chemical changes or were not formed by simple mechanisms (El Bouseily, A.M. and El Sokkary, A.A .1975).

Comparison of REE abundances between the Kasika leucogranite and the Kadubu metaturbidite respectivelly , and Twangiza albitite demonstrate the genetic relationship between the albitite and the leucogranite ,but not between the albitite and the metaturbidite (Fig.II.99) as a possible source for direct partial melting of the Twangiza albitite intrusion. The Kadubu metaturbidites have different REE patterns from the Twangiza albitite, yet the Twangiza albitite has similar REE patterns to those of the Kasika granite. (Fig.II.100). Compared to Kasika leucogranite, the Twangiza albitite shows an enrichment in V, Cr, Ni, Sr,Y, Nb, Ta, U and depletion in Rb, Pb (Fig.II.101).

Sodium –rich fluids may have been generated by alkalic (or carbonatitic ?) intrusions at depth. There are significant differences in initial Sr isotopic signatures between the Kasika granite and the Twangiza albitite, but a strong similarity in initial Nd isotope signatures.

These data also suggest a relationship between the Twangiza albitite and the spatially associated Kasika granite. Based on major element chemistry, the experimental data of Kjarsgaard and Hamilton (1989), are consistent with an immiscibility relationship between the Kasika granite and the Twangiza albitite. Plotted on a ($SiO_2 + Al_2O_3$), ($Na_2O + K_2O$), and ($CaO + FeO + MgO - MnO$), (Fig.II.102), there is a compositional gap between albitite and granite which also supports an immiscibility model.

The same behavior is seen in the ($Na_2O + K_2O$) versus SiO_2 diagram (Fig.II.103), where there is a distinct gap between the two groups of rocks.

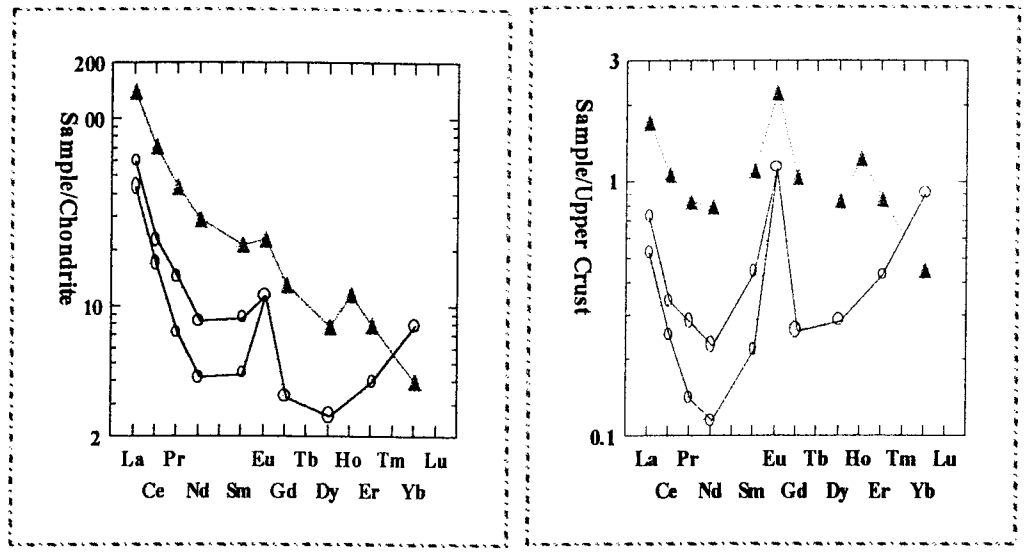


Fig.II.99:- Comparison of REE abundance , demonstarting genetic independence between the metaturbidite of the Kadubu area as a possible source for direct partial melting of the Twangiza albitite intrusion.

Twangiza albitite
Kadubu metasediments

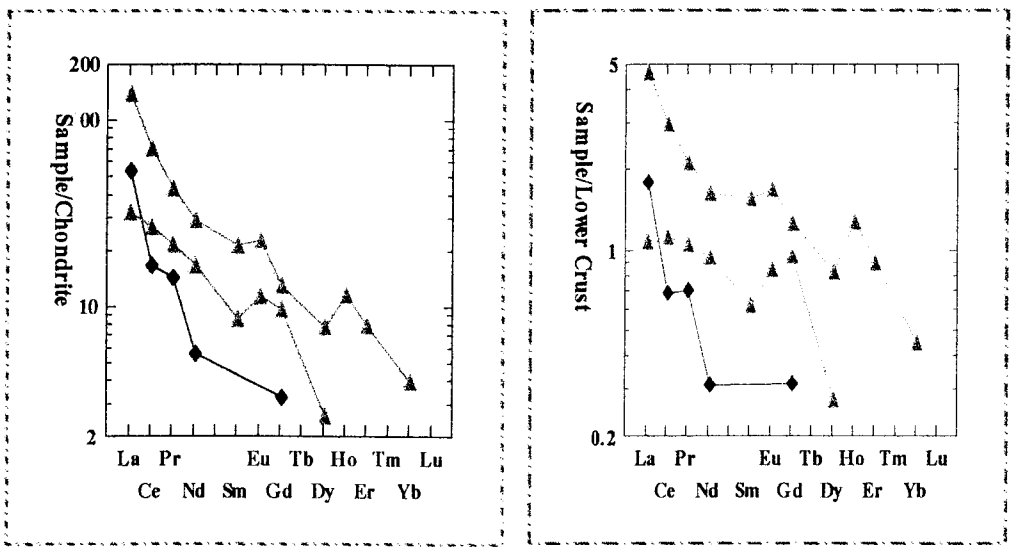


Fig.II.100:- Comparison of REE abundances demonstrating genetic dependence between the Kasika leucogranite and the Twangiza albitite.

Kasika granite
Twangiza albitite

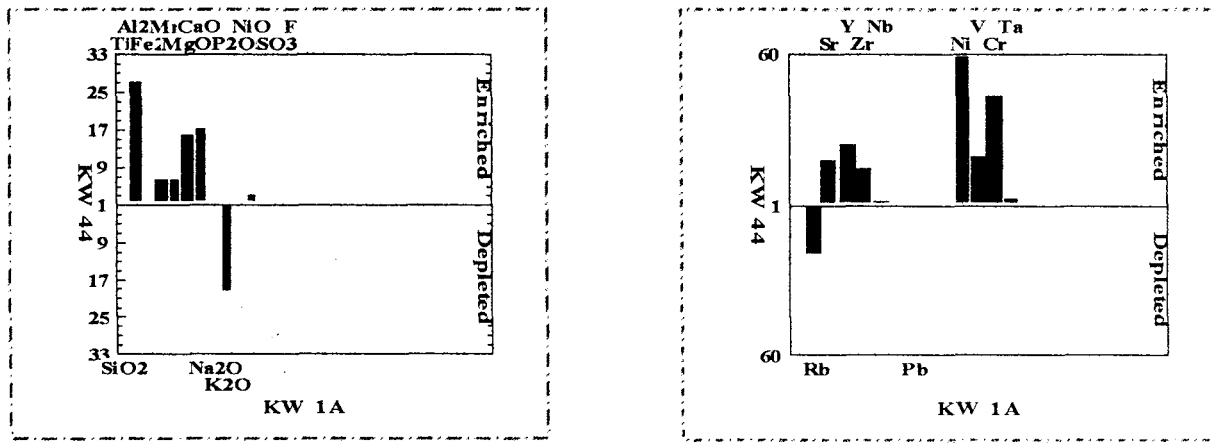


Fig.II.101:- Enrichment - depletion diagram showing the enrichment factors for selected major and trace elements from the Kadubu area The Diagram compares the relative concentrations of the Twangiza albitite and the Kasika granite (KW 44).

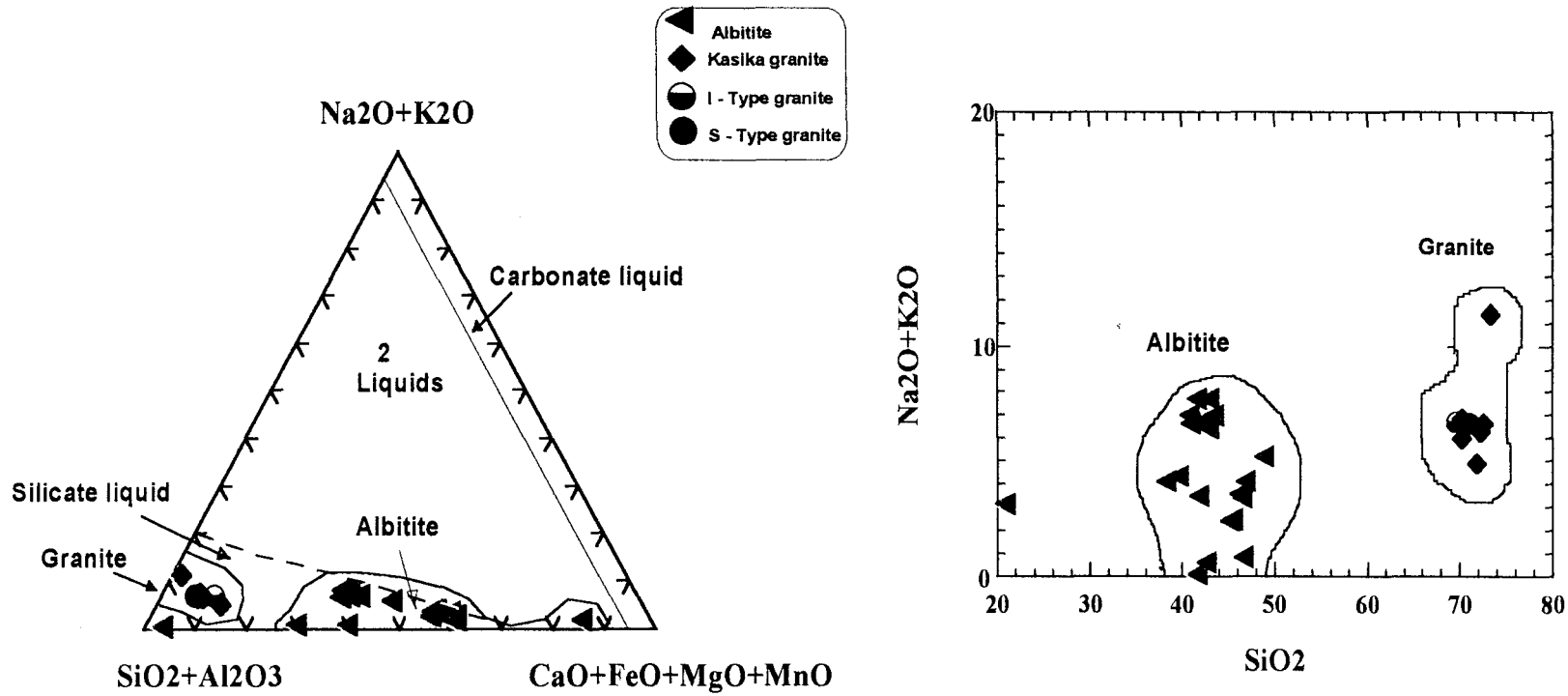


Fig.II.102:- Kasika granite and Twangiza albitite within the ternary diagram of Kjarsgaard and Hamilton (1989).

Fig.II.103:- The binary plot of SiO2 versus total alkalis of Twangiza albitite and Kasika granite.

The fields of the Twangiza albitite and Kasika granite are depicted in an SiO_2 versus Y diagram in Fig.II.104, and showing albitite field described in this study exhibiting considerable gap between these two rocks. Fig.II.105 is a plot of TiO_2 versus Zr showing the fields for the Twangiza albitite porphyry and the Kasika granite in the Kadubu area. The diagram illustrates the overlap between the Kasika granite and the Twangiza albitite with the albitite plotting in the higher TiO_2 part of the granitoid field, corresponding to the more mafic members.

Albitization of granite - a review.

Albitization is often regarded as one of the most typical features of mineralized granites (Beus et al., 1962, 1970, Stemprok, 1971). In most literature, the word " albitization" is usually used in the sense of Na-metasomatic addition of albite (e.g. by albitization of K-feldspar, or by albitizaton of plagioclase which involves the coupled exhange reaction Na^{+} for Ca^{2+} and Si^{4+} for Al^{3+}).

According to Haapala, (1997), albite in granitic rocks may be formed by several processes :

1*- magmatic crystallization ; 2*.- exsolution of alkali feldspar ;

3*.- de-anorthitization of plagioclase ; 4*.- Na-metasomatic albitization.

Although magmatic albite is very rare, albites formed by processes (2), (3) and (4) are " postmagmatic " . Only case (4) involves inevitably sodium metasomatism.

It is probable that formation of intergranular albite rims and grains by exsolution and minor recrystallization is more common than generally thought. Much of the albite described in the literature as a product of albitization is actually intergranular albite formed by exsolution and minor recrystallization. De-anorthitization involves destruction of the anorthite molecule of plagioclase, not necessarily sodium metasomatism.

In the case of the Kasika granite and Twangiza albitite, it is considered that secondary albite has been formed by all the processes (2) $\rightarrow$ (4), but with exsolution and Na-metasomatism having been the major mechanisms. Rock /fluid interaction between albitite and host-rocks is well displayed as petrographical and geochemical zonal patterns in response to Na-metasomatism.

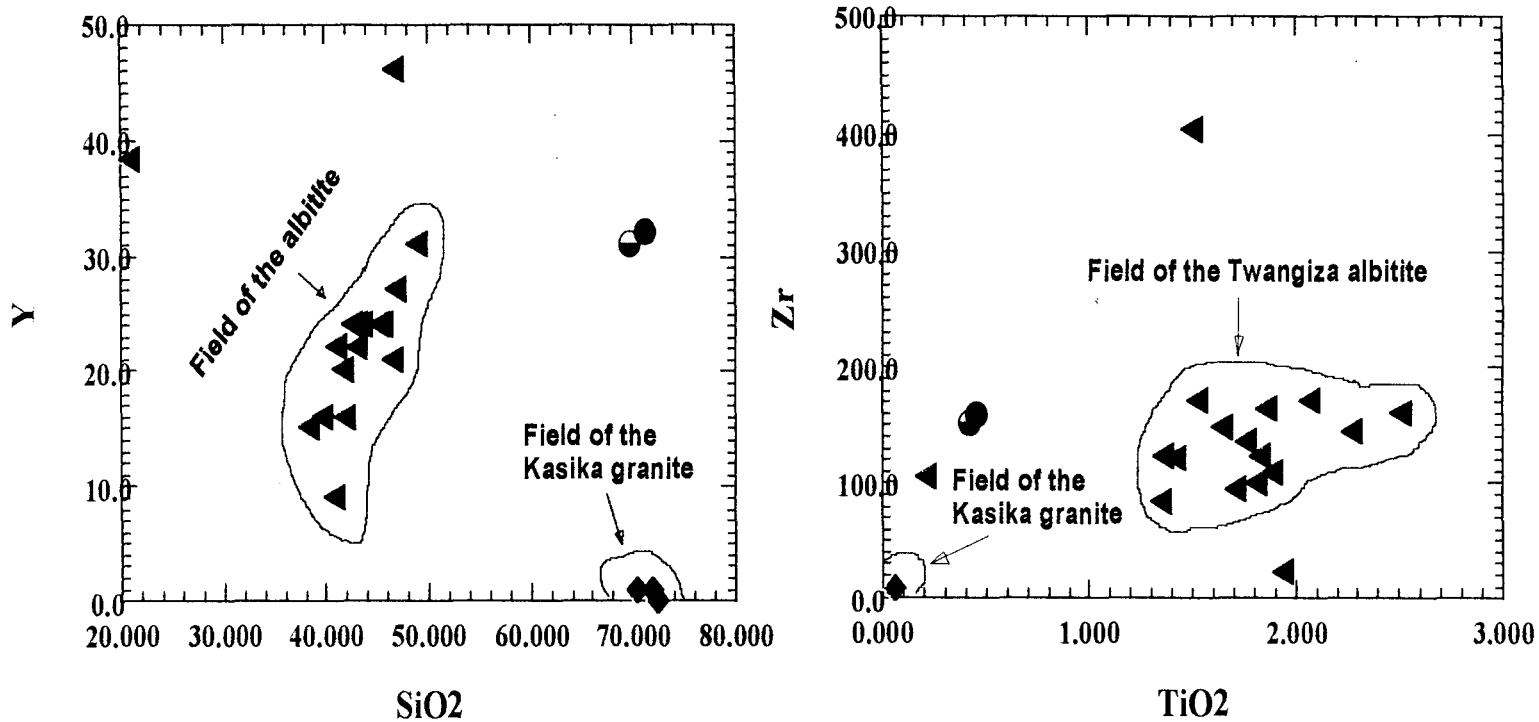


Fig.II.104:- Y versus SiO2 showing albitite field comparatively to granite field described in this study.

Fig.II.105:- Zr verus TiO2 showing respectively fields of Twangiza albitite and spatially associated Kasika granite. The diagram shows no overlap between Twangiza albitite porphyry and Kasika leucogranite.

A variety of genetic explanations for the formation of albitite rock have been proposed by differents authors :

*.-Korzhinsky, 1959; considered post-magmatic metasomatic rocks to be characterized by two main features: their location is generally determined by post-intrusive fractures and the appearance of metasomatic zoning with a varying number of minerals and displaying sharp mutual boundaries.

*.-Beus, 1970, differenciated two types of albitite formation depending on their relations with parental alkalic intrusive rocks formed at a depth of 1.5-3 km and more rarely, at a depth of 3-4 km: rare-metal albite apiogranites and rare-metal albitites of alkalic rocks.

*.- Korzhinsky, 1969 stressed that ,the metasomatic zoning reflect the temporal and spatial sequence of their formation . They indicate the tendency of the increase in acidity in the course of a metasomatic process asociated with decreasing temperatures and may result from differential mobility of the components.

Monomineralic microcline and albitite zones are consequently formed during maximum metasomatic alteration. (Borodin and Pavlenko, 1974).

*.- Beus, 1970 pointed out that a regular change in the relative activity of acids and bases in the process of a drop in temperature and a migration of the solutions into the areas of lower pressure finds its expression in a consecutive replacement of the stages of postmagmatic metasomatism in the intrusive rocks, this being: early potassium feldspathization – early albitization – high-temperature silicification – late albitization – late potassium feldspatization. A reflection of the stages outlined is a metasomatic zoning in the albitite deposit. It is in the metasomatic fronts developed in the frontal zones of high – temperature silicification (mostly in the albite zone) that maximum concentrations of the majority of rare elements are found. (Beus , 1970).

*.- Sorensen, 1974 , assumed that the source of matter and energy is subcrustal (" transmagmatic"). The successive infiltration of the solutions through sialic rocks,could generate, respectively and successively calc-alkaline, subalkaline and alkaline magmas.

*.- Pollard., 1983, pointed out that mineralization in many rare-element deposits associated with late-stage granitoids is related to the formation of K-feldspar-rich , albite-rich and greisenised rocks. K-feldspar-rich and albite-rich rocks may be formed by magmatic and/or postmagmatic processes.

The term " Na-feldspathization " is used here to describe the magmatic processes that lead to the development of albite-rich rocks in association with rare-element mineralization. (Table.II.12; Fig.II.106).

Albitization may be produced during late –stage aqueous phase saturation in association with the breakdown of sodium-fluor-rare element complexes. At the postmagmatic stage, Na-feldspathization (albitization) , is a common phenomenon in rare-element deposits. Albitization may occur on a regional scale but is most strongly developed in the apical zones of the final intrusive phase, especially adjacent to fractures where albitites and quartz-albitites may occur. This alteration may occur above the zone of K-feldspathization and there may be a gradual transition between the two zones.

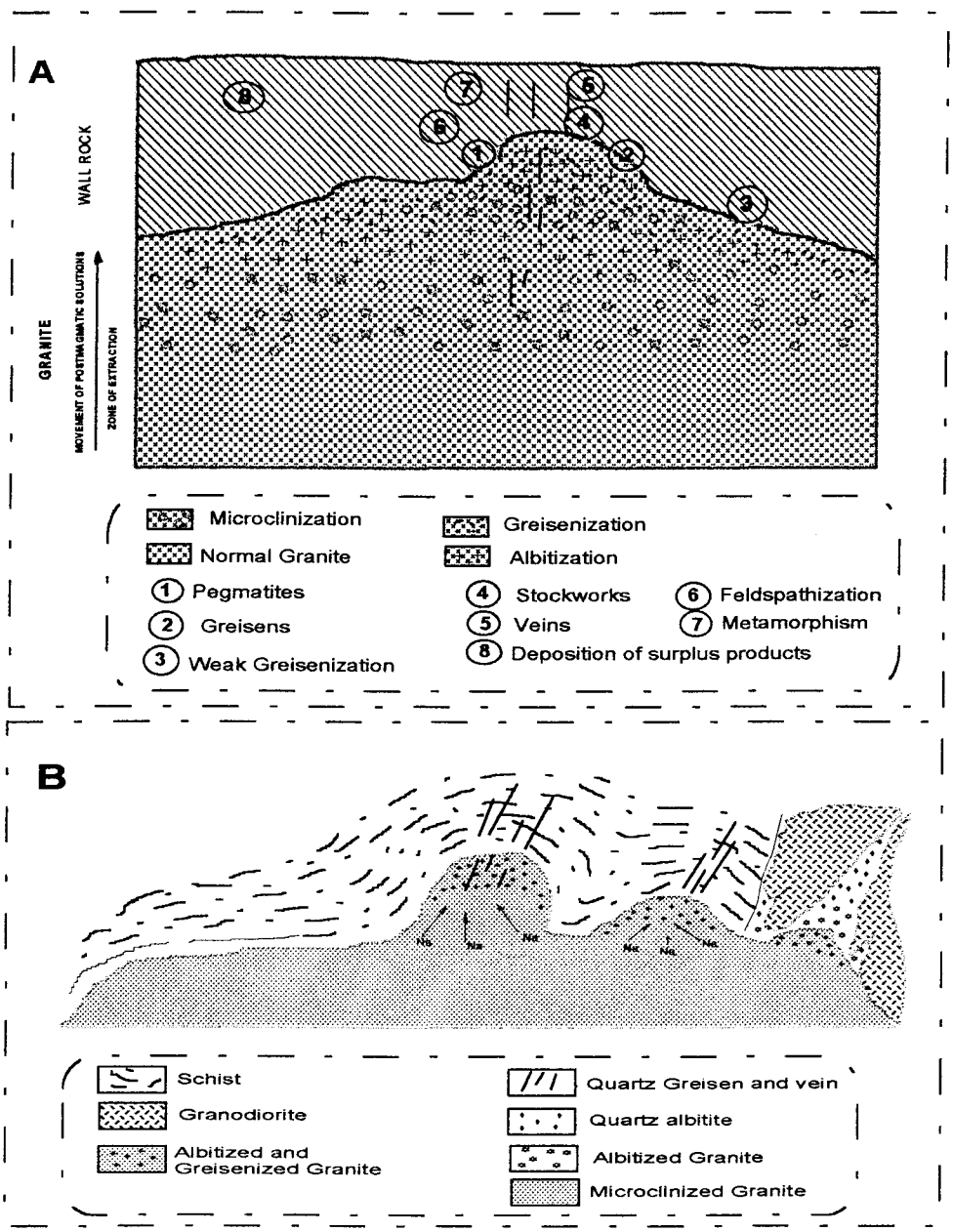
5.6.- SUMMARY AND DISCUSSION.

The Kadubu area is made up of a metaturbidite sequence exhibiting characteristic Bouma cycles in the western branch of the East African rift system, with two structural zones bordered by major thrust-faults. The investigated area is composed of two different geological groups subdivised into seven formations intruded by igneous rocks, quartz-veins and covered in the north by recent rift related basaltic formation.

The two groups are the Upper Kadubu group with four formations and the Lower Kadubu group with three formations. This classification scheme is based on the broad lithologic characteristic. The Upper Kadubu group is comprised mainly of an alternation of conglomeratic, slaty phyllitic and arenaceous metasediments, whereas, the Lower Kadubu group consists of a monotonous cyclic sequence of psammitic and phyllitic horizons. A tectonic contact; the Tshondo fault, demarcates this abrupt change in lithologic character. The Lower Kadubu group and upper Kadubu group, are in tectonic contact with the Kibaran basement.

This sequence has been intruded by a late to post-orogenic, alkaline, metaluminous albitite rock. In the Twangiza region, gold mineralization is often, but not always associated with albitite rock. Petrographic and geochemical (major and trace elements) data show the Twangiza albitite intrusion to be of igneous origin; related to a a deep-seated alkalic magmatism.

Fig.II.106:- Models for postmagmatic alteration in rare - element granitoids.
A*.- Autometamorphic zonation (after Shcherba, 1970)
B*.- Postmagmatic metasomatism in greisen granites
(after Beus and Zalashkova, 1964).



KM Walemba, 2000

Table. II.12:- MAGMATIC AND POST MAGMATIC PROCESSES AND PRODUCTS IN RARE - ELEMENTS GRANITOIDS.

K - Feldspathization	Magmatic	K -feldspar - rich granites, Pegmatites, Stockscheiders.
	Postmagmatic	Microclinization, K - feldspar megacrysts.
Na - Feldspathization	Magmatic	Albite granites, Aplites, Ongonites.
	Postmagmatic	Albitized granites, Albitite.
Greisenization	Postmagmatic	Greisens and greisenized rocks.

The diversity of REE minerals, such as hydrothermal monazite, supports the source of sodium -rich fluids from a deep -seated alkalic (or carbonatitic) intrusion. A regional granite is also intruded into the Kibaran metasediments in the southwesternmost corner of the study area. This granite is a leucocratic, SiO_2- and K_2O- rich, peraluminous, subalkaline, granite/alkaligranite of syn-collisional and post-orogenic type.

$^{39}Ar/^{40}Ar$, Rb/Sr and Sm/Nd constrain the history of magmatism. Both radiogenic ages and field evidence indicate a Neoproterozoic event. This granite yielded mean ages of 529 ± 5 Ma and 436 ± 8 Ma ($^{39}Ar/^{40}Ar$) and 703 ± 14 Ma (Rb/Sr). The albitite rock yielded an age of 1078 ± 27 Ma implying that this albitite is related to a Kibaran granite. The initial Sr isotope ratios ($^{87}Sr/^{86}Sr$) for respectively feldspar (albitite) and apatite &mica (granite) have a mean of 0.734298 ± 0.0001 and (0.885419 ± 46 & 18.277000 ± 26) respectively. Sm/Nd iostope ratios for feldspar (albitite) and apatite (granite) are respectively 0.14852 and 0.36422.

The initial $^{143}Nd/^{144}Nd$ ratios (0.512590 ± 23) of albitite is consistent with that of the Kasika granite (0.512669 ± 29) and again suggest a genetic link between these two rocks. The samples that have a correspondingly similar Nd ratio can be assumed to have evolved from the same source. The field and geochemical relationships between the Kasika granodiorite and the Twangiza albitite suggest a genetic connection between these two types of igneous rocks.

Despite some geochemical similarities to late-orogenic granites, the Kasika leucogranite is best interpreted as a syn-to post- orogenic granite which was probably formed by partial melting of lower –upper crustal /upper mantle source rocks. A mixed crustal / upper mantle source is also indicated by mixed, S and I-type characteristics (e.g. initial $^{87}Sr/^{86}Sr$ of 0.885419) and LIL/HFS element ratios. Intense crystal fractionation produced highly differentiated pegmatites from a granitic melt which may have originated by partial melting of crustal/upper mantle source rocks. The most plausible source for the Kasika granite is the Kibaran gneissic metasediments, which are relatively mature, and contain older crustal materials. Formation probably occurred in a deep Kibaran gneissic and/or granitic environment and at high temperatures (> 800 ^0C). Radiogenic isotope constrain a common crustal / upper mantle source for these two rocks with some contamination. The magma could have been generated from crust that had been through a cycle of subduction or continent –continent collision magmatism and probably emplaced during intraplate rifting .

CHAPTER 6.- STRUCTURE AND DEFORMATION.

6.1.- INTRODUCTION.

The results carried out from complementary techniques [Remote sensing, field structural analysis and geochronology ($^{39}Ar/^{40}Ar$ and Rb/Sr)], reveal that tectonics in the Kadubu area have acted at different times, through two main periods: the Neoproterozoic period and the Phanerozoic period related to present -day rifting with the reactivation of previous structures by rifting mechanisms.

Polyphase regional deformation has affected the Kadubu terrane which forms a major lithologic and structural entity with the presence of broad doubly plunging anticlinoria and synclinoria. Bedding, lineations, (intersection lineations), and /or crenulation folding can be observed.
On the basis of the differences in the metasediments, igneous rocks and structural style, the Kadubu area has been subdivided into two tectonic zones which are bordered by major faults. These bounding faults together with major internal, high-angle reverse and normal faults are thought to have a listric geometry and flatten at depth.
The detailed structure of the Kadubu area is used to place constraints on the regional structure. The implications of the structural style in the Kadubu metasediments is examined for models of tectonic development of the region and the types of crustal structure that may be expected in the Itombwe synclinorium. The importance of a detachment surface(s) and the response of the mantle lithosphere during the deformation of the Kadubu area are highlighted.

6.2.- TECTONOSTRATIGRAPHY.

The area is characterized by a large-scale succession of deeply SE-plunging synclines and anticlines succession and, by a number of parasitic folds on a variety of scales. Three deformational events can be recognized D_1 : compression; D_2 : compression; D_3 : extension and accompanying thermal event.

Major angular unconformities, which may be the result of regional tectonic events, have been identified by field mapping. Two such unconformities may bound a number of sequences, which together constitue a megasequence.(Fig.II.7).

The graben system related to the recent rifting event, overprint and/or superimpose the structural framework of the Kadubu area with several periods of reactivation and no noticeable changes in the directions of throw. Such grabens have created small rift lacs in the eastern part of the study area: The Kasandja lake and the Luhimbole lake.

6.2.1.- FOLD GEOMETRY.

The metaturbidite sequence is upwards facing and folded about upright to steeply east or west-dipping and north, northwest –trending axial surfaces. Fold axes are generally gently north or south plunging. Major folds are usually continuous for distances in excess of several kilometres along their axial direction and exhibit tight to isoclinal types, symmetric to west-verging profiles. Fold wavelengths range from 200m to about 600m. Interlimb angles range from 15^0 to 85^0, though angles from 25^0 to 45^0 are typical. The axial traces of the folds are either straight or curvilinear in flattened S patterns, indicative of right lateral slip on the wrench fault. Parasitic or minor folds are infrequently developed on the limbs of major folds, as within Twangiza fold.

Two domains; the Tsibangu and the Mudubwe of differing structural style are separated by a major fault zone;-the Tshondo fault zone . Within the domains, the fold style is not grossly affected by lithostratigraphic variations at the present level of exposure. Marked variations in the fold style occur across the cross -section in the western extremity (Fig.II.16). Still further to the west, folds become more markedly asymmetric and west verging, and have overturned western anticlinal limbs and may be termed ; recumbent folds (Fig.II.16).
Fold vergence is consistent with the dominant fault movement sense and indicates westward tectonic transport during regional deformation .The macroscopic fold geometry is illustrated in cross-section (Fig. II.16).

The following small-scale structures have been recognized within the study area:

1 .- a dominant slaty cleavage (S_1 , in lower group); (S_2 , in upper group).

2 .- a steeply dipping crenulation cleavage that defines well-developed tectonic banding ,(S_2)

3 .- Chevron folds and kink bands. Chevron folding is developed by kinking and results in saddle reef formation .

4.- *En- echelon* folds.

6.2.2.- FAULT SYSTEM.

6.2.2.1.- NORMAL AND HIGH-ANGLE REVERSE FAULTS, THRUST-FAULT.

The Kadubu fault system is made up of a number of major northwest-trending faults within an 50km broad zone which transect the Kadubu area and trends more westerly than the axis and borders of Itombwe trough. (Fig.II.7).

Each fault is characterized by older rocks overlying younger rocks , causing thickening of the stratigraphic section beneath the main fault. Faults are marked by prominent continous topographic features and terminate by simple dying out, or by curving and dying out, or by segmenting into *en echelon* sets of small extension fractures. The geometry of the major fault zones throughout the study area, is consistent with large-scale west-wards tectonic transport .

Two **major high-angle reverse faults** (Twangiza and Bugoyi faults), die out upsection in the Tsibangu formation rocks . These major faults are respectively termed here Twangiza and Bugoyi fault after the Twangiza deposit and the Tshondo locality through which they passe. At the scale of outcrop, many small-scale reverse faults have been observed. These range from apparently ductile structures with no sign of cataclasis or brittle fracture to entirely brittle faults marked by discrete fractures.

Some major **(extensional) listric (downward-flattening) normal faults** , particularly the Tshondo and Bulongo faults and the Eastern bounding fault, with their antithetic and synthetic, smaller-scale, associated fault arrays, have been also observed.

It is suggested that the hanging -wall deformations above these listric normal faults produced a characteristic roll-over anticlines with associated superposed crestal collapse graben structures within the Itombwe Formations of the Kadubu area. Their migration being towards the main detachment surface (fault breakway) and the direction of extension being to the east. The Kibaran basement acting as a rigid-body footwall. (Fig.II.16).

- The **Tshondo fault** is a major structural discontinuity which separates the Tsibangu and Mudubwe /Kalama formations, and hence the Upper and Lower Kadubu groups. This fault is very extensive and extends out of the study area. It is defined by a zone of crushed rocks and fault gouge from a few centimete to several metres wide. The fault surface is more or less a straight line (rectilinear), dipping east more steeply in the Tsibangu formation .
- The **Eastern bouding fault** is an extensional normal fault with 10 km or more downward displacement -to-the-east-northeast.
- The **Bulongo fault zone** is defined by two normal high-angled faults which are, NNE trendin, east dipping and more or less parallel.

The western bounding **thrust-fault** exhibits a low to moderate east-dipping reverse movement which probably represent D_1 backthrusting, with listric deep geometry to the East and displaying positive inversion tectonics. In the northern part, the thrust-fault curves to the west, shallows in dip, and trends approximately perpendicular to the direction of movement.
The inversion structure in the Kabubu area is exhibited in the extreme west where the Kadubu lower group clastic metasediments are preserved in the footwall of a major north-south verging thrust –fault.(Fig.II.16). The term " inversion " is used here to describe reversal of sense of motion along this western bounding thrust-fault .

6.2.2.2.- UNCONFORMITIES.

Three discontinuities with critical exposure occur within the area, namely the Nya-Kasiba angular unconformity, the Tshondo tectonic contact and the western bounding thrust-fault .

- The Nya-Kasiba angular unconformity (Eastern bounding fault) separates the Kadubu area (Itombwe synclinorium) from the Kibaran formations.

- The Tshondo tectonic contact could be interpreted as related to a rollover formation rather than to syndepositional E – W shortening, and separates the Lower from the upper Kadubu groups.
- A Low-to moderate- angle thrust -fault occurs along the western boundary of the metasedimentary pile , and separates the Kadubu area (Itombwe synclinorium) from the Kibaran metasediments (Fig.II.7; Fig.II.16).

6.2.2.3.- CATACLASITES.

Within the study area, cataclasites and fault breccias are exposed at two main locations on the Nya-Kasiba and Tshondo faults zones. The cataclasites are derived respectively from the adjacent metasediments and consit of clay matrix and quartz porphyroclasts. The matrix is commonly dark brown to dark green in color. Quartz porphyroclasts are rounded in shape, commonly 1mm to 10cm in diametre, rarely as large as 15cm in diametre.

6.3.- TIME SEQUENCE OF DEFORMATION.

In this study, the interpreted folding events and axial planar foliations produced during the successive deformations (compressions and extension) are designated with a subscripted number that relates to the deformation event: for example, the S_2 foliation and F_2 folds were produced during D_2 , deformation At least, three phases of deformation (D_1, D_2 & D_3), affected the Kadubu area.

6.3.1.- D_1 PHASE OF DEFORMATION: COMPRESSION.

This phase of deformation has been recorded only in the lower Kadubu group. The D_1 event is characterized by mesoscopic to macroscopic, upright to reclined, open to tight, northwest trending F_1 folds with a steeply dipping S_1 axial surface. This first phase is responsible for the generation of folds with an axial plane slaty cleavage (S_1)

D_1 regional folds include the Kitogo and Kitwabaluzi anticlines and the Ruzimu syncline.

Parasitic F_1 folds are commonly tight. The oblique relationship of F_1 and F_2 fold axes means that fold interference patterns are relatively common and occur on mesoscopic and macroscopic scale

6.3.2.- D_2 PHASE OF DEFORMATION : COMPRESSION.

North to northwest –trending structures , referred to here as " D_2 " , correspond to the second and more pervasive structures throughout the study area. The D_2 deformation produced upright regional F_2 folds with variably developed S_2 foliation, as well as D_2 faults and shear zones.

These structures generally trend N to NW , recording E-W shortening. Prominant D_2 folds in the supracrustal succession are the Twangiza anticline, and the Bugoyi syncline (Fig.II.7). D_2 regional folds include also the Kahanda, the Mohe and the Gahinga synclines and the Bugoyi, and Kasandja anticlines (Fig.II.7).

The D_2 event is characterized by mesoscopic to macroscopic, tight to isoclinal F_2 folds with an axial surface (S_2), defined by preferred dimensional orientation of micaceous minerals and quartz grain recrystallization. On a mesoscopic scale, the F_2 folds axes trend mostly north to northwest. Parasitic F_2 folds are commonly tight.

Slaty cleavage (S_2) is pervasive throughout the study area. It is not as intense as to erase completely the bedding particularly within the coarse-grained metagreywacke, sandstone and quartzitic layers.

A strong **crenulation cleavage** ; (S_2) overprints S_o, in the central and eastern The S_2 folding areas represents a widespread crenulation cleavage grading progressively to centimetre scale chevron folds and is found along the Bugoyi anticline. The cleavage is statistically parallel to the fold axial surfaces. This crenulation cleavage is well developed in the western part of the study area, particularly within the Kalama formation.

The cleavage dip direction changes along the strike from dominantly north in the southern part to north and northwest in the northern part . Kink and chevron folds , however, also occur in these metasediments. Small – scale F_2 folds show steeper plunges , and most D_2 faults are inferred to be listric to the east.

All the later structures (crenulation, kink band) ,occurring in the study area ,are indicative of nearly vertical shortening. D_2 -D_3 transition from dominantly compressive to (transpressive) extensive deformation occurred throughout the study area .

6..3.3.- D_3 PHASE OF DEFORMATION: EXTENSION.

D_3 deformation resulted in a variety of late stage ,locally developed ,meso-scale structures and is related to extensional faulting and shearing.

The Kahanda shear zone (KSZ) located mainly within the conglomerate and the Ludjo shear zone (LSZ) corresponds to the most highly sheared zone in *domain 1* (Fig.II.7).
Dextral shearing with a flat –lying strong tectonic banding, related to low-angle shear-zones, and late kink-bands has been observed. A significant amount of cataclastic deformation observed particularly within albitite rock, could be a result of dextral brittle shear.
Normal faults with dominant parallel shear fractures and subordinate conjugate shear fractures have been observed. These shear fractures are mostly associated with extensional normal faulting.
Four major extensional (***dextral & sinistral) strike-slip faults*** (Twangiza, Kahanda, Bugoyi, Tshondo) occur in the Kadubu area. These faults have been traced over at least 25 km.

The Kadubu strike-slip fault system is characterized by three distinct sets of principal displacement faults.(Fig.II.7). The first set comprise north-trending faults (e.g.,the Bugoyi fault), while the second fault set comprises northwest-trending faults (e.g., the Twangiza fault), the last set comprises east-west trending faults (e.g., the Tshigola fault).
Kink bands exist in all areas where S_1 has not been disturbed by crenulation cleavage S_2 , particularly in the central part.

6.4.- KINEMATIC INTERPRETATION.

6.4.1.- INTRODUCTION.

Three phases of deformation have been observed in the Kadubu area.
In the *lower Kadubu group*, the first deformation phase (D_1) is a large-scale, NNW- verging set of closed to tight folds developed during the early phase of compressional deformation.
The second major deformation phase (D_2) is related to a large NW- verging asymmetrical to recumbent fold , which deforms the previous folds.

These two phases were folowed by the third phase (D_3) related to extensional strike-slip faulting and shearing.

In the *upper Kadubu group*, only the second phase (D_2) and the third phase of deformation (D_3) have been recorded . The second phase is related to a large N to NNW- verging tight to isoclinal folds. The deformation phase D_2 is characterized by large coaxial isoclinal folds of a kilometre size, which are a result of compression and thrusting.

The constrast in the tectonic evolution between the upper and lower Kadubu groups in the study area indicates the existence of a detachment between the two. This is manifested by the Tshondo fault which could be regarded as a major tectonic break.

6.4.2.- COMPRESSIVE PHASES.

Major compressive structures encoutered within the study area, comprise tight to isoclinal folds, chevron folds, high-angle reverse faults, thrust-faults and fault-induced propagation folds.

The deformational phases D_1 and D_2 are related to east-west compresional stress due to crustal thickening and shortening probably during the Pan African orogeny.

Timing of D_2 deformation is inferred from the $^{39}Ar/^{40}Ar$ age dating of metamorphic muscovite from a phyllite and a hydrothermal muscovite from albitite rock. The Twangiza albitite, syn-to-post tectonic that intrudes the Tsibangu formation of the upper Kadubu group, gives a Neoptroterozoic age which is supported by field evidence.

6.4.3.- STRIKE-SLIP PHASE.

Movement on vertical or high-angle faults with straight traces are commonly strike-slip. In the Kadubu area, deviated stream channels, small valleys, ridges or hills, sag ponds, small *en echelon* ridges, *en echelon* fractures, are all indicative of strike-slip movement. Large –scale, ductile and brittle, dextral and sinistral strike –slip faults and shear zones are observed throught out the study area. These shear zones are revealed by heterogeneously distributed, syn-to late metamorphic C/S fabrics and from Landsat imagery and aeromagnetic map.

Shear-sens as indicators throughout the area, are mostly asymetrical pressure-shadows and deformed vein systems. The small- scale fracture patterns and shear fabric indicate dextral offsets. ***Kinematic indicators*** in the polymitic conglomerate rock of the upper Kadubu group include shear bands, " foliation fish " and rotated porphyroblasts that indicate rigth-lateral northwest-southeast shear (Fig. II.107).
Details of fault-zone characteristics and kinematic indicators include cataclastic NNW -directed Twangiza fault zone in the Twangiza deposit.

The geometric relation of the secondary faults to the main traces of the major faults correspond to the orientation of the synthetic set of Riedel Shears (in the terminology of Tchalenko and Ambraseys, 1970), characteristic of a wrench-fault system. (Fig.II.108). Minor *en echelon* north-trending faults near or aligned with the northwest-trending Bugoyi fault are suggestive of right –slip on this major fault.
The average trend of the faults of the Kadubu system is about N 45 ^{0}W. (Fig.II.5 ,Fig.II .7), along which , movements are primary right-slip.

On faults that trend more north-south, tension components of movement are evident, and on those that trend more east-west, compression components are involved. The north and northwest-trending faults , generally dip steeply ($> 75^{0}$) to the east with a dominant dextral movement. In contrast, the east-west –trending faults dip steeply to the north.

The major features of the Kadubu strike-slip fault system are multiple dextral strike-slip faults , subsidiary structures such as intersecting and overstepping faults and multiple displacement of the litho-stratigraphic succession. There is not enough evidence for crosscutting relationships of these differents sets of faults.

It is interpreted that the fault system was generated during one deformation event with different phases and dextral / sinistral strike-slip faulting along the Kadubu area occurred in a transpressional setting.

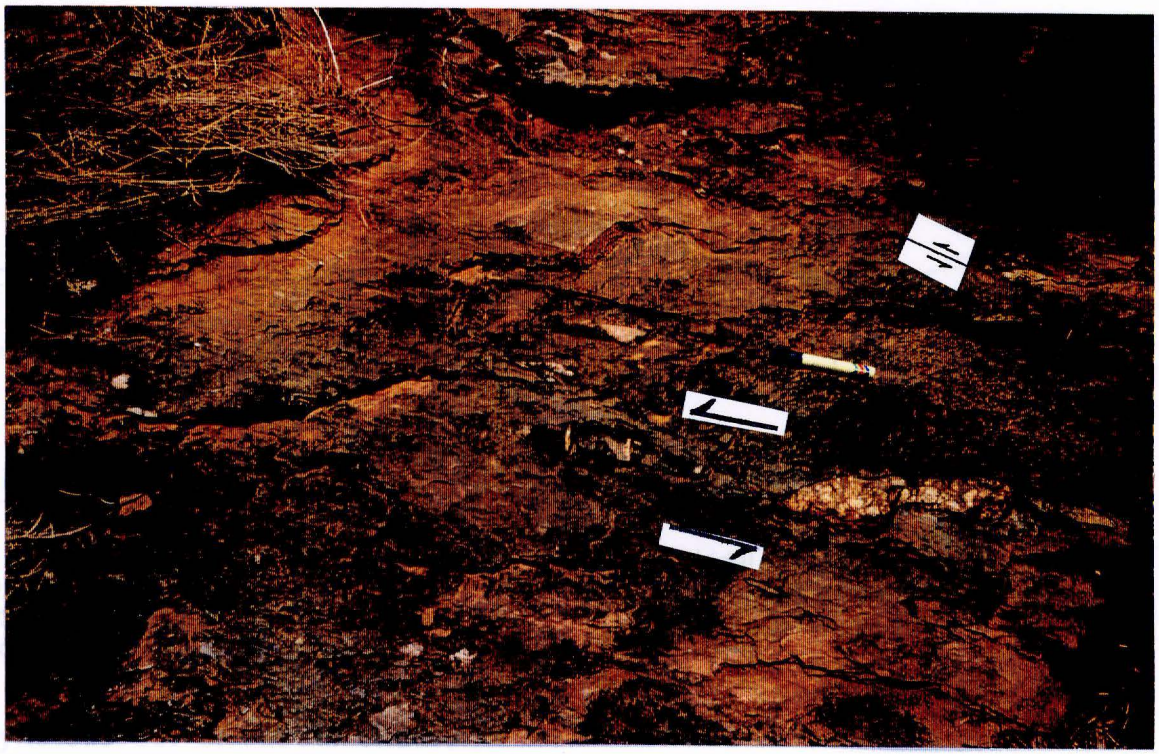
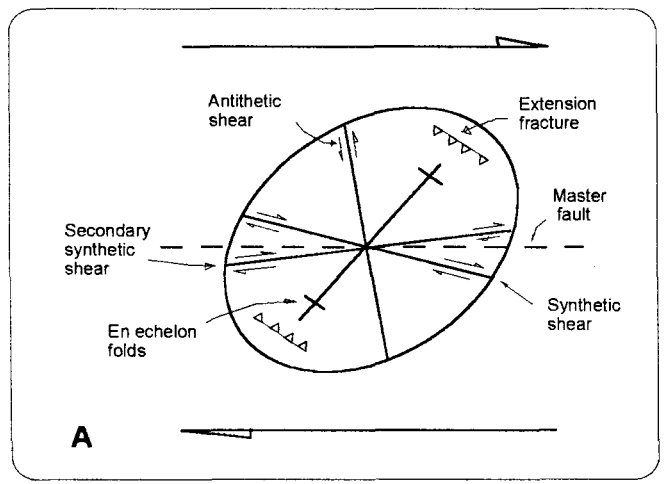
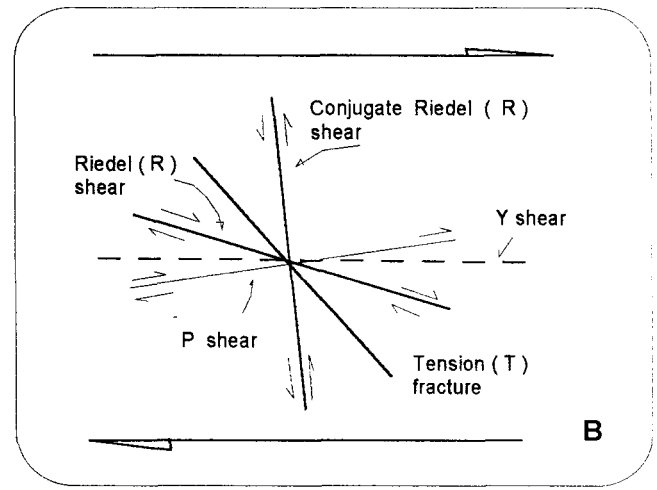


Fig.II.107:- Kinematic indicators within the polymitic conglomerate .



A:- Terminology largely from Wilcox et al., (1973), superimposed on a strain ellipse for the overall deformation.



A:- Riedel shear terminology, modified from Tchalenko and Ambrasey (1970) and Barlett et al., (1981).

Fig.II.108:- Synthetic set of Riedel shears.

The angular relations between structures that tend to form in right - lateral simple shear under ideal conditions, compiled from clay - cake models and from geologcal examples. Arrangements for structures along left - slip faults may be determined by viewing the figure in reverse image.

6.4.4. THE RELATIONSHIP BETWEEN THE TWANGIZA AIBITITE AND D_2 STRUCTURES.

The internal structures of syntectonic albitite intrusion shows an outward progression from magmatic to solid-state cataclastic and/or mylonitic fabrics. In its core, magmatic foliation and lineations are well-defined by slight alignment of tabular, euhedral plagioclase (albite)crystals . The albitite margins are dominated by low-temperature deformation, which occurs as localized millimetre - to centimetre -wide bands that overprint more widespread high temperature fabrics. (Fig.II.109).

These planar and linear fabrics reflect an evolution as temperature progressively decreased. They remain parallel to one another , which suggests a synkinematic emplacement and cooling (Paterson et al ., 1989) of the Twangiza albitite relative to the NNW-dipping D_2 Twangiza fold and fault. The emplacement of albitite rock is interpreted to be synkinematic relative to the D_2 event.(Fig.II.109; Fig.II.110; Fig.II.111; Fig.II.112).

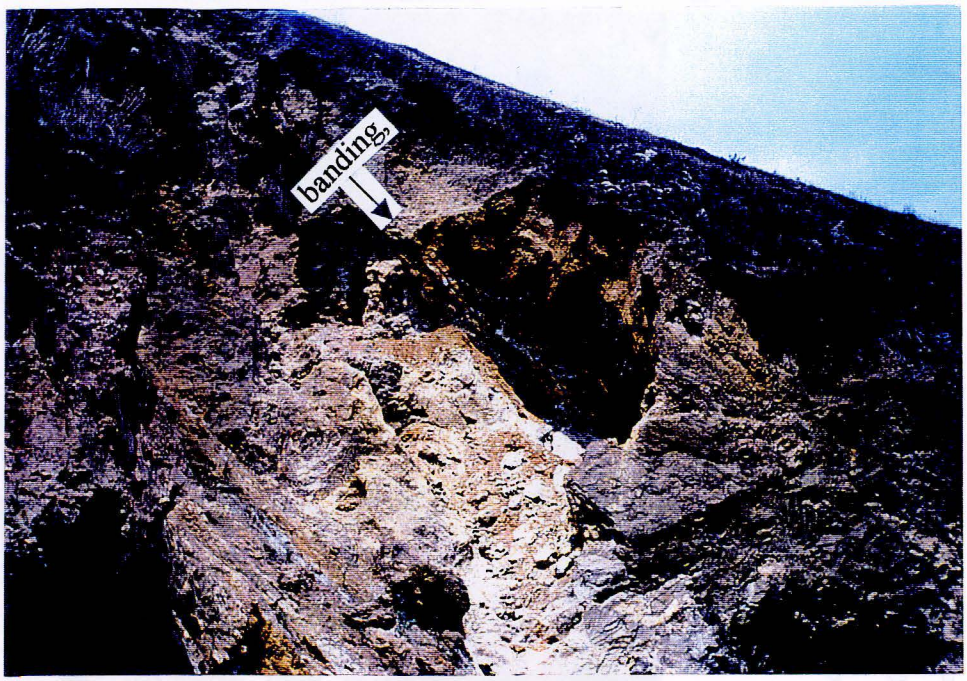
Fault –controlled dilation (i.e., the pull-apart model) is invoked for a similar pluton passively emplaced along , and during the development of either strike-slip faults (Hutton and Reavy ., 1992, Ferre et al., 1995) or extensional faults (Hutton et al ., 1990 ; Koukoukevlas and Pe-Piper, 1991) (Fig.II.113). The existence of marginal injections within outcrop-scale releasing bends and extensional structures, (Fig.II.114) is roughly consistent with their emplacement within dilatant positions along dextral oblique-slip and extensional D_2 faults respectively.

6.5.- SUMMARY AND DISCUSSION.

One of the main structural features of the Kadubu area, is the juxtaposition along the Tshondo fault of two crustal blocks with markedly different lithostratigraphic and structural characteristics: The lower and upper Kadubu groups.

On the basis of differences in metasediments, igneous rocks and structural style, the Kadubu metaturbidite sequence has been subdivided into two structural zones which are bordered by major faults.

These bounding faults and internal, normal faults, shear-faults, strike-slip faults and high-angle reverse faults are interpreted to have a listric geometry and to flatten at depth to form an inferred major mid-crustal detachement fault zone forming a west-vergent thrust system.



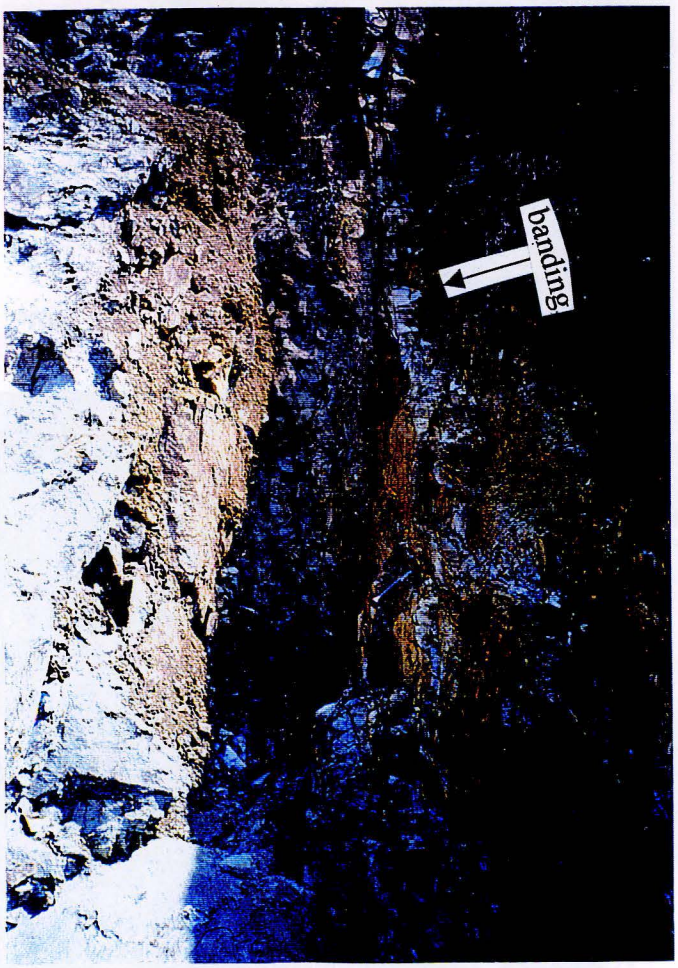


Fig.II.109:- Albitic margins occuring as mm to cm wide bands. Twangiza gold deposit.

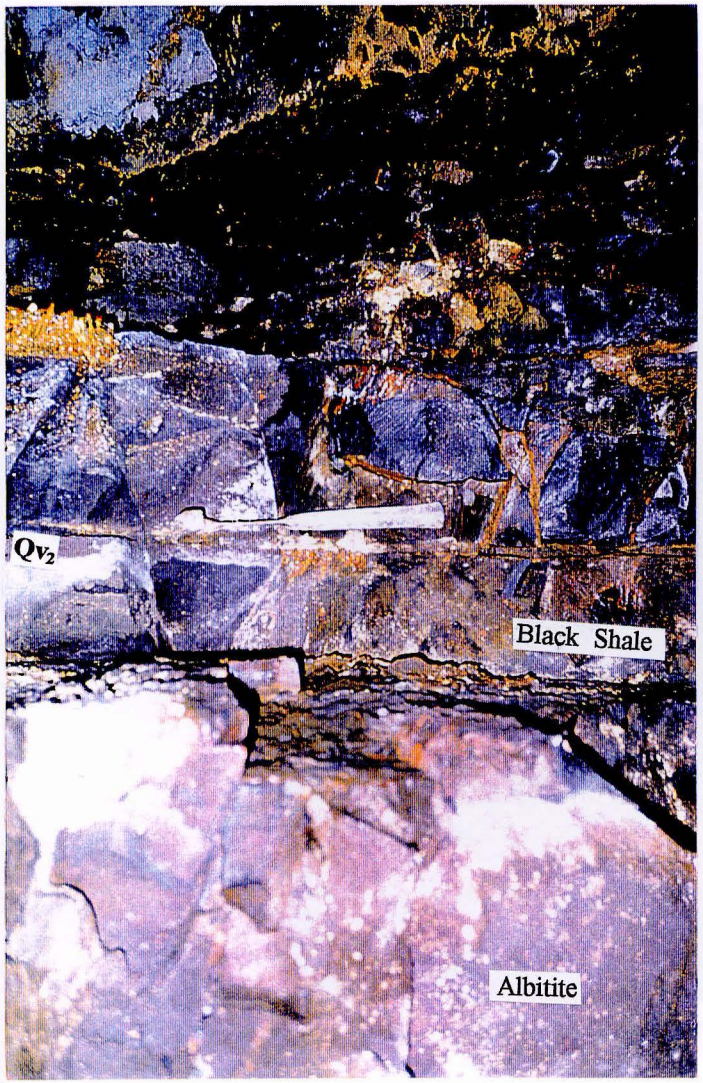




Fig.II.110:- Contact of albitite and black shale in oxide zone showing brecciation .

Adit G20 , level 2130 ; Twangiza gold deposit.

Fig.II.111: - Contact of albitite and black shale showing no deformation and albitization of black shale suggesting passive emplacement of albitite pluton.

Adit G19 , level 2130 ; Twangiza gold deposit.

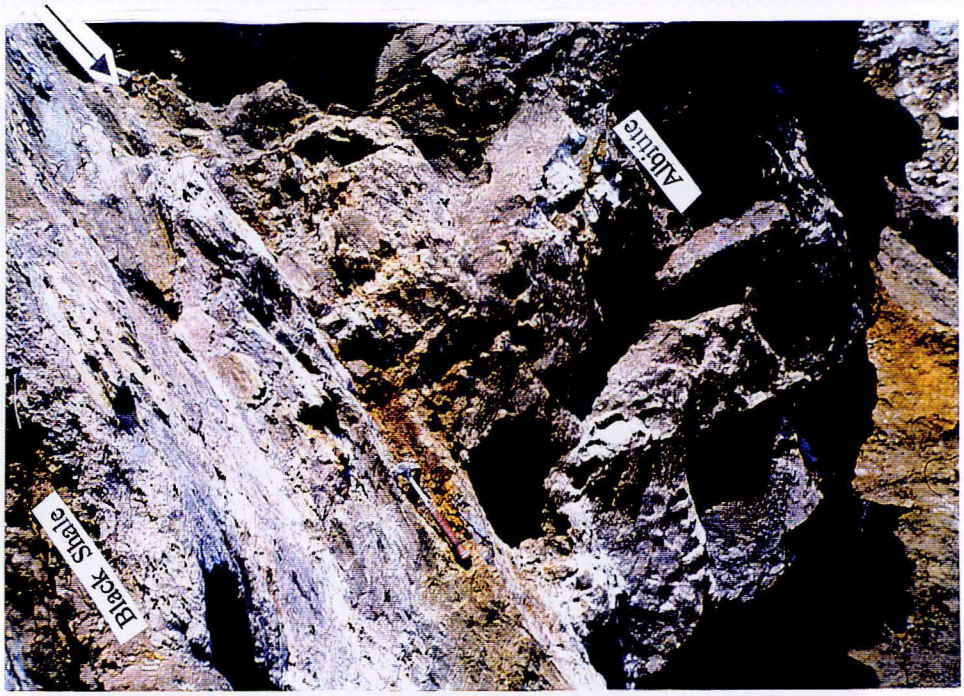


Fig.II.112:- Contact of albitite and black shale showing margin banding . Twangiza gold deposit.

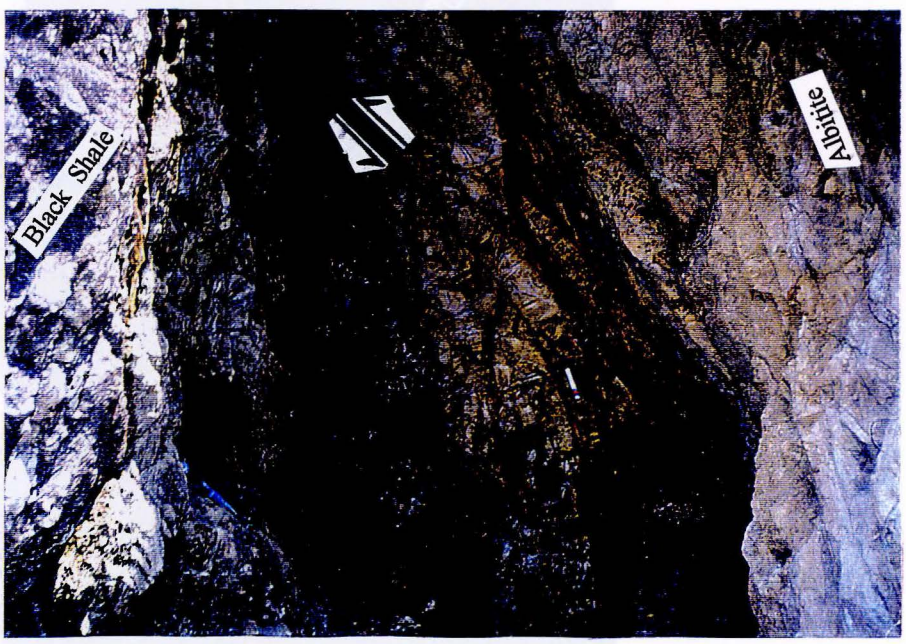


Fig.II.113:- Thrust -fault zone within albitite .

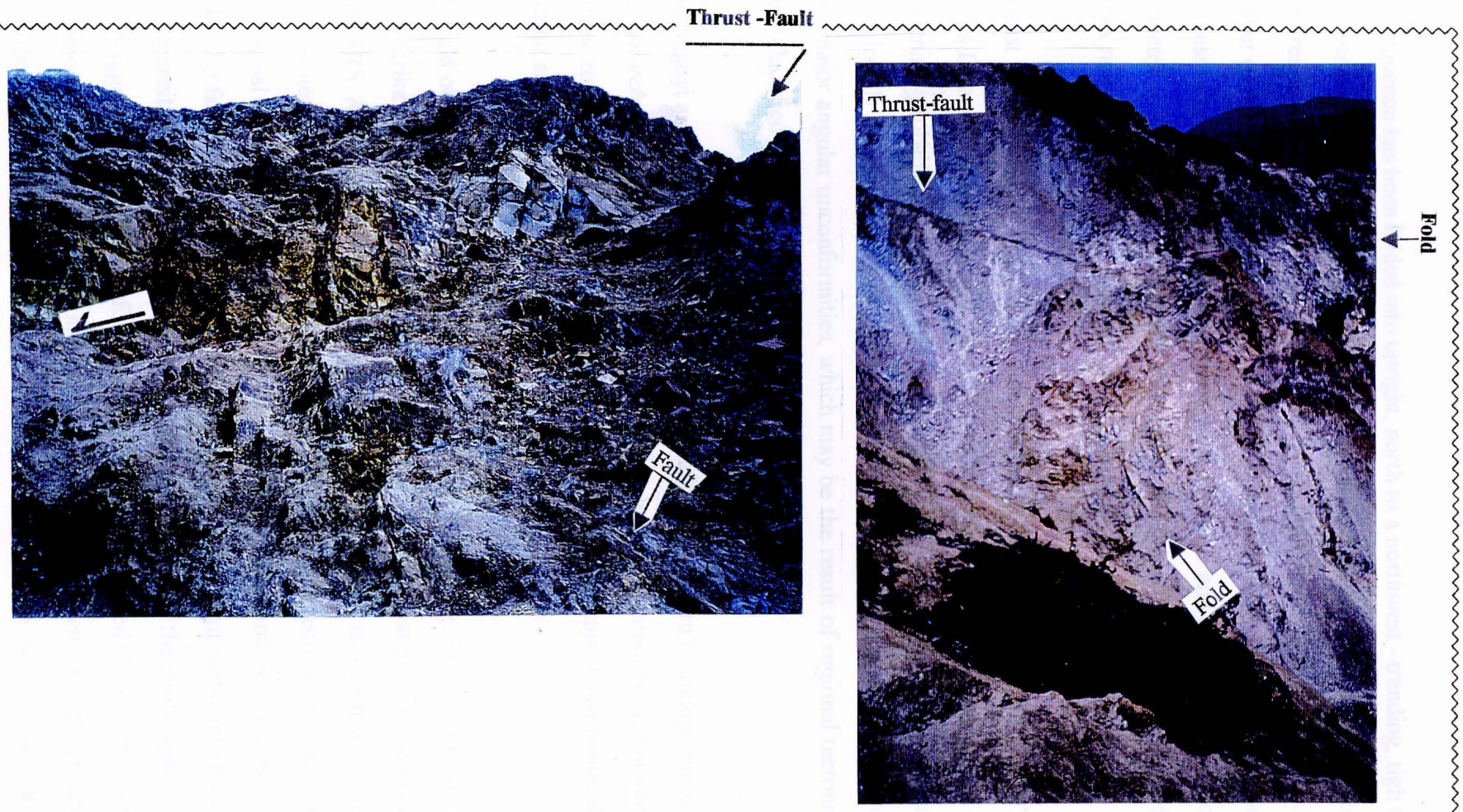


Fig. II.114:- :- Folded albitite rock exhibiting D_2 deformation and thrust -fault zone within albitite rock and suggesting a synkinematic emplacement and cooling of albitite pluton.

This sequence has been folded into upright, north to a northwest –trending, tigh to isoclinal fold succesSsion intruded by late to post-orogenic, alkaline, metaluminous albitite rock.
The area is deflected by large-scale, steeply SE-plunging synclines and anticlines and, by a number of parasitic folds on a variety of scales. Major folds are usually continuous for distances in excess of several kilometres along their axial direction and exhibit tight to isoclinal types with symmetric to west-verging profiles. Fold wavelengths range from 200m to about 600m. Interlimb angles range from 15^0 to 85^0, though angles from 25^0 to 45^0 are typical.

At least three phases of deformation affected the Kadubu area : D_1 ; D_2 ; D_3 . The deformation phases D_1 and D_2 are related to east-west compresional stress due to crustal thickening and shortening probably during the Pan african orogeny. D_3 deformation resulted in a variety of late stage, locally developed meso-scale structures and is related to extensional faulting and shearing. Two major angular unconformities, which may be the result of regional tectonic events , have been identified .

The Bugoyi and Twangiza high-angle reverse faults, the western bounding thrust- fault, chevron and *en-echelon* folds, are evidences of crustal shortening concentrated within a remarkably narrow zone. Subvertical extension associated with subhorizontal shortening due to folding , faulting and cleavage are part of an overall plane strain.

The field observations indicate a large -scale sinistral shearing. Strike –slip movements parallel to the strike of the Itombwe synclinorium, appear to be associated with the development of the WBEARS. Although, the exact kinematic relationship between strike-slip and extensional faulting in this system still remains unclear. From the chronology of tectonic events, it is probable that extensional faulting in this region was kinematically linked and was a direct result of dextral strike-slip faulting. The distribution of rheologically competent units and preexisting structural heterogeneity might explain the D_2 structural development in the study area.
It is suggested that these deformations may have occurred during the same progressive compression eventwhich was followed by an extension event. Faults and shear zones that developed early in the deformation history of the Kadubu area, were re-activated.

The phase of shear folding known in Kivu, has been dated at 648 ±12 Ma. (Cahen et al.,1979). The youngest movements also included reactivation of major D_1 and D_2 structures by rifting and seismicity.

Northwest – trending chevron folds, kinks, shear zones and faults , locally accompanied by a foliation, have overprinted D_1 - D_2 structures.The emplacement of albitite rock is interpreted to be synkinematic relative to the D_2 event.

CHAPTER 7.- METAMORPHISM.

7.1.- INTRODUCTION.

In the Kadubu area, metamorphic grade increases gradually towards the west across the Upper Kadubu group (the lower tectonostratigraphic level) from subgreenschist to greenschist facies. This observation is based on differences in the intensity of deformation and foliation, and on regional variations in the distribution of the textural zones of metamorphism.

Metamorphic reactions related to synkinematic intrusion and cooling of the Kasika leucogranite, are found as an aureole surrounding the pluton in the southwesternmost corner of the study area. Contact metamorphism around the Twangiza albitite is not noticeable.

The metamorphism of the overall area can not be completely described, largely because the disposition of mineral parageneses and isograds has not yet been fully mapped.

The Tshondo fault zone can be regarded as a true major tectonic and metamorphic break within the Kadubu area.

7.2.- PETROGRAPHY AND PHASE RELATIONS.

In order to constrain the metamorphic conditions, about 147 polished and thin-sections have been studied.

7.2.1.- MINERAL ASSEMBLAGE .

The main common and critical mineral assemblage throughout the Kadubu area, recognized in the course of this study is : quartz, albite, chlorite, white mica, (muscovite, sericite), plagioclase (oligoclase), epidote, actinolite, biotite and opaques (hematite, goethite, limonite).

This mineral assemblage occurs in 75% or more of the samples from each stratigraphic unit. In addition to the common mineral assemblage noted above, other minerals can include calcite, ankerite, apatite, graphite, magnesite, rutile, talc and kaolinite. Tourmaline, pyrite, arsenopyrite and zircon as weel as lithic fragments are common additional constituent:

*.- Chlorite is present in all the mineral zones and is due probably to prograde reactions in the S_1 and S_2 schistosisty. It is a typical constituent of the interstitial matrix of all metagreywackes.

*.- Muscovite (sericite) is present in all the lithologies but (mica) increases in amount westwards into the lower Kadubu group. It occurs in three habits : (a) as clusters of fine-grained laths in albite porphyroblasts replacing alkali-feldspars; (b) in the groundmass as individual flakes of detrital or neometamorphic origin; (c) as variably sized streaks that either are derived from argillaceous fragments or represent the original mud matrix .

*.- Plagioclase is patchily altered to fine-grained sericite.It occurs throughout the sequence. Plagioclase grains range from large, euhedral, compositionaly zoned crystals to subangular grains.

*.- Biotite crystallized all along the prograde metamorphic path. A few flakes of biotite in the matrix may represent relics of biotite which has largely been altered to chlorite.

*.- The presence of actinolite and of pale green biotite in several samples from the Lower Kadubu group, indicates upper greenschist facies conditions.

*.- Most quartz grains are monocrystalline quartz, but rare polycrystalline quartz grains have been also observed. Monocrystalline quartz is commonly rounded to sub-angular, undulose or not, sometimes showing common orientation.

Most polycrystalline quartz grains consist of > 2 crystals. The contacts between the sub-grains are straigth to sutured. Inclusions of rutile, tourmaline, are sometimes present within both mono and polycrystalline forms.

7.2.2.- WHOLE -ROCK COMPOSITIONS.

In order to asses the role of whole-rock compositions on the mineral assemblage, four samples (phyllites, diamictite , and metagreywacke) from respectively the upper and lower Kadubu groups, were selected for bulk-rock analysis

KW 88 and KW 107B are respectively a phyllite and a diamiticte from the Kadubu Upper group. KW 341A and KW 330 are respectivelly a phyllite and a metagreywacke from the lower Kadubu group. (Fig.II.115, Table II.13). The compositions show systematic differences.

Compared to the phyllite from Lower Kadubu group, phyllite from Upper Kadubu group are enriched in TiO_2, Al_2O_3, MgO, Na_2O, K_2O, V, Cr, Rb, Sr, Zr, Nb, and Ba and depleted in F_2O_3, MnO, P_2O_5, LOI, Co, Zn, and Y. (Fig.II.115).

The diamictite from the upper group show a enrichment in CaO, MgO, MnO, Fe_2O_3, V, Cr, Co, Zn, Rb, Sr, Ba and a depletion in Al_2O_3 and U.

The data suggest also that the occurrence of upper greenschist is sensitive to the content of total iron . (< 2 wt% Fe_2O_3)

7.3.- MICROTECTONISM AND METAMORPHISM.

7.3.1.- INTRODUCTION.

Three phases of deformations D_1, D_2 and D_3 , characterized by various microstructures (schistosity and crenulations) have been recognized in the metasediments of the study area. The analysis of fabric relations demonstrates that two phases of penetrative deformation, (S_1 & S_2), are associated with low-grade metamorphic crystallizations.

The detailed analysis of some metasediments samples from differents units, has allowed the relationship between the microstructures related to D_1 , D_2 and D_3 , and the mineral associated with M_1 , M_2 , M_3 parageneses to be established . These data define three tectono-metamorphic phases: D_1 -M_1 , D_2 -M_2 and D_3-M_3 .

TABLE. II.13 :- WHOLE - ROCK COMPOSITIONS ON THE MINERAL ASSEMBLAGE FROM PHYLLITES, DIAMICTITE AND METAGREYWACKE OF THE KADUBU AREA.

Sample	SiO2	Fe2O3	MnO	MgO	CaO	Na2O	P2O5	LOI	Total	FeOT	FeO	Fe2O3T
KW 107B	64.01	6.92	0.11	3.68	4.4	1.48	0.26	-	95.84	46.13	39.8	51.14
KW 112	65.68	6.73	0.19	2.23	0.88	1.54	0.25	3.06	99.12	44.87	38.72	49.75
KW 152	62.78	6.31	0.01	1.13	0.06	0.45	0.23	-	97.71	42.07	36.3	46.64
KW 330	85.84	1.98	0.02	0.65	0.07	1.34	0.07	0.95	99.24	13.2	11.39	14.63
KW 341A	60.25	4.82	0.02	0.47	0.03	0.31	0.04	5.96	99.68	32.13	27.72	35.62
KW 341B	54.52	5.13	0.03	0.05	0.02	0.32	0.04	6.65	98.68	34.2	29.51	37.92
KW 65	69.56	1.4	0.01	0.22	0	0.74	0.05	4.01	-	9.33	8.05	10.34
KW 70	65.77	0.6	0	0.44	0	0.69	0.04	3.72	100.46	4	3.45	4.43
KW 88	49.39	2.21	0.01	0.64	0	0.45	0.03	5.13	100.01	14.73	12.71	16.33

Sample	Ba	Y	Zr	Nb	Th	Pb	Zn	Cu	Ni	V	Cr	Ta	Co	U
KW 107B	602	17	158	10	16	14	51	4	36	102	76	3	14	1
KW 112	-	-	-	-	-	-	-	-	-	-	-	-	-	-
KW 152	1073	23	222	19	23	3	71	174	79	171	109	8	19	0
KW 330	171	14	170	13	-	-	21	-	-	39	45	-	12	11
KW 341A	902	37	282	28	-	-	30	2	15	181	165	-	4	-
KW 341B	978	46	327	30	-	-	29	-	12	203	189	-	2	-
KW 65	-	-	-	-	-	-	-	-	-	-	-	-	-	-
KW 70	-	-	-	-	-	-	-	-	-	-	-	-	-	-
KW 88	2987	27	321	72	-	-	10	-	16	782	1027	-	3	-

Sample	W	Sn	Mo	Au	La	Ce	Pr	Nd	Sm	Eu	Gd	Tb	Dy	Ho	Er	Tm	Yb	Lu
KW 107B	-	-	1	-	23	40	5	14	4	-	2	-	1	-	-	-	-	-
KW 112	-	-	-	-	-	-	-	-	-	-	-	-	-	-	-	-	-	-
KW 152	5	-	-	-	-	-	-	-	-	-	-	-	-	-	-	-	-	-
KW 330	-	-	2	-	-	-	-	-	-	-	-	-	-	-	-	-	-	-
KW 341A	-	-	-	-	-	-	-	-	-	-	-	-	-	-	-	-	-	-
KW 341B	-	-	-	-	-	-	-	-	-	-	-	-	-	-	-	-	-	-
KW 65	-	-	-	-	-	-	-	-	-	-	-	-	-	-	-	-	-	-
KW 70	-	-	-	-	-	-	-	-	-	-	-	-	-	-	-	-	-	-
KW 88	-	-	-	-	-	-	-	-	-	-	-	-	-	-	-	-	-	-

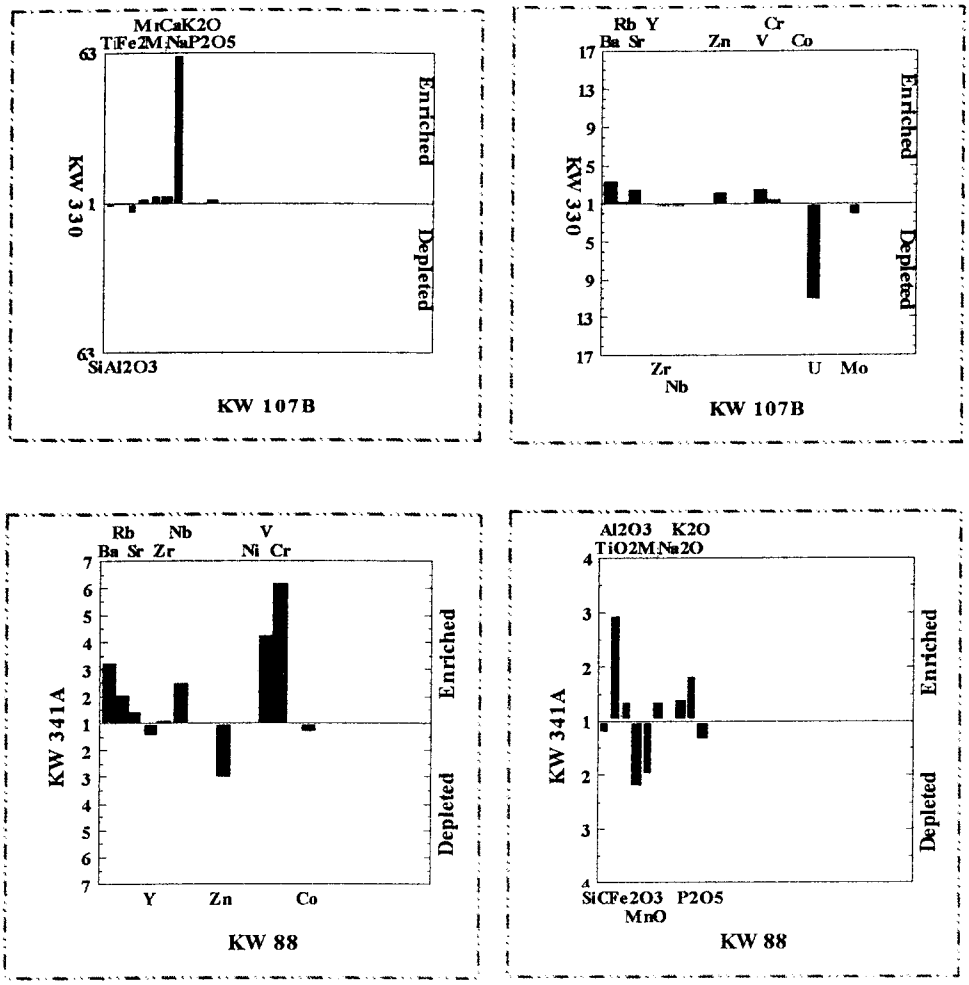


Fig.II.115:- Enrichment / depletion diagrams showing the enrichment factors for selected major and trace elements in samples from Kadubu area.
The diagrams compare the relative concentration respectively of the Upper Kadubu polymictic conglomerate (sample KW 107B) and phyllite (sample KW 88) and lower Kadubu group metagreywacke (KW 330) and sample (KW 341 A).

7.3.2.- TECTONO- METAMORPHIC PHASE : $D_1 - M_1$.

This phase has been observed only on lower Kadubu group metasediments. The microstructures characteristic of this phase are essentially slaty cleavage (flow cleavage) with quartz pressure-shadows. S_1 is orientated NW- SE and subparallel to S_o . S_1 is deformed by S_2 (microstructure S_2). F_1 folding of the bedding S_o induced the shistosity S_1, which can only be recognized in thin section as relics overgrown by D_2 minerals.

During D_1 deformation , the rocks passed through low to moderate pressure conditions and the assemblage ; quartz-muscovite-chlorite, was formed. This is the M_1 phase.

The metamorphism M_1 (synkinematic D_1) is manifested by the recrystallization of the following minerals : biotite, muscovite, chlorite, opaque minerals.

7.3.3.- TECTONO – METAMORPHIC PHASE: $D_2 - M_2$.

In the lower Kadubu group, this phase is chracterised by the deformation and /or cataclasis of the minerals aligned along S_o-S_1. S_2 crenulation cleavage and strain slip are orientated NNW-SSE.

In the upper Kadubu group, not affected by D_1, the second phase of deformation is accompanied by the M_2 phase of metamorphism which occurred during D_2 deformation.

Most of the rocks in the upper Kadubu group, have well-developed foliations defined by the shape and preferred orientation of micas (sericite), shear- band orientations, S-C fabrics and quartz textures.

The mineral paragenesis associated with this phase is : quartz, muscovite, sericite, chlorite and opaque minerals with neoformation minerals having an S_2 orientation .

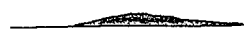
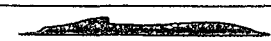
7.4.- METAMORPHIC EVOLUTION.

Prograde greenschist facies metamorphism has affected the Kadubu area and it is concluded that one regional metamorphic event with distinct phases occurred.

7.4.1.- GROWTH AND STABILITY OF THE MINERALS.

The relative grow and stability of the minerals during the metamorphic and deformational evolution is summarised in the following Table.II.14.

Table. II.14.

Tectonic event / Mineral phases	$D_1 - M_1$	$D_2 - M_2$	$D_3 - M_3$
Quartz			----------
Chlorite			----------
Plagioclase	.....		.....
Muscovite	----------		----------
Biotite Garnet			.....

Based on mineralogical assemblages in the system K_2O-FeO-MgO-TiO_2-Al_2O_3-SiO_2-H_2O, two main metamorphic zones have been recognized with the following minerals : quartz, muscovite, chlorite ,(always present); with or without biotite and garnet.

These two metamorphic zones correspond also to the two structural zones defined previously.

7.4.2.- CHRONOLOGY AND TECTONIC FRAMEWORK : $^{39}Ar/^{40}Ar$ DATING.

7.4.2.1.- INTRODUCTION.

The $^{39}Ar/^{40}Ar$ age spectrum study was initiated to establish the time of regional metamorphism and associated compressive deformation in the Kadubu area. Radiometric dating of minerals is also a useful tool in the quantificafion of T-t paths during cooling of metamorphic terranes and such paths are an important test for tectonic models of orogens. (Cliff, 1985 ; Zeitler, 1989).

The $^{39}Ar/^{40}Ar$ age spectrum technique can yield detailed information on the age of thermal events, because of its potential to resolve ^{40}Ar gradients within minerals, thus allowing identification of disturbed samples. In metamorphic terranes, radiogenic argon, ^{40}Ar , may diffuse from minerals during thermal overprinting. Argon thus released into the metamorphic fluid, as well as argon released from minerals during recrystallization, may be incorporated into other minerals.

The interpretation of isotopic ages in terms of the thermal evolution of crustal sections during orogeny has been discussed , and several points have been recognized as pertinent to the establishment of precise thermal histories of terranes (Harrison et al., 1979).

These are the following :

1.- Metamorphic terranes may have experienced more than one phase of mineral growth, with the result that different generations of minerals may coexist or overgrow each other;

2.- Quantitative accumulation of a radiogenic daughter only occurs subsequent to cooling of a mineral below its closure temperature;

3.- Mineral growth may not exactly coincide with the most extreme temperatures or pressure experienced by the system;

4.- A mineral outside its stability field may undergo alteration, exsolution, recrystallization , polymorphic alteration, or weathering.

All these processes may interfere with interpretation of isotopic ages.

In the present study, geochronological information is supported by an assessment of the petrological and structural relations of relevant mineral assemblages.

In terranes where minerals have crystallized at metamorphic temperatures greater than the closure temperature for argon diffusion, ages are interpreted as recording cooling of the rocks following the peak of metamorphism. The closure temperature of white micas (muscovite) for argon is quoted to be 350^0 C (Jager , 1979) or 330^0 C (Wijbrans and McDougall, 1988).

7.4.2.2.- SAMPLE DESCRIPTION.

Sample KW 152 , a carbonaceous,sericite –quartz schist, come from the confluence of the Mwana and Kadubu rivers, within the Tsibangu formation of the upper Kadubu group.

The rock is an extremely fine-grained, carbon-rich, sericite-quartz schist. The micaceous component defines a crenulation cleavage with carbon being concentrated along the axes of this cleavage at a high angle to the schistosity. The rock is traversed by quartz-chlorite veins which, to some extent, parallel the carbon stringers. (Fig.II.116).The sample is foliated and the main phases are sericite, quartz, chlorite, carbon and rutile; a low temperature assemblage .

The composition and texture of the sample is as follow (estimation abundances are in vol. %):

Sericite: 72 vol. % , Somewhat iron-stained, oriented flakes, up to 0.04 mm long, defining a schistosity.

Quartz : 15 vol. % , (i) Deformed veins, up to 3 mm wide, transecting the rock at high angle to foliation.

(ii) Very fine grains , < 0.03 mm accross, concentrated in lenticular streaks parallel to foliation.

Chlorite: 2-3 vol. % , forming the outer zone of quartz veins .

Carbon: 10 vol. % , Extremely fine , poorly crystalline material between the mica flakes and concentrated linearly along axes of crenulation cleavage.

Rutile: < 1 vol. % ,Very small grains distributed throughout sericite.

7.4.2.3.- RESULTS AND INTERPRETATION.

$^{40}Ar/^{39}Ar$ laser probe analytical results for a single muscovite are presented in Table II.15 . The Ca/K ratio from $^{40}Ar/^{39}Ar$ ratios is included. Step-heating analyses were undertaken on seven muscovite grains from sample KW 152 at Anglo American Research Laboratory by Dr N. Philipp, Mrs V.M. Robb and Mrs G.B. Kiviets. The grains were very small and only single analysis steps could be undertaken. All the grains except, grain KW 152-1 , released insignificant amounts of argon and no age calculations could be made. Due to its small size, muscovite grain KW 152-1 degassed in a single step producing an age of 575 +/- 83Ma.

This dated muscovite comes from within the D_2 - NNW- directed tight to isoclinal –dominated structural domain and the interpreted age coincides with the F_2 folding event. The plateau age of 575 ± 83 Ma is interpreted as recording initial mica growth during D_2 deformation and associated regional metamorphism. This age is likely to date cooling following initial metamorphic recrystallization and concomitant cleavage development.

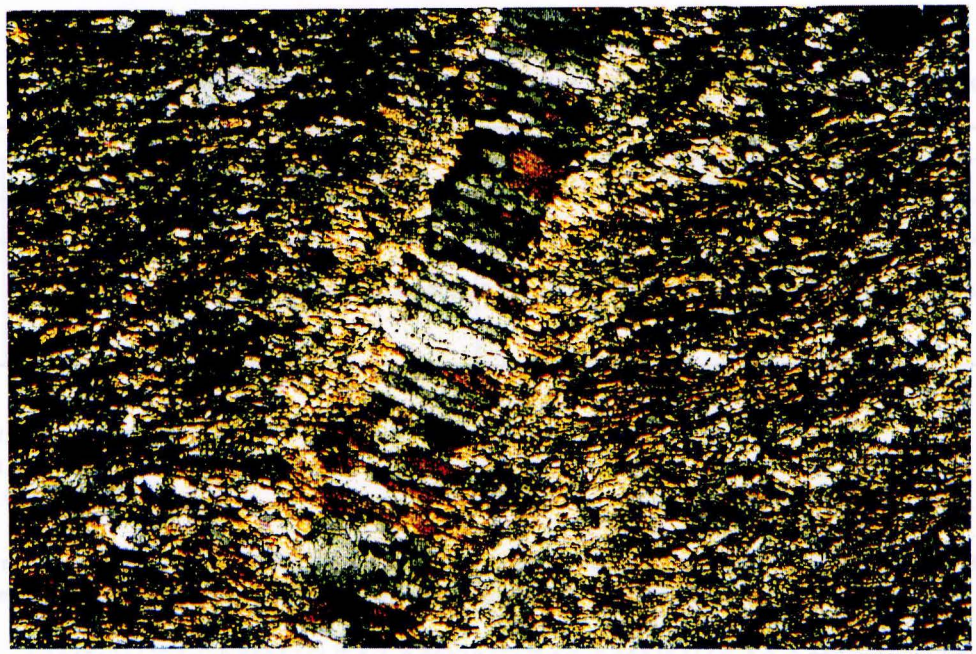


Fig.II.116:- - Photomicrograph of a carbonaceous- sericite- quartz schist (KW 152), from the upper Kadubu group.

Table.II.15:- $^{40}Ar/^{39}Ar$ LASER PROBE ANALYTICAL RESULTS FOR SINGLE MUSCOVITE GRAIN FROM BLACK SHALE . KADUBU AREA.

MINERAL	GRAIN	STEP	INTERFERENCE - CORRECTED PEAK HEIGHTS					$^{37}Ar_{ca}/^{36}Ar_{k}$	ATMOS	AGE (Ma)
	No.	No.	^{40}Ar	^{39}Ar	^{38}Ar	^{37}Ar	^{36}Ar		%	
MUSCOVITE	KW 152-1	1	0.0376+/-0.0002	0.00041+/-0.00002	0.00049+/-0.00003	0.0001+/-0.0001	0.00007+/-0.0001	0.092+/-0.092	5344	575+/-83

J-Value for KW 44, KW 622A = 0.0086+/-0.0001
J-Value for KW 705 = 0.009+/-0.0001
J-Value for KW152 = 0.0087+/-0.0001

Isotope peak heights are corrected for system blanks, mass discrimination, radioactive decay of ^{37}Ar and ^{39}Ar,and reactor induced interferences on masses 40, 39,38 and 36. Values are recorded as volts (V).

Typical blank levels are: 0.00461 V (^{40}Ar), 0.0001 V (^{39}Ar), 0.00010 V (^{38}Ar), 0.00346 V (^{37}Ar), 0.00030 V (^{36}Ar)

7.5.- SUMMARY AND DISCUSSION.

In the Kadubu area, metamorphic grade increases gradually towards the west (the lower tectonostratigraphic level) across the Upper Kadubu group, from subgreenschist to greenschist facies.

The common mineral assemblage throughout the Kadubu area is : quartz, albite, chlorite, white mica (muscovite, sericite, phengite), plagioclase (oligoclase), epidote, actinolite, biotite, opaque (hematite, goethite, limonite). This mineral assemblage occurs in 75% or more of the samples from each unit. Other minerals associated include calcite, ankerite, apatite, graphite, magnesite, rutile, talc and kaolinite. Lithic fragments, tourmaline, pyrite, arsenopyrite and zircon are common additional constituents .

Three phases of deformations D_1, D_2 and D_3 , characterized by various microstructures (schistosity, crenulations) have been recognized in the metasediments of the study area. The analysis of fabric relations demonstrates that two phases of penetrative deformation, (S_1 & S_2), are associated with low-grade metamorphic crystallization . The detailed analysis of some metasediments samples from differents units, has allowed the relationship between the microstructures related to D_1 , D_2 and D_3 , and the associated mineral parageneses (M_1, M_2, M_3) to be established.

These data define, three tectono-metamorphic phases: D_1-M_1 , D_2-M_2 and D_3-M_3.
The microstructures characteristic of the tectono-metamorphic phase D_1-M_1 are essentially slaty cleavage and flow cleavage with quartz pressure-shadows. S_1 is orientated NW- SE and is subparallel to S_o . S_1 is the deformed by microstructure S_2 .

In the upper Kadubu group, the D_2-M_2 tectono-metamorphic phase has a well-developed foliation (S_2), defined orientated micas (sericite), orientated shear- band, (S-C fabrics) .

Compared to the phyllite from the Lower Kadubu group, phyllites from the Upper Kadubu group are enriched in TiO_2, Al_2O_3, MgO, Na_2O, K_2O, V, Cr, Rb, Sr, Zr, Nb, and Ba and depleted in Fe_2O_3, MnO, P_2O_5, LOI, Co, Zn, and Y.
The diamictite from the Upper group shows an enrichment in CaO, MgO, MnO, Fe_2O_3, V, Cr, Co, Zn, Rb, Sr, Ba and a depletion in Al_2O_3 and U.

The geochemical data suggests the development of the upper greenschist metemorphic assemblage is sensitive to the total iron content. (< 2 wt% Fe_2O_3).
The Tshondo fault zone is a clear tectonic and metamorphic discontinuity within the Kadubu area.

$^{40}Ar/^{39}Ar$ dating of metamorphic mica (muscovite) in cleaved phyllite gives an age of 575 ± 83 Ma ; This dated muscovite comes from within the D_2 - NNW- directed tight to isoclinal – dominated structural domain and the interpreted age coincides with the F_2 folding event .

The plateau age of 575 ± 83 Ma is interpreted as recording initial mica growth during D_2 deformation and associated regional metamorphism. This age is likely to date cooling following initial metamorphic recrystallization and concomitant cleavage development.
Both the field evidence and age dating give a Neoproterozoic age.

CHAPTER 8.- GEOCHEMISTRY AND TECTONIC SETTING OF CLASTIC METASEDIMENT.

8.1.- INTRODUCTION.

This chapter examines the geochemistry of the clastic metasediments, and by using their geochemistry in relevant discriminant diagrams, determine the tectonic depositional setting.

An attempt is also made :

1:- to interpret the origin of protolith and its transformation identifying the source and provenance of these metasediments ;

2:- to elucidate the conditions and setting of protolith formation and the significances for local history of the earth of the conglomeratic Formations found in the Kadubu area.

The reconstruction of geodynamic settings in metamorphosed and strongly deformed sequences is associated with a number of fundamental problems. The first significant problem is the degree to what the primary rock composition has been preserved in the regional metamorphism. The second problem is the correlation between the composition of ancient rock complexes and the recent ones, which can serve as indicator for certain geodynamic settings (Makrygina and Petrova, 1998).

Holland and Winchester (1989) pointed out that certain element concentrations are essentially unaffected by metamorphic and structural influences and record, with surprising fidelity, the chemistry of the pre-metamorphic and pre-tectonic assemblages. The apparently largely isochemical of metamorphism allows the sedimentary record to be identified and evaluated.

Geochemical characteristics of metasediments in the Kadubu area and the Itombwe Synclinorium in general , have not yet been done undertaken.

While much work remains to be done before a comprehensive coverage of the entire region is achieved, preliminary results for the Kadubu area show that their geochemistry is a useful meams for identifying original sedimentary type and for geodynamic reconstruction where recrystallisation during metamorphism has occurred .

8.2.- GENERAL GEOCHEMICAL FEATURES AND CLASSIFICATION.

In this study, 20 samples of black shale, 3 samples of phyllite, 2 sample of conglomerate and 2 samples of greywackes from lower and upper Kadubu groups were chemically analysed (Representative data in Table II.16, and chemical composition of average shale and major sandstones types in Table.II.17).

In general, the metasediments are broadly acidic in composition with normally 53 – 70 wt.% SiO_2 for black shale, 64 wt.% SiO_2 for conglomerate, 49.39- 60.25 wt% for phyllite and 85 wt.% SiO_2 for greywacke. Higher values are exhibited by the more silicified (and /or siliceous) black shale and phyllite. The lowest value [40 wt.% SiO_2] is recorded in a weathered black shale sample.

The metasediments are characterized by $Na_2O/K_2O > 1$, and a narrow range of Al_2O_3/Na_2O (1.53- 2.59) and Al_2O_3/TiO_2 (17.20 – 15.44) indicative of chemical maturity because typical greywackes have $Al_2O_3/Na_2O \approx 10$. (Garrels and McKenzie, 1971 ; Pettijohn, 1975).

Large-ion-lithophile (LIL) are often very variable with , for example, K_2O, 0.03 – 8.66 wt.% , although LIL element ratios are relatively uniform . (Tables II.13).

Total REE contents are variable (sometimes > 100 ppm) and exhibit well-fractionated light to heavy REE ratios (La/Lu > 2) .

Mg, Fe and all transition trace elements are highly variable and reflect the proportion of phyllosilicates in the metasediments representing the clay component of the original sediments.

Variations in the major element geochemistry are shown on Harker diagrams (Fig.II.117). Notice the negative correlation of SiO_2 versus TiO_2, Al_2O_3, Fe_2O_3, Fe_2O_{3T} and K_2O.

Two main populations can be identified on the Na_2O-SiO_2 diagram. Those with low and hose with high Na_2O values (Fig.II.117). The population with high Na_2O (3.7- 12.0 wt%) represente the metasediments closely associated with the albitite rock, and this high Na_2O content may due to post-depositional albitization. High Na_2O values from Twangiza black shale [3.7 – 12.02 wt.%], and low Na_2O values for the black shale of the remaining area [0.05 – 1.54 wt.% :], could also indicate that some units of black shale and phyllite are derived from relatively immature sediments.

TABLE.II.16 : - CHEMICAL COMPOSITION OF THE KADUBU METASEDIMENTS.

Sample	SiO2	TiO2	Al2O3	Fe2O3	MnO	MgO	CaO	Na2O	K2O	P2O5	F	LOI	Total	FeOT	FeO	Fe2O3T
KW 107B	64.01	0.7	1.58	6.92	0.11	3.68	4.4	1.48	2.42	0.26	-	-	95.84	46.13	39.8	51.14
KW 112	65.68	0.81	14.49	6.73	0.19	2.23	0.88	1.54	3.25	0.25	-	3.06	99.12	44.87	38.72	49.75
KW 152	62.78	0.9	20.92	6.31	0.01	1.13	0.06	0.45	4.63	0.23	-	-	97.71	42.07	36.3	46.64
KW 203	58.83	1.2	23.88	1.92	0.01	1.05	0.06	0.55	7.08	0.2	0.05	-	94.89	12.8	11.04	14.19
KW 203A	49.68	2	31.59	1.92	0.03	0.86	0	0.39	8.66	0.01	-	5.7	100.9	12.8	11.04	14.19
KW 204	79.89	0.79	8.8	5.59	0.05	0.04	0	0.05	1.14	0.09	-	4.08	100.5	37.27	32.16	41.32
KW 205B	52.58	0.86	18.85	13.91	0.03	0.57	0	0.13	4.33	0.16	-	8.07	99.51	92.73	80.02	102.81
KW 207	61.72	1.03	19.96	5.45	0.01	0.51	0	0.21	4.26	0.06	-	6.95	100.2	36.33	31.35	40.28
KW 330	85.84	0.51	6.41	1.98	0.02	0.65	0.07	1.34	1.4	0.07	-	0.95	99.24	13.2	11.39	14.63
KW 341A	60.25	1.24	22.55	4.82	0.02	0.47	0.03	0.31	3.97	0.04	-	5.96	99.68	32.13	27.72	35.62
KW 341B	54.52	1.4	25.12	5.13	0.03	0.05	0.02	0.32	4.94	0.04	-	6.65	98.68	34.2	29.51	37.92
KW 429	61.84	1.31	22.77	1.31	0	0	0	0	0.03	0.05	-	11.34	99.28	8.73	7.53	9.68
KW 429A1	58.58	1.39	26.86	0.72	0	0.01	0	0	0	0.04	-	12.54	100.2	4.8	4.14	5.32
KW 429A2	56.01	1.57	28.28	0.3	0	0	0	0	0	0.03	-	12.48	98.7	2	1.72	2.21
KW 438	43.8	4.12	34.08	1.78	0.01	0.37	0	0	1.99	0.06	-	13.75	99.97	11.87	10.24	13.16
KW 438B	44.28	1.81	36.7	2.45	0	0	0	0	0.31	0.06	-	14.69	100.7	16.33	14.09	18.1
KW 439A	51.17	0.26	5.54	32.01	0.03	0.41	0	0	0.03	0.69	-	9.86	100	213.4	184.2	236.61
KW 439B	39.91	1.02	32.14	8.52	0.01	0.49	0	0.02	2.04	0.1	-	15.91	100.2	56.8	49.01	62.97
KW 439C	62.43	0.76	20.75	4.49	0.01	0.11	0	0	0.56	0.1	-	10.66	99.88	29.93	25.82	33.18
KW 439D	73.04	1.01	13.99	3.16	0.02	0.19	0	0	0.97	0.05	-	7.42	99.85	21.07	18.18	23.36
KW 448A	56.02	1.17	2.13	4.74	0.02	0.66	0.04	7.77	1.99	0.06	-	6.36	98.95	31.6	27.26	35.03
KW 448C	65.11	0.83	12.96	6.55	0.01	0.34	0.03	9.83	0.21	0.05	-	4.84	100.8	43.67	37.68	48.41
KW 621B1	65.87	0.87	16.02	3.53	0.03	1.67	0.14	10	0.43	0.1	-	2.21	100.9	23.53	20.3	26.08
KW 621B2	63.88	0.93	19.47	1.25	0.02	1.59	0.08	10.8	1.15	0.07	-	1.76	101	8.33	7.18	9.23
KW 622A	70.38	0.03	12.34	1.68	0.04	0.45	0.69	3.71	1.52	0.23	0.05	-	91.17	11.2	9.66	12.41
KW 622A1	63.38	0.93	19.55	1.29	0.03	1.98	0.08	11.32	1.08	0.07	-	0.45	100.2	8.6	7.42	9.53
KW 622B	62.73	0.94	18.38	0.85	0.01	1.76	0.43	12.02	0.87	0.08	-	2.24	100.3	5.67	4.89	6.28
KW 622D	57.44	0.87	14.03	11.76	0.08	1.35	0.39	5.76	0.21	0.28	-	6.7	98.87	78.4	67.65	86.92
KW 65	69.56	1.05	18.9	1.4	0.01	0.22	0	0.74	4.05	0.05	-	4.01	-	9.33	8.05	10.34
KW 70	65.77	1.13	22.64	0.6	0	0.44	0	0.69	5.43	0.04	-	3.72	100.5	4	3.45	4.43
KW 88	49.39	3.72	31.08	2.21	0.01	0.64	0	0.45	7.33	0.03	-	5.13	100	14.73	12.71	16.33
KW2 448A	53.19	1.24	18.63	3.39	0	1.63	0.14	3.7	2.54	0.12	0.06	-	86.32	22.6	19.5	25.05
KW2 448C	63.18	0.75	11.58	5.68	0.01	0.86	0.13	4.2	0.29	0.14	0.07	-	-	37.87	32.68	41.99
KW2 621B	58.97	0.89	16.61	1.42	0.01	1.81	0.22	4.11	1.27	0.18	0.06	-	85.71	9.47	8.17	10.5
UpCC	-	-	-	-	-	-	-	-	-	-	-	-	-	-	-	-

Sample	Ba	Rb	Sr	Y	Zr	Nb	Th	Pb	Ga	Zn	Cu	Ni	V	Cr	Ta	Co
KW 107B	602	85	144	17	158	10	16	14	-	51	4	36	102	76	3	14
KW 112	-	-	-	-	-	-	-	-	-	-	-	-	-	-	-	-
KW 152	1073	198	23	23	222	19	23	3	-	71	174	79	171	109	8	19
KW 203	1409	284	23	3	415	25	9	1	-	29	-	2	145	118	5	5
KW 203A	2025	412	31	18	600	35	-	-	-	62	11	11	226	211	-	8
KW 204	62	67	13	14	284	18	-	-	-	-	10	9	62	48	-	7
KW 205B	1043	224	16	19	194	19	-	-	-	14	82	22	166	148	-	-
KW 207	974	222	13	27	245	19	-	-	-	-	-	-	154	142	-	7
KW 330	171	57	54	14	170	13	-	-	-	21	-	-	39	45	-	12
KW 341A	902	136	48	37	282	28	-	-	-	30	2	15	181	165	-	4
KW 341B	978	147	52	46	327	30	-	-	-	29	-	12	203	189	-	2
KW 448A	238	92	14	37	235	22	-	-	-	-	-	-	257	118	-	16
KW 448C	28	25	14	25	213	19	-	-	-	-	21	26	106	68	-	19
KW 621B1	25	42	13	30	215	19	-	-	-	-	0	23	94	102	-	18
KW 621B2	153	71	17	37	191	20	-	-	-	-	-	9	153	135	-	9
KW 622A	113	68	16	37	192	20	-	-	-	-	-	-	147	135	-	9
KW 622A1	-	133.7	18.05	5.04	-	-	11.19	10.89	-	60.94	-	-	17.7	-	-	-
KW 622B	72	58	15	36	194	19	-	-	-	-	-	-	140	140	-	11
KW 622D	6	34	11	27	212	19	-	-	-	9	-	60	86	77	-	33
KW 65	-	-	-	-	-	-	-	-	-	-	-	-	-	-	-	-
KW 70	-	-	-	-	-	-	-	-	-	-	-	-	-	-	-	-
KW 88	2987	296	70	27	321	72	-	-	-	10	-	16	782	1027	-	3
KW2 448A	267	99	19	38	252	24	29	4	-	23	-	0	276	173	-	7
KW2 448C	34	19	17	23	224	18	26	9	-	28	-	24	103	60	9	15
KW2 621B	99	66	19	34	191	20	13	-	-	28	-	0	121	103	-	5
UpCC	700	110	350	22	240	25	10.5	15	-	-	-	20	60	35	-	10

Sample	U	W	Sn	Mo	Au	As	La	Ce	Pr	Nd	Sm	Eu	Gd	Dy	Er	Yb
KW 107B	1	-	-	1	-	-	23	40	5	14	4	-	2	1	-	-
KW 112	-	-	-	-	-	-	-	-	-	-	-	-	-	-	-	-
KW 152	0	5	-	-	-	-	-	-	-	-	-	-	-	-	-	-
KW 203	17	6	12	7	24.2	36	16	16	1	3	1	1	1	1	1	2
KW 203A	11	-	20	-	24.2	62	22	22	2	6	2	1	1	1	1	2
KW 204	12	-	-	-	0.05	37	-	-	-	-	-	-	-	-	-	-
KW 205B	18	-	-	-	-	41	-	-	-	-	-	-	-	-	-	-
KW 207	15	-	-	-	-	129	-	-	-	-	-	-	-	-	-	-
KW 330	11	-	-	2	-	-	-	-	-	-	-	-	-	-	-	-
KW 341A	-	-	-	-	-	-	-	-	-	-	-	-	-	-	-	-
KW 341B	-	-	-	-	-	-	-	-	-	-	-	-	-	-	-	-
KW 439B	-	-	-	-	-	-	-	-	-	-	-	-	-	-	-	-
KW 439C	-	-	-	-	-	-	-	-	-	-	-	-	-	-	-	-
KW 439D	-	-	-	-	-	-	-	-	-	-	-	-	-	-	-	-
KW 448A	8	-	-	3	0.35	4033	-	-	-	-	-	-	-	-	-	-
KW 448C	12	-	-	4	0.2	1302	-	-	-	-	-	-	-	-	-	-
KW 621B1	7	-	-	4	-	97	-	-	-	-	-	-	-	-	-	-
KW 621B2	9	-	-	3	-	48	-	-	-	-	-	-	-	-	-	-
KW 622A	12	-	-	3	-	76	2	3	-	-	-	-	-	-	-	2
KW 622A1	11.19	-	7.94	-	-	-	-	-	-	-	-	-	-	-	-	-
KW 622B	10	-	-	4	-	52	-	-	-	-	-	-	-	-	-	-
KW 622D	20	-	-	4	0.1	1972	-	-	-	-	-	-	-	-	-	-
KW 65	-	-	-	-	-	-	-	-	-	-	-	-	-	-	-	-
KW 70	-	-	-	-	-	-	-	-	-	-	-	-	-	-	-	-
KW 88	-	-	-	-	-	-	-	-	-	-	-	-	-	-	-	-
KW2 448A	4	-	-	4	-	5776	35	67	8	32	4	1	4	2	1	2
KW2 448C	0	8	-	3	0.2	1622	18	36	4	13	3	1	2	2	1	2
KW2 621B	-	8	-	3	-	14	19	40	4	7	2	-	3	3	1	1
UpCC	-	-	-	-	-	-	30	64	7.1	26	4.5	0.88	3.8	3.5	2.3	2.2

Table.II.17:- Chemical Composition of Average Shale and Major Sandstones Types .

	Average Shale (%)	Ortho-Quartzite(%)	Graywacke (%)	Arkose (%)
SiO_2	58.1	95.4	66.7	77.1
Al_2O_3	15.4	1.1	13.5	8.7
Fe_2O_3	4.02	0.4	1.6	1.5
FeO	2.45	0.2	3.5	0.7
MgO	2.44	0.1	2.1	0.5
CaO	3.11	1.6	2.5	2.7
Na_2O	1.3	0.1	2.9	1.5
K_2O	3.24	0.2	2	2.8
CO_2	2.63	1.1	1.2	2.8
C	0.8	*	0.1	*
H_2O	5	0.3	3	0.9

Data from Pettijhon 1975

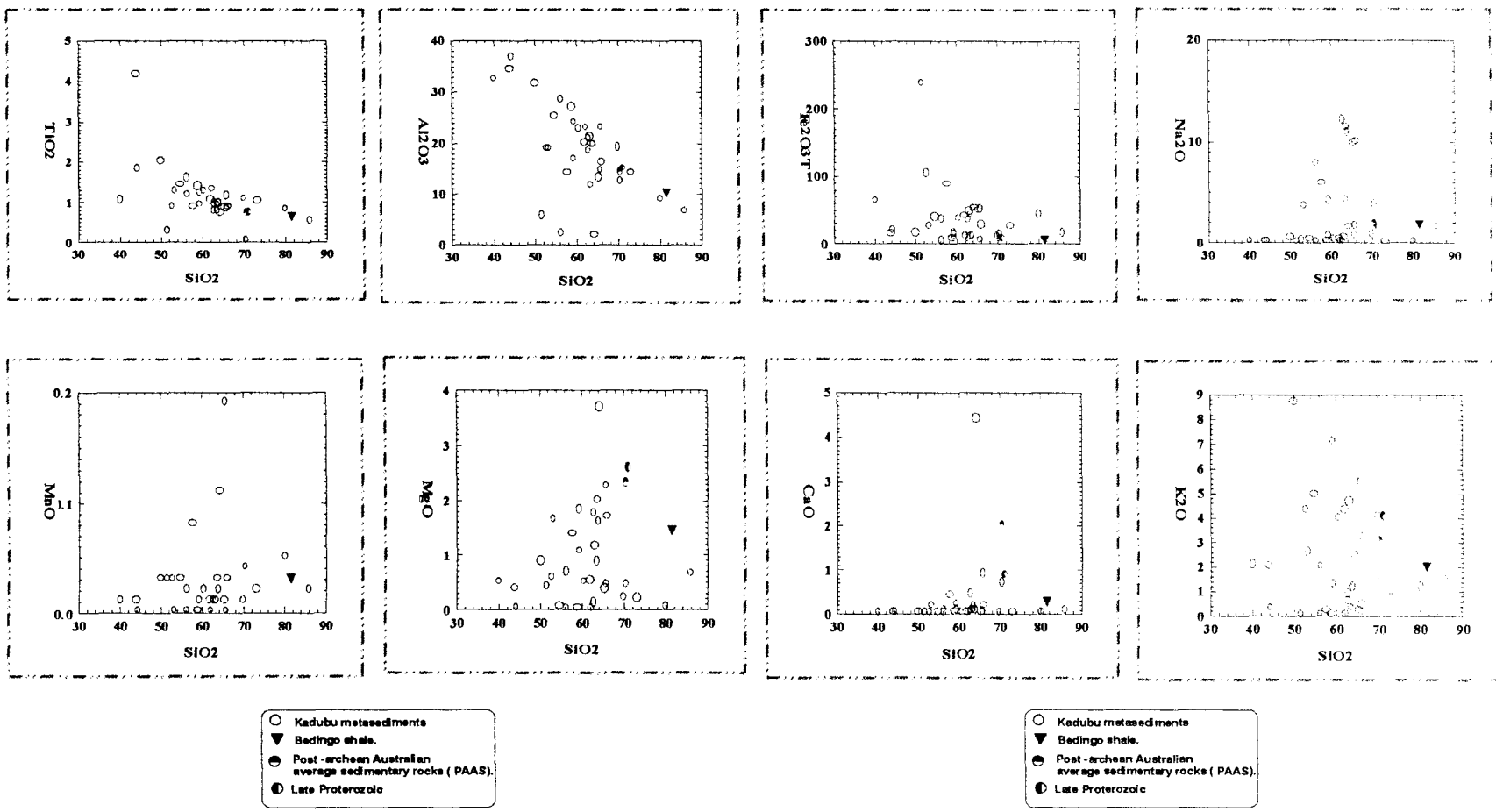


Fig.II.117:- Covariation of major elements versus SiO2 for the Kadubu metasediments.

Both major and trace LIL element has been used in this study to characterize the metasediments chemically. Most LIL elements would be trapped in the micaceous components of the phyllite on metamorphism. Chemical classification of sediments often depends on LIL elements, such as Na and K, that may mobilized during metamorphism.

The same degree of lithological distinction is not achieved in each diagram. The Kadubu metasediments are shown to represent an original mixture of relatively mature clastic materials, such as greywackes, and minor lithic sandstones. (Fig.II.118; Fig. II.119 ;Fig.II.120) shows that most of the clastic metasediments are classified as magmatogenic greywackes with Ni abundances typical of acidic and intermediate rocks .

The elements Nb, Zr, and Y are incompatible during most igneous processes and are generally resistant to change during weathering and alteration processes ; therefore they tend to be enriched in felsic relative to mafic rocks. (Taylor and McLennan , 1985 ; Bhatia and Crook, 1986).

In the studied metasediments, abundance of these elements exhibit a widespread distribution suggesting more than one source. (Fig.II.121).

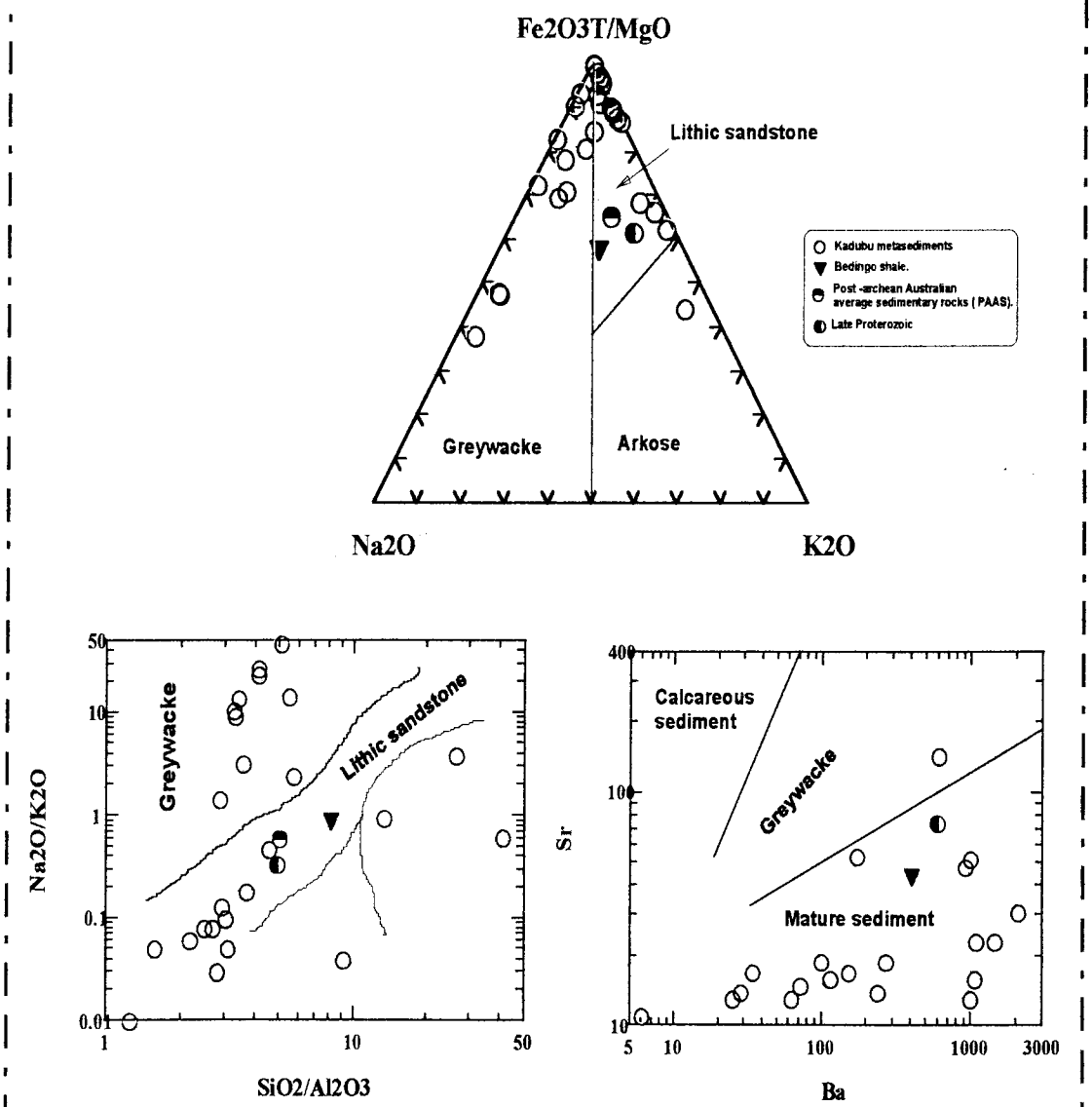
The plots of Cr versus Ni and Co versus V show high contents of Cr and Ni relative to the average upper continental crust of Taylor and McLennan, 1985). (Fig. II.122)

The Kadubu metasediments contain high concentrations of ferromagnesian elements (Cr, Ni, Co, V) and it is more likely that the salic fraction of the sediments has been physically mixed with mafic sedimentary debris.

The two component plots which involve Y versus CaO, P_2O_5, Sr, and Rb versus K_2O , Sr (Fig.II.123) suggest that both geochemical groups of the studied area contain non –calcareous metasediment as shown by minor differences in their concentrations of Ca, Y, P, Sr, and Rb. There is a strong correlation between Rb versus K_2O, and V versus Cr .

Discriminant diagrams (Fig.II.124) of the Kadubu metasediments show one main chemical grouping, an exception is for Ba versus Sr plot which show two chemical groups.

The highly matured and recycled nature of the Kadubu metasediments is reflected in their relative enrichment of K_2O, Na_2O and depletion of CaO compared to the average granite. (after Le Maitre, 1976). (Fig.II.125).



Fi.g.II.118:- Chemical classification of the Kadubu metasediments as predominantly metagreywackes and lithic sandstones.

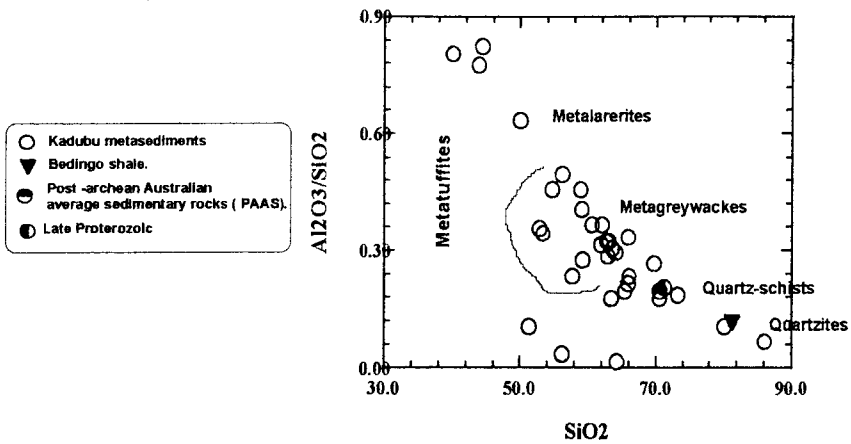


Fig.II.119:- Position of the Kadubu metasediments on Al2O3/ SiO2 versus SiO2 diagram after Lisitsyn , 1978.

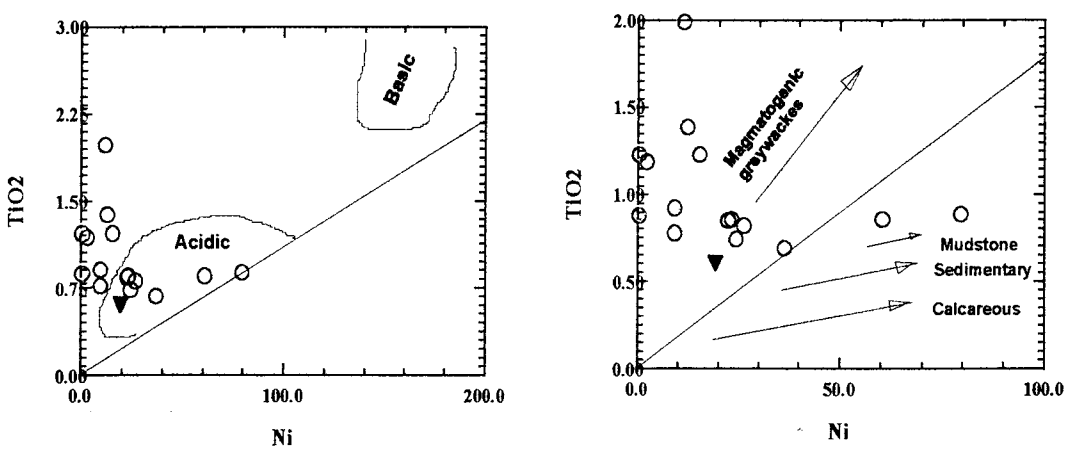


Fig.II.120:- Bivariate plots of Ni versus TiO2 .

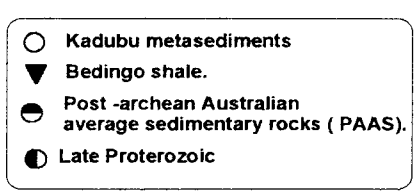
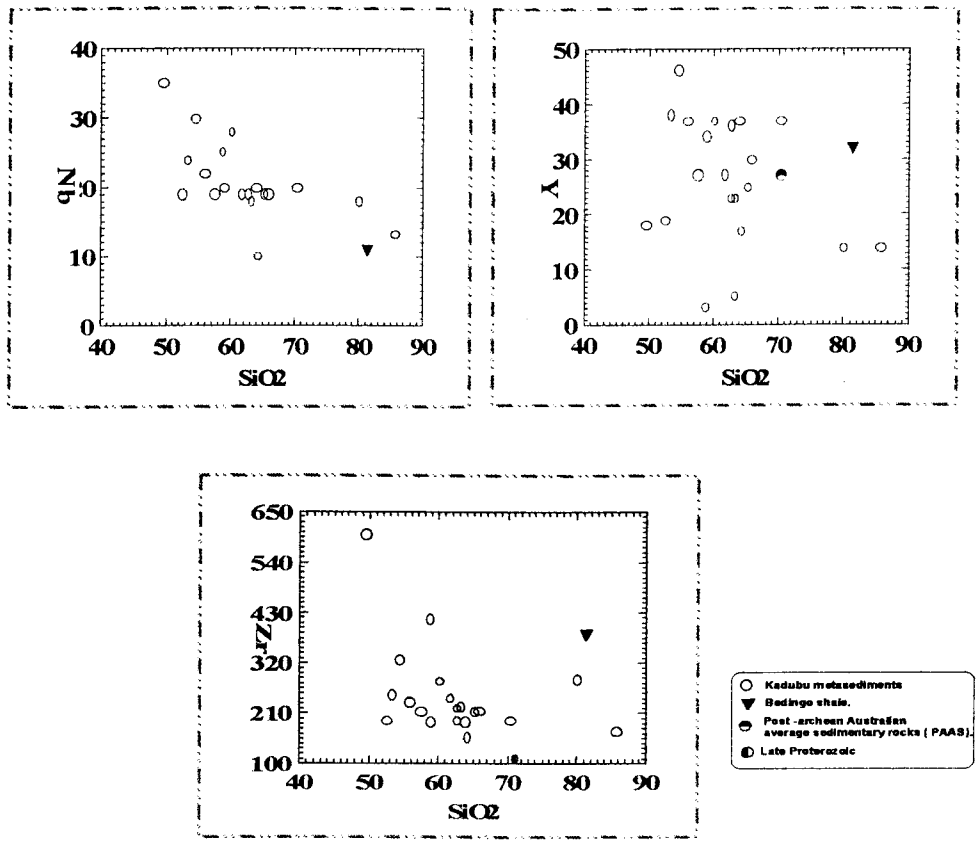


Fig.II.121:- Plot of incompatible trace elements (Nb, Y, Zr) against SiO2 content.



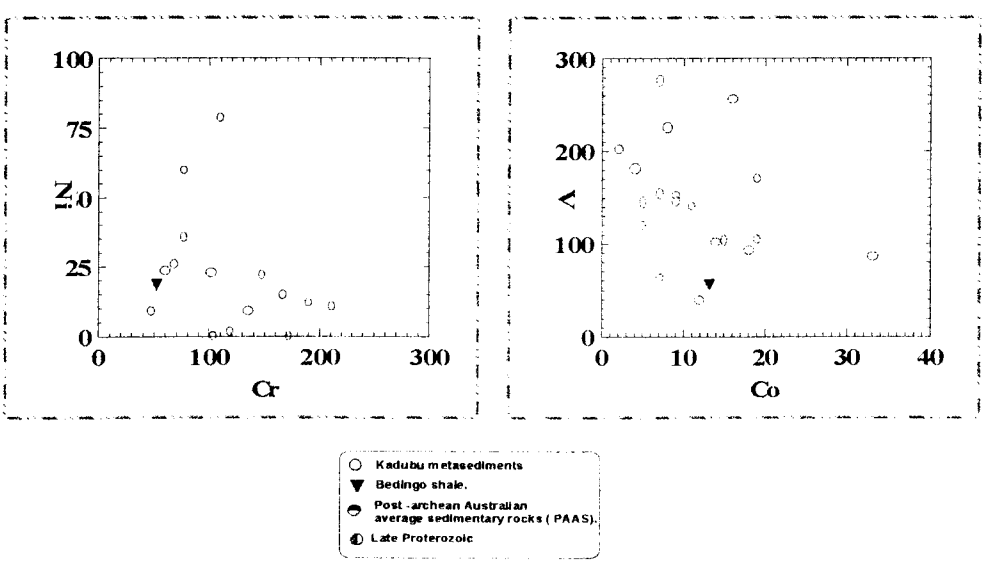


Fig.II.122:- Binary plots of Cr versus Ni and Co versus V for Kadubu metasediments.

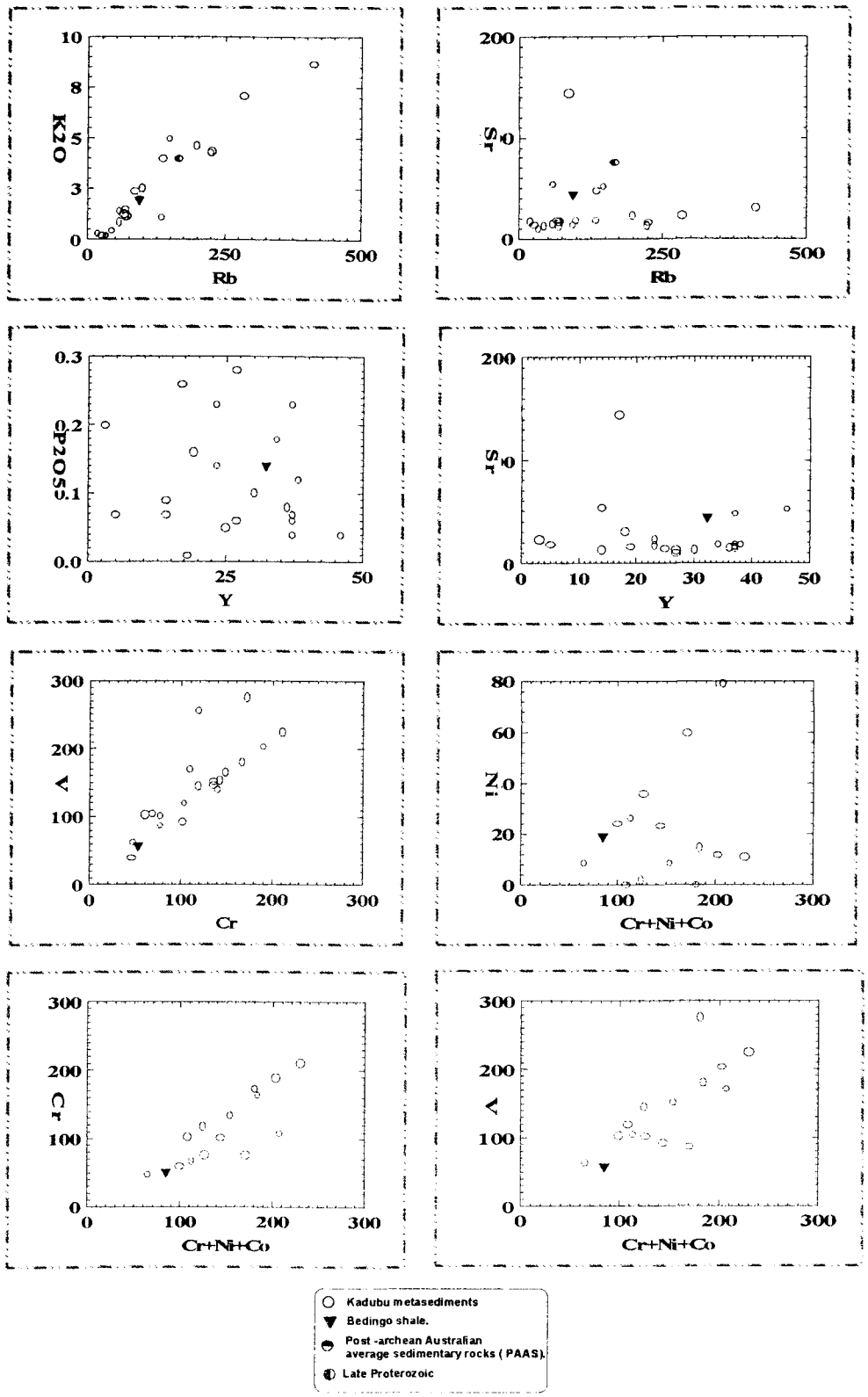


Fig.II.123:- Binary plots of Rb versus K2O , Sr , Y versus P2O5 , Sr and V versus Cr, and Cr + Ni + Co versus Ni, Cr, V

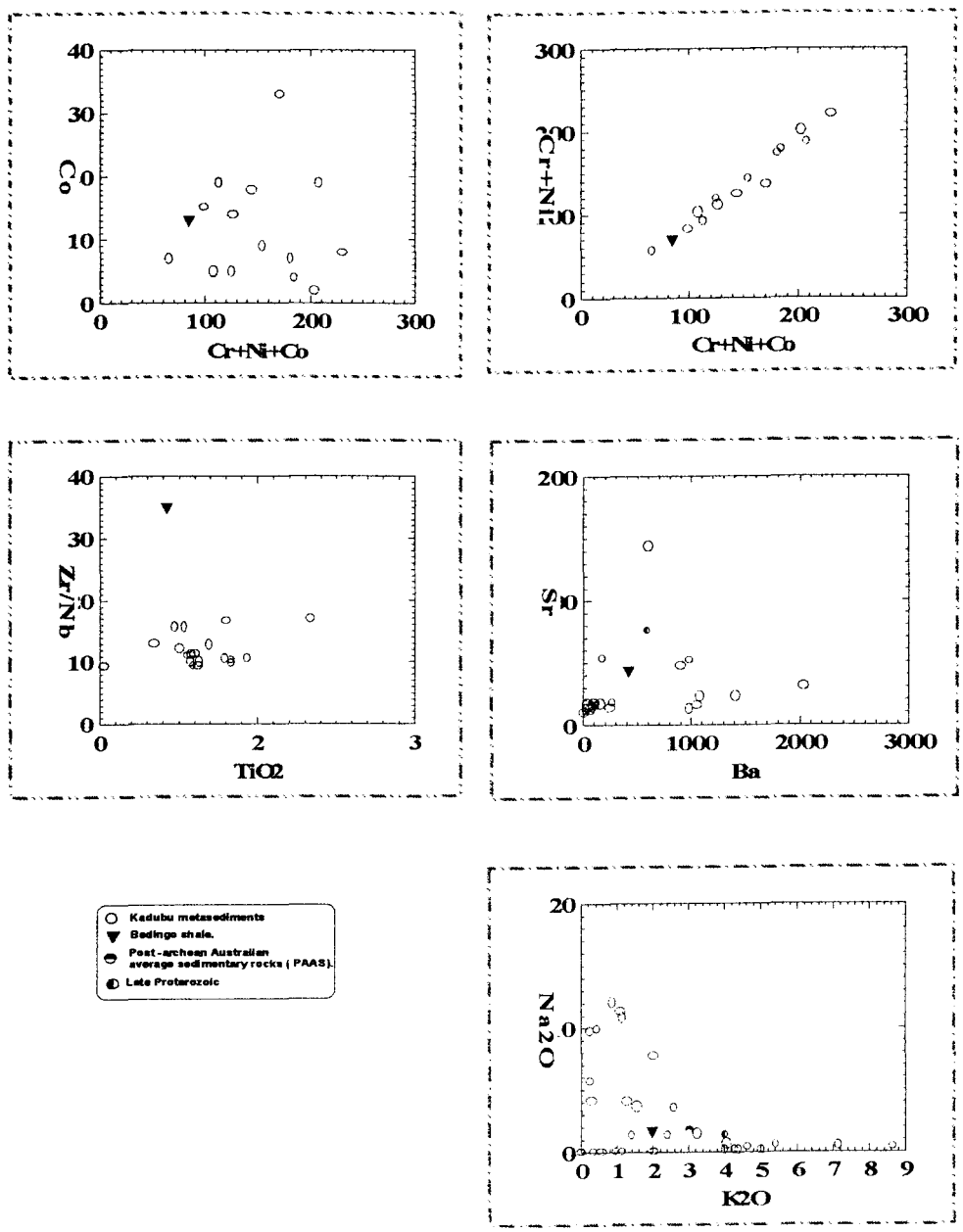


Fig.II.124:- Binary plots of Cr+Ni+Co versus Co, Cr+Ni ; and Ba versus Sr, and K2O versus Na2O , and TiO2 versus Zr/ Nb

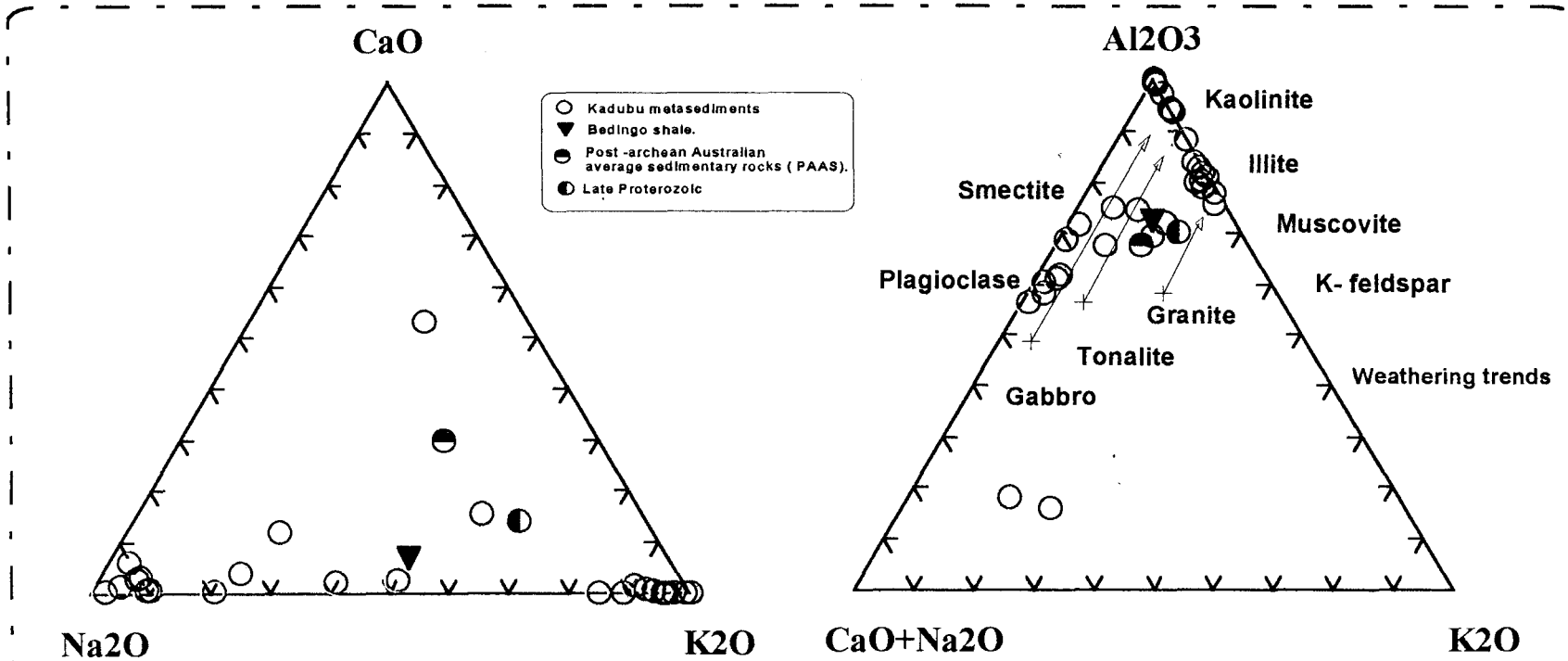


Fig.II.125:- Kadubu metasediments on the Ternary diagram (K2O-Na2O-CaO) of le Maitre, (1976).

Fig.II.126:- Kadubu metasediments on the weathering discrimination diagram of Nesbitt and Young (1984, 1989).
(Major molar proportions plot [(CaO+Na2O)- K2O-Al2O3]

On the weathering discrimination diagram of Nesbitt and Young (1984,1989), (Fig.II.126) they plot mostly on the Al_2O_3 - K_2O and Al_2O_3 - (Na_2O + CaO) joins, in the position of gabbro and granite–derived metasediments. Total CaO is plotted because none of the samples was calcareous.

This is suggestive of a continental source. Although the possibility of some diagenetic alteration of the major element composition, particularly potassium metasomatism can not be excluded (Nesbitt, 1992; Fedo et al., 1995). A continental platform environment, with slight igneous activity could be the source of the sediments.

There is an enrichment in TiO_2, Al_2O_3, MgO , Na_2O, K_2O , V, Cr, Ni, Rb, Sr, Zr, Nb, and Ba and depletion in SiO_2, Fe_2O_3, MnO, P_2O_5, Co, Zn, Y in the phyllite from the upper Kadubu group KW 88 in comparison with the phyllite from lower Kadubu group, KW 341. (Fig.II127). Compared to the metagreywacke of the lower Kadubu group, (KW 330), the matrix supported conglomerate of the upper Kadubu group is enriched in MgO, Rb, Ba, Sr, V, Y, Cr, Zn and depleted in Nb, U, Zr. (Fig.II.128). This suggests an active continental margin which uderwent large chemical weathering process.

8.3.-SOURCE CHARACTERISTIC AND DEPOSITIONAL ENVIRONMENT.

8.3.1.- COMPOSITIONAL CHARACTERISTICS.

The analysis of the compositional characteristics of the Kadubu metasediments provides the data needed to elucidate the conditions and setting of protolith formation. Elements such as Zr, Hf, Y, Ti, Nb, Ta, Sc, V, Th, U, and REE are particularly useful in determining the source materials and depositional environment. Those elements are rapidly incorporated into sediments, or quickly transported to depositional sites as immature detritus via turbidity currents (e.g. greywackes), and hence provide evidence for the composition of the source. (Mc Lennan et al., 1980).

Major element discrimination function analysis (Bhatia, 1983) and selective stable trace element distributions (Bhatia and Taylor, 1981, Floyd and Leveridge, 1987) can achieve some degree of chemical discrimination of the depositional area, particularly in sandstone.

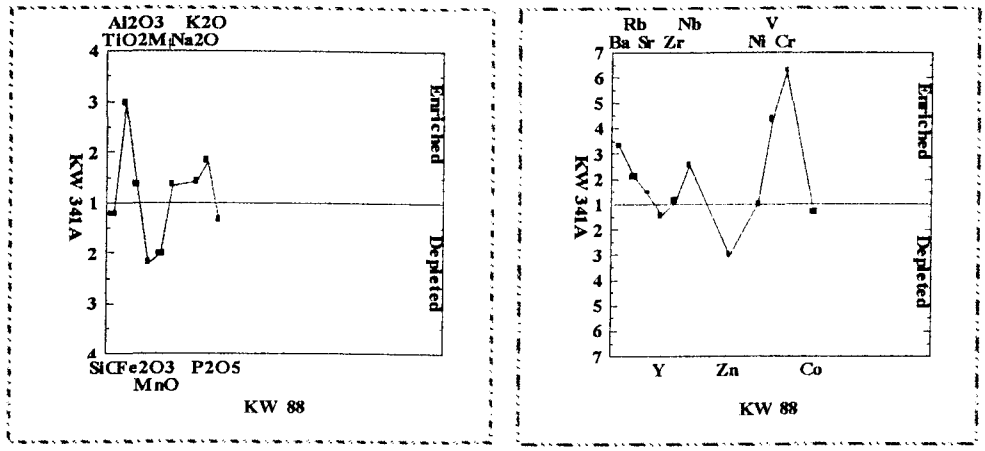


Fig.II.127:- Upper (sample KW 88) and Lower (sample KW 341) Kadubu group phyllites on the enrichment / depletion diagram.

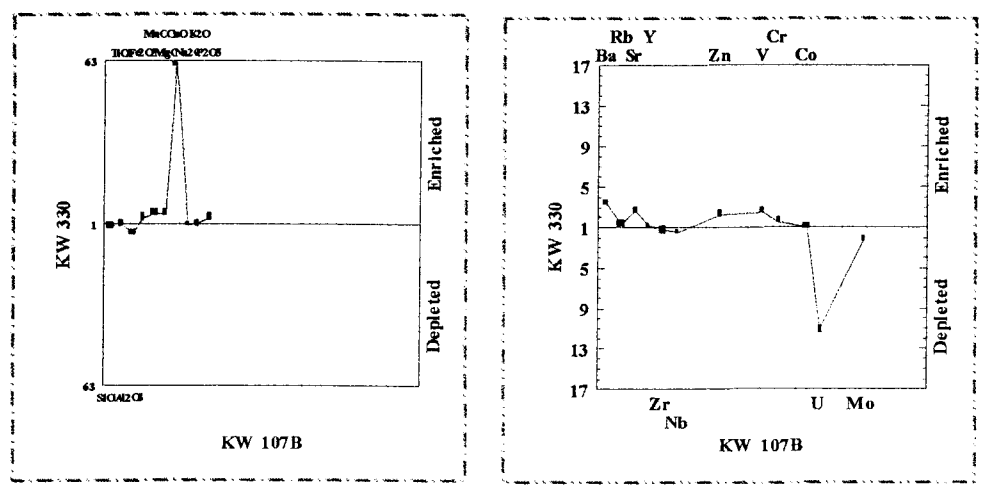


Fig.I.128:- Enrichment - depletion diagram showing the enrichment factors for selected major and trace elements from Kadubu area.
The diagram compares the relative concentration of the polymictic conglomerate (sample KW 107B) from the Upper Kadubu group and the metagreywacke (sample KW 330) from the Lower group.

Major element compositions of the metasedimentary rocks were plotted on discriminant diagrams devised by Bhatia (1983) to illustrate tectonic setting.

On the Fe_2O_{3T} + MgO versus K_2O/Na_2O , TiO_2 , and Al_2O_3/SiO_2 discriminant diagrams, most of the metasedimentary rocks plot within " Oceanic island arc ", while some of the points plot close to this field.(Fig.II.129). An Active continental margin and Passive continental margin setting for the Kadubu metasediments is suggested by the discriminant diagram of K_2O/Na_2O versus SiO_2 (Roser and Korsch, 1986). (Fig.II.130).

In terms of $CaO+Na_2O+K_2O$ / Fe_2O_{3T}+MgO/ Al_2O_3 ternary diagram, (Fig.II.131), derivation from a mixed source is suggested .

Most aspects of major and trace element chemistry (especially of Cr, Ni, and Y) can be explained by mixtures of mafic and felsic igneous rocks. (Fig.II.132). The concentrations of mafic elements (Ni, V, Cr, Co,TiO_2, MgO) are positively correlated with the concentration of Fe_2O3; excepte for Cr, and TiO_2 .(Fig.II.133). These trends indicate that the Kadubu greywackes were formed by mixing schist-like debris with less ferroan detritus.

The concentration of these elements are high comparatively to the upper continental crust and suggest that a significant amount of mafic rock existed in the provenance of the Kadubu sedimentary sequence.

There is not a strong correlation between MgO and various ferromagnesian elements (MnO, Fe_2O_{3T}, Cr+Ni, Cr+Ni+Co), (Fig.II.134) and this is suggests that the chlorite and epidote minerals didn't control the distribution of these elements.

The binary relation TiO_2 vs Ni suggests that the metasediments were largely derived from a magmatic source and that was dominantly acidic or acid/intermediate (Fig.II.120).

In the plots of Al_2O_3 versus TiO_2, V, MgO, K_2O and Na_2O (Fig.II.135), some positive correlations for most of them suggests that the source rock of these metasedimentary rocks underwent significant chemical weathering processes. V correlates positively with Cr, but Au doesn't correlate with Co. (Fig.II.136).

Fig.II.129:- Kadubu metasedimentary rocks on the tectonic discriminant diagrams of Bathia, 1983.

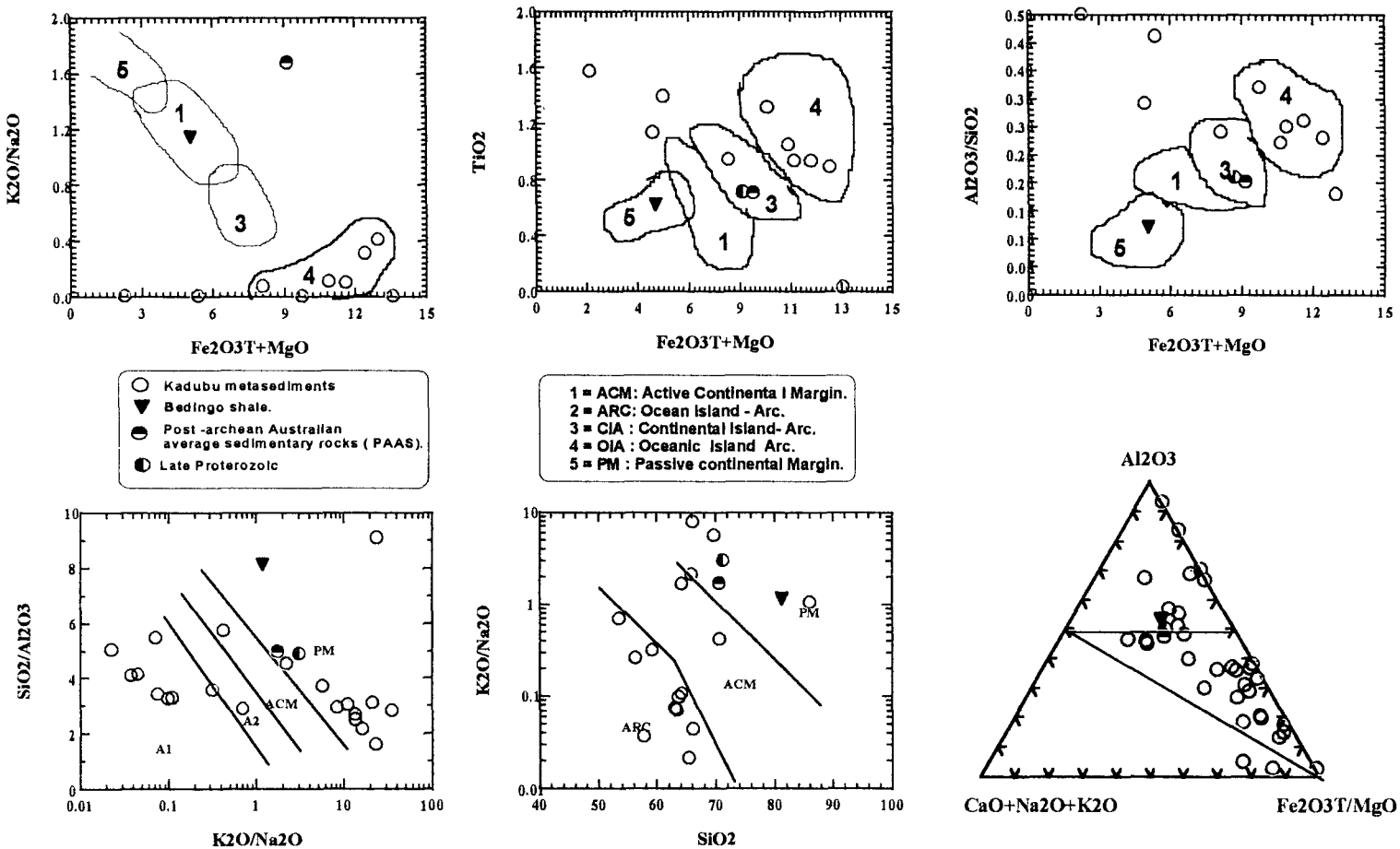
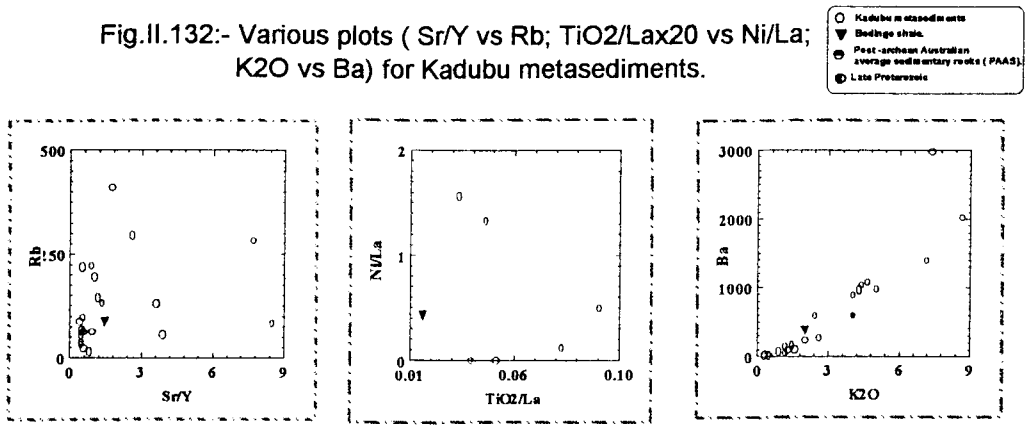


Fig.II.130:- Kadubu metasediments on the tectonic discriminant diagrams of Roser and Korsch, 1986.

Fig.II.131:- Kadubu metasediments on the ternary diagram [Al2O3 - Fe2O3T/MgO - (CaO- Na2O - K2O)]

Fig.II.132:- Various plots (Sr/Y vs Rb; TiO2/Lax20 vs Ni/La; K2O vs Ba) for Kadubu metasediments.



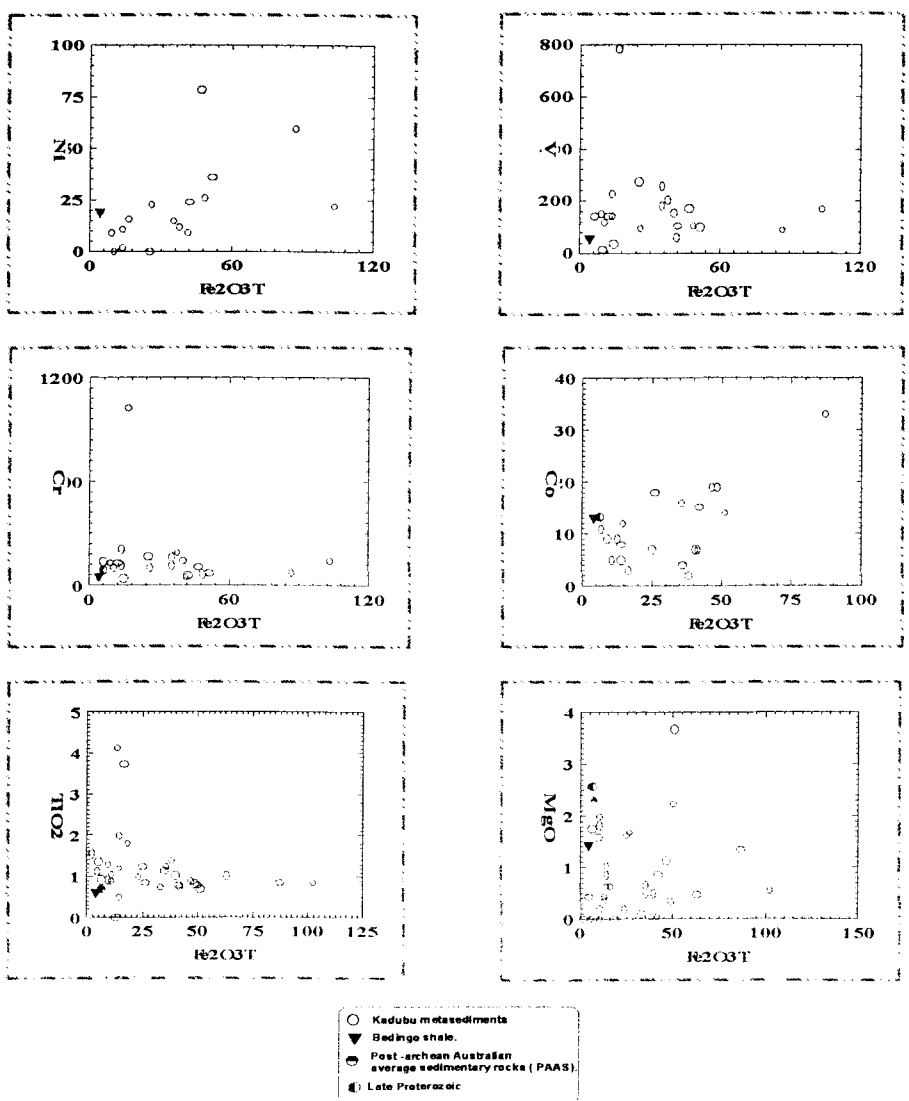


Fig.II.133:- Binary plots of Fe2O3T versus mafic elements (Ni, V, Cr, TiO2, MgO) for Kadubu metasediments.

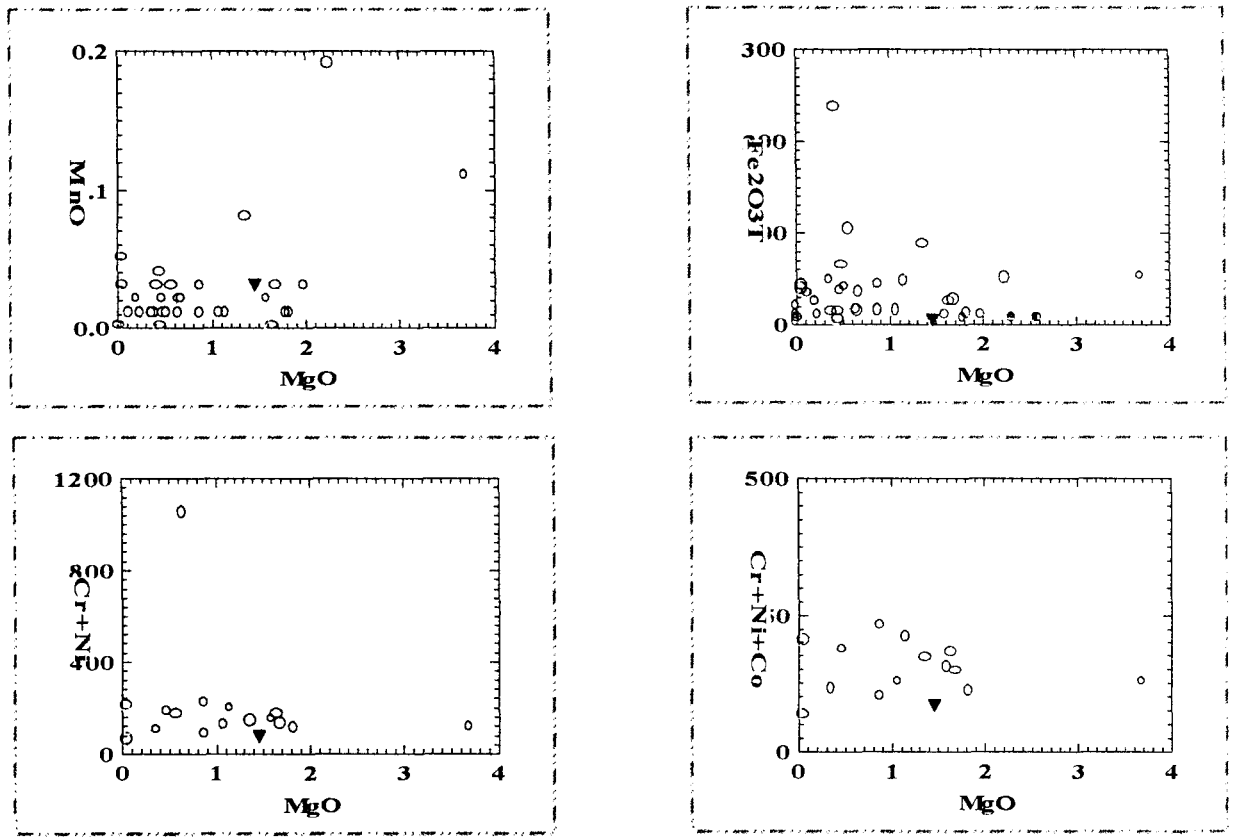


Fig.II.134:- Binary plots of MgO versus ferromagnesian elements (MnO, Fe2O3T, Cr+Ni+, Cr+Ni+Co).

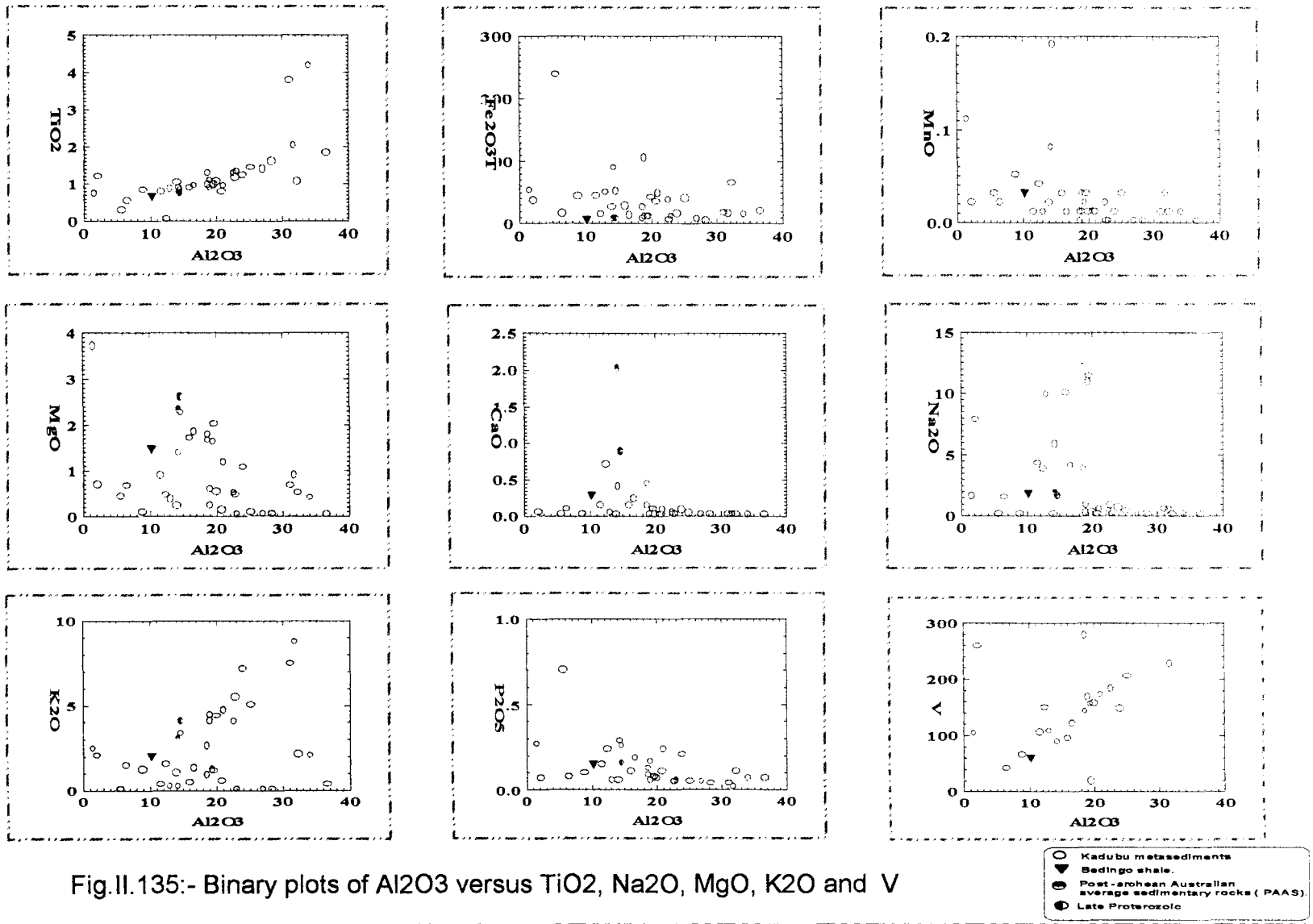


Fig.II.135:- Binary plots of Al2O3 versus TiO2, Na2O, MgO, K2O and V

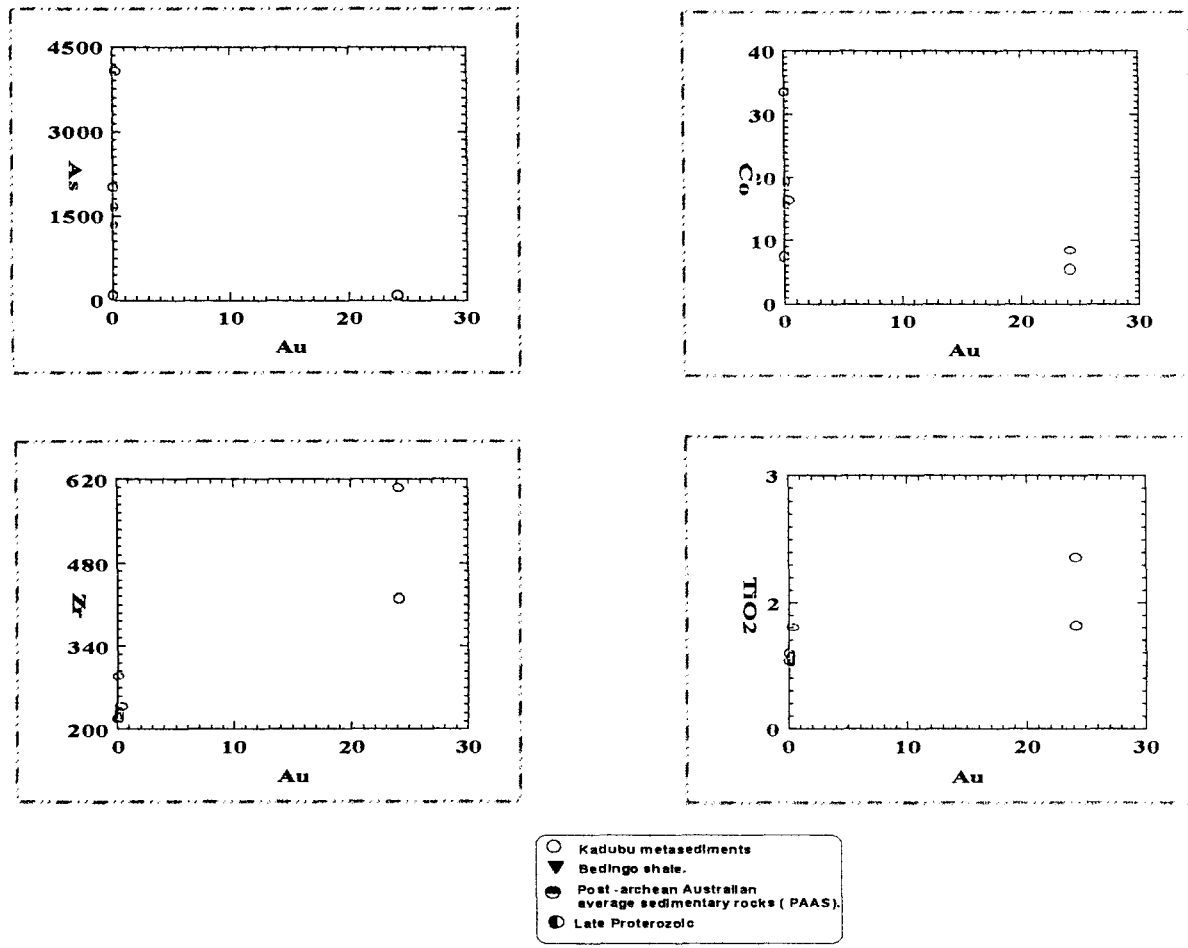


Fig.II.136:- Binary plots of Au versus As, Co, TiO2, Zr, for Kadubu metasediments

The conglomerates and greywackes are rich in S, Mo, Ag and B. The granitoid clasts (unfoliated granite, minor granitic gneiss, gneiss, and vein quartz) from matrix -supported conglomerate (tillite) of the upper Kadubu group are petrographically similar to the Kasika leucogranite and the Kibaran gneiss and hence suggest a derivation from the Kibaran basements. Compositions of pebbles and matrices suggest that the source of the conglomerate is in the continental nuclei.

Passive Margin (PM) sediments are largely quartz-rich, derived from plate interiors or stable continental margins, associated with ocean floor spreading, failed rifts and Atlantic-type continental margins. Active Continental Margin (ACM) sediments are quartz-intermediate and derived from tectonically active margins such as uplifted areas associated with strike-slip faults and deposited in pull-apart basins; subduction- related basins,and continental collision basins, whilst , Oceanic Island Arc (OIA) sediments are quartz-poor volcanic in origin derived from oceanic island arcs and; subduction – related basins. (Pearce, 1983, Bathia, 1983; Roser and Korsch, 1986, Makrygina and Petrova, 1998).
Roser and Kosch, (1986) pointed out that care is needed when assessing the tectonic setting of sediments deposited in basin related to active plate boundaries because these basins (trench, forearc , intraarc, backarc) can be related to either a continental margin magmatic arc (ACM) or an Island Arc,(ARC).

The high content of quartz and high ratio of $K_2O/Na_2O > 1$, allow us to classify the Kadubu metasediments as OIA in ACM.

In the Chondrite-normalized REE diagram, (Fig.II.137) for Kadubu metasediments, the patterns are not the same as typical post- Archean shales showing LREE-enrichment, a positive Eu-anomaly, and no flat HREE patterns. McLennan ,(1993) pointed out that in detail, a wide range of REE patterns is found in active tectonic settings, but the signature of intracrustal differentiation, in the form of negative Eu-anomalies, is present to varying degrees in most samples.
The Europium enrichment in the Kadubu metasediments could be related to a high normative plagioclase content, due to a local accumulation of feldspars during sedimentary processes, without wider implication. The enrichment of Eu is also observed in the Archean sedimentary rocks (Nance and Taylor, 1976).

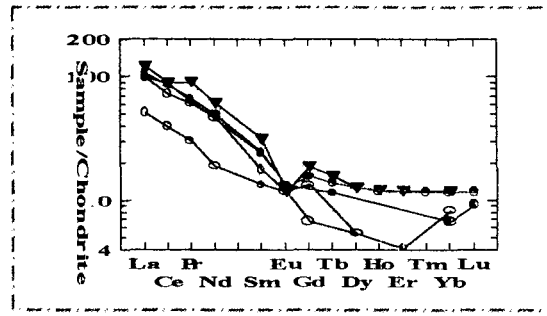
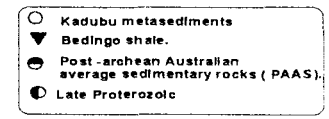
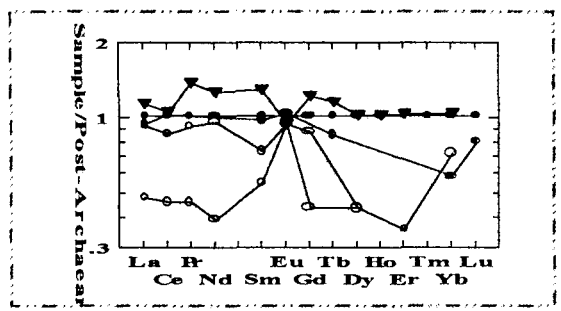


Fig.II.137:- Chondrite - normalized REE diagram for Kadubu metasediments.





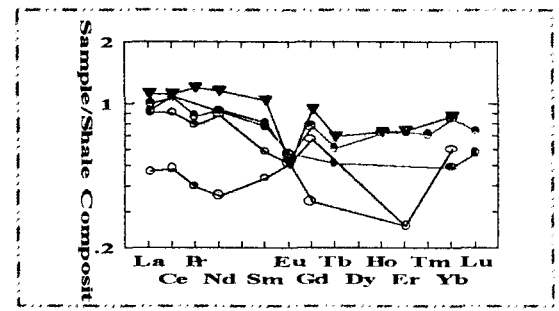
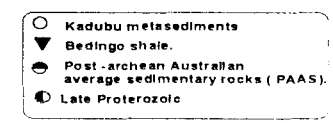
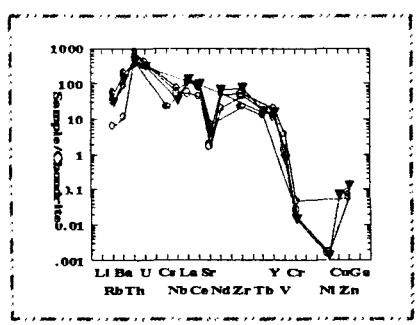
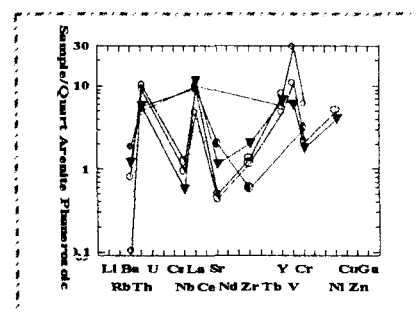


Fig.II.138:-
PAAS - normalized REE diagrams, and Shale - composite NA - normalized REE diagram for the Kadubu metasediments.







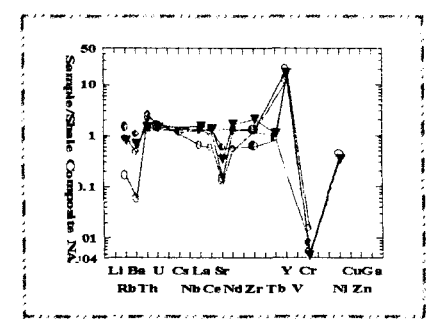
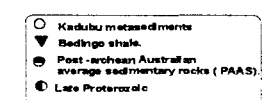


Fig.II.139: -
Spider diagrams of the Kadubu metasediments.



The plots of PAAS (Post-Archaean Average Australian sedimentary rock. Mc Lennan,1989), -normalized REE pattern, Shale composite NA- normalized REE pattern, and Upper crust - normalized REE pattern shows an essentially curve pattern with high left hump and positive Eu anomaly (Fig. II.138).

Spider diagrams of these metasediments are shown in Figure.II.139 . The type of patterns found are not identical to post-Archean shales and could be typical of acidic continental crust differing only in having lower total REE abundances, probably reflecting a mantle source signature or igneous history of the provenance of the metasediments.

The predominantly high to intermediate silica and no PAAS-like compositions of the Kadubu clastic metasediments indicates derivation from a dual –source area : continental upper crustal materials mixing with a mafic source. Erosion of the local Kibaran gneissic basement could represent the "end member" source composition of the metasediments.

Structural and geochronological evidence suggests that the Kadubu area is a Neoproterozoic supracrustal sequence with the chemical data from the clastic metasediments appearing to confirm a Proterozoic rather than an Archaean age. (Taylor and Mc Lennam,1985)

The chemical variation exhibited is therefore largely interpreted as the result of mixing between a dominant continental source and a mafic source.

On a discriminant function diagram devised to determine the depositional environments of sandstones using major elements, the Kadubu clastic metasediments plot dominantly within the "active continental margin " field.

The plotted position of these samples therefore suggests that this diagram may not be able to discriminate between continental subduction-related and rift-related depositional environments.

The presence of black shale suggest that sedimentation occurred under reducing conditions probably within a shallow basin.

The composition of the sand grains and pebbles in matrix -supported conglomerate is broadly consistent with derivation from a terrane of silicic igneous rocks and clastic metasediments as seen in the Kibaran basement today, together with reworking of older sediments in the basin.

The plate tectonic significance of the tillite clasts suggest derivation from the Kibaran basement. The dominance of quartz grains composed of only one, two or three crystals and the minor importance of polycrystalline quartz grains in the Kadubu metasediments, suggests that granitic and /or gneissic rocks were dominant in the source areas. The conglomerates and quartzites represent crustal stability.

The Congo craton and the Kibaran basement are thus the oldest stable terranes known in the region.

8.3.2.- GLACIOGENIC DEPOSITS : PALEOCLIMATE SIGNIFICANCES AND GEOCHRONOLOGICAL IMPLICATIONS .

This section deal with the significances for local history of the earth of the conglomeratic Formations found in the Kadubu area. Four levels of conglomeratic rocks have been recognized in this study area : Kigogo conglomerate Formation, Nya-Kasiba basal conglomerate Formation, Mukuka oligomictic conglomerate of the Nya -Kasiba Formation and Polymictic conglomerate of the Tsibangu Formation. The sedimentological and paleoclimatic significance of these different conglomerates were not yet appreciated at this time.

The criteria for identification of glacial bed deposits (unsorted sediments, angular clasts, striated boulders, water-worn clasts ....), and their classification, has been much debated (Harland et al., 1966, Brodzikowski and Van Loon, 1991). Therefore, it may be difficult to discrimate between glacially (glacigenic, glacifluvial, and glacilimnic) and no glacially formed tillites when dealing with the conglomeratic metamorphic Formations such as of the Kadubu area. The sedimentological evidence for a glacial origin is not absolutely convincing .

Following the approach of Nesbitt and Young; (1982), the chemical index of alteration (CIA) of diamictite matrix materials , from the Polymictic conglomerate of the Tsibangu formation ,was calculated to give an idea of the source, using molecular proportions, { $CIA = [Al_2O_3 / (Al_2O_3 + CaO^* + K_2O] \times 100$ where CaO^* is the amount of CaO incorporated in the silica fraction of the rock }.

Chemical analyses of the fine -grained portion of the matrix of five diamictite samples yielded CIA mean value of 51.94548. These average values for the diamictite matrix material supports the glacial origin of the Polymictic conglomerate of the Tsibangu Formation. (Table.II.18).

Lower CIA values from the Tsibangu formation suggest that, following deposition of this formation, there was a cooling climatic trend. It is suggested that the Polymictic conglomerate of the Tsibangu Formation was laid down as marine, dominantly glaciogenic sediments as part of a glacial episode of continental : snowball Earth.

The rhytmic alternation of coarse and fine layers in the Mukuka oligomictic conglomerate of the Nya-Kasiba Formation may possibly represent seasonal increase or decrease in meltwater produced from the glacier. The presence of dropstones, together with occurrence of striated clasts, strongly support the idea that deposition of this conglomerate was related to glacial conditions. (Fig.II.21).

Glacial influence on deposition of the Neoproterozoic Kadubu area (Itombwe synclinorium) is well established. Polymictic conglomerate of the Tsibangu Formation, Mukuka Oligomictic conglomerate and Kigogo conglomerate Formations are here interpreted as glaciomarines.

The glacial interpretation is based on :

1*- Chemical index of alteration (CIA) of the matrix materials of the Polymictic conglomerate;

2*- Presence of dropstones , angular to subangular quartz grains, laminated facies exhibiting multiple -graded layers , and rare striated stones for Mukuka oligomictic conglomerate ;

3*- Presence of extremely angular quartz grains, and striated clasts for the Kigogo conglomerate. Overlying the Kigogo conglomerate, there is a classic cap dolomite of the kind that commonly overlies upper Proterozoic glacial diamictites in Australia and north west Africa (Williams, 1976 ; Deynoux and Trompette, 1976) ;

The inference of a marine, as opposed to a possibly glaciolacustrine setting rests mainly on stratigraphic and paleotopographic relation. A long-lived marine basin, witnessed by carbonaceous and metaturbidites metasediments, is recorded in the Kadubu study area. The difficulty of global chronocorrelation of Upper Proterozoic deposits are widely appreciated. (Cahen ,1979). Hence, more detailed sedimentologic study is needed as proof for glaciogenic origin of these conglomerates.

Table.II.18:- Chemical composition of the fine-grained portion of the diamictite matrix from the polymictic conglomerate of the Tsibangu Formation.

	KW 105A	KW 105B	KW 107B	KW 650A	KW 650B
SiO2 wt%	65.32	65.75	64.01	65.85	65.86
TiO2	0.76	0.75	0.7	0.99	1.01
Al2O3	11.57	11.49	11.58	13.53	13.56
Fe2O3	5.99	5.85	6.92	7.28	7.18
MnO	0.13	0.13	0.11	0.14	0.14
MgO	4.03	4	3.68	3.88	3.9
CaO	3.62	3.61	4.4	2.94	2.9
Na2O	1.35	1.36	1.48	1.51	1.55
K2O	2.3	2.32	2.42	2.65	2.67
P2O5	0.14	0.14	0.26	0.18	0.19
LOI	5.15	5.06		1.53	1.54
TOTAL	100.38	100.45	95.84	100.49	100.51
CIA	50.6244	50.3935	47.0004	55.8502	55.8589

CIA = [Al2O3 / (Al2O3 + CaO* + Na2O + K2O)] x 100
Where CaO* is the amount of CaO incorporated in the silicate fraction of the rock.

These conglomeratic Formations have not been directly dated but are thought to be correlative with the 520-550 Ma glacial tillites of Western Africa (520-550 Ma) (Hamley and Harland, eds., 1981) and of Schwarzrand diamictites of the Nama Group (550 Ma), (Meert and Van der Voo , 1994), all belonging to the latest Vendian/ Sinian glaciation (625 - 540 Ma), (Meert and Van der Voo, 1994).

8..4.- SUMMARY AND DISCUSSIONS.

The Kadubu metamorphic complex consists of two geochemically and structurally distinct groups: the lower Kadubu group and the upper Kadubu group. The structure of the Kadubu area is essentially a "detachment (nappe) – thrust " stack that has resulted from compressional thrust tectonics that was later transformed into strike-slip dominated tectonics.

The structure and age (530- 540 Ma) of the complex accords with a Pan African collisional *(Kuunga orogen*) history which is one of the major conclusions of this work with regard to the thermal-tectonic development of the Kadubu area. It is assumed that the orogeny resulted from a collision between the Congo and the Tanzania plates. [continent – continent collision].

In formulating the models of geodynamic evolution of the Itombwe basin, and taking into account the different geodynamic models of the Kibaran basement, the following scenarios are proposed:

*- The Itombwe basin was formed in a strike-slip setting as a pull-apart basinal structure with transitions from compressional (transpression) to extensional (transtension) regimes. The pull-apart basin was associated with strike-slip displacements along oversteping *en -echellon* faults.

*- The geochemistry of the clastic metasediments suggests a tectonic model for the Kadubu area (Itombwe Supergroup), as an intracontinental extensional rift receiving clastic detritus from the adjacent uplifted Kibaran basement .

*- Geochemical results from the diamictite matrix material support the interpretation that it was deposited in a glacially -influenced environment. Diamictite of the Tsibangu formation is considered to be glaciogenic and may provide independent evidence of a cooling climatic trend beginning after deposition of the Tsibangu Formation. Polymictic conglomerate of the Tsibangu Formation, Mukuka Oligomictic conglomerate and Kigogo conglomerate Formations are all interpreted as glaciogenic deposits related to the latest Vendian/ Sinian glaciation (625 - 540 Ma).

*- The development of the Itombwe basin (and subsequent Kadubu area) which is controlled by fault movements and reactivations, is related to its location at divergent plate boundaries (Congo and Tanzania cratons), and /or active margin (western branch of the East African Rift system).

CHAPTER 9.- INTERPRETATIONS.

Making use of all the data collected from the Kadubu area, a reconstruction of the tectonometamorphic evolution of this part of the Itombwe synclinorium belt has been attempted. Glacial influence on deposition of the Neoproterozoic metasediments of the Kadubu area within the Itombwe Supergroup is also discussed.

The synclinorium could be interpreted as a pull-apart basin developed along a strike-slip fault system or as a pull- apart basin formed by overall sinistral shear .
At the begining of continental collision, the eastern part of the Kibaran belt corresponded to a broad continental margin covered with a thick sedimentary sequence.
During the early stage of the collision, a first phase of crustal thickening induced low-grade metamorphism in the lower Kadubu group sediments. The thickening is interpreted as having been related to a compressional tectonic event that occurred between the Congo craton and the Tanzania craton during the *Kuunga orogen*. It is proposed that the western bounding faults represent an inversion structure, superposed on the basal thrust .

Following its burial, the lower Kadubu group was thrust to the desection suggesting eastward transfer of its principal zone to deeper structural levels. Furthermore, deformation (D_1) within a structurally thickened sedimentary wedge was initiated in the west, while sedimentation was still ongoing in the basin to the east. At the end of this sedimentation, a second deformational event (D_2) with a low grade metamorphism (M_2), occurred. ^{40} Ar/ ^{39}Ar dating of the uppermost phyllite in the Tsibangu group suggest that (D_2) deformation took place at ca 575 ± 83Ma.

It is suggested that these deformations may have occurred during the same progressive compressional event and following extensional event. Faults and shear zones that developed early in the deformation history of the Kadubu area, were re-activated particularly during rifting event. The extensional shear zone is superposed on earlier NW-verging compressional fabrics. Northwest - trending chevron folds, kinks, shear zones and faults, locally accompanied by a foliation, have overprinted D_1 - D_2 structures.

The Neoproterozoic interval (1000-540 Ma) contains a series of glacial intervals. These includes: the 750-700 Ma Sturtian glaciation, the 625-580 Ma Marinoan -Vendian glaciation and the 600-550 Ma Sinian glaciation. (Meert and Van der Voo, 1994).

Neoproterozoic climate presents the following paradox and mysteries (Harland, 1964 ; Williams,1993 ; Kirschvink, 1992, Hoffman and Schrag, 2000):

- Low -elevation continental glaciations that occurred at tropical latitudes (< 25^0C). How glaciers could have survived the tropical heat ? ;
- The occurrences of glacial debris near sea level in the Tropics ;
- Mixed in with the glacial debris are unusual deposits of iron-rich rock ;
- Rocks known to form in warm water seem to have accumulated just after the glaciers receded. Neoproterozoic glacial deposit is found blanketed by carbonate rocks. Such rocks typically form in warm, shallow seas: This explains so sudden a change from glacial to tropical climates.

All these paradox are found united within the four conglomeratic Formations of the Kabudu area.

For explaining Neoproterozoic glaciation in low palaeolatitudes, the " global glaciation " hypothesis of Harland (1964), recently dubbed " Snowball Earth " (Kirschvink, 1992, Meert and van der Voo, 1994; Hoffman and Schrag., 2000) and the " large obliquity " hypothesis of Williams (1993) and Williams et al.,1995, for low latitude (0 - 30^0) glaciation with strong seasonality are the two principal and longstanding hypotheses .

For the Tsibangu-diamictite, the " snowball earth " model better fits the available geochnological data of the Kadubu metasediments and the fact that, Williams's hypothesis of a large obliquity in the geological past applies only to the pre-Ediacaran, because he postulated that during the late Vendian - Ediacaran (approximately 600-540 Ma), the obliquity underwent reduction from > 54^0 to a value approching that of today. (Williams et al., 1995).

Overall, the snowball earth hypothesis explains many extraordinary observations in the geological record of the Neoproterozoic world : the carbon isotopic variations associated with the glacial deposits, the paradox of cap carbonates , the evidence for long-lived glaciers at sea level in the tropics, and the associated iron deposits. (Hoffman and Schrag., 2000).

According to Eyles (1993), Late Proterozoic glacially-influenced strata occur on all seven continents and falls into two tectonostratigraphic types. In the first category are thick successions of turbidites and mass flows deposited along *active, compressional plate margins* recording a protracted and complex phase of supercontinent assembly between 800 and 550 Ma. The most characteristic deposit in such settings is the diamictite / turbidite facies association.

The second tectonostratigraphic category of Late Proterozoic glacial strata includes successions of glacially-influenced mostly marine strata deposited along *rifted, extensional plate margins*. Kadubu glaciogenic deposits fall into the first tectonostratigraphic type.

CHAPTER 10.- SUMMARY OF THE GEOLOGY AND TECTONIC EVOLUTION OF THE KADUBU AREA.

The Kadubu area constitutes the type area of the Itombwe synclinorium supergroup and is located approximately between the 28 ^{0}33' – 28^0 50' longitude east and the 2^0 45' – 2^0 57' latitude south, covering about 750 s.q.km, (30 km x 25 km). The synclinorium is an arcuate north-south trending tectonic unit extending for about 125 km, from the Luemba village, in south, (~ 4^0 00' south), to the Masisi locality (~ 1^0 30' north), in north. It is up to 35km wide.

The most striking physiographical features of this area are the moutain ranges of the western branch of the east African rift system, (WBEARS) which have deeply incised valleys with rain forest within them. The area experiences a semihumid, tropical climate. Deep weathering profile, is strongly developed producing some distinctive landforms.

The Kadubu river drains a large part of the study area and has a basin area of ≈ 25,000 sq km. Various terrace levels can be developed up to 350m above the present level of some streams. The Kadubu river and its tributaries run along very narrow to incised valleys bordering the west side of the extension zone of the WBEARS .

The northern part of the sudy area is overriden by the Ngweshe basalt and seems to have been dammed off by volcanic activity and its products. Some relics of underlying metasediments are seen on the top of mountains.

The Kadubu area is made up of metaturbidite sequence exhibiting characteristic Bouma cycles , with two structural zones bordered by major thrust-faults. These bounding faults and internal, normal faults, shear-faults, strike-slip faults and high-angle reverse faults are interpreted to have a listric geometry and flatten at depth with inferred major mid-crustal detachement faults forming a west-vergent thrust system.

This metaturbidite sequence consists of two geochemically and structurally distinct groups: the lower Kadubu group and the upper Kadubu group. The Upper Kadubu group is comprised mainly of an alternation of conglomeratic, slaty phyllitic and arenaceous metasediments, whereas the Lower Kadubu group consists of a monotonous cyclic sequence of psammitic and phyllitic horizons. The Tshondo fault zone is a clear tectonic, metamorphic and geochemical discontinuity within the Kadubu area.

This sequence has been folded into upright, north to northwest –trending, tight to isoclinally folded successsion. The dominant trend of the belt is NW to NNW with two main fabric/lineament directions running NNW-SSE and NE-SW.
It has been suggested that this deformation may have occurred during the same progressive compressional event ; with two phases compressional, followed by extension event. Faults and shear zones that developed early in the deformation history of the Kadubu area, were re-activated. Northwest – trending chevron folds, kinks, shear zones and faults, locally accompanied by a foliation, have overprinted D_1 - D_2 structures. Two major shear zones running respectively N-S and E-W have been observed.

Three phases of deformations D_1, D_2 and D_3 , characterized by various microstructures (schistosity, crenulations, ...) have been recognized in the metasediments of the study area. The analysis of fabric relations demonstrates that two phases of penetrative deformation, (S_1 & S_2), are associated with low-grade metamorphic crystallization. The detailed analysis of metasediment samples from differents units, has allowed the relationship between the microstructures related to D_1, D_2 and D_3, and the associated mineral parageneses (M_1 , M_2, M_3) to be established. Hence, these data define three tectono-metamorphic phases: D_1 -M_1 , D_2 -M_2 and D_3-M_3.

The microstructures characteristic of the tectono-metamorphic phase D_1 -M_1 are essentially slaty cleavage and flow cleavage with quartz pressure-shadows. S_1 is orientated NW- SE and subparallel to S_0. S_1 is deformed by microstructure S_2.

In the upper Kadubu group, the D_2 -M_2, tectono-metamorphic phase has well-developed foliations (S_2), defined by the shape and preferred orientation of micas (sericite), shear- band orientation, S-C fabrics and quartz texture.

In the Kadubu area, metamorphic grade increases slowly towards the west; (the lower tectonostratigraphic level), across the Upper Kadubu group , from subgreenschist to greenschist facies.

The main common and critical mineral assemblage for the whole Kadubu area is: quartz, albite, chlorite, white mica, (muscovite, sericite, phengite), plagioclase (oligoclase), epidote, actinolite, biotite, opaque (hematite, goethite, limonite).

Additional minerals include calcite, ankerite, apatite, graphite, magnesite, rutile, talc, kaolinite. Lithic fragments, tourmaline , pyrite, arsenopyrite and zircon can also occur.

$^{40}Ar/^{39}Ar$ step-heating of mineral separates and laser probe fusion of single grains have been used in conjunction with petro-structural observations to delineate the cooling / tectonic history of the Kadubu area. $^{40}Ar/^{39}Ar$ dating of metamorphic mica (muscovite) growth, in cleaved phyllite gives an age of 575 $\pm$ 83 Ma ; This dated muscovite comes from within the D_2- NNW- directed tigh to isoclinal –dominated structural domain and the interpreted age coincides with F_2 folding.

The plateau age of 575 $\pm$ 83 Ma is interpreted to record initial mica growth during D_2 deformation and associated regional metamorphism . This age is likely to date cooling following initial metamorphic recrystallization and concomitant cleavage development.

This sequence has been intruded by a late to post-orogenic, alkaline, metaluminous albitite rock. In the Twangiza region, gold mineralization is often, (but not always) associated with albitite rock. Petrographic and geochemical (major and trace element) data show the Twangiza albitite intrusion to be of igneous origin ; related to deep-seated alkalic magmatism .

The diversity of REE minerals, such as hydrothermal monazite, suggests that the source of sodium –rich fluids may have been a deep -seated alkalic (or carbonatitic) intrusion.
A regional granite is also intruded into the Kibaran metasediments in the southwesthernmost corner of the study area. This granite is leucocratic, SiO_2- and K_2O- rich granitic/alkaligranitic, peraluminous, subalkaline, syn- to post collisional, and fits the criteria for S-type granite.
Combined field, geochemical and isotopic data enables constraints to be placed on the origin of the Kasika granite and the Twangiza albitite. $^{39}Ar/^{40}Ar$, Rb/Sr and Sm/Nd constrain the history of magmatism . Both radiogenic ages and field evidence indicate a Neoproterozoic event.

This granite yielded mean ages of 529 ± 5 Ma and 436 ± 8 Ma ($^{39}Ar/^{40}$) and 703 ±14 Ma . (Rb/Sr). The albitite rock yielded an age of 1078 ± 27 Ma implying that this albitite is related to a Kibaran granite. The initial Sr isotope ratios ($^{87}Sr/^{86}Sr$) for respectively feldspar (albitite) and apatite &mica (granite) have a mean of 0.734298 ± 0.0001 and (0.885419 ± 46 & 18.277000 ± 26) respectively.
Sm/Nd iostope ratios for feldspar (albitite) and apatite (granite) are respectively 0.14852 and 0.36422 suggesting a mantle source in origin.

The initial $^{143}Nd/^{144}Nd$ ratios (0.512590 ± 23) of albitite is consistent with that of the Kasika granite (0.512669 ± 29) and again suggests a genetic link between these two rocks. The samples that have a correspondingly similar Nd ratio can be assumed to have evolved from the same source. The field and geochemical relationships between the Kasika leucogranite and the Twangiza albitite suggest a genetic connection between these two types of igneous rocks.

Despite some geochemical similarities to late-orogenic granites, the Kasika leucogranite is better interpreted as a syn-to post- orogenic granite which probably was formed by partial melting of lower –upper crustal /upper mantle source rocks. A mixed crustal / upper mantle source is also indicated by mixed, S and I-type characteristics (e.g. initial $^{87}Sr/^{86}Sr$ of 0.885419) and LIL/HFS element ratios.

Intense crystal fractionation produced highly differentiated pegmatites from granitic melt which may have originated by partial melting of crustal/upper mantle source rocks.
The most plausible source for the Kasika granite is the Kibaran gneissic metasediments which are relatively mature and contain older crustal materials. Formation probably occurred in a deep Kibaran gneissic and/or granitic environment and at high temperatures (> 800 ^{0}C). Radiogenic isotope suggests a common crustal / upper mantle source for these two rocks with some contamination. The magma could have been generated from crust that had been through a cycle of subduction-zone or continent –continent collision magmatism.

The structure of the Kadubu area is essentially a "detachment (nappe) – thrust " stack that has resulted from compressional thrust tectonics that was later transformed into strike-slip dominated tectonics. The structure and age (530 - 540 Ma) of the complex accords with a Pan african collisional history. It is assumed that the orogeny [continent – continent collision.] resulted from a collision between the Congo and the Tanzania plates.

In formulating the models of geodynamic evolution of the Itombwe basin, and taking into account the different geodynamic models of the Kibaran basement, the Itombwe basin has been considered evolved in a strike-slip setting as pull-apart structures with transitions from compressional (transpression) to extensional (transtension) regimes.

The geochemistry of the clastic metasediments suggest a tectonic model for the Kadubu area (Itombwe synclinorium), as an intracontinental extensional rift receiving clastic detritus from the adjacent uplifted Kibaran basement. Geochemical results from the diamictite matrix material support the interpretation that it was deposited in a glacially - influenced environment. Polymictic conglomerate of the Tsibangu Formation, Mukuka Oligomictic conglomerate and Kigogo conglomerate Formations are all interpreted as glaciogenic deposits related to the latest Vendian/ Sinian glaciation (625 - 540 Ma).
The development of the Itombwe basin, and subsequent Kadubu area is related to its location at divergent plate boundaries (Congo and Tanzania cratons), and /or active margin (western branch of the East African Rift system).